2012

# Evaluation of shoreline change using optical satellite images, case study of Progreso, Yucatan

Garcia-Rubio, Gabriela

# EVALUATION OF SHORELINE CHANGE USING OPTICAL SATELLITE IMAGES, CASE STUDY OF PROGRESO, YUCATÁN

**GABRIELA GARCÍA RUBIO**

A thesis submitted to the University of Plymouth in partial fulfillment of the requirements for the degree of

**DOCTOR OF PHILOSOPHY**

School of Marine Science and Engineering

**December 2011**

# Abstract

**Evaluation of shoreline change using optical satellite images, case study of Progreso, Yucatán**

Gabriela García Rubio

A technique to extract the shoreline from optical satellite images has been developed, evaluated and applied to the case study site of Progreso, Yucatán, México. This site was chosen as it is frequently subject to hurricanes, shows shoreline erosion and has a paucity of coastal data. The area under investigation is an 8 km length of shoreline that faces north into the Gulf of México.

A novel method to extract satellite-derived shorelines (SDS) was developed ensuring the maximum contrast between sea and land. The SDS was validated using quasi-simultaneous *in situ* shoreline measurements from one day in two different years (2008 and 2010). The *in situ* shoreline measurements recorded the instantaneous shorewards extent of the wave run-up when walking along the beach.

The validation of SDS revealed that the SDS locates consistently seawards of the *in situ* shoreline, explained by: a) the water depth that an optical satellite image requires to identify a pixel either as sea or land, and b) the shorewards extent of the wave run-up. At Progreso, the overall distance between SDS and *in situ* shoreline is 5.6 m on average and standard deviation of 1.37 m (in the horizontal) over 8 km of shoreline.

For an accurate location of the mean SDS, estimation of the shorewards extent of the wave run-up, tidal level and inter-tidal beach slope were required. *In situ* measurements regarding the beach profile, shoreline location and water levels were taken into consideration to achieve this.

The shoreline change observed over a 6.5 year period allowed the estimation of intra-annual and inter-annual shoreline changes and progressive changes in the shoreline location. The intra-annual shoreline change revealed seasonality in the shoreline position. The shoreline position from late winter (March 20, 2004) was landwards (approx. 5 to 9 m) in relation to the earlier winter shoreline position (November 11, 2003). The assessed SDSs from the hurricane season (June to November) are at the landwards envelope limit during the year, between -30 to 15 m in relation to the estimated mean SDS. The largest landward movement (100 m) is related to Hurricane Ivan, detected 13 days after the hurricane passed by Yucatán. The inter-annual shoreline change highlighted that an approximate length of 6 km of shoreline is retreating at a rate between -2.4 and -1.2 m per year. Such estimates of shoreline change would not be possible using other available coastal information at this site.

The results of this research show that optical satellite images can be used to study shoreline change over large spatial scales (> 5 km), as well as in short (< 1 yr) and long (> 5 yrs) temporal scales.

**Keywords:** coastal erosion, shoreline detection, coastal dynamics, remote sensing.

# Contents

# List of Figures

# List of Tables

# Acknowledgements

I would like to acknowledge my supervisors David, Paul and Ken, for their important feedback, particularly David, who has given me great support and supervision since the very beginning of this research project. Thanks for all the discussion, guidance and advice!

I also want to thank Luciana Esteves and Victor Abbot; their important feedback allowed me to improve this research.

Thanks to CONACyT, who supported me during the PhD, allowing me to work full time in this research. I am grateful to my external contacts in México, especially to Ismael Mariño from CINVESTAV, Mariana, Aleph and Edilberto; without their help fieldwork and data collection in Progreso would not have been possible. Also to the personnel from the Mexican Navy based at Progreso and at México city, particularly Tte. Iván Gutiérrez. In addition, I would like to express my gratitude to CONAFOR who gave me access to images at the very beginning of this research.

I would also like to acknowledge Emma P., Bex, Siân, and very especially Victor, for reading my chapters. Also I would like to thank Tim Scott, for his help to analyse sediment samples in the laboratory, and Dan Buscombe, for taking photographs to sediment samples, both from the CPRG group.

Thanks also to my friends Floortje, Bex, Marta, Leyla, Siân, Charlie, Marieka and Joachim, Iman, Paola and Salo, Thomas and Linda, Rob and Jane, Victor and Judith, Emma P., Raúl, Vanessa and Markus, José and Corina, Sean, Frankie, Phil, Daniel, Donella, Emma R., Rob, Ant, Jamie, Sola, Emlyn, people who made my days easier and happier in Plymouth. The times together, the laughs, the outdoors, the cake and the wine were great! My friends in México were important as well. Thanks to Lina, Ana, Israel, Gaby Sampedro, Anta and Vic, Alex, Sandy. Thanks as well to all the miles that kept my mind working, giving me strength and health.

Finally I would like to thank my wonderful loving parents, Don José Antonio and Doña Lupita, who made my writing-up days full of cheer and love. My sweet sisters for all their love, Claudia, Laura and Fabiola, and my cute and gorgeous nieces and nephew, Gigi, Lucien and Isabelle, especially to Gigi who has the most wonderful laugh!

# Author's declaration

At no time during the registration for the degree of Doctor of Philosophy has the author been registered for any other University award.

This study was financed with the aid of a studentship from the Mexican Council of Research and Technology (CONACyT).

Relevant scientific seminars and conferences were regularly attended at which work was often presented. One conference paper has been presented at an International Conference.

**Publications** :

García-Rubio, Gabriela; Huntley, David; Kingston, Kenneth and Esteves, Luciana. Shoreline identification using satellite images. Impacts of Human Activities on Dynamic Coastal Processes, 7-11 September 2009, Tokyo, Japan. paper no. 117.

**Oral presentations and conferences attended** :

Young Coastal Scientists and Engineers Conference, Oxford, 27 May 2008.

Plymouth Marine Sciences Partnerships Symposium, 7 April 2009, Plymouth, UK, Oral presentation: Shoreline change identification using optical images (SPOT) in the Yucatán Peninsula, México.

Coastal Dynamics, 7-11 September 2009, Tokyo, Japan, Oral presentation: Shoreline Identification using satellite images.

Remote Sensing and Photogrammetry Society, 15-17 March 2010, Plymouth, Oral presentation: Spectral differences between sea and land with optical satellite images.

Young Coastal Scientists and Engineers Conference, 29-30 March 2010, London (UCL), Oral presentation: Assessing shoreline change using satellite images.

Coastal Processes Rearch Group Symposium, 11 November 2010, Plymouth, Oral presentation: Shoreline identification using satellite images.

Third Annual Conference, Marine Institute, 20 December 2010, Plymouth, Oral presentation: Capabilities of satellite images to assess shoreline change.

Young Coastal Scientists and Engineers Conference, 30 March 2011, Liverpool (NOC), Oral presentation: Accuracy assessment of shoreline change using satellite images.

Plymouth Marine Sciences Partnerships Symposium, 12 December 2011, Plymouth (PML), Oral presentation: Evaluating optical satellite images for shoreline change studies.

**External Contacts:**

Centro de Investigación y de Estudios Avanzados (CINVESTAV), Mérida, Yucatán.

Secretaria de Marina, México.

**Word count of main body of thesis: 56,500**

**Signed:** _____

**Date:** _____

# Chapter 1

# Introduction

Shorelines are features vulnerable to erosion, floods, storms and hurricanes. Moreover, they are inherently dynamic features that mark the transition between land and sea. Shorelines change their location over time, and at different spatial scales due to waves, winds, nearshore currents, storms and by human modification.

It is estimated that there are more than 347,984 km of shoreline in the world and that 60% of the world's population lives within 100 km of the sea (Vitousek et al. 1997). In addition, considering the sea level rise produced by climate change, monitoring shoreline change becomes particularly relevant to estimate shoreline erosion and coastal flooding (Douglas et al. 2001; FitzGerald et al. 2008; Gutierrez et al. 2011). The shoreline erosion and coastal flooding were pointed among the gravest effects of climate change by the IPCC (1990). Within this context, the shoreline has been also recognised as one of the 27 global geo-indicators referred to by the International Union of Geological Science in order to monitor shoreline change over the coasts (Li et al. 2003).

The implementation of coastal monitoring and shoreline change studies is costly and beyond human and budget capacities for developed and developing countries. Therefore, to monitor shoreline change covering large spatial scales, a cost-effective approach is required, particularly for those places where there are concerns about shoreline erosion, paucity of coastal data and/or limited access to carry out *in situ* shoreline mea-

surements on a regular basis. The research presented here assesses the capabilities of optical satellite images to identify the shoreline and study shoreline change.

There are multiple data sources that can help to identify the shoreline, such as satellite imagery, aerial photography, radar, video and field surveying techniques. Optical satellite images have been widely used to map the shoreline, offering the potential to update maps covering large areas as often as every one to eight days (Frihy and Lotfy 1997). The spatial resolution of optical satellite images has been improving in the last 20 years, from 20 m to 0.4 m pixel size, allowing access to images with a much better resolution offering the possibility of building a long database (> 20 years) to study shoreline change in places where otherwise it would not be monitored.

Optical satellite images have been previously used to study shoreline change (Mason et al. 1995; Chen and Rau 1998; White and El-Asmar 1999; Li et al. 2003; Liu and Jezek 2004; Muslim et al. 2006; Dinesh-Kumar et al. 2007; Li et al. 2008; Wang et al. 2010), showing their value in coastal studies. However, the shoreline identified by images has not been validated using *in situ* shoreline measurements, indicating potential errors on its detection. This research developes a novel method to extract satellite-derived shorelines (SDS), validates the SDS with quasi-simultaneous *in situ* shoreline measurements and assesses shoreline change using confidence intervals for the case study area of Progreso, Yucatán, México.

Progreso is frequently impacted by hurricanes and storms, shows erosion from Hurricane Gilberto's direct impact in 1988, is densely populated and has a paucity of coastal data. These characteristics make Progreso an interesting location to study shoreline change using SDS.

The analysis of SDSs in this region helped to estimate the intra-annual and inter-annual shoreline change in a 6.5 year period (December 2003 to July 2010). At certain locations shoreline change larger than 20 m was found, as well as areas with changes

as large as 100 metres. Moreover, it was found that Progreso has overall erosion with a shoreline rate of change between -2.4 m and -1.2 m per year. The assessment of SDSs shows the value of exploring shoreline change using SDS and demonstrates their applicability at other locations.

## 1.1 Aim

To explore the use of optical satellite images to study shoreline change using an objective and systematic approach.

## 1.2 Objectives

1. To develop an objective, systematic and practical method to identify the shoreline (as a vector) from satellite optical images, including adjustment to a standard water level.

2. To validate the feature extracted as a shoreline from satellite optical images using *in situ* shoreline measurements and to define confidence bounds for the satellite-derived shoreline.

3. To assess shoreline change over the longest period of time that available images allow in the case study area of Progreso, covering the period of December 2003 to July in 2010, and to determine locations with large shoreline change (> 30 m) and/or progressive shoreline retreat.

4. To interpret the observed shoreline change in relation to winds and waves, as well as to artificial barriers of sediment, presence of hurricanes and storms and to relate the change observed with factors that could be driving shoreline change in the case study area.

## 1.3 Thesis outline

Following this introductory chapter, the literature review (chapter 2) addresses topics related to the study of the shoreline, such as the definition of the shoreline, the natural variation of the shoreline and water levels, different shoreline indicators and the existing data types and techniques used to map and study shoreline change over time.

Chapter 3 explores the capabilities of satellite images to distinguish sea and land as separate groups, and investigates different techniques to identify the shoreline (filters, manual identification and soft classification). The exploration of the satellite capabilites and the investigation of different techniques are shown to be useful to clarify which technique to use for shoreline detection and, therefore, for the development of a method to identify the shoreline from optical satellite images.

Chapter 4 describes the case study area and details the meteorological and coastal processes in the region using the available ancillary data (winds, waves, tides) that was compiled from diverse sources. Tidal measurements are assessed using predicted tides in this chapter in order to ensure that the tidal levels for the shorelines extracted with satellite images are as accurate and consistent as possible over time.

In chapter 5 the case study area is used to validate SDS using *in situ* shoreline measurements over 8 km. Two inter-comparisons from different years are used here, one quasi-simultaneous (2010) and one with 11 days between *in situ* shoreline measurements and SDS (2008). The two inter-comparisons allow estimation of the mean displacement between the SDS and true *in situ* shoreline measurements, as well as the variables involved in the shoreline identification using satellite images. This chapter defines confidence bounds for further use in the calculation of shoreline change. Finally, this chapter assesses shoreline change using SDS from 2008 and 2010 in relation to shoreline change calculated using the *in situ* shoreline measurements.

Chapter 6 examines shoreline change in a six and a half year period in the case study area. The assessment of the shoreline change takes into consideration the artificial barriers of sediment, storms and cyclones. The change of the shoreline location is explored over time in order to detect if there is progressive erosion at the case study area.

Chapter 7 provides a general discussion of the main topics covered through this thesis, as well as suggestions for future studies to pursue for the development of this topic.

Chapter 8 gives overall conclusions of the contents of this thesis.

The Appendix includes (all these contents are in the digital version of this thesis):

1. The cyclone reports of the cyclones mentioned in this thesis from the National Hurricane Center (NHC). The cyclones reports from NHC include information such as track, wind velocities, atmospheric pressure, surges and resulting damage.

2. The conference paper presented at the International Conference of Coastal Dynamics in 2009. The conference paper covers the ealier research from chapter 5.

3. The location and the beach profiles taken during fieldwork conducted in 2010.

# Chapter 2

# Literature Review

## 2.1 Introduction

This literature review puts into context the topics related to shoreline identification and shoreline change using optical satellite images. The topics addressed here are:

1) Shoreline definition and water level variations that modify shoreline location. This section describes the most common tidal datums, as well as the tides, surges, wave set-up and wave run-up.

2) Shoreline indicators: this section reviews different shoreline indicators used to identify the shoreline.

3) Data sources used to map the shoreline over time. This section reviews the different types of data used to survey and map the shoreline, the spatial resolution, the year when they became available to the scientific community and the cost. This section also shows the value of exploring satellite images to identify the shoreline and to study shoreline change.

4) Techniques already developed for shoreline identification using optical imagery. The existing techniques have been in constant development and a review of them provides the background needed to ascertain which approaches or techniques could be applied to identify the shoreline using optical satellite images. This section reviews some of the

developed techniques for shoreline identification. Most of the developed methods are for video (e.g. Argus), however their main principles might be applicable for optical satellite images.

5) Shoreline change studies covering long time-spans. This section reviews some studies that have attempted to study shoreline change over time-spans longer than a decade by using different sources of data and a variety of analytical approaches to identify shoreline change. Although the time-span of the shoreline change covered in this research is shorter than a decade, this section is included to highlight the main considerations when studying long-term shoreline change, as well as the main difficulties when integrating different types of data to monitor the shoreline and to study shoreline change.

## 2.2 Shoreline definition and water level variations

The shoreline, defined as the edge of the sea, marks the transition between land and sea and is the intersection of the sea over the beach. It is a time-dependent feature, that may exhibit substantial short-term variability due to changes in water levels and beach morphology (Morton 1991). As a consequence, the shoreline definition has to consider a timescale (Gens 2010).

### 2.2.1 Water level variations

This section describes the water level variations and the different timescales over which they occur, including the tides, surges and wave run-up.

Water level variations occur over a variety of temporal and spatial scales. Some of them occur slowly (years) while others can be very rapid (minutes). They can also occur over local (<100 km), regional or global scales (> 10,000 km) (Figure 2.1).

The observed sea level, assuming an averaging timescale, is the combined result of

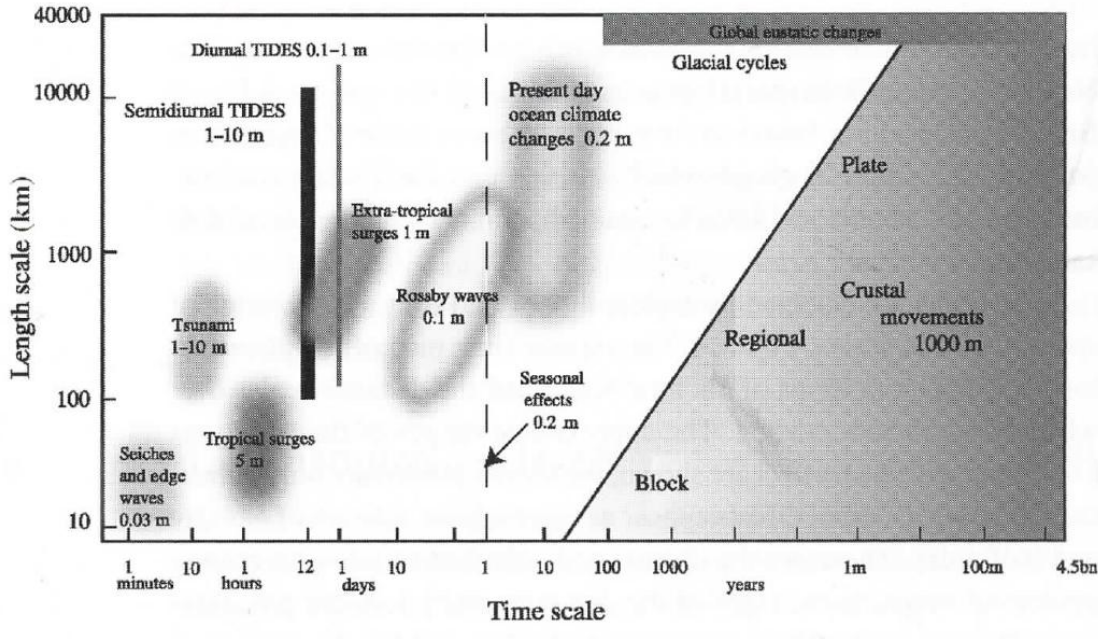


*Figure 2.1:* Factors that change sea level over different geographic (km) and time (minutes to years) scales, from Pugh (2004).

three main factors: tides, surges and mean sea level. The tides are the main cause of sea level change, with a timescale that varies from 12 hrs to one day and a spatial scale of length up to 10,000 km. The surges, in contrast, can last as long as 10 days and can cover a spatial scale of 1,500 km.

Seasonal variations have timescales up to a year and inter-annual changes cover timescales longer than a year. Spatially, inter-annual changes can cover geographic areas as large as 50 km. The temporal scales (up to 6 yrs) and spatial scales (up to 8 km) covered in this research include changes in water levels related to tides, surges, seasonal and inter-annual changes.

### 2.2.2 Tides

This section describes tides and surges and their effects on sea level.

Tides are mainly caused by the gravitational forces of the moon and sun. The range and period are the main tidal features of any sea level record. The range is the height between high and low water, the period is the time between one high (or low) water and the next high (or low) water. The range and the period vary greatly from one site to another.

Figure 2.2 shows the different phases of a diurnal, semidiurnal or mixed tide. Semidiurnal tides are the most dominant regular pattern and have a tidal cycle of 12 hrs 25mins. This tidal cycle spans half a day, with a range that typically increases and decreases cyclically over a fourteen-day period. Diurnal tides have one tidal cycle with a period of 24 hrs 50 mins. Therefore in one day there is one high tide and one low tide. Mixed tides are composite tides, whereas the diurnal tides are similar in magnitude to the semidiurnal tides.

The maximum range, called spring tides, occur one or two days after both new and full moons. These times are termed syzygy, when the moon, earth and sun are aligned. The minimum ranges, called neap tides, occur shortly after the first and last quarters of the moon. When the moon is at its maximum distance from the earth, known as lunar apogee, semidiurnal ranges are less than when the moon is at its nearest approach, known as perigee. The variation from apogee to perigee is repeated every 27.55 solar days. Therefore, big semidiurnal tidal ranges occur when spring tides and perigee coincide, whereas small semidiurnal ranges occur when neap tides and apogee coincide.

To measure the tidal range a datum is used as a reference or as a benchmark. There are a variety of tidal datums, some of the most commonly used are defined in the next section.

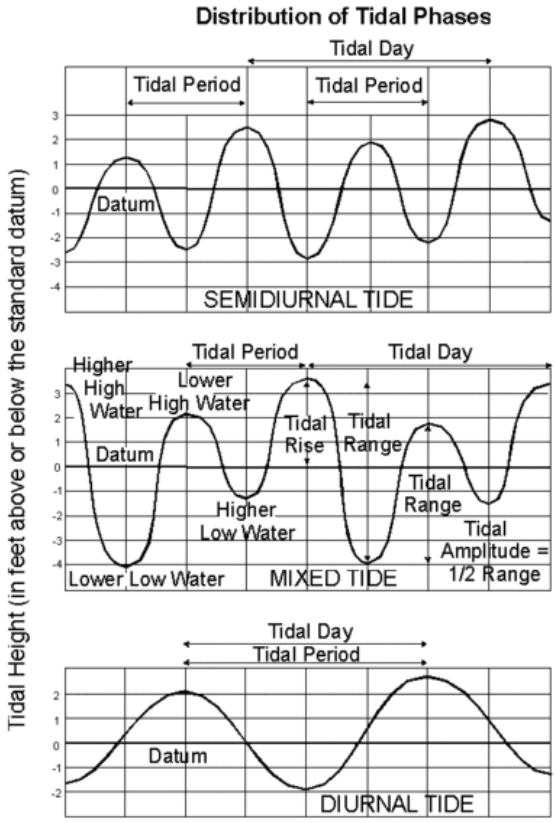


*Figure 2.2:* Different types of tides: semidiurnal (top), mixed (middle) and diurnal (bottom). The plot from the middle show different tidal datums. Diagram from NOAA (1998).

### 2.2.3 Tidal datums

This section outlines the most commonly used tidal datums that are also defined as shoreline indicators. Section 2.3 describes shoreline indicators and it will refer to these tidal datums.

A tidal datum is a stable height used as a reference zero for sea level measurements against which the tidal height can be registered. Tidal datums refer to the intersection of the water level with the land at a specific tidal datum. There are different tidal datums, which are used as a reference to locate the shoreline and for shoreline change studies.

Tidal datums are also used as a benchmark for navigation, coastal management plans and other applications, for example:

- **Mean Sea Level (MSL).** This is defined as the average level of the sea water column measured relative to a fixed level on the land and identified by a network of fixed benchmarks. It can be calculated as the average over a specified long period such as a month, a year, or an 18.6 year nodal cycle. As it is an average calculation, mean sea level does not consider waves but very long-period tides and storm effects can be included in the mean sea level.
- **Mean Water Level (MWL)** This is defined as the average height of the water column.
- **Mean High Water (MHW).** This is defined as the average of all the high water heights observed using a specific tidal datum as a reference, over a specific period of time.
- **Mean High Water Level (MHWL)** This is defined as the average of all the higher high water height of each tidal day observed using a specific tidal datum as a reference, over a specific period of time (Figure 2.2).
- **Mean Lower Low Water Level (MLLW).** This is defined as the average of the lower low water height of each tidal day observed using a specific tidal datum as a reference over a period of time (Figure 2.2).

Each of these tidal datums shows variations in water levels due to waves and winds and these considerations will be mentioned later in this chapter (2.3.2).

### 2.2.4 Surges

Surges are the difference between predicted tides and observed water levels. This difference from the predicted levels is due to the combined effect of atmospheric pressure,

winds and waves. The term 'storm surge' is used for the excess sea levels generated by a severe storm. When weather conditions increase water levels it is known as a positive surge and when lower levels occur it is called a negative surge. Positive surges can cause coastal flooding, whilst negative surges reduce water depths and are a hazard for navigation. Surges are associated with strong currents that can be important agents of erosion and geological change.

Surges are the result of the combined effect of the atmospheric pressure and the wind response. The hydrostatic link between sea levels and atmospheric pressure is clear. The atmospheric pressure modifies water level and produces changes in the pressure forces acting vertically on the sea surface. Open coast storm surge water levels consist of a wind shear forcing component, generally referred to as wind set-up. The wave set-up component caused by wind, induces waves by transferring momentum to the water column. The biggest effects are observed when strong winds blow over shallow water (Pugh 2004).

The response in the water level due to the atmospheric pressure is called the inverted barometer effect. The general rule is that an increase of one mbar corresponds to a fall in the sea level of 0.01 m. However, this general rule is for static conditions. If a system is in movement the response in the sea level will vary in terms of the bathymetry, size, wind velocity and direction of the system.

The wind stress on the sea surface is towards the direction of the wind and it is proportional to the square of the wind speed. Therefore, in storms conditions, the wind effect can be very significant. Moreover, the wind response will be affected by the Earth's rotation, water depth and wind velocity.

In the Atlantic basin, there are hurricanes every year. From Florida to Cape Hatteras there is a great risk of flooding. One of the largest records of surge was in August 1969 when Hurricane Camile, with a recorded atmospheric pressure of 909 hPa and

estimated surface winds of up to 305 $kmh^{-1}$ (190 mph), raised water levels by up to seven metres on the Mississippi coast (ESSA 1969). The low atmospheric pressure alone does not explain this large positive surge but the dynamic effect of the wind velocity, its landfall, and bathymetry conditions, plus the tidal conditions, increased the surge to that magnitude.

### 2.2.5 Wave set-up

When waves break into the shore, they produce a set-up, a rise in the mean water level above the still water elevation of the sea (Komar 1998). The wave set-up ($\partial\eta$) is the time-averaged water level, the super-elevation of still water at the shoreline, due to breaking waves. The wave run-up, in contrast, is the time-varying fluctuation of water level elevation at the shoreline. To clarify, the wave run-up is the water level variation occurring from wave to wave, while the wave set-up is the average of these water level variations during a period of time (Figure 2.3).

The beach slope and the significant wave height are the main factors that modify the wave set-up, which can be as large as the tidal range. Therefore, when locating the shoreline, it is important to take them into consideration otherwise the *in situ* shoreline location might have an offset as large as several metres in the horizontal.

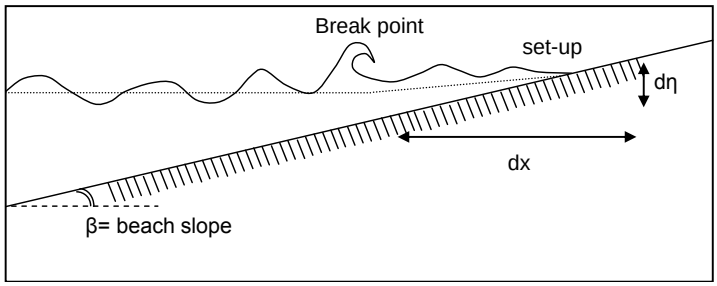


*Figure 2.3:* Wave set-up diagram. Horizontal distance from the break point ($\partial x$) elevation produced by the wave set-up ($\partial\eta$) over a determined beach slope ($\beta$).

The wave set-up is a function proportional of the breaker criterion $\gamma$=$(H/d)_b$, where H

is the wave height and d the depth of the breaking wave. The general rule is that sea level at the shoreline level will rise about 10 to 20 % of the significant wave height in deep water (Komar 1998).

The relationship for the maximum set-up elevation at the shoreline depends on the breaker criterion, which for monochromatic waves is approximately 0.78. The equation is as follows:

$$\frac{\partial \eta}{\partial x} = \frac{tan\beta}{1 + \frac{8}{3\gamma^2}}$$

The elevation ($\eta$) at the shoreline level is independent of the beach slope. It varies with the breaker criterion and the breaking wave height.

For example, a breaking wave of 0.5 m ($\gamma$=0.78) will produce the same elevation over a range of beach slopes of (tan $\beta$) 0.03, 0.05 and 0.1, obtaining an elevation of 0.12 m. This elevation has a $\frac{\partial \eta}{\partial x}$ which will produce a horizontal excursion of 4, 2.4 and 1.2 m respectively. In contrast a $\gamma$ of 0.5 will produce a $\eta$ at the shoreline level of 0.09 m. Nine centimetres of elevation will produce a horizontal excursion of 2.9, 1.7 and 0.9 m respectively.

This example illustrates that the $\eta$ due to the wave set-up can move the shoreline position by a magnitude of approximately a quarter of the breaking wave height. Furthermore, that the associated horizontal excursion will be larger with a flatter beach slope.

## 2.3 Shoreline indicators

Shoreline indicators are used to represent and study the shoreline position. Therefore, shoreline indicators should be robust, consistent with the available data, practical, repeatable and must be adequately defined (Pajak and Leatherman 2002). If not, their

use will limit the study of shoreline change over time. Boak and Turner (2005) categorise shoreline indicators into three groups, visually discernible, tidal datum based, and based on image processing techniques.

### 2.3.1 Visually discernible

The first group of shoreline indicators refers to features that are physically seen. This type of shoreline indicator is mostly used with aerial photographs, charts, different types of images and in field surveys. Some of the features used as shoreline indicators are the High Water Line (HWL), wet/dry boundary, the instantaneous extent of the wave run-up, vegetation line, and dune vegetation line.

The HWL has been widely used as a shoreline indicator. It can be observed using aerial photography as a tonal contrast between wet intertidal beach and dry beach. It can also be estimated by noting the vegetation, driftwood, discoloration of rocks, debris line, or any other visible signs left after the highest tide (Shalowitz 1964). This feature has been reported most frequently in earlier records, as seen in charts and maps (Anders and Byrnes 1991). It has also been used as a shoreline indicator on the US East Coast (Stafford 1971; Leatherman 1983; Anders and Byrnes 1991) and it has been considered the best shoreline indicator for many years because it is easily field-located and identifiable by aerial photography (Crowell et al. 1991).

The position of the HWL is highly variable. It is derived from the combination of tide levels, wave energy, seasonal beach changes, storm events, wind forcing. Furthermore, the position of the HWL can change with the type of data used to identify it (Ruggiero et al. 2003; Moore et al. 2006). Differences in wave height and period during high tide can also result in significant differences in the HWL position due to wave run-up, beach slope and sediment type (Morton and Speed 1998). For example, Pajak and Leatherman (2002) show that the HWL on sandy beaches with a foreshore slope of between 8° and

10° shows differences of up to 13 m for a precise period of time. In addition, Shalowitz (1964) found an estimated error of 3-4 m when comparing the HWL found *in situ* and in aerial photographs. These examples illustrate that the HWL changes with the type of beach and the type of data used to identify the HWL.

The wet/dry boundary has been used to identify different features, such as the dry and wet beach boundary, the maximum run-up limit or as the HWL (Dolan et al. 1978; Overton et al. 1999). Therefore, when using this shoreline indicator, it is important to be clear about which feature is being referred to. Furthermore, it should be noted that any of the features usually identified as the wet/dry boundary constantly change due to tides, winds and wave set-up. Its horizontal and vertical variation has to be considered when analysing the change over time of this shoreline indicator.

There are other shoreline indicators based on the vegetation present on the beach, such as the vegetation line and dune vegetation line. The vegetation line is the boundary between vegetated and non vegetated places, whereas the dune vegetation line, refers to the seawards edge of dune vegetation.

The main advantage of using vegetation as an indicator is that its location does not change with the wave set-up, tides or winds. This indicator can be used to study shoreline change over long-term timescales. This approach can be practical for research where the change in the vegetation line is more relevant, for example in studies such as Chen and Rau (1998); Li et al. (2003); Shaghude et al. (2003) and Chu et al. (2006). Moreover, vegetation-based shoreline indicators can be used for widely vegetated regions without a beach. For example, at the Sinnamary River, French Guiana, the presence of mangroves was used as a shoreline indicator, thus enabling study of the evolution of the coastline over 48 years. This approach proved to be very useful for regular monitoring of the mangrove and coastal dynamics (Fromard et al. 2004).

Although there are some general considerations of visually discernible shoreline indi-

cators that should be acknowledged, they also have some disadvantages. Firstly, they are not linked to an elevation; their position is determined by a pair of coordinates (latitude and longitude). Secondly, in general they are identified by visual interpretation, a process which is not objective, making future replication difficult. Thirdly, all visually discernible shoreline indicators, with the exception of vegetation indicators, show variations in their location depending on the wave set-up, winds and tides. The use of vegetation indicators are useful for regular shoreline change monitoring covering long-term timescales. However, is limited to places where vegetation is present and where the coastal vegetation is not under constant human modification, which can be impractical when studying shoreline change in urbanised locations.

### 2.3.2 Tidal datum based

The second group of shoreline indicators refers to the intersection of the coastal profile with a specific vertical elevation. This vertical elevation is defined by the tidal datum of a particular location, such as the Mean High Water (MHW) and Mean Water Level (MWL), among others. The chosen tidal datum of reference has to be fixed at a determined height (Parker 2003). The technique used to identify this type of shoreline indicator has to measure elevation, such as the LIDAR (Light Detection and Ranging), microwave sensors and field surveying techniques. Tidal based shoreline indicators are better defined in position than visually discernible indicators, because their location includes three coordinates rather than two (Ruggiero et al. 2003). However, the inter-annual and seasonal shoreline change has to be considered when studying longer temporal scales (> 10 yrs). Moreover, at longer temporal time scales any tidal datum will change due to the effect of solar heating on ocean currents and atmospheric pressure (Pugh 2004).

Research has been carried out to identify which tidal datum can be most reliable when studying shoreline change over time. Moore et al. (2006) compared the use of the

MHW and HWL shorelines and found that there is an average horizontal offset between the MHW and the HWL shorelines of 18.8 m. This is due to the fact that the HWL is not simply a mark left on the beach by the most recent high tide, it is a complex feature that, when identified by aerial photography, is the product of a combination of tide levels and wave energy. The MHW, in contrast, corresponds to a precise tidal datum obtained from measurements. Thus, between the HWL and MHW has a consistently lower elevation than the HWL. As the findings of Morton et al. (2004) show, the combination of different shoreline indicators should be considered for shoreline change studies in order to reduce the short-term variability that HWL exhibits.

### 2.3.3 Image processing techniques

The third group of shoreline indicators are features identified from digital coastal images that are not necessarily visible to the human eye. These include: Colour Band Divergence line (CBD), Pixel Intensity Clustering (PIC) and Artificial Neural Networks (ANN). The interpretation of these features is abstract and their definition relies much more on the type of analysis performed on the image to find a boundary between the sea and the land. The main consideration for these types of shoreline indicators is that they omit the field interpretation. To clarify, the feature which is identified by the technique does not have a direct link to a visually observed feature in the field (e.g. vegetation line, the wet/dry line and high water line), or to a tidal datum. However, image processing techniques can be systematic and consistent.

For shoreline identification purposes using satellite images it is desirable that the shoreline indicator used is visually identifiable on the beach, as well as ensuring systematicity and consistency over time.

## 2.4 Data resources to map the shoreline

This section gives an overview of the resources that have been used over time to map the shoreline. The focus of this section is to show the development of the resources used to map the shoreline, emphasising the development of satellite images to date, in order to show their capabilities as a resource to map the shoreline.

For centuries there has been interest in identifying the shoreline on a map, mainly for navigation purposes. However, this type of information is also relevant for shoreline change studies and for coastal management applications. For this research it is of particular interest to review the different resources previously used to map the shoreline and to explore their main advantages and disadvantages. In long-term shoreline change studies one difficulty is the lack of consistency in the shoreline indicators and the type of data, limiting the shoreline change that it is possible to detect. Therefore, recording a consistent shoreline indicator over time allows real shoreline change to be determined and to compare findings in other shoreline change studies.

There are a variety of resources for shoreline mapping. Data resources and techniques are being developed in parallel. Some of the resources for shoreline identification include charts and aerial photography. Since the 1970s more resources have become available to identify the shoreline. In the 1990s systems such as Argus systems, LIDAR, microwave systems and modern equipment for field surveying techniques such as Global Positional Systems (GPS), Differential Geopositional Systems (DGPS) and Real Time Kinematic (RTK) became commercially available, increasing accuracy and reducing the time frames of field survey techniques.

The utility of remote sensing in shoreline detection is well understood and it can be applied to monitor shoreline change (Gens 2010). However, each data type has different characteristics, which have to be considered before its application.

Table 2.1 provides an overview by summarising the available data types, their resolution, cost, the surface area that they cover, temporal availability and the date they became available to the scientific community. This information is necessary in order to identify which data types can be used to build long records of shorelines for further studies in coastal change.

*Table 2.1:* Data types that can be used for shoreline identification and details of their date of availability, resolution, cost, type of measurement and how often it is possible to get the data.
$^{+}$Topographic Survey Chart from the National Ocean Service (USA).
*Stereo view is a pair of images from the same location with different angles over the same plane.
$\star$ For archived images from 1986 to 2006.

| **Data source** | **Date of availability** | **Spatial resolution** | **Cost** | **Data type** | **Revisit time** |
|---|---|---|---|---|---|
| Charts$^{+}$ | 1800 | 1:20,000 | £20 to £40 | HWL | Variable according to the location |
| Aerial photography | 1909 | Varies from location | Varies from specific space regulations | Intensity | Varies according to flight schedule (vulnerable to weather conditions) |
| Landsat | July 1972 | 80, 50, 30m pixel size, 185 km (swath) | Free | Reflectance from 0.45 to 1.1 $\mu$m | 16 days |
| SPOT 1,2,3,4,5 | February 1986 | 20, 10, 5, 2.5m pixel size, 60km (swath) and stereo view* | £1,052 to £7,107 per image, £0.3$\star$ to £1.3 per km$^2$ | Reflectance from 0.50 to 1.74 $\mu$m | 2 to 3 days |
| ERS-1,2 | July 1991 and April 1995 | 26.3 to 30 m pixel size, 100 x 294 km (swath) | €440 to €600 per image | Microwave: 5.3 GHz, C band, VV polarization, bandwidth 15.5 to 0.06 MHz. | 35 days |

*Table 2.1* continued...

| Data source | Date of availability | Spatial resolution | Cost | Data type | Revisit time |
|---|---|---|---|---|---|
| Argus images | 1992 | Varies from specific stations | main cost is the installation (aprox. €35,000) | Intensity of the wavelengths in the visible spectrum. Single snapshots, averaged images, variance images, etc | Continuous |
| LIDAR | 1993 | 15cm (vertical), 1m to 5m (horizontal) | £230 to £463 per $km^2$ | Time taken to reflect a laser beam on to the surface | Varies according to flight schedule (vulnerable to weather conditions) |
| RADARSAT-1 | 1995 | 8m to 100m pixel size, 50km to 500km (swath), stereo view* | €960 to €2,860 per image | C-band wavelengths (5.6 cm) | 24 days |
| SAR | 1996 | 1.25m to 4m (horizontal) 0.3m to 5m (vertical) | | Reflectance from 0.50 to 1.74 $\mu$m | Varies according to flight schedule (vulnerable to weather conditions). |
| IKONOS | January 1996 | 1m pixel size (PAN), 4m pixel size (MS), stereo view*, 11.3 km (swath) | €20 to €38 per $km^2$ | Reflectance in wavelengths 0.526 to 0.929 $\mu$m | 3 to 5 days |

*Table 2.1* continued...

| Data source | Date of availability | Spatial resolution | Cost | Data type | Revisit time |
|---|---|---|---|---|---|
| QUICKBIRD | 2001 | 0.61m to 0.72m pixel size (PAN), 2.4m to 2.9m (MS), 17.5km (swath), stereo view* | €28 to €40 per km$^2$ | Reflectance in wavelengths 0.45 to 0.9 $\mu$m | 1 to 3 days |
| FORMASAT-2 | May 2004 | 2m (PAN), 8m (MS), 24km (swath), stereo view* | €2,500 to €4,600 per image | Reflectance 0.45 to 0.85 $\mu$m | 2 to 5 days |
| WORLD VIEW-1 | September 2007 | 0.5m pixel size (PAN), 17.6km (swath), stereo view* | €28 to €40 per km$^2$ | Reflectance 0.45 to 0.65 $\mu$m | 2 to 5 days |
| RADARSAT-2 | December 2007 | 3m to 8m pixel size, 50km to 500km (swath), stereo view* | €2,670 to €3,430 per image | C-band wavelengths (5.6cm) | 24 days |

*Table 2.1* continued...

| Data source | Date of availability | Spatial resolution | Cost | Data type | Revisit time |
|---|---|---|---|---|---|
| GEOEYE | September 2008 | 0.41m to 1m pixel size (PAN) 2m to 4m (MS), 15.2km $^2$, stereo view* | €25 to €40 per km$^2$ | Reflectance from 0.45 to 0.8 $\mu$m | 3 to 8 days |
| WORLD VIEW-2 | October 2009 | 0.46m to 0.52m pixel size (PAN), 1.8m to 2.08m pixel size (MS), stereo view*, 17.6km (swath) | €14 to €63 per km$^2$ | Reflectance in wavelengths 0.526 to 0.9 $\mu$m | 1 to 4 days |

### 2.4.1 Maps and charts

The earliest records of shoreline mapping are contained in nautical charts. The United Kingdom (UK) and United States of America (USA) have the oldest records of the shorelines in nautical charts. The shoreline indicator that these charts used was the HWL. Charts and maps became more accurate around 1750 in the UK, and in the mid 1800s in the USA, due to clearer standards of HWL identification (Anders and Byrnes 1991). The spatial scale of the earliest maps allowed detection of 200 m on the ground as the smallest feature distinguishable in one centimetre of the map, limiting shoreline change studies to at least magnitudes of 200 m.

In the USA, before 1941 the allowable error to map the shoreline in charts was 20 m. Currently, the allowable error of the National Oceanic Service in Topographic and Nautical charts is 8.5 m at 1:10,000 and 10.2 m at 1:20,000 spatial scales (Moore 2000). When using maps and charts to study shoreline change, the translation of the information from maps to a digital format is required, allowing comparisons and further analysis to be conducted. Digitisation is a common practice to translate earlier charts into a digital format. However, digitisation can add an error from 2.6 m to over 5 m (Anders and Byrnes 1991). Therefore, the original resolution from charts will increase from 20 m to 22.6 m to 25 m and that has to be considered when interpreting shoreline change. The value of information contained in the earlier maps and charts, however, has been recognised by a number of authors and cannot be provided by any other source of data for long-term studies (Leatherman and Douglas 2003; Boak and Turner 2005).

### 2.4.2 Active remote sensing systems

This section describes different types of active remote sensing systems. Active remote sensing systems send a pulse of energy from the sensor to the surface and then receive the energy reflected or backscattered from the surface. They record the elevation and

horizontal position of a predetermined place. The use of this type of data makes the identification of tidal datum shoreline indicators possible.

**Light Detection And Ranging**

Light Detection and Ranging (LIDAR) systems became available in 1993. LIDAR systems are based on the measurement of the time taken for a laser beam to leave and return to the instrument after reflecting on a surface (Cracknell 1999). Knowledge of the speed of light allows a distance to be calculated, and the use of differential GPS specifies the precise location.

Surveys using LIDAR systems are similar to surveys with aerial photographs where factors such as the altitude, angle and tilt of the aircraft will have an effect on the resulting images. However, although the laser beam can go through clouds, it is preferable that surveys are taken with a clear sky. LIDAR allows surveying of large areas to take place but not instantaneously, it usually takes about an hour to survey 50 $km^2$.

The wavelengths of the electromagnetic spectrum typically used are ultraviolet, visible, or the near infrared range. The vertical accuracy is approximately 15 cm and the horizontal resolution varies between one and five metres. The revisit rate will depend on the flight schedule and nowadays the cost range is approximately £232 to £463 per $km^2$.

Robertson et al. (2004) used this type of data to identify the shoreline, finding differences less than 6.1 m in relation to aerial photographs. Their estimated error is largely associated with the processing of aerial photographs rather than with the LIDAR capabilities. However, the acquisition of this type of image will depend on the scheduling of a flight, as well as the weather conditions. Although some satellites use active systems, covering a range of wavelengths, none of them use light detection, which can be a limitation when building a long time series of LIDAR images from a predetermined

study area.

### Radio Detection and Ranging

The first Radio Detection and Ranging (RADAR) systems started in the 1940s for military applications. They emit pulses repeatedly. The emitted energy is in the form of electromagnetic waves in the microwave part of the spectrum, typically between P-band, at about 300 MHz, and K-band, at about 30 GHz. The microwave energy is directed towards the ground, either directly below the remote sensing platform or obliquely. The same antenna measures the ground reflection of the microwave pulses. The emitted pulse depends on the functionality of the radar; it may be long or short, of uniform frequency or a swept frequency, that creates a chirped pulse. An altimeter, producing a pulse-limited footprint, allows measurement of the travel time, shape and strength of echoed pulses. The scatterometer has a large footprint, achieving a coarse resolution by Doppler filtering. Nadir-pointing radar enables the estimation of the altitude (Robinson 2004). Radar systems vary in the timing of the transmit/receive cycle and generally satellite radar use a single antenna both to transmit and to receive. Different classes of satellite radar have a different interleaving between the emission of pulses and their echoes.

The use of radar images has enabled the development of coastal studies as the study of Galal and Takewaka (2008) shows. This study explored the longshore movement of mega-cusps covering 5 km of shoreline over a two-year period.

### Synthetic Aperture Radar

The first commercial Synthetic Aperture Radar (SAR) system was available in 1996. It gathers information about a point on the ground, calculating the distance based on the return period of the signal and signal strength (Richards and Jia 1999). It allows the study of large spatial areas. SAR satellite images are available, as well as surveys that

can be taken from a flight or from a fixed position.

The accuracy varies with the band specifications: in the horizontal from 1.25 to 4 m and in the vertical from 0.3 to 5 m, covering 10 x 10 km. The data can be used to develop intertidal digital elevation maps, which have a height accuracy of around 20cm. This error can become smaller depending on the methodology used and the beach slope. An example of a study that uses this type of data is Niedermeier et al. (2000).

One disadvantage of images produced by active sensors is that they are speckled; the visibility largely depends on the incidence angle that illuminates objects on the ground and the roughness of the surface to survey. Features with high slopes or with high roughness can blend with other objects, they can also produce shadows and mirror-like features. Therefore, although active sensors can go through clouds, their speckled nature can make further analysis difficult.

### 2.4.3 Passive remote sensing systems

Passive remote sensing systems measure the energy that is reflected or emitted from the surface. Therefore, this type of remote sensing system requires the sunlight or a different source of energy.

#### Aerial photographs

Aerial photographs first became available in 1909 and have been available for the developed world since the 1940s. At this time the resolution of cameras was not good enough to make quantitative comparisons between images until in the 1960s, the optics of cameras and the processing techniques improved (Anders and Byrnes 1991; Pajak and Leatherman 2002). The processing of aerial photographs varies with the type of photograph, geometric distortions, and specific conditions when photographs are taken (e.g. altitude, angle, tilt of the aircraft). Changes in altitude along a flight line produce scale variations; taking a photograph from a completely vertical angle is very difficult

and corrections need to be made during analysis. Therefore, the use of aerial photographs for shoreline identification will include errors due to the conditions when the photograph was taken and the inherent errors of the shoreline identification methods.

The resolution of aerial photographs (approx. 1:3,000) is comparable to the geographic scale of modern charts and maps, although it varies depending on the survey, operator and country. Their use allows the identification of both visually discernible and image processing based shoreline indicators.

**Argus systems**

The Argus system became commercially available in 1992. An Argus station consists of a number of video cameras attached to a host computer that serves as both system control and communication link between the cameras and central data archives (Holman and Stanley 2007). Argus cameras can collect time-averaged images as well as instantaneous images. The data is very rich; the stations routinely collect three types of image products each hour, such as a single snapshot, a 10 minutes time exposure and a 10 minutes variance image.

The identification of the shoreline can be done using either visual or image processing techniques. The resolution varies according to the camera location and angle. The images are oblique hence the images have a distortion that has to be corrected with Ground Control Points (GCP). Argus stations provide a low-cost accessible system for long-term studies, allowing the study of shoreline change and beach morphology. However, Argus stations have some disadvantages in relation to satellite images, for example the budget required for their installation and maintenance and the fact that the study area is limited to the location of the station, covering a few hundred metres of shoreline. In contrast, satellite images allowed the survey of any location on Earth over the long-term with a moderate to high spatial resolution and without the installation of

a station to acquire images.

Some studies that have used this type of data are described in Armaroli et al. (2004) and Pearre and Puleo (2009) demonstrating their value to the study of shoreline variability within short timescales covering relatively small areas. The spatial resolution varies with the viewing distance and imaging system, it can be in the cross-shore of about 0.25 m up to 500 m of shoreline from the Argus station.

**Optical satellite imagery**

The first satellite image was taken in 1959. The Landsat program, launched in 1972, made satellite imagery commercially available.

Satellite images vary in data type, resolution, revisit time, orbit and cost. Some satellites use active sensors, such as SAR, Radarsat-1 (launched in 1995), and Radarsat-2 (launched in 2007); while others are passive (e.g. Landsat, SPOT, IKONOS), receiving the reflected sunlight from the ground. This section is focused on passive sensors, the active sensors are explained in section 2.4.2. The continuous development of satellite imagery is significant. For example, the Landsat satellite initially had 80 m pixel size but by 1982 the Thematic Mapper sensor had a 30 m pixel size. In 1986 the SPOT satellite was launched starting with 20m pixel size, and now it has improved to 2.5 m pixel size in multispectral (MS) images (further details about SPOT images are given in chapter 4). Many other satellites are available and have also seen an improvement in resolution, as well as spectral capabilities, providing the acquisition of stereo view. Stereo view consists of a pair of images of the same location taken a few minutes apart with different angles (approximately 60° and 90°). Stereo view images allow elevation to be estimated at a determined location.

Satellites like Ikonos, GeoEye and QuickBird, provide high resolution images between 4 and 2.4 m pixel size in MS images. However, the resolution in Panchromatic (PN) has

improved even more in relation to MS images, achieving 0.41 m pixel size. However, a higher spatial resolution means a decrease in the swath. For example, while SPOT images provide a 60 km swath images, GeoEye and Ikonos have 15.2 km and 11.3 km respectively, covering at least four times less surface than SPOT images. Moreover, the frequency of satellite coverage of a specific location has been improving, allowing the acquisition of an image of any location to take place as frequently as 1 to 8 days. This is becoming a valuable resource when monitoring the shoreline and shoreline change.

Optical satellite imagery has assisted the understanding of coastal erosion over large areas of shoreline, as well as the exploration of local coastal dynamics and shoreline change, in places with no earlier sources of data for shoreline location and where any data can provide useful information on past changes (Blodget et al. 1991; Chen and Rau 1998; White and El-Asmar 1999; Shaghude et al. 2003; Fromard et al. 2004; Trebossen et al. 2005; Chu et al. 2006; Zakariya et al. 2006; Dinesh-Kumar et al. 2007; Hanamgond and Mitra 2008; Li et al. 2008; Chen and Chang 2009; Klemas 2009; Kumar and Jayappa 2009; Wang et al. 2010; Kuleli et al. 2011).

The accuracy of the geometric correction, the difference in water levels between images and the magnitude of the shoreline change are some of the difficulties involved with the study of shoreline change using satellite images. The geometric correction must be as precise as possible to give resulting errors smaller than the pixel size. In this way, when comparing images taken at different times, it would be possible to detect real changes rather than differences related to the geometric location of images. This difficulty was overcome by White and El-Asmar (1999) by using *in situ* GCP and following strict controls on the error of the geometric correction, keeping the error smaller than half of the pixel size. By following this approach they were able to estimate shoreline change rates over a three-year period with a magnitude of up to 113 m. The difference between magnitudes measured by images and those in the field can be due to different water

levels and the temporal spacing of the images.

Another limitation of detecting shoreline change with satellite images is the pixel size, specifically for areas showing little shoreline change. This could also be overcome by using techniques to identify the shoreline at a super-resolution level, as Foody et al. (2005) show in their research, thus locating the shoreline with an error of less than 3m in images of 20 m pixel size. However, the shoreline detected with super-resolution methods was not compared using *in situ* shoreline measurements and was not linked to the tidal levels on the ground either, which is important to achieve a better and precise definition of the shoreline.

Different techniques used in optical images to identify the shoreline are described later in this chapter.

### 2.4.4 Field surveying techniques

The shoreline can be registered using field surveying techniques involving leveling instruments, such as theodolites, measuring tape, among others, with a high accuracy (<5cm). Nowadays field surveying techniques are based on global positioning system technologies. They also allow the identification of any feature on the beach in order to study changes in beach morphology and shoreline change over time.

#### Global Positioning System

Global Positioning System (GPS) became available to the public in 1996. It is a space-based global navigation system that provides the location and the time of any feature of interest in all weather, at all times, anywhere on or near the Earth. The GPS receiver calculates its position by timing the signals sent by GPS satellites high above the Earth. The Global Navigation Satellite System (GLONASS) has 24 satellites which continuously send information to the receivers. Through triangulation this determines a precise location on the ground.

### Differential Global Positioning System

Differential Global Positioning System (DGPS) uses a network of fixed, ground-based reference stations. The difference between the positions indicated by the satellite systems and the known fixed positions allows location of a specific position in time and space. The locations acquired by the DGPS require post-processing, which means that the position is corrected using two simultaneous measurements. Once corrected, the spatial location taken with DGPS has a resolution of about 4 cm in the horizontal and about 10 cm in the vertical.

### Summary

The data types reviewed show that there are a variety of resources that could be used to study shoreline change in the long-term. The use of satellite optical images has the advantage of instantaneously covering a large geographic distance on a frequent basis (1 to 8 days), without the need to install a station or schedule a flight, aerial photography, LIDAR, Radar, and Argus images all require. Although satellite optical images have a coarser spatial resolution in comparison to aerial photography, LIDAR, Radar and Argus images, the surface they cover and the frequency of the images shows that they are a valuable resource. Satellite optical images can enable assessment of almost any location on the Earth's surface with moderate and high spatial resolutions since the 1990s (Table 2.1).

## 2.5 Techniques used in optical images for shoreline identification

This section describes various existing techniques for shoreline identification using images.

There are different approaches to the analysis of satellite imagery for coastal and shoreline detection studies. The development of techniques is constantly evolving, improv-

ing their precision and speed of application. Shoreline identification can be achieved either by visual interpretation or by automatic and semi-automatic methods.

The different techniques and algorithms for shoreline identification are aim to find edges, reduce noise, increase sharpness between the sea and land. Some techniques are: segmentation, edge detection, canny filters (White and El-Asmar 1999; Zakariya et al. 2006; Liu et al. 2007; Chen and Chang 2009; Wang et al. 2010; Kuleli et al. 2011) and the classification of sea and land (Aarninkhof 2003; Kingston 2003; Ekercin 2007; Dinesh-Kumar et al. 2007; Plant et al. 2007). Furthermore, super-resolution methods have been developed (Foody et al. 2003, 2005; Muslim et al. 2006) to predict the shoreline position within the pixel size. Moreover, inter-tidal digital elevation models and sediment transport (Mason et al. 1997, 1999, 2001; Mason and Garg 2001) can be estimated from images. Thus, the technique to follow depends on the research objectives, the availability of data and the characteristics of the type of beach to study.

### 2.5.1 Automatic and semi-automatic techniques

Automatic and semi-automatic techniques reviewed in this section include classification techniques and the use of filters.

The use of automatic algorithms to identify the shoreline largely depends on the ability to separate sea from land. The sea and land have an inherent difference in intensities. Therefore, some techniques first reduce the variation within the image being analysed, applying filters, histogram stretching or equalization, to improve the contrast and brightness of images before using an edge detection algorithm (Liu and Jezek 2004; Liu et al. 2007; Chen and Chang 2009).

#### Classification

The classification of images is based on the differences of intensity values between different features in the image. The classification process can be based on sample

sites of the groups (e.g. hard classification). The classification can also be performed without using sample sites, identifying groups based on the variety of intensities within each image (e.g. soft classification). Further details about the soft classification are provided in chapter 3.

Dinesh-Kumar et al. (2007) used a hard classification to estimate erosion and accretion in Sagar Island in India. However, the shoreline was not extracted from the images. Their analysis used the pixel as a unit of area, which has the disadvantage that the pixel location changes from image to image, affecting the resulting estimation of erosion and accretion. An indication of the error involved in their calculation is not provided in this study.

Foody et al. (2003) and Muslim et al. (2007) developed a method (contouring soft classification) to extract the shoreline at a super-resolution level using a soft classification. They use satellite images degraded at 20 m pixel size, from original one metre pixel size images, enabling them to identify the shoreline with a horizontal accuracy of 3.2m, using a soft classification, and 6.5 m error using a hard classification. The accuracy was estimated using a one metre pixel size image as a reference. Li et al. (2003) also agree that the soft classification offers greater accuracy than hard classification methods, allowing identification of the shoreline at a super-resolution level.

Aarninkhof (2003) and Plant et al. (2007) used a pixel intensity clustering method to group pixels into sand or water from Argus images. They converted intensity values in the red, green and blue channels into grayscale intensities. This method is data-adaptative, based on the intensity values of the image, and works well for dissipative beaches. The error in this technique is 0.2 m in elevation.

Kingston (2003) used artificial neural networks to differentiate wet pixels from dry pixels, using Argus images, to identify the shoreline. The method is data-adaptative and can be trained to compensate for the variation in image quality. Using this method

it is possible to solve complex geometries such as submerged sandbars, sand pits and inlets. This model has previously been used to identify dry and wet pixels, using as sample sites, locations of dry and wet pixels. The estimated accuracy of this method is about 0.2 m in elevation.

### Filters

Filters are designed to enhance, contrast and remove certain ranges of optical wavelengths. Therefore, they are used to enhance the contrast between the sea and the land to identify the shoreline.

The application of filters like edge detection, kernel, canny or segmentation, requires a threshold to be specified to distinguish between sea and land. However, setting a determined threshold, raises the problem that each image has slightly different conditions, such as sunlight angles, cloudiness, suspended particles in the water and atmospheric conditions. These conditions not only change over time, they also change from location to location. For this reason some authors, such as Liu and Jezek (2004) and Wang et al. (2010), have generated adaptive thresholds rather than static thresholds. In this section we consider methods that use the change in intensities to identify the shoreline and the nearshore depth. Chapter 3 provides more details about edge detection techniques.

Other research has used a mix of filtering techniques such as edge detection and the contouring of images for further integration into digital elevation models in order to find the shoreline. The latter has shown good results for SAR images. Mason et al. (1995) developed the water-line method (Mason et al. 1995), estimating the inter-tidal digital elevations using SAR images. One disadvantage of this method is the loss of coherence between corresponding pixels due to 'different beach drying conditions' and to the low radiometric response of wet sand in SAR images. Only the high resolution achieved using aircraft altimetry and aerial stereo photography makes it possible to

obtain resolutions of < 10 cm in height and 1 m in horizontal.

Plant and Holman (1997) developed the Shore Line Intensity Maximum (SLIM) method, based on swash motions. The generation of foam parallel to the shore produces a high light intensity in time exposure images. This high light intensity is detected using Gaussian-shaped functions along a cross-shore profile. This approach has been used to derive nearshore bathymetric studies using Argus images. The SLIM method has worked well on steep beaches with a well defined swash zone. However, it is sensitive to variations in the surf similarity parameter.

Turner et al. (2001) developed a Colour Channel Divergence model that relies on the divergence in intensity values of the blue and red light at the shoreline level, with the aim of overcoming the problems that the SLIM method exhibits on shallow beaches. The shoreline is identified by the pixels that first exceed a threshold based on the difference in intensities between the blue and red colour channels. The determination of a precise threshold requires the survey of the specific location under investigation.

Lafon et al. (2002) study the reflectance attenuation in seawater to estimate the depth in the nearshore zone. This approach allows determination of migration rates of submerged sandbanks using SPOT images (20 m pixel size).

Figure 2.4 shows the reflectance spectra from emerged sand to submerged sand at different depths. This change of intensities with depth allows its estimation. There are detectable differences in reflectance between emerged sand and water depths of one metre, particularly with the Near Infra Red (NIR) wavelengths. The green and red wavelengths, in contrast, penetrate as much as 15 m deeper in the water conditions of the estuary from Banc du Chien (Lafon et al. 2002*(a)*).

The relevance of the Lafon et al. (2002) study is that it shows that optical satellite images are sensitive enough to detect specific water depths. Therefore, the shoreline,

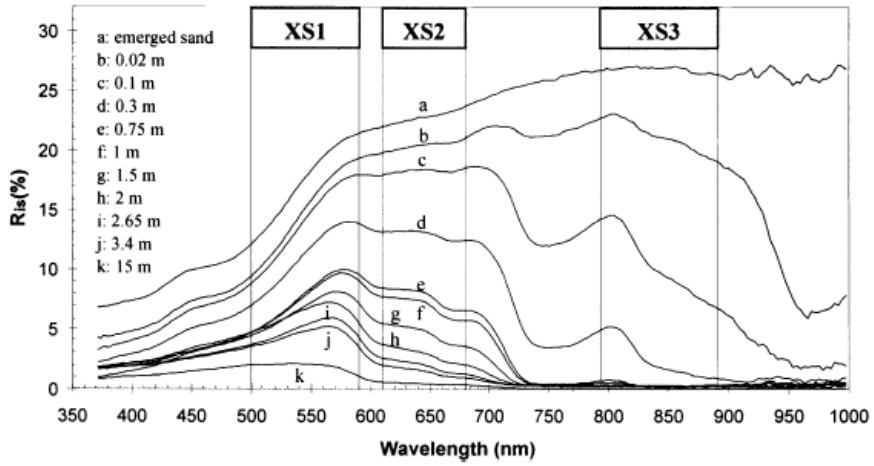


*Figure 2.4:* Reflectance spectra (Ris) of emerged sand (a), shallow water (b to j) and deep water (k) in Banc du Chien, France. Figure from Lafon et al. (2002).

as a specific depth contour that lies between the sea and the land, might be detectable using the change of intensities.

### 2.5.2 Visual interpretation

Some studies have used the manual extraction of the shoreline, such as Chen and Rau (1998); Li et al. (2003); Shaghude et al. (2003) and Chu et al. (2006). The visual interpretation of the shoreline is sometimes preferred over automatic processes, where images have a high spatial resolution to visually distinguish the shoreline.

Manual identification can involve shoreline extraction in 3-D, as the work of Li et al. (2003) shows using Ikonos stereo panchromatic image of one metre pixel size. This type of image requires a geometric correction to achieve a spatial resolution < 5 m otherwise the spatial resolution decrease by 25 m in the horizontal and 22 m in the vertical. Li et al. (2003) first corrected the images by applying rational functions and then manually identified the shoreline. The accuracy of the extracted shoreline is between 2 and 4 m. This shows that the visual interpretation of images is valuable for shoreline identification and that it is useful to explore the capabilities of satellite images with stereo

view.

## 2.6 Shoreline change studies

To study shoreline change covering long periods of time (decades), it might be necessary to gather shorelines from different data types with different spatial resolutions. This increases the total error, due to the addition of the inherent errors of each data type. Studies such as Miller and Fletcher (2003) and Kumar and Jayappa (2009) were able to cover 76 and 38 years of shoreline change respectively by using different data types with an integrative approach. Chen and Chang (2009) were able to cover 13 years of shoreline change based on optical satellite images.

Miller and Fletcher (2003) used aerial photography to study historical shoreline change and beach profiles to study the short-term shoreline change. The aerial photographs were digitised and geometrically corrected using DGPS. In total they covered a 76 year period of study of Waikiki beaches. The aerial photography and beach profiles complement each other, allowing the estimation of volumes of change on the beach, with orders of magnitude between -1,492 and 233 $m^3yr^{-1}$. The location with the highest retreat of the shoreline has a rate of $0.6 \pm 0.1$ $myr^{-1}$. This estimation was made using the re-weighted least squares regression, where each shoreline is considered according to the accuracy of each observation, in such a way that the shorelines with the least accuracy or spatial resolution have the least significance, and vice versa, in the overall estimation of the shoreline change rates.

Kumar and Jayappa (2009) studied shoreline change using a topographic map and satellite imagery which was acquired at low tide by the Indian Satellite IRS-1C for three different dates between 1967 and 2005. Their estimated shoreline change considered the images and beach profiles. They found changes of up to 160 m of accretion and 220 m of erosion in a beach stretch close to a river mouth. This hybrid approach allowed them

to draw conclusions about the maximum and minimum changes in the shoreline over a 38-year period of study, as well as to identify beach stretches showing the largest shoreline change. However, the calculation of a mean shoreline change was not achieved due to the large time span between images, which made it difficult to distinguish between short-term changes (tide, surges and seasonal) and long-term changes.

Chen and Chang (2009) studied shorelines extracted from satellite images, taking into consideration the water levels and the beach slopes of the shorelines. This approach allow them to determine the rate of change of the shoreline using a linear regression. The change in the shoreline position is possibly related to sand supply, waves and nearshore currents.

## 2.7 Discussion

### Shoreline definition

The shoreline definition used in this research has been determined according to the detectable feature using a snapshot in a satellite image. The satellite will capture the instantaneous plan view of the shoreline at a precise time its backwards and shorewards extent in the alongshore. So, the shoreline is defined as the boundary between the sea and the land at the tidal level when the satellite image passes over the study area. This definition considers the shoreline position on a temporal scale, which will vary due to tidal levels, wave set-up and surges, and that can be verified *in situ*. The comparison of the shoreline identified by satellite images and the *in situ* will enable estimation of the magnitude of the errors involved in the shoreline identification (see chapter 5). This shoreline definition can also be related to a tidal vertical datum and a visual feature, which allows the translation of the shoreline location using different datums, offering the possibility of comparing its location with shorelines identified at other times (Ruggiero et al. 2003).

### Data types

There are a great variety of data types that can potentially be used for shoreline identification, such as maps, aerial photographs, radar and satellite imagery. The development of satellite imagery, in terms of its spatial resolution, spectral properties and diversity of products, is significant and is in continuous development. Currently, it is possible to acquire images with a pixel size of 0.25 m, whereas 20 years ago the high resolution images had 10 m pixel size and the earlier optical satellite images had 90 m. Their optical properties have been developing as well, including narrower ranges of the wavelengths and stereo views. In addition, satellite images cover a footprint of at least 220 $km^2$ as often as every 1 to 8 days.

Although other types of data such as radar and aerial photographys can cover large footprints with higher spatial resolutions than satellite imagery, satellite imagery has the advantage of providing an instantaneous picture of a determined location with moderate (< 20 m) and high resolutions (< 5 m). The range of wavelengths included in optical satellite images have different applications in coastal research as the literature review shows. Moreover, they allow the assessment of different locations on the Earth without requiring the installation of a station or scheduling of a flight as is required for Argus systems and aerial photographs. Furthermore, satellite images are taken with specific characteristics (horizontal inclination, spectral mode and pre-processing level), whereas the characteristics of surveys in a flight will depend on the local wind speed, turbulence, and the skill of the pilot. So, satellite optical images are a source of data that is useful to the study of shoreline change in the long-term. The earliest images with a relatively high spatial resolution (10 m) are from the 1980s. One disadvantage of optical images is that the presence of clouds represents an obstacle to detection of features below. This disadvantage is overcome by the frequent re-visiting of satellites to a study area, increasing the possibility of acquiring a cloud-free image.

**Techniques used for coastal interpretation**

The literature review shows that shoreline identification is a complex problem when using any data type or technique. Shoreline extraction involves a series of processes to successfully obtain a vector that indicates the shoreline location. The use of a single process to identify the shoreline as a vector would not be successful. For that reason, manual identification has been widely used. However, the accuracy of a manual extraction of the shoreline relies on the individual skills of the interpreter (McBeth 1956; May et al. 1983; Anders and Byrnes 1991), making its replication difficult and time consuming, especially for long-term shoreline change studies. In contrast, the use of automatic techniques can facilitate systematization when monitoring shoreline change.

The number of algorithms and techniques that have been developed to identify the shoreline is vast, and they are constantly progressing. The different techniques include all types of data such as optical images, radar and aerial photographs. Each technique has its own limitations and each technique identifies a specific feature that can be used as a shoreline indicator.

For shoreline identification using optical satellite images the pre-existing algorithms can be useful. However, further research would be required to determine which technique is best to use and also to successfully identify the shoreline as a vector. Chapter 3 describes the method developed in this thesis to identify the shoreline, which can be applied to shoreline change studies.

Different types of filters have been applied by White and El-Asmar (1999); Liu and Jezek (2004); Chen and Chang (2009) and Mason et al. (1995) to identify the shoreline. Other authors have used classification techniques, such as Foody et al. (2003) and Muslim et al. (2006), to identify the shoreline at a resolution beyond the pixel size. In addition, a number of researchers have followed a manual approach, such as Li et al. (2003); Shaghude et al. (2003) and Chu et al. (2006). The diversity of approaches for shoreline identification does not give a clear indication of which method might be the most accurate. The largest estimated error is 72 m for the horizontal (White and El-Asmar 1999), using a classification technique. Liu and Jezek (2004) estimate the error of their method to be approximately one pixel using a visual interpretation, whereas Muslim et al. (2006) estimate an error of 3.2 m (horizontal) using a classification technique. However, these estimations have not been verified using *in situ* shoreline measurements. The lack of *in situ* verification was also noted by Liu and Jezek (2004), which is an important consideration when assessing the accuracy of their developed methods.

Whichever technique or data type is used to identify the boundary between sea and

land, the consideration of water level variations such as tides, wave run-up and surges is required. These water level variations depend on the study area location and the type of beach.

In chapter 3 filters, manual identification and a soft classification technique are explored using optical satelite images to assess their potential use for shoreline identification and shoreline change studies.

**Shoreline change**

Although satellite imagery can be a valuable source of information for shoreline change studies and coastal management applications, its use requires consideration of waves, nearshore bathymetry and beach morphology to understand the coastal processes driving shoreline change. The study of shoreline change covering longer periods of time, also raises several points to consider. The use of images from the same season and avoidance of post-storm photographs is recommended (Crowell et al. 1991). However, when the data is sampled unevenly, it is important to consider the magnitude of seasonal shoreline changes, as well as the magnitude of change during storms (Moore 2000).

Another factor to consider when studying shoreline change in the long-term (> 5 yrs) is the difficulty of building a series of shorelines with consistent shoreline indicators over time. This may be because the data is not be available or it may come from diverse data types, including different datums or shoreline indicators. Thus, when estimating shoreline change using shorelines from different shoreline indicators, the error in the overall shoreline change estimation will increase.

The use of satellite imagery can help to build the longest record (1986) that the available images allow with a moderate resolution (< 20 m) in order to identify the shoreline in the long-term and to assess the seasonal shoreline change with a different type of data, such as beach profiles or field surveying techniques.

## 2.8 Conclusions

1. Shoreline identification requires a precise and consistent definition, that includes the use of a tidal datum as a reference. The definition used in this research is the boundary between sea and land at a given tidal level when the satellite passes the study area.

2. Multiple data sources can help to identify the shoreline, such as satellite imagery, aerial photography, radar, video and field surveying techniques.

3. Satellite optical imagery is progressing rapidly with the spatial resolution, improving from 10 to 0.4 m in the last 20 years, providing a visual image covering a footprint of at least 220 $km^2$ as often as every 1 to 8 days. Therefore, the development of a technique for shoreline identification using satellite optical images would be very useful to study shoreline change and for coastal management applications.

4. Several algorithms have been developed to extract the shoreline from optical images (Foody et al. 2003; Liu and Jezek 2004; Muslim et al. 2007; Wang et al. 2010), with errors between 72 m (White and El-Asmar 1999) and 3.2 m (Foody et al. 2005). However, the difference between the shoreline identified by satellite and the shoreline identified with *in situ* measurements has not yet been assessed.

# Chapter 3

# Shoreline identification

## 3.1 Foreword

Shoreline identification using satellite optical images is possible in principle due to the inherently different physical characteristics of sea and land. Sunlight must pass through the Earth's atmosphere to reach the surface. There are three types of interaction with the surface which might take place: reflection, absorption or transmission. Satellite images measure the reflected sunlight energy. The fundamental premise of remote sensing is based on the idea that Parker and Wolff (1965), p.21 expressed as follows "Everything in nature has its own unique distribution of reflected, emitted, and absorbed radiation. These spectral characteristics can, if ingeniously exploited, be used to distinguish one thing from another or to obtain information about their shape, size, and other physical and chemical properties".

Identifying the shoreline from satellite images is challenging and many techniques have been developed for its identification, as reviewed in chapter 2. The shoreline, a feature located in between two extensive features, might be identified, for instance, by identifying its surrounding features: sea and land. The sea and the land have very different physical and chemical properties and therefore differ in their absorption, reflection and transmission of sunlight.

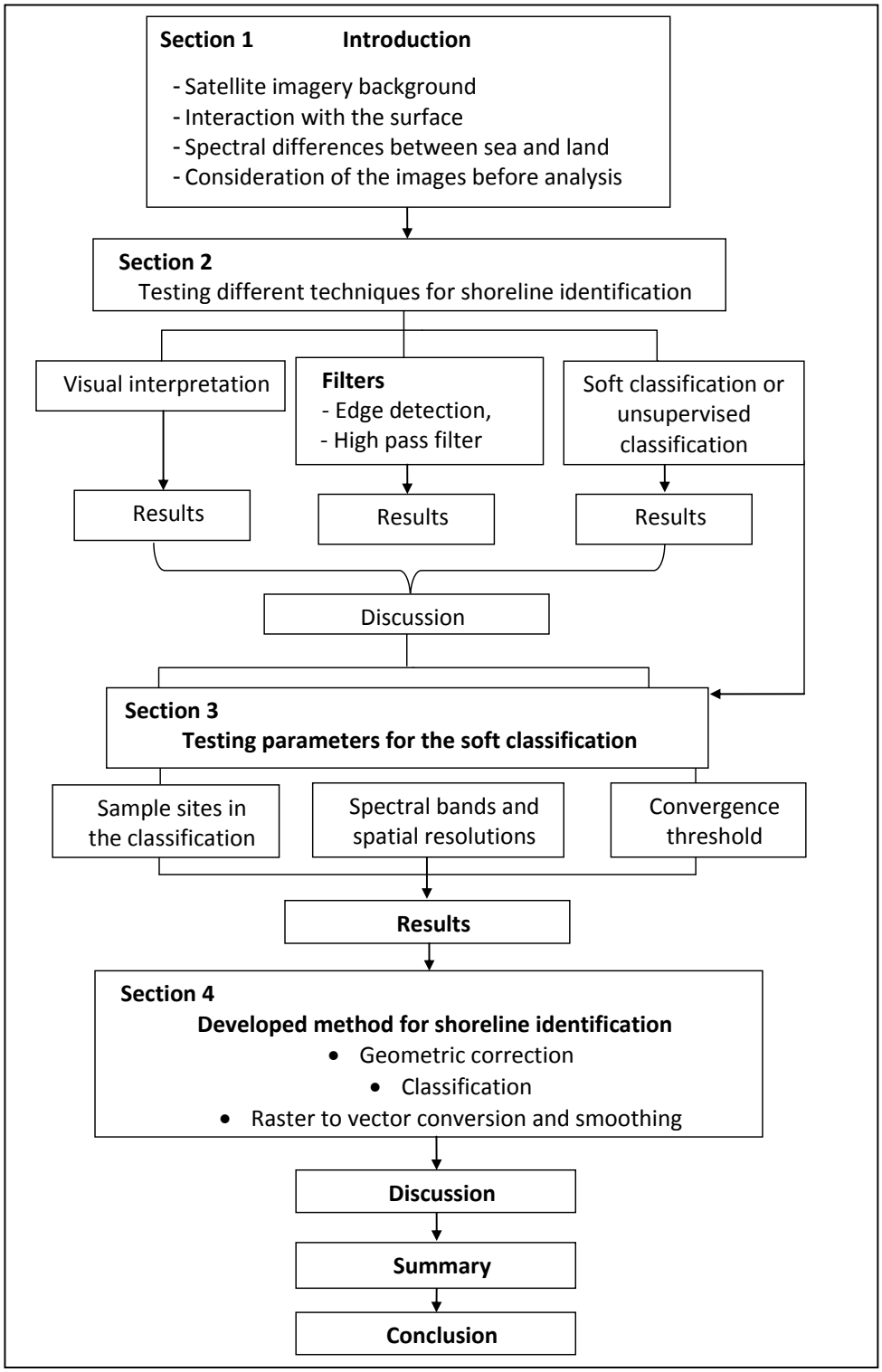


*Figure 3.1:* Chapter 3 structure summary.

## 3.2 Introduction

This chapter describes the developed method to identify the shoreline from optical SPOT images and is divided into four main sections. Figure 3.1 summarises the chapter structure. The first section examines the variation in intensities between sea and land on cross-shore and alongshore sections, with the aim of determining how sensitive the reflectance at the shoreline level is and whether it is possible to separate sea from land to identify the shoreline.

The second section explores different techniques to identify the shoreline, a manual identification, filters and classification are explored with the aim to determine a method which is objective, consistent and practical to identify the shoreline as a continuous feature.

The third section investigates the parameters to use in the soft classification method determined to identify the shoreline from images. The parameters defined in this section ensure that sea and land have the largest difference in their intensities.

The fourth section describes the developed method for shoreline identification using SPOT images. This method is the result of the previous exploration of the different techniques as described in the earlier sections of this chapter. The method developed here is validated using *in situ* shoreline measurements and is described in chapter 5.

### 3.2.1 Satellite imagery

The SPOT satellite was launched in 1986 and has provided optical images since then. Currently there are five SPOT satellites in orbit. The orbit has an altitude of 832 km, and an inclination of 98.7°. The satellites are placed in a circular polar orbit, phased and sun-synchronous. The inclination of the orbital plane, combined with the rotation of the Earth around the polar axis, allows the satellite to fly over any point on Earth within 26 days.

The sensors are passive, meaning that they receive the reflected sunlight from the ground. The satellite consists of two identical sensing instruments, a telemetry transmitter and magnetic tape recorders. The two sensors are known as High-Resolution Visible and Infrared instruments (HRVIR). The HRVIR can be operated in two modes, the Panchromatic (PN) and the Multispectral (MS). In the PN mode, the sensor is sensitive across a range of wavelengths including green and red. In this mode, the sensors provide a fine spatial detail but records a broad spectral range. In the MS mode, the HRVIR instrument is sensitive to four spectral ranges, including the green, red, near infrared (NIR) and short wave infrared (SWIR). Therefore, in MS mode the sensor records finer spectral ranges but coarser spatial resolution (Table 3.1). The green band has the smallest wavelength, followed by the red, near infrared and short-wave infrared. Satellites SPOT 4 and 5 cover the same wavelength ranges in MS and PN modes but SPOT 4 has a coarser pixel size than SPOT 5 (Table 3.1).

An image from SPOT covers a footprint of 3,600 $km^2$ at resolutions from 20 to 2.5 m, depending on the type of sensor mode and satellite. The images come in raster format, which is as an array of values composed of pixels. Each pixel is a separate unit, which can always be located within the image by its row and column coordinates. The values that the pixels have are intensity values of the reflected energy from the Earth's surface on a scale from 0 to 256. Each pixel in each spectral band has a single value and in the case of SPOT imagery each line of data is treated as a separate unit. Thus, in the case of MS images, they are composed of four data matrices with reflectance intensity values, while PN images are composed of a single data matrix or an individual image.

### 3.2.2 Interaction with the surface

Figure 3.2 shows the different interactions that the sunlight can have when it reaches the surface (reflection, absorbtion and transmission). The proportions of each interaction of the energy, reflected, absorbed or transmitted, will depend on the nature of the surface,

*Table 3.1:* Electromagnetic range covered by the spectral bands of SPOT satellite.

| Spot satellite | Spectral bands | Pixel size (m) | Spectral resolutions |
|---|---|---|---|
| 5 | Panchromatic | 2.5 or 5 | 0.48 to 0.71 $\mu$m |
| | Green | 10 | 0.50 to 0.59 $\mu$m |
| | Red | 10 | 0.61 to 0.68 $\mu$m |
| | Near infrared | 10 | 0.78 to 0.89 $\mu$m |
| | Short-wave infrared | 10 | 1.58 to 1.75 $\mu$m |
| 4 | Monospectral | 10 | 0.61 to 0.68 $\mu$m |
| | Green | 20 | 0.50 to 0.59 $\mu$m |
| | Red | 20 | 0.61 to 0.68 $\mu$m |
| | Near infrared | 20 | 0.78 to 0.89 $\mu$m |
| | Short-wave infrared | 20 | 1.58 to 1.75 $\mu$m |

the wavelength, and the illumination angle. The unique response from each surface at different wavelengths facilitates the recognition of different features using satellite imagery. Sea absorption increases with increasing wavelength, so most of the red light is absorbed before it can be scattered out through the surface but there is high reflection of the blue wavelength (Morel 1974), which explains why the colour of the sea is blue and not red.

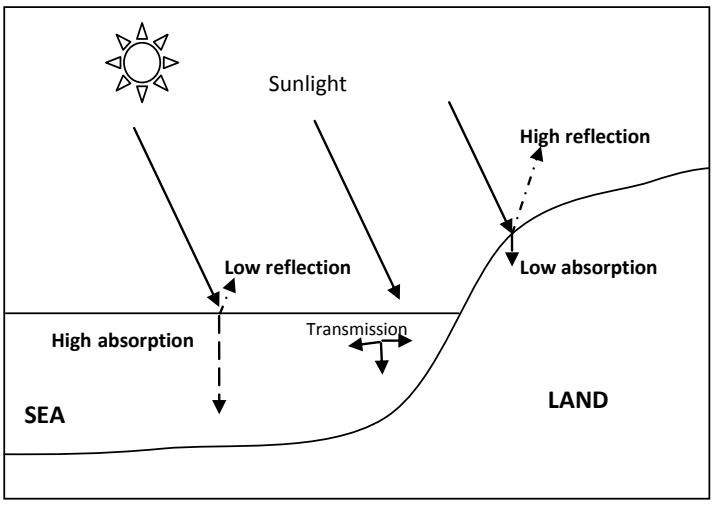


*Figure 3.2:* Interaction with the surface of sunlight in a cross-shore view.

For ocean studies, the wavelengths from the visible spectrum provide valuable information concerning the presence of phytoplankton, primary production, dissolved organic

material and suspended particles. The Near Infra Red (NIR) band is not usually considered for marine research because almost all the NIR radiation is quickly absorbed. However, if the research interest relies on the identification of the shoreline, the NIR can be of great value due to the sharp contrast between sea and land (Robinson 2004).

Back scattering on land is more complex than at sea. There are many different inland features e.g. vegetation, urban surfaces, soil, sand, which each have very different back scattering patterns. Therefore, in spite of their inherent differences, it would be necessary to identify all such features as a uniform group when using satellite images for shoreline identification.

## 3.3 Spectral differences between sea and land

This section reviews the spectral behaviour over the sea and land for MS and PN images.

Figure 3.3 shows an extract of a SPOT image that covers a shoreline longer than 1.5km from Yucatán (see chapter 4), which was used to explore the differences between land and sea with PN and MS image scenes. The land is covered by an urban area. The sea in this region has very low nutrient levels and very low primary productivity and is therefore considered to be an oligotrophic sea. To clarify, this means that the environment is low in the nutrients required to sustain life. Therefore, the main backscattering detected in the sea will be due to suspended particles and depth variation.

Histograms of intensities and cross-shore spectral profiles are useful to explore the distribution of intensities. The presence of crests in a histogram can be matched to specific features located in the image (e.g. sea, vegetation, land). Cross-shore profiles allow observation of the variation in intensities along a specific cross-section within the image.

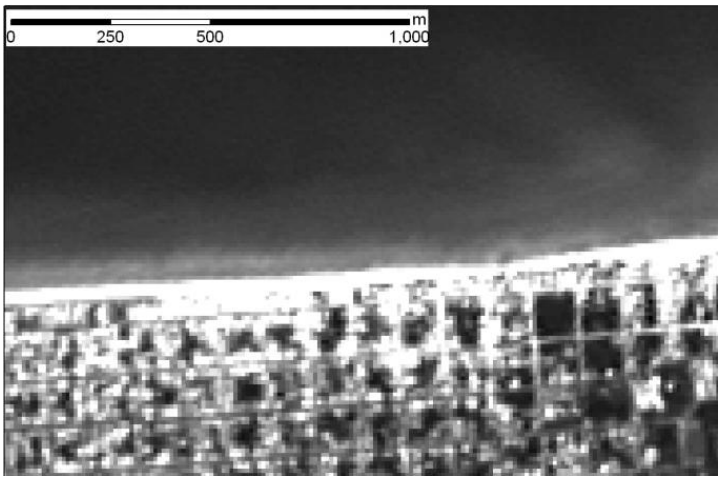


*Figure 3.3:* Extract of a PN image, 10 m pixel size, from Progreso (beach segment 5), Yucatán, México (see Figures 4.2 and 4.10 in section 4.3 to view the geographic location).

### 3.3.1 Panchromatic images

Figure 3.4 shows the distribution of intensities, ranging from 0 to 256. There is one clear crest at 52 intensity with no values between 0 and 50 and no obvious peaks between 70 and 150. The smaller intensities are associated with the sea, which quickly absorbs the sunlight with very little backscattering, and the higher intensities are associated with the land.

Figure 3.5 shows the interpolated cross-shore spectral surface. There is a clear contrast between intensities associated with the sea and the land. However, as the land is approached there is a slope with values between 70 and 100, followed by a sharp edge with values ranging between 150 and 200, decreasing further inland between 100 and 150. The slope might be related to suspended material in the water column. The higher intensities are inland features, showing a large range of intensities, some even smaller than the values on the slope. The wide range of intensities of the land can make it difficult to separate both sea and land into two groups.

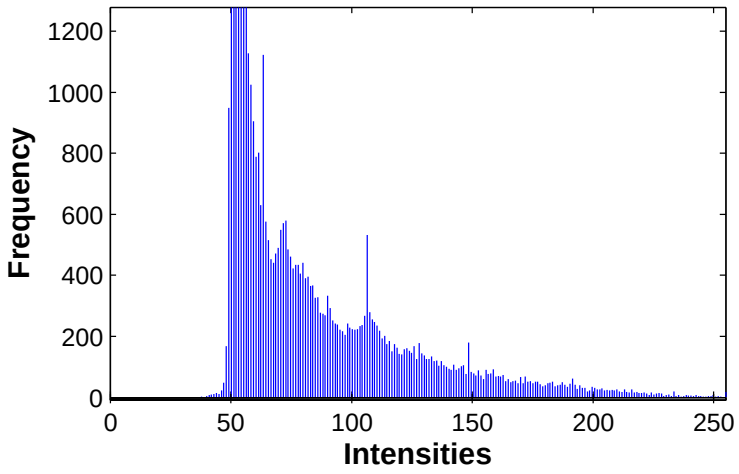


*Figure 3.4:* Histogram of the intensities of PN image extract (Figure 3.3). The wavelengths range is from 0.48 to 0.71 $\mu$m.

### 3.3.2 Multispectral images

Figure 3.6 shows the distribution of intensities covering the same location shown in Figure 3.3 over the four spectral bands. The four spectral bands have two clear crests. The first crest is associated with sea values and the second crest, at higher intensities, is related to inland features. The intensity from the first crest with the green spectral band is the largest of the four spectral bands (50-75), whereas red has intensities between 25 and 50, NIR between 25 and 50, and SWIR has between 12 and 28. The larger the distance between the two crests the clearer the difference between the groups. The largest distance between crests is in the NIR and SWIR. Therefore, using these two spectral bands will allow better differentiation between the sea and the land.

The difference between the NIR and SWIR is that the SWIR show a large amount of pixels in the higher intensities. The pixels in the higher intensities could be interpreted as saturation over this spectral band. However, the saturation of the SWIR does not have any negative consequences for shoreline detection; on the contrary, the saturation

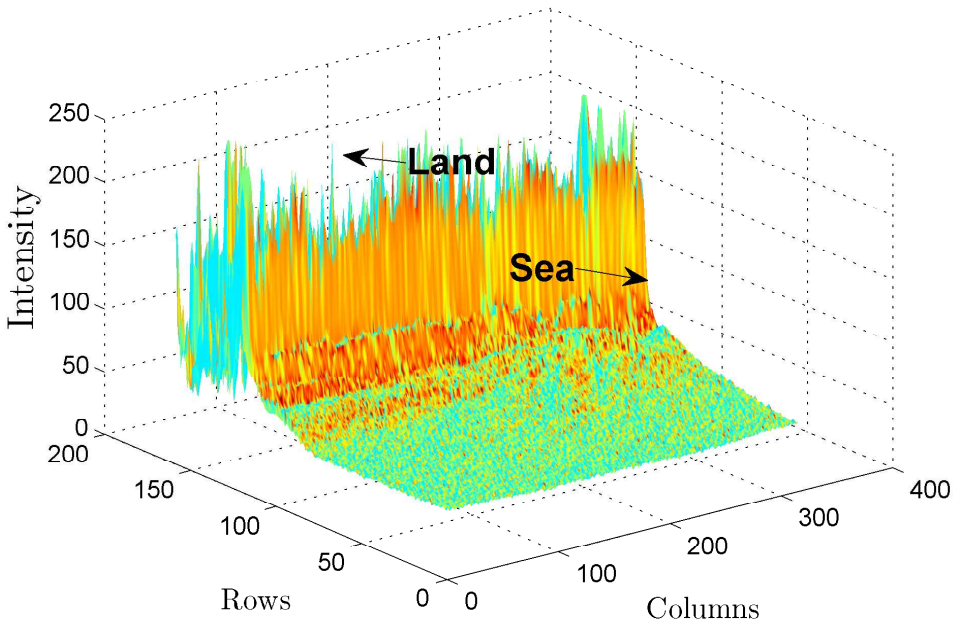


*Figure 3.5:* Interpolated cross-shore spectral surface from the PN image extract from Fig. 3.3.

of features inland allows the definition of land features with a relatively homogeneous range of intensities and makes the distance between both crests larger in the NIR (160) than in the SWIR (220).

Figure 3.7 shows the cross-shore intensity profile for each spectral band. The sea pixels for the four bands are fairly homogeneous. The land pixels have a large range of intensities, particularly over the green and red spectral bands. The green, red and PN spectral surfaces (Figure 3.5) have a slope in between the land and sea. The PN includes the same range of wavelengths as the green and red spectral bands (Table 3.1). The NIR and the SWIR in contrast do not have any slope, and show a clear edge between relatively homogeneous high and low intensities. The NIR has the largest difference in intensities between sea and land in relation to the other spectral bands, changing from 38 to 105 from one pixel to the next. In contrast, the green spectral band has the smallest drop,

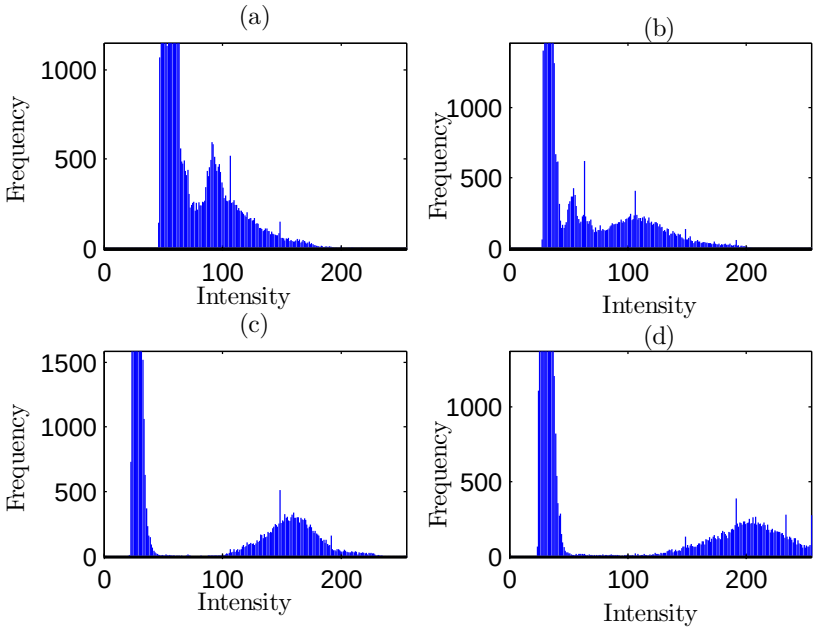


*Figure 3.6:* Histograms of distribution of intensities for each spectral band. (a) Green (0.5 to 0.59 $\mu$m), (b) red (0.61 to 0.68 $\mu$m), (c) NIR (0.78 to 0.89 $\mu$m) and (d) SWIR (1.58 to 1.75 $\mu$m) from an image extract shown in Fig. 3.3.

changing from 99 to 124 over the same distance.

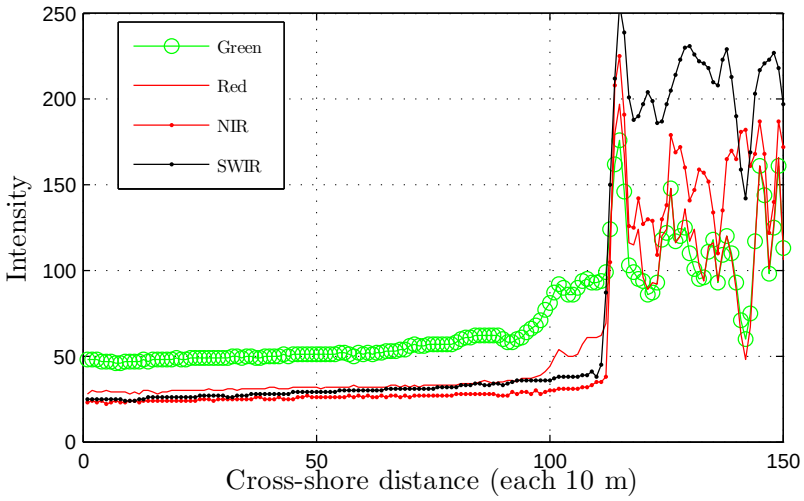


*Figure 3.7:* Cross-shore spectral profile in intensity values along the shoreline level. The horizontal axis is spaced by the pixel size (10 m).

This exploration of the change in the intensities using satellite optical images shows that the differences between sea and land are clear, in particular in the NIR and SWIR from MS images, whereas the intensity differences in a PN are not as clear for identifying the sea and land: their histograms only show one crest rather than two.

### 3.3.3 Considerations of the images before analysis

Prior to the analysis of the images a visual examination was carried out on all the images analysed in this research in order to consider whether each image was suitable for further analysis. Variables such as the cloud percentage, the presence of haze, brightness, striping or banding are described in this section.

### 3.3.4 Cloud percentage

Clouds are an obstacle that restrict sunlight from reaching the surface so their presence results in a loss of data. The default maximum cloud coverage is 10 % of the whole image. However, this percentage can be flexible depending on where the clouds are located. In this research, the cloud percentage was flexible, with the location of the clouds being more important than the total percentage of clouds in the image. For example, an image with 10 % cloud coverage might seem feasible to analyse but when the 10 % of clouds are over the shore then such analysis is not recommended. In contrast, when an image has 15 % of clouds but all of them are located far away from the shore, analysis should be possible.

### 3.3.5 Presence of haze

The presence of haze might not allow clear identification of features on the ground thus introducing uncertainty into the image. There is no standard threshold to assess whether the haze is high or low in an image, this is based on the judgment of the interpreter.

### 3.3.6 Brightness

Some images can have excessive brightness; this is also called specular reflection and it occurs when the angle of reflection equals the angle of incidence (Lillesand et al. 2008). This mostly occurs on flat surfaces, such as water bodies that create mirror-like reflections. Excessive reflection causes saturation of the intensities. Therefore, it is not possible to estimate the % sunlight that is reflected when reaching the ground. Specular reflection cannot be fixed.

### 3.3.7 Striping or banding

Striping or banding is produced by systematic noise. Noise can totally mask the data, removing the possibility of analysing the image. The striping or banding can be fixed by interpolating the intensities where the stripes or bands occur. In this research, the analysed images did not show this type of noise. More information about this can be found in Lillesand et al. (2008).

### 3.3.8 Distortions which might occur on the images

Images from on-board satellite sensors have a number of distortions which can affect the accuracy of the extracted information.

Images can be acquired with different pre-processing levels. Images can be acquired in almost raw form or they can include radiometric corrections and geometric corrections for systematic effects such as the Earth's rotation, curvature and variations in the satellite's orbital altitude. Also the images can be rectified to match a standard map projection (UTM WGS 84). This is done using a global Digital Elevation Model with a spacing of one kilometre, in the case of SPOT images. The model used is based on known viewing parameters such as precise orbital information, altitude and time and does not use external measurements. The images used in this research have the standard corrections mentioned above, hence they can be projected on to a standard map

to allow further processing. This type of pre-processing level is called 2A. However, although the image scene has a geographic projection, its geographic coordinates do not coincide with sufficient accuracy with *in situ* coordinates. Therefore, a geometric correction is required to accurately locate the features seen in the image with ground features. Details about geometric correction performed on the images are described in section 3.6.1 in this chapter.

## 3.4 Different techniques for shoreline identification

This section explores three different techniques in order to assess their further application in shoreline detection. First is a visual interpretation; second, a high pass filter and an edge detection filter are used to enhance the shoreline; third, a soft classification is applied to separate pixels into the two groups, sea and land. The desired output is the definition of sea and land as separate groups, where it is possible to differentiate a clear and continuous boundary that can be further applied for shoreline identification.

### 3.4.1 Visual interpretation

The manual identification of the shoreline was performed to evaluate its further use in optical satellite images. This is also an alternative method in the case that an automatic technique fails. Chen and Rau (1998); Li et al. (2003); Shaghude et al. (2003) and Chu et al. (2006) applied a manual approach, allowing the addition of their personal expertise and judgement for shoreline identification.

The shoreline used as an example in this thesis includes diverse coastal features such as harbours, inlets, villages and vegetated areas, thus providing a range of conditions to identify the shoreline. The shoreline was identified using a single image made up of three spectral bands (NIR, red and green), covering 60 km of shoreline, with a fixed close up of 1:5,000 in ArcMap software.

### Results

The band combination of the NIR, red and green, provides a high contrast to differentiate between sea and land. Figure 3.8 (A) and 3.8 (C) are examples of two areas where the identification of the shoreline is clearer due to the features next to the shore. The inland vegetation, enhances the contrast between sand and water. In contrast, figures 3.8 (B) and 3.8 (D), the urban areas, with similar colours to the sand, make it more difficult to distinguish between sea and land. Therefore, only the difference in colour and the shape of the coast gives an indication of the shoreline's location. Moreover, an image with 10 m pixel size does not provide the detail needed to distinguish specific features on the beach. Further in this chapter (section 3.5.2), a visual identification of the shoreline using a PN image with 2.5 m pixel size is shown.

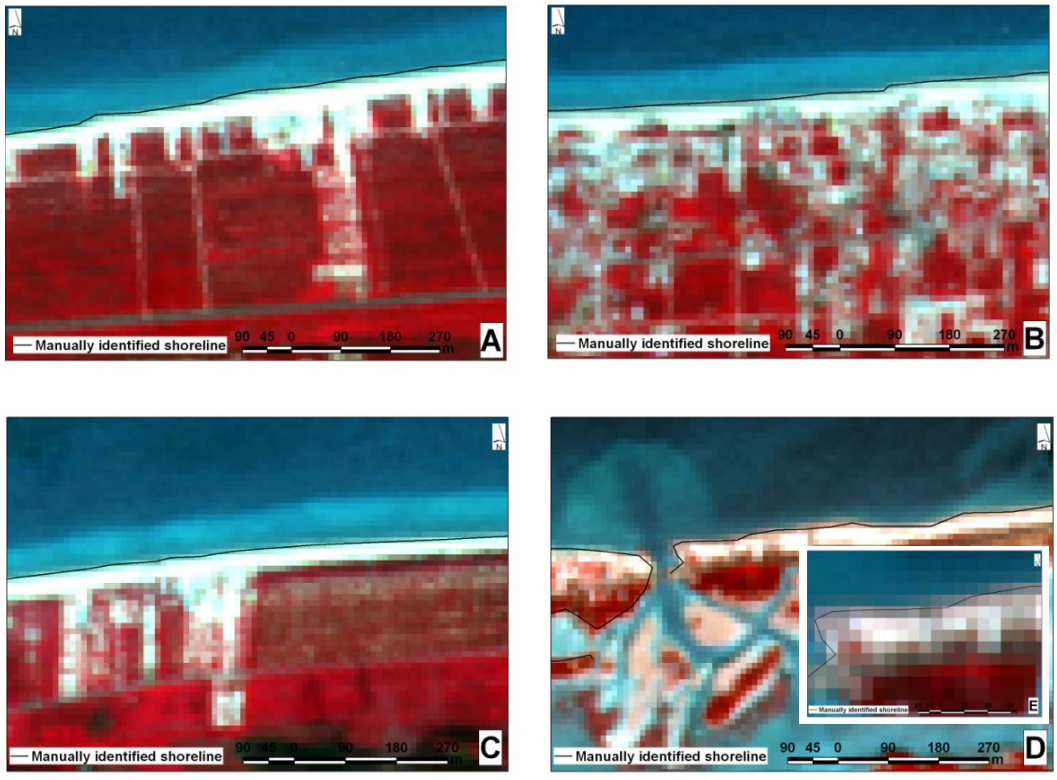


*Figure 3.8:* Visually identified shoreline at four locations in Telchac, México, using a 10 m pixel size image. A, C and D are sparsely populated, while B is a heavily populated village. E is a close-up within D's location.

The colour of the images, however, depends on the spectral bands used. Each spectral band enhances different features in the image due to their interaction with the sea and the land.

Figure 3.9 A and B displays the channel of an inlet with water depths shallower than 2 m depth, using the red and NIR spectral bands respectively. The NIR has a larger contrast than the red. The sea looks mostly dark, even in the channel of the inlet, with intensity values between 60 and 80. The land is much brighter, with intensities ranging between 130 and 200. This is because the NIR is absorbed more rapidly by the sea than the red. The red can detect shallow features in the nearshore region because it goes deeper into the water column. The channel of the inlet is clearly differentiated from the sand with the NIR but not so clearly using the red, showing that the use of the NIR or red as a reference to visually identify the shoreline can lead the interpreter to different locations.

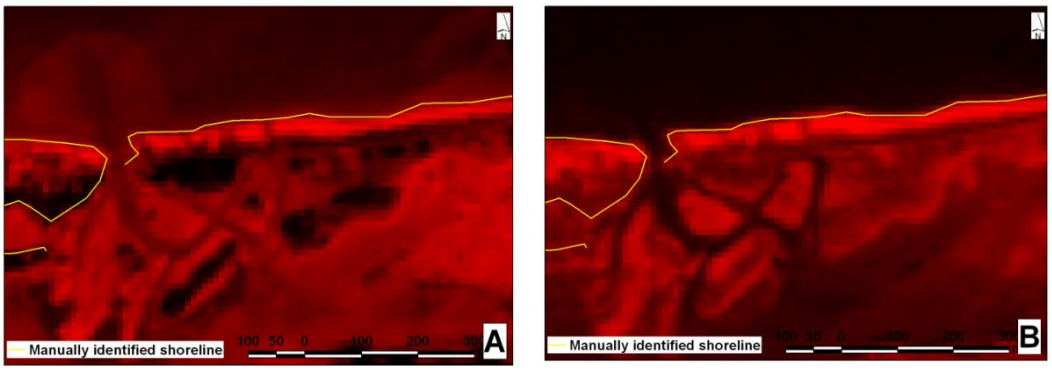


*Figure 3.9:* Satellite image displayed using the red spectral band (A) and the NIR spectral band (B). The yellow line is the shoreline visually identified using the NIR, red and green spectral bands.

### 3.4.2 Filters

This section explores two filters and their application in shoreline detection, high pass and edge detection. First the way in which the filters work is described, then the results (after their application into the image) are shown. The application of filters is widely

used for image interpretation to enhance and increase the contrast between different features, which otherwise would be difficult to detect by eye. Filters have been used for shoreline identification by authors such as Mason et al. (1995, 1997); White and El-Asmar (1999); Liu and Jezek (2004); Chen and Chang (2009) and Wang et al. (2010).

**High Pass**

The high pass filter is widely applied to highlight edges in images. This filter allows the high frequency component to pass through, bringing out the edges between relatively homogeneous groups of pixels (Campbell 1996).

The spatial frequency of an image changes within a determined matrix size. The matrix is used as a filter and is often called a kernel. A $3 \times 3$ matrix was used in this test, with values of the same order in magnitude as those found at the shoreline level in satellite images.

The value in the middle of the matrix is filtered using the numbers in the vicinity of the original image. Some examples are shown below to describe how this process works:

$$\begin{pmatrix} 150 & 155 & 120 \\ 110 & 105 & 115 \\ 100 & 120 & 118 \end{pmatrix} \times \begin{pmatrix} -1 & -1 & -1 \\ -1 & 9 & -1 \\ -1 & -1 & -1 \end{pmatrix} = \begin{pmatrix} & -43 & \\ & & \end{pmatrix}$$

The values in the first row are slightly larger than the values in the second and third rows. Therefore, the location between the first and second rows could be interpreted as a border. The value in the centre of the matrix (105) is multiplied by the kernel, the denominator is 1 (because the sum of the coefficients in the kernel makes zero), resulting in:

[(150*-1+155*-1+120*-1) + (110*-1+105*9+115*-1) + (100*-1+120*-1+118*-1) /1)]
= -43

This process runs pixel by pixel using the values within a $3 \times 3$ matrix.

In the next example, the values in the kernel are all the same in a scenario without borders. Because the filter used is $\left(\begin{smallmatrix} 0 & 0 & 0 \\ 0 & 9 & 0 \\ 0 & 0 & 0 \end{smallmatrix}\right)$, it can also be interpreted as the result of $\left(\begin{smallmatrix} 0 & 0 & 0 \\ 0 & 8 & 0 \\ 0 & 0 & 0 \end{smallmatrix}\right)$ + $\left(\begin{smallmatrix} 0 & 0 & 0 \\ 0 & 1 & 0 \\ 0 & 0 & 0 \end{smallmatrix}\right)$. When this is applied to a $3 \times 3$ matrix the result will be the same value within the kernel, in this case 150. This indicates no change in or presence of borders.

$$\begin{pmatrix} 150 & 150 & 150 \\ 150 & 150 & 150 \\ 150 & 150 & 150 \end{pmatrix} \times \begin{pmatrix} -1 & -1 & -1 \\ -1 & 9 & -1 \\ -1 & -1 & -1 \end{pmatrix} = \begin{pmatrix} \\ 150 \\ \\ \end{pmatrix}$$

**Edge Detection**

Edge detection filters are a different type of high pass filters, that increase in particular the contrast between neighbouring pixel intensity values (Campbell 1996). A $3 \times 3$ matrix was used in this test. In these examples the same scenarios are used as were previously used in the high pass filter. In a kernel with values suggesting a border between the first and second rows the result is -148, a value larger in magnitude than in the high pass because the filter used is one unit smaller thus the negative values are larger.

$$\begin{pmatrix} 150 & 155 & 120 \\ 110 & 105 & 115 \\ 100 & 120 & 118 \end{pmatrix} \times \begin{pmatrix} -1 & -1 & -1 \\ -1 & 8 & -1 \\ -1 & -1 & -1 \end{pmatrix} = \begin{pmatrix} \\ -148 \\ \\ \end{pmatrix}$$

Alternatively if all the values within the kernel are the same, when the values are added the result is zero. This is because all the values within the kernel will make zero when added together, indicating that there are no borders within that kernel.

$$\begin{pmatrix} 150 & 150 & 150 \\ 150 & 150 & 150 \\ 150 & 150 & 150 \end{pmatrix} \times \begin{pmatrix} -1 & -1 & -1 \\ -1 & 8 & -1 \\ -1 & -1 & -1 \end{pmatrix} = \begin{pmatrix} \\ 0 \\ \\ \end{pmatrix}$$

Both types of filters enhance borders within a kernel. The high pass magnifies the difference between values that are relatively similar; whereas the edge detection gives the largest values when there are relatively different values within the kernel.

**Results**

**Edge detection and High pass**

Figures 3.10 A and B show the resulting image after the application of the edge detection and high pass filters. Both filters enhance features in the image, mainly over the urban area, highlightling features such as streets and buildings, whereas the sea appears homogeneous. The boundary between sea and land is detected by both filters, as well as features on the land such as streets, buildings and vegetation. The details identified inland are not the desired output because enhancing features on land increases the hetereogeneity, making it difficult to define the land as a single homogeneous group. Therefore it is not appropriate to apply filters for the purpose of shoreline detection in this thesis.

The main challenge when trying to group the sea and land as separate and homogeneous groups is due to the hetereogeneity in intensity values inland, whereas the sea has relatively homogeneous intensities.

### 3.4.3 Soft classification

This section explores the results obtained after the use of a classification technique to separate the sea and land.

Soft classification, or unsupervised classification, identifies groups with similar inten-

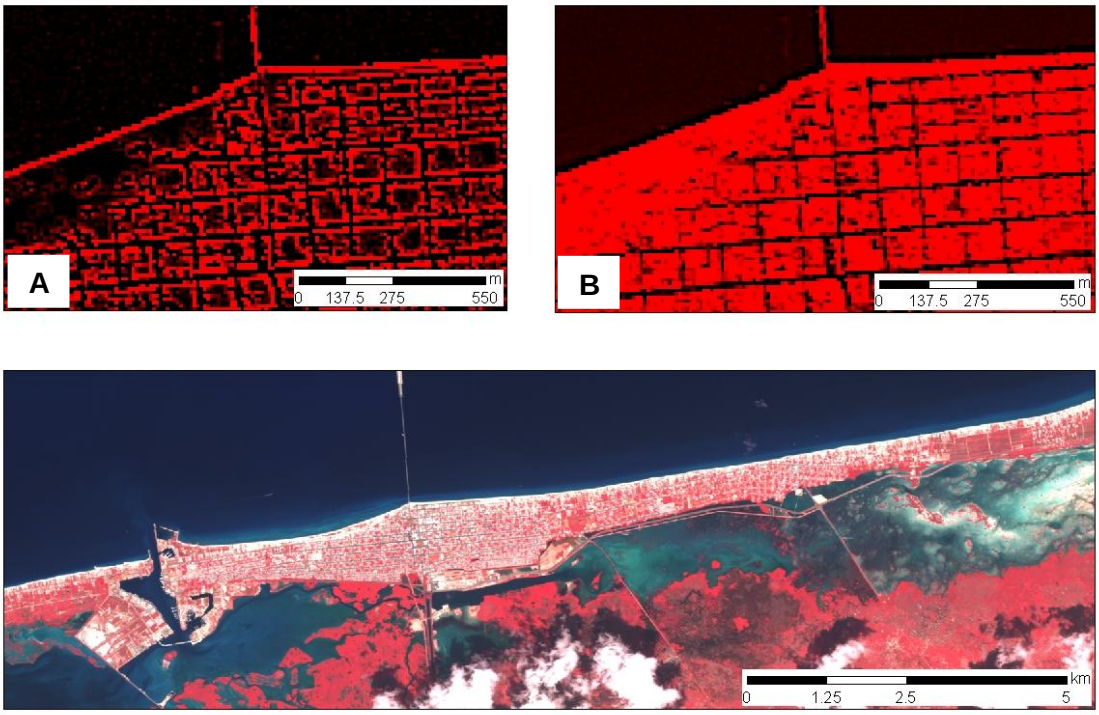


*Figure 3.10:* Close up of the filtered image with edge detection (A) and a high pass filter (B) using the NIR. Bottom: Original image, displayed with the NIR, red and green spectral bands.

sities within an image. This technique has been used in other research on shoreline change such as Foody et al. (2005). The classification process is based on the existing spectral groups within a raw image. The basic premise is that values within a class should have a similar spectral pattern. Conversely, intensities from a different class should be relatively well separated (Lillesand et al. 2008). The identified groups will be based on the distribution of intensities within an image. The soft classification was executed in Erdas software, using single or three spectral bands for the classification process.

The mean of each group is used to identify the pixels belonging to it. The mean of each group is calculated several times, in an iterative process, using all the pixels from the image. The pixel analysis compares each pixel value to the mean of each group, assigning each pixel to the group that has the minimum intensity distance.

Figure 3.11 shows how the number clusters are determined for the first calculation. After each iteration a new mean for each cluster is calculated, replacing the arbitrary initial calculation. The new mean values are used to define clusters in the next iteration. Therefore each pixel is classified several times, assigning each pixel to the group which has the minimum intensity distance to the pixel value.

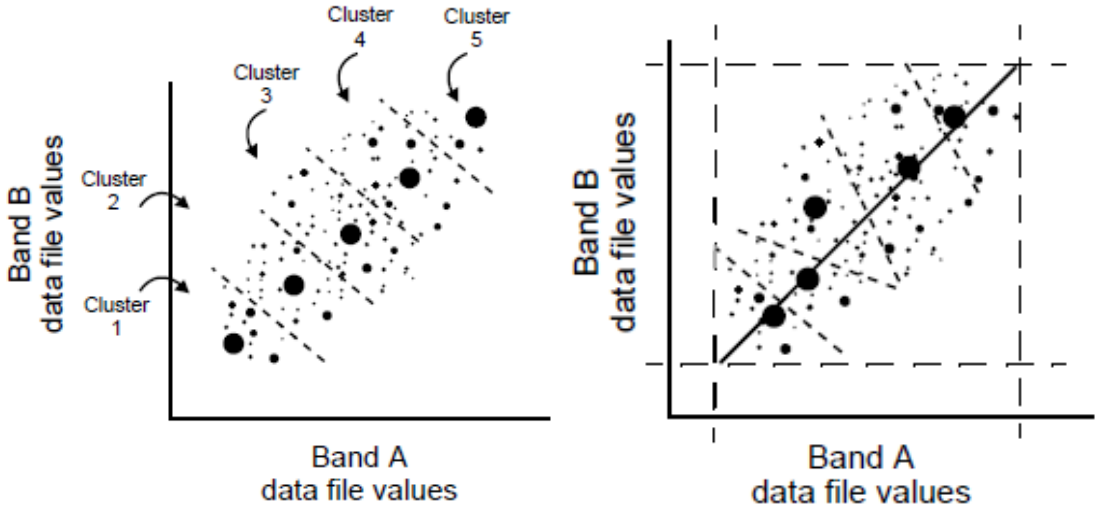


*Figure 3.11:* Schematic of the assignment for the initial cluster means in the first iteration, using five clusters and two spectral bands (A). Second iteration, where the means are recalculated and shifted (B). Figure from Swain (1973)

This iterative classification process implies that a number of pixels might be classified into different groups from iteration to iteration. The number of pixels not allowed to change membership from one group to another during one iteration is called convergence threshold. A very high convergence threshold will allow only a few pixels to be classified as a different class in the next iteration, whilst a very low convergence threshold allows more pixels to be classified into a different group. The classification finishes when the convergence threshold has been met (Swain 1973). This classification technique is highly successful at finding spectral groups that are inherent in the data. The location of the initial arbitrary cluster does not affect the results if enough iterations are

performed.

In this research, the classification was set to identify two groups (sea and land), using three spectral bands (NIR, red and green), with a convergence threshold of 95 %, allowing 5 % of the pixels to change membership from iteration to iteration. Section 3.5.3 shows the different results in the classification using different convergence thresholds.

**Results**

Figure 3.12 (bottom) shows the output of the classification process. The pixels from the original image were successfully grouped either into sea or land. Although the land intensities have an ample range of values (see section 3.3), the inland surface was grouped into the same class. Some pixels were classified as sea that was located further inland, which correspond to a coastal lagoon, showing that these pixels are accurately classified. There are also some sparse pixels located inland and classified as sea, which might correspond to cloud cover and cloud shade present in the original image. However, although these pixels do not correspond to sea or land features, their presence does not affect the ability to identify the shoreline.

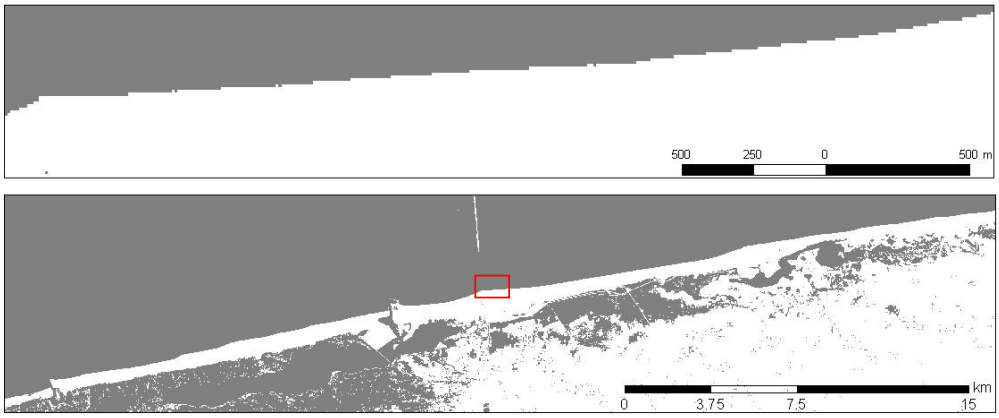


*Figure 3.12:* Close-up of the classified image (top). Classified image into two classess: sea (grey) and land(white) at the bottom. The area within the red square is shown in the close-up.

Figure 3.12 (top), shows that the pixels classified as sea or land are homogeneous

separated groups. This is an important consideration for getting a continuous contour that runs between both groups.

The use of a soft classification to identify a continuous border between the two classes seems promising for shoreline identification. Moreover, the soft classification is a robust algorithm, which is systematic and practical. The images are rapidly processed, allowing large numbers of images to be analysed, which is an important consideration for monitoring shoreline change studies. In addition, soft classification has been previously used to identify the shoreline and study shoreline change in diverse studies such as Foody et al. (2003); Li et al. (2003); Foody et al. (2005); Muslim et al. (2006); Dinesh-Kumar et al. (2007); Muslim et al. (2007).

### 3.4.4 Discussion

The different techniques explored show, that the visual interpretation of the shoreline location has differences depending on the spectral bands used. Therefore, the consistent use of a specific spectral band or combination of bands would avoid the uncertainty in shoreline identification caused by using different spectral bands. Furthermore, the filters applied (edge detection and high pass) increase the hetereogeneity inland, rather than decreasing the variation of intensities inland. Finally, the soft classification successfully identifies the sea and the land as separate and homogeneous groups.

The edge detection and high pass filter increase the heterogeneity of the land even when using the NIR, which is the spectral band that provides the largest contrast between sea and land (see section 3.3 and 3.5.2). The edge detection filter highlights the borders between any feature within the image, such as streets, buildings, vegetation, and the sea, as an homogeneous feature. However, the edge detection filter detects not only an isolated pixel as a boundary but identifies several pixels as borders. So, it is difficult to identify which of the selected pixels represent a border between features. Moreover,

in order to separate the sea and the land as homogeneous groups, the hetereogeneity of the land is enhanced with the edge detection filter rather than being reduced. Therefore, the further separation of sea and land can be less clear after using the edge detection filter. In contrast, the high pass filter detects the land as a less hetereogenous group, but it fails to filter the low intensities from the streets and vegetation that are present in the land.

The result of applying these two filters is that a more heterogeneous group is produced, which is the opposite of the required output. As a result, the use of filters was not pursued further in this research.

Shoreline identification using visual interpretation was achieved. The uncertainty on its location when different spectral bands are used shows that manual identification with satellite optical images might not be suitable for shoreline change studies. Thus, shoreline identification through satellite optical images seems to be more difficult and more subjective than using aerial photographs. However, regardless of the subjectivity, it is recognised that the interpreter's judgement is an advantage (McBeth 1956; May et al. 1983; Anders and Byrnes 1991) when analysing the study area, since it can use other features such as shapes and colours that algorithms do not consider.

The soft classification provides an efficient separation between the sea and the land intensities in a systematic and practical way. However, it is not clear which wavelengths will prevent the overlapping between intensities associated with sea or land. This is addressed in the next section (3.5.2).

When exploring these techniques, it was helpful to define the shoreline as the border between sea and land. However it was noted that shoreline representation as a vector requires a change on its data type, from raster to vector. This conversion will produce a jagged vector. The steps of the vector, related to the pixels' size and position from the original image, add an error when compared with other shorelines.

Liu and Jezek (2004) produced a smoother vector from the original jagged vector. However their smoother vector has some corners, indicating the presence of curvatures in the shoreline. Foody et al. (2003) obtained a contour from the classified image, located at 50 % and 50 % from the classified sea and land, producing a smoother result. However, the contour obtained by Foody et al. (2003) and Liu and Jezek (2004) has being developed to represent as accurately as possible the shoreline and not for its further application in shoreline change studies. In contrast, in this research, the emphasis is on obtaining a shoreline from satellite optical images that accurately marks the shoreline and that can be further applied in shoreline change studies.

## 3.5 Testing parameters for soft classification

This section explores the different parameters to perform soft classification, such as the the use of single or a combination of spectral bands and different convergence thresholds. Prior to the assessment of different parameters, the advantage of using sample sites of different sizes (using a mask) was assessed in order to determine whether the use of a sample site could improve the identification of sea and land.

### 3.5.1 Using sample sites in the classification

This section assesses the effect on the classification output of the use of two different sized sample sites (masks), one of 16.6 km and another of 1.5 km (Figure 3.13 (a), (b)). The classification results might be different if the area to analyse covers a larger extent of the image because soft classification uses the inherent existing groups in an image.

Figure 3.14 shows that classification can change after the use of a mask. The longer wavelengths (NIR) showed little change in classification. The classification using the shorter wavelengths (green and red) degrades with the narrower mask. For example, the mean of the groups of the classified sea increases from 20 to 80 with the narrower mask, and the mean of the groups of the classified land decreases from 220 to 140.

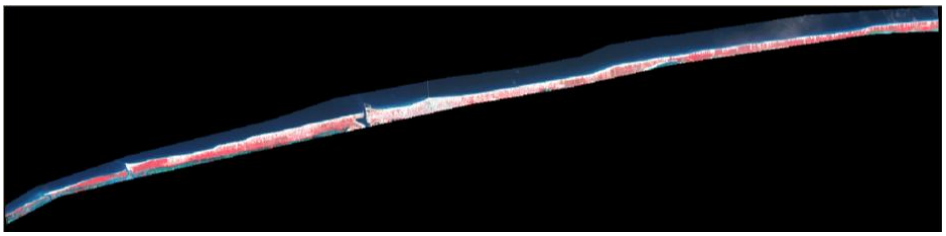

*(a)*

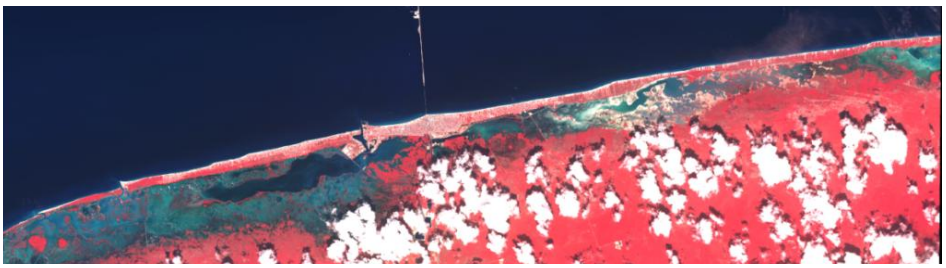

*(b)*

*Figure 3.13:* Sample site including 1.5 km across the shoreline (a). Sample site including 16.6 km across the shoreline (b).

This suggests that a narrower mask removes the variation within each group, which is required to determine the means of the groups that represents the sea and land.

These results confirm that the use of a mask provides little change in the classification in longer wavelengths and that in shorter wavelengths its use can produce an unclear defintion of sea and land. Therefore, the use of sample sites or masks was not included in the analysis.

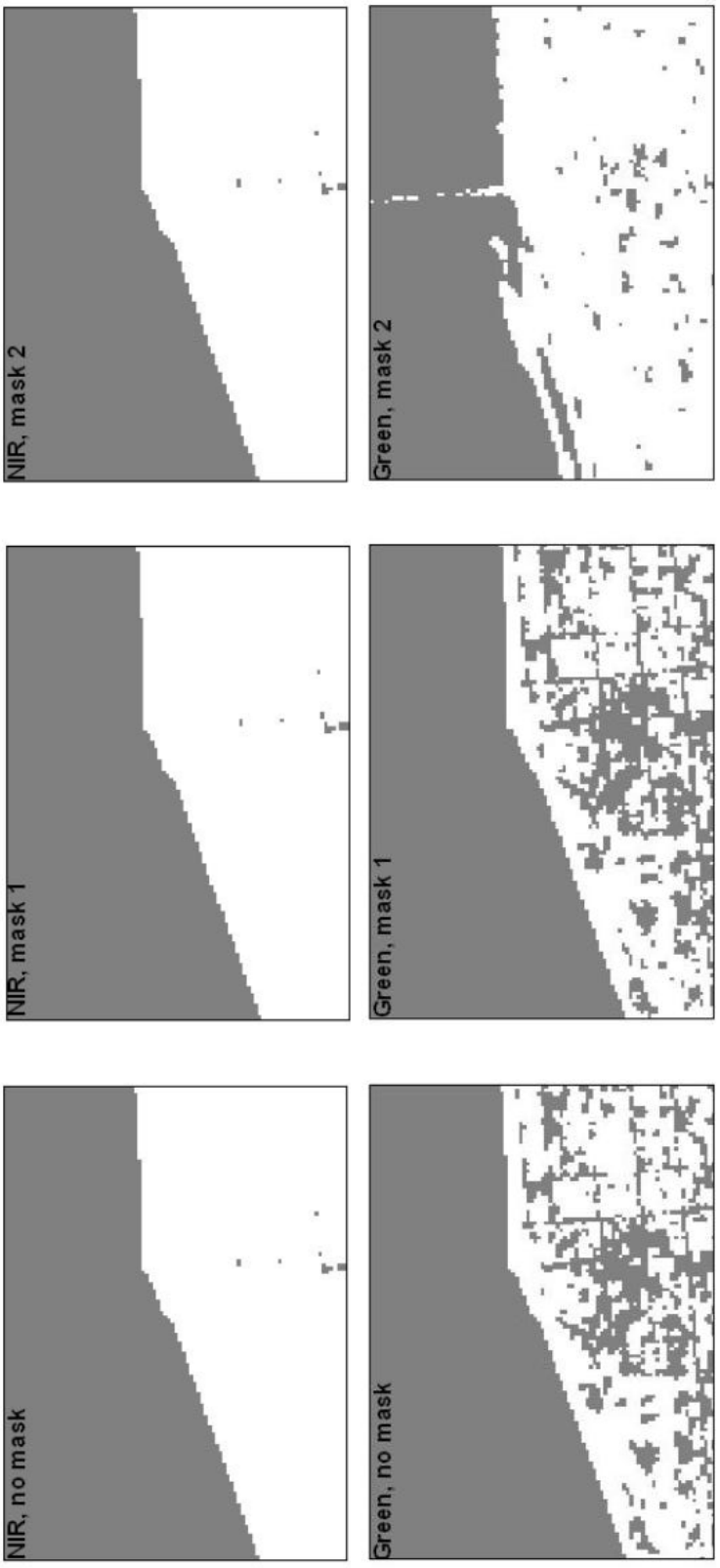


*Figure 3.14:* Classified image using the NIR (first row) and green (second row) spectral bands. First column has no mask, second columnn has a sample site (mask) of 16.6 km and third column has a sample site (mask) of 1.5 km.

### 3.5.2 The use of different spectral bands

This section explores the classification results using images of MS with 10 m pixel size (Figure 3.13 *(b)* and Figure 3.15, bottom) and PN with 2.5 m pixel size (Figure 3.15, top). Each band from the MS image, as well as a combination of spectral bands, is used to classify the image. The use of different wavelengths in the classification could give a different definition of sea and land due to different wavelengths highlighting different features on the ground. These comparisons will show which spectral bands provide the clearest definition of sea and land, with the largest distance possible between sea and land, so as to avoid misclassification between groups. Later in this section a quantitative estimation of the classification accuracy is shown.

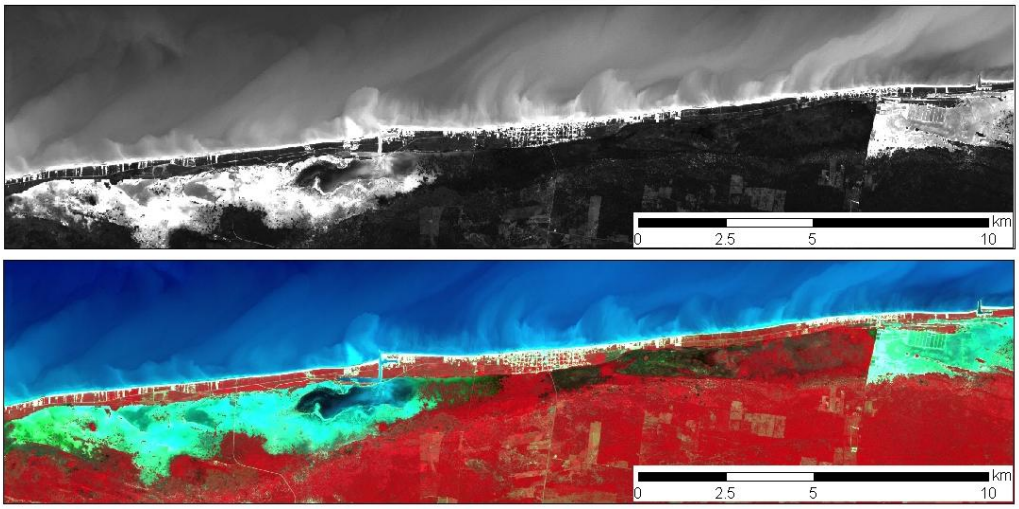


*Figure 3.15:* PN (top) and MS (bottom) images from the same location and time (Nov. 24, 2005).

The images assessed in this section are from September 20, 2008 and November 24, 2005. The MS images cover two different locations in Yucatán (Progreso and Telchac), with different turbidity conditions in the nearshore region. Therefore, their comparison will allow determination of which spectral band provides the clearest definition of sea and land. The PN and MS images in 2005 are simultaneous images, covering the same

location at the same time, but the PN image has 2.5 m pixel size, which is four times smaller than MS images. Therefore their comparison will allow assessment of whether the use of an image with better spatial resolution can provide a better definition of the sea and the land.

**Results**

Figures 3.16 and 3.17 show the classification results in two different locations using each spectral band separately. The results vary between the two locations. The classification at Progreso, a location with little suspended particles, has a clear definition of sea and land. The classification shows similar results with each spectral band and the two composites. In contrast, the classification at Telchac, a location with a more significant amount of suspended particles than Progreso, has a clear misclassification of pixels using the PN and the shorter wavelengths (green and red). The longer wavelengths (NIR and SWIR), in contrast, successfully separate sea and land. These results show that the longer wavelengths can distinguish between sea and land, even in the presence of suspended particles in the water column. Furthermore, when there are low suspended particles (visibly) in the water column any spectral band can distinguish between sea and land.

Interestingly, the good spatial resolution of the PN does not provide a better classification result in the shoreline identification, showing that the wavelengths included in the spectral band are more important than the spatial resolution.

Typically in the nearshore region suspended particles occur in the water column. Therefore, for shoreline identification, the suspended particles in the nearshore region can often be a frequent difficulty. So, the use of longer wavelengths, such as the NIR and SWIR, can prevent misclassification between sea and land even with suspended particles in the water column.

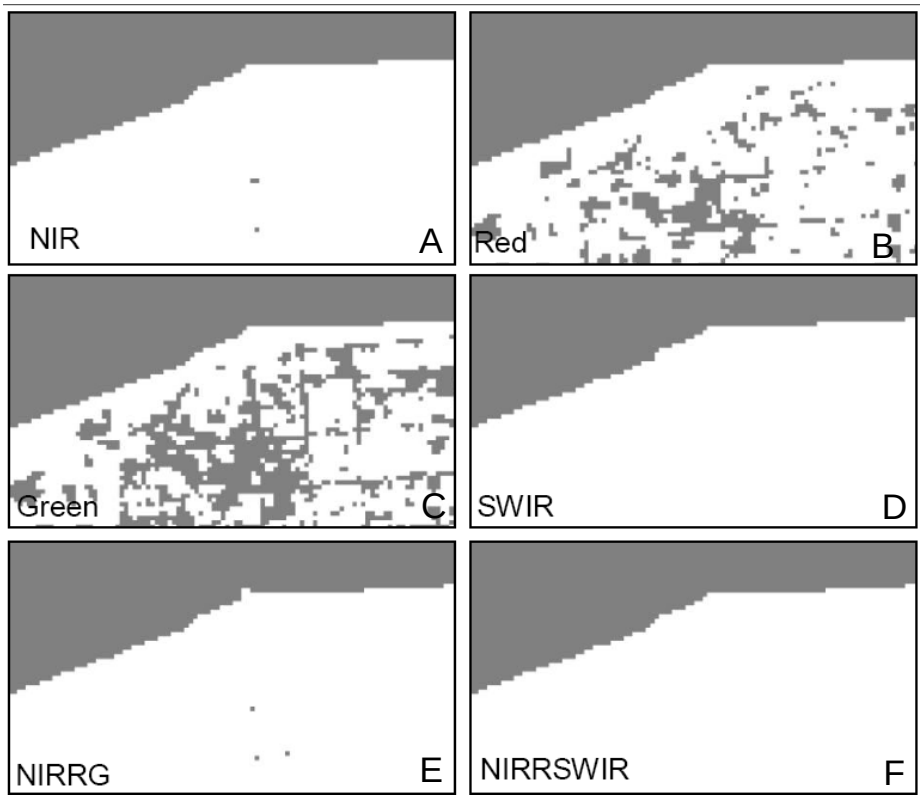


*Figure 3.16:* Classified images in sea (grey) and land (white) using single bands (A to D) and two different composites, NIR+Red+Green (E) and NIR+Red+SWIR (F) at Progreso on September 20, 2008.

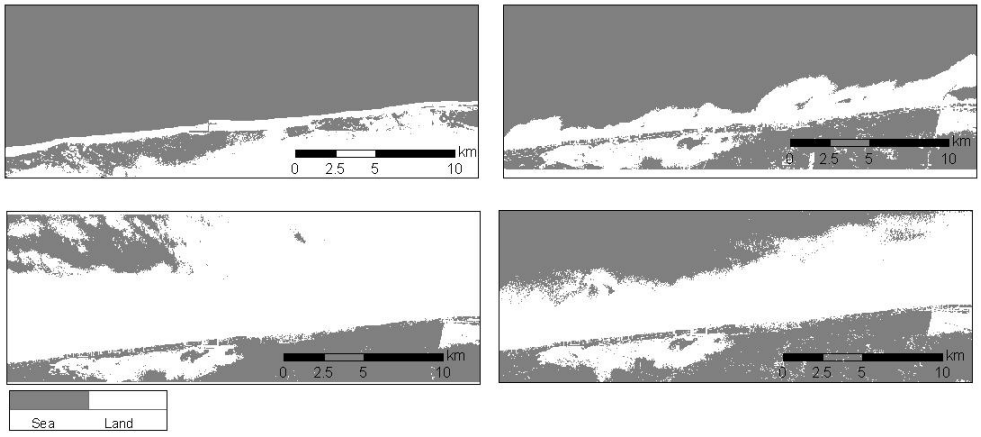


*Figure 3.17:* Classified images in sea (grey) and land (white) using the NIR (top left), red (top right), green (bottom left) and PN image (bottom right) at Telchac on November 24, 2005.

The differences between classified images using each spectral band confirms the capabilities of each wavelength to go through the water column. The green wavelength, which can go deeper (15 m) than the red (0.5 m) Lafon et al. (2002(a), detects a broader area as land than the NIR.

Overall the classification using the two composites (Figure 3.17 E to F) have similar results. Both can clearly distinguish between sea and land.

**Distance between the classified sea and land**

Although it was visually determined that longer wavelengths provide a clearer definition of sea and land than shorter wavelengths, it is necessary to develop a quantitative measure to evaluate their separability. The transformed divergence is widely used as a measure of how much two groups or variables change together.

The transformed divergence is based on the covariance-weighted distance between the means of the groups. The larger the transformed distance, the greater the statistical distance between groups therefore the higher the probability of a correct classification of groups.

The classified images using a single spectral band and a combination of three spectral bands were used to calculate the transformed divergence, including the images from Telchac (MS and PN) and Progreso from November 2005 and September 2008 respectively.

Figure 3.18 shows the probability of correct classification as a function of pairwise transformed divergence (dij). Values lower than 1.5 x $10^3$ indicate that the groups are from spectrally similar classes, and therefore have the lowest probability of be correctly classified.

Table 3.2 shows that, overall, all the spectral bands have a transformed divergence larger than 1500, with the exception of the PN (1386). The green has a transformed di-

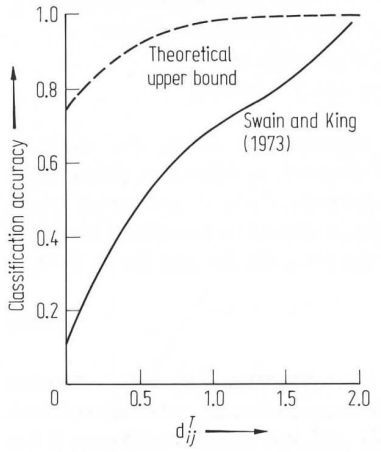


*Figure 3.18:* Probability of correct classification as a function of the transformed divergence (d*ij*). The values of the horizontal axis are x $10^{-3}$. Figure from Swain (1973).

vergence only slightly above 1500, showing that the classification of sea and land with the PN and the green could be considered spectrally the same. The highest likelihood of a correct classification is with the NIR and SWIR. The transformed divergence with the NIR remains large, with a clearer water column and with suspended particles in the water column, with values of 1998 and 2000 respectively in the image from Telchac (Figure 3.15) and from Progreso (Figure 3.13). The classified images that include a combination of bands show the largest transformed divergence, as the NIR exhibits. This might be because the NIR was included in the classification, as the red and the green alone have much lower transformed divergence. Due to the fact that the NIR alone shows a large transformed divergence, there is no reason to perform the classification using other spectral bands that have lower transformed divergence. These results, therefore, provide evidence that the use of the NIR alone has the largest difference between sea and land, ensuring the correct classification of both groups. So, it will be further used for the identification of the shoreline.

Figure 3.19 shows that the intensities between sea and land, with the NIR and SWIR, have opposite intensity values; in contrast, the green and red, have a intensity values

*Table 3.2:* Transformed divergence for each spectral band classified for the image from Progreso on September 20, 2008 and Telchac on November 24, 2005.

| | Transf. div. | |
|---|---|---|
| Spectral bands | Sept. 2008 | Nov. 2005 |
| Green | 1980 | 1503 |
| Red | 1930 | 1750 |
| NIR | 1998 | 2000 |
| SWIR | 1996 | |
| PN | | 1386 |
| NIR+R+G | 2000 | |
| NIR+R+SWIR | 2000 | |

are closer to one another, which allows visualising their lower transformed divergence between the classified sea and land.

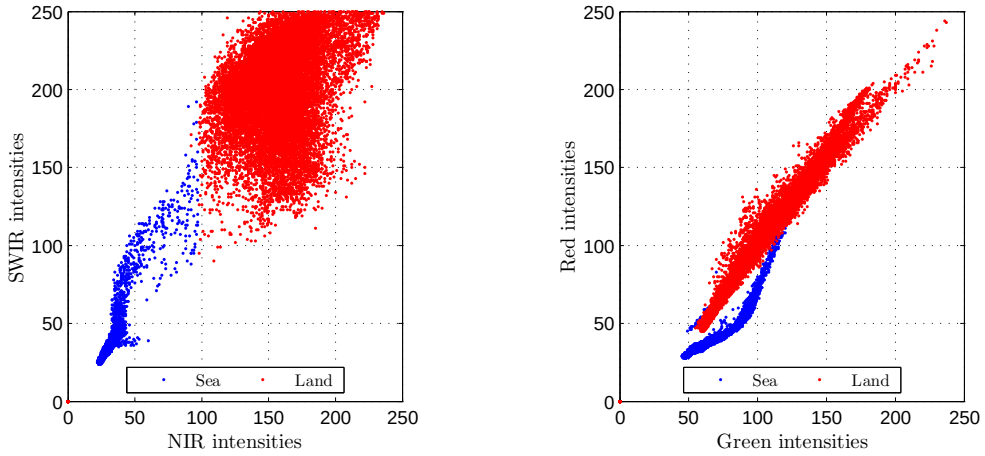


*(a)* *(b)*

*Figure 3.19:* Intensities from the classified sea and land with the NIR against SWIR (a) and with the green and red (b).

The sea intensities with the NIR have a narrower distribution, with values between 23 and 96. In comparison, the land intensities, have diverse intensities ranging between 93 and 250. Those closer to the lower limit of intensities of the land and those closer to the upper limit of the sea are from pixels that can potentially be misclassified, even though the transformed divergence using the NIR is the highest. However, the geographic

location of these pixels was verified, and it was found that their location is far away from each other. These pixels are associated with streets and vegetation, which have both high and low intensities, as do the land and the sea. Therefore, although there could be misclassification of these pixels, their location is far from the boundary between sea and land.

**Visual interpretation of a PN image**

The PN image was visually interpreted to identify the shoreline. The manually identified shoreline was compared with a classified image, using the NIR spectral band. This comparison shows whether the visually identified shoreline matches the border between the classified sea and land. Earlier in this chapter a visual shoreline identification was performed with 10 m pixel size MS images. The results suggest that a better spatial resolution could provide a better accuracy in shoreline identification. Therefore, visual interpretation using a 2.5 m pixel size image is a good opportunity to address this issue.

Figure 3.20 (a) and (b) show two locations where the shoreline has been visually identified with a PN image (2.5 m pixel size), overlapped with the boundary between the classified sea and land from an MS image (10 m pixel size). The difference between the visually identified shoreline and the boundary between both classes has an overall cross-shore difference of 1.7 m over 57 km of shoreline. However, locations with high intensities (> 150) in the nearshore, associated with suspended particles, have differences as large as 35 m. This comparison shows that even though the PN image has a smaller pixel size, the range of wavelengths included in this type of images cannot discriminate the high intensities in the nearshore suspended particles from the intensities from inland. Which is probably best explained because shorter wavelengths can go deeper in the water column than longer wavelengths (Lafon et al. 2002). Therefore, the use of PN images for shoreline identification can mislead an attempt to locate the shoreline when suspended particles are present in the nearshore region.

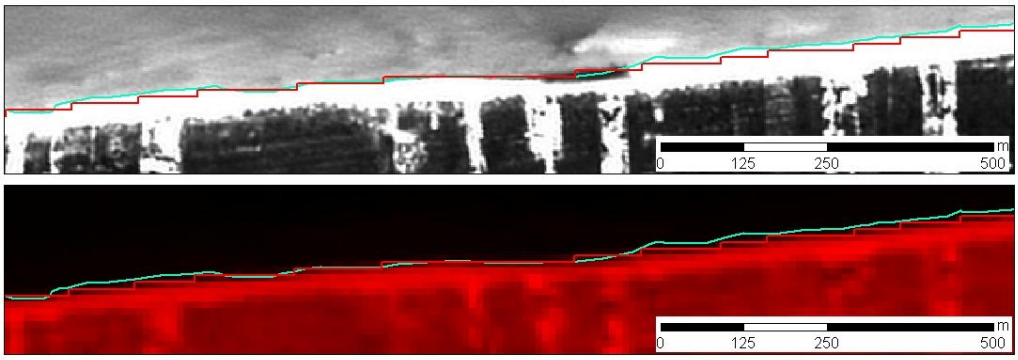


*(a)*

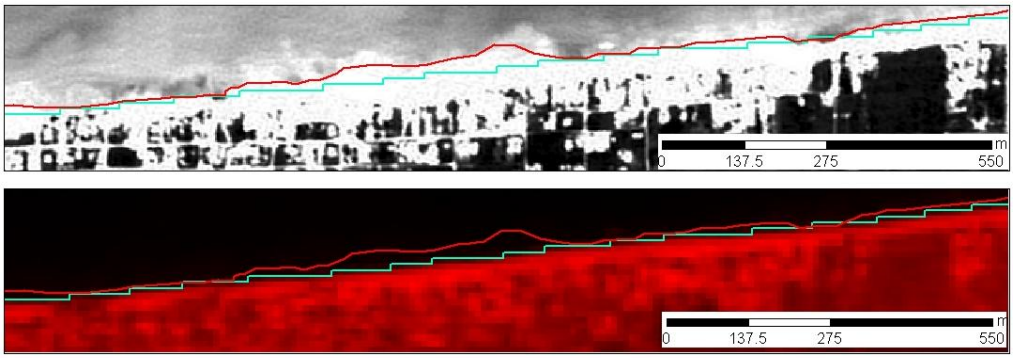


*(b)*

*Figure 3.20:* Visual identification of the shoreline (red line) using a PN image (top) 2.5 m pixel size, overlapped with the boundary of the classified sea and land (blue) using the NIR spectral band (bottom) in two locations (a) and (b).

### 3.5.3 Convergence threshold

Different convergence thresholds were used to determine which convergence threshold gives the best classification of sea and land. The convergence threshold determines the number pixels which are allowed to change their membership from one group to another, between iterations. The higher the convergence threshold the fewer pixels are allowed to move between iterations, resulting in more iterations required to reach the convergence threshold set.

The thresholds tested here ranged from 0 to 100 %. A zero convergence threshold is

the result of only one iteration, without comparing the classification results with other iterations.

Figure 3.21 shows the classification result with different convergence thresholds. The definition of the sea and land with no threshold, where the classification is the result after the first iteration, is relatively good; it is able to identify the sea and land as different groups, although with a broader definition. The number of pixels classified as sea or land does not change with a threshold of either 10 or 95 %, showing that with at least two iterations the pixels identified as sea and land remain the same during the eight iterations required to achieve a 95 % convergence threshold. This suggests that the difference between the identified groups is clear and that between iterations the membership of the pixels remains the same.

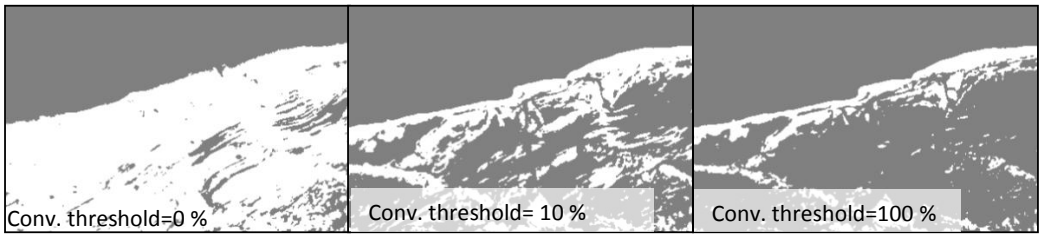


*Figure 3.21:* Classification of sea (grey) and land (white) with convergence thresholds of 0, 10 and 100 %.

In the tests, a threshold of 100 % was achieved after executing 12 iterations and the output was a narrower definition of the land. However, a threshold this high does not allow any flexibility in the classification process. If in the second iteration some pixels are identified as a different group to in the first iteration, then a third iteration is required until the same pixels are selected as part of the same group. This process can run indefinitely and for that reason a threshold this high might never be reached.

The advantage of using higher rather than lower convergence thresholds is that a higher threshold will produce a classification that is consistent between iterations and more likely to be correct than a low convergence threshold.

The results of testing convergence thresholds shows the advantages of using a convergence threshold that is high enough to allow enough iterations, whilst also providing some flexibility for a number of pixels to change their membership from one group to the other. Therefore, the convergence threshold that will be used in this research is 95%, allowing 5 % of the pixels to change their membership between iterations.

## 3.6 Developed method for shoreline identification

This section first summarises the whole process of obtaining a satellite-derived shoreline (SDS), as well as explaining each step followed of the method developed to identify the shoreline using optical images. The shorelines extracted through this method will allow assessment of shoreline changes.

The developed method is the result of the tests described earlier in this chapter. These tests have been helpful to determine the adequate parameters, such as the algorithm to use, the spectral bands and the convergence threshold, which produce the clearest definition of the shoreline from satellite optical images.

Figure 3.22 shows a diagram which summarises the method followed to extract SDS from optical images.

The first step is a geometric correction of the image. As was explained earlier in sections 2.4.4 and 3.3.8, SPOT images used in this research are not Geometrically Corrected using *in situ* Ground Control Points (GCP). Therefore, a geometric correction will adjust the image to *in situ* coordinates. Once the image is geometrically correct, the sea and the land are identified using a soft classification (unsupervised classification). Then a series of process are applied to the classified image to get the border between the classified groups of sea and land. The resulting vector denotes the shoreline. The estimation of the water level when the image was taken is essential for further comparisons with other shorelines of the same nature and that are adjusted to a common

vertical tidal datum. In chapter 5, this vector is validated using quasi-simultaneous *in situ* shoreline measurements.

### 3.6.1 Geometric correction

The geometric correction was executed in Erdas using *in situ* GCP located over the image. The features used as GCP were distinguishable at precise locations, such as highways and streets intersections. A linear model was used, which finds new coefficients and adjusts to the locations identified in the image and to the corresponding *in situ* GCP. The adjustment of the image involved a translation of coordinates. The Root Mean Square (RMS) between the *in situ* GCP and their location in the image, which is calculated by the model, was kept as small as is possible. The smaller the RMS, the closer the coordinates from the geometrically corrected image are to the *in situ* coordinates.

#### GCP *in situ* collection

GCP were chosen from the case study area in September 2008 using mainly street and highway intersections. The study area location is described in chapter 4. Forty GCP were located using a Differential Geographic System (DGPS), with a base station and mobile rover, within a radius of 15 km. The base station was located at a known fixed location and the GCP registered with DGPS were corrected by the comparison of simultaneously measured signals from the base and mobile stations. The base station was placed at least 30 minutes before starting the collection of points to allow the signal to stabilise and thus to get a better quality of measurements. The mobile antenna was programmed to record the position every three seconds and the survey involved staying at each GCP location for three minutes, recording 60 points for each GCP.

The location of the base station was corrected using the continuous data set from the closest available antenna (Merida). The measurements in Merida are continuous mea-

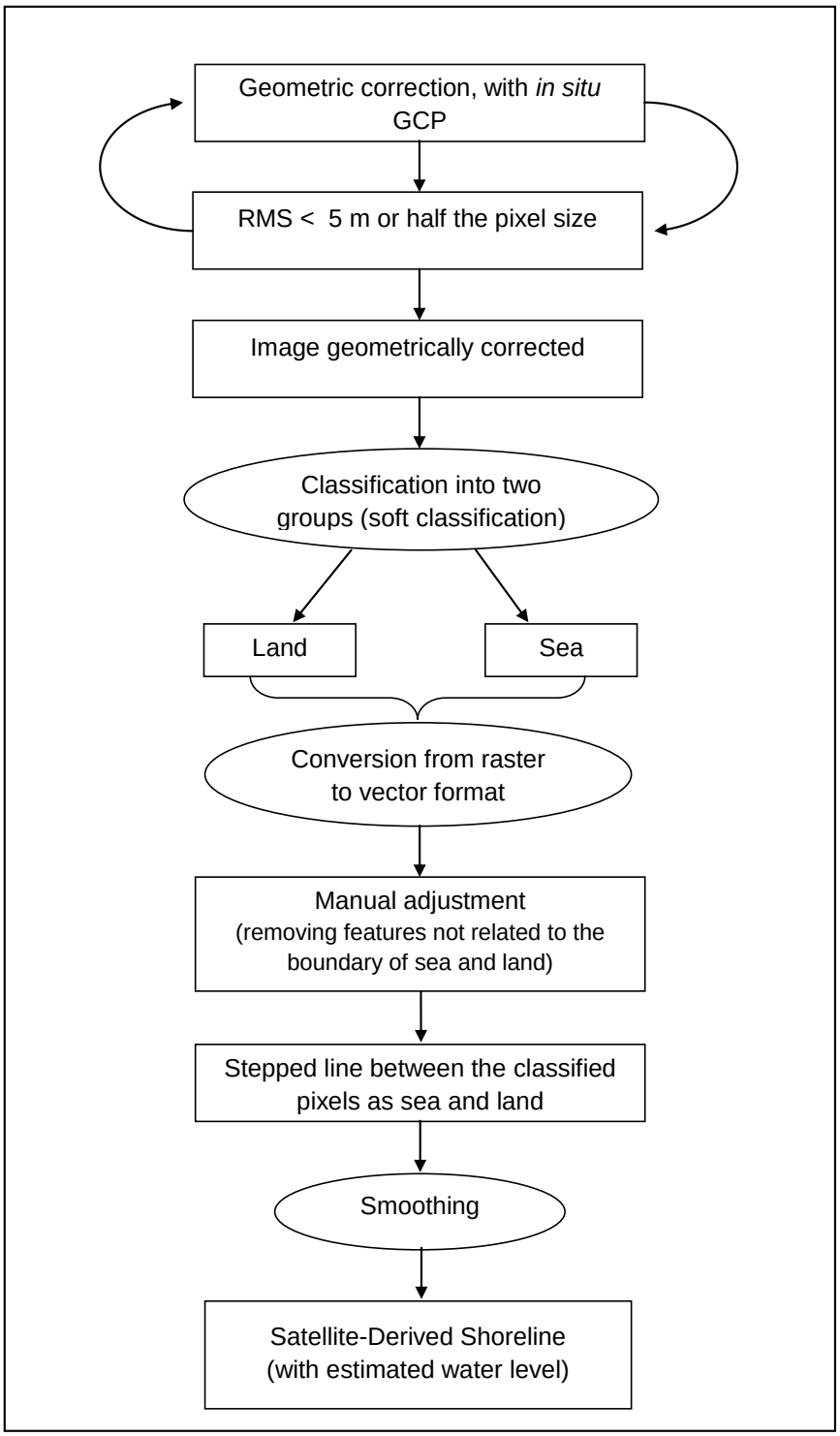


*Figure 3.22:* Diagram summarising the developed method for shoreline identification using satellite optical images.

surements that are simultaneous with the base station. The comparison of both signals corrects the location of the base station used in field measurements with the mobile receiver locations. After the correction of the received signal, the precision of the DGPS improves to around 10 cm, which is a suitable spatial resolution for our images of 10m pixel size.

GCPs were distributed as widely as possible. The location of each GCP was determined according to the location of the main streets and highways. Therefore, areas without any highways or streets do not have any GCP, resulting in some gaps in between locations within the image.

Figure 3.23 shows that the standard deviation of the GCP in most of the recorded points ranges between 0 and 20 cm. This variation may be due to changes in the ionosphere, presence of large buildings or dense vegetation obstructing the signal, the verticality of the antenna, and the distance of the mobile antenna from the base station. The GCP showing the largest standard deviation (> 10 cm) are further away from the base station. However, the accuracy of GCP with a deviation between this range is adequate to geometrically correct images of 10, 5 and even 2.5 m pixel size (White and El-Asmar 1999; Robinson 2004; Lillesand et al. 2008).

**Georeference process**

For this thesis, for 10 m pixel size images the maximum RMS accepted was 5 m, ensuring that the variation is within the pixel size.

The outputs of the model are the linear coefficients of the equations used to translate the original coordinates to the new eastern and northern locations.

As an example, the series of equations:

xnew= 19130.5 + 1.001x - 0.008y,

ynew= 12286.5 + 0.001x + 0.994y

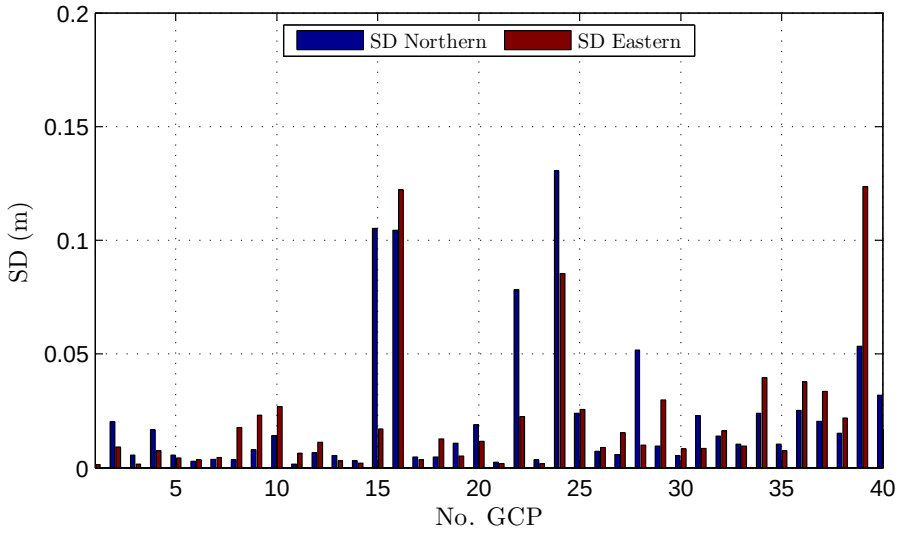


*Figure 3.23:* Standard deviation (m) of the *in situ* GCP in their northern and eastern coordinates.

where xnew and ynew are the new pair of coordinates and x and y are the original coordinates, were used to correct the image from September 20, 2008. Applying the equations produces a translation of the image.

### 3.6.2 Vectorisation of the classified image

The identification of sea and land is only the first step towards shoreline identification using satellite images. The result after the classification is an image of pixels grouped as sea and land. Thus, to obtain a shoreline that can be used in shoreline change studies, it is necessary to identify the shoreline as a line that runs between the grouped pixels of sea and land, which can be compared with other shorelines of the same nature. This has several implications: the shoreline has to be located systematically within the pixel size and the vector indicating the shoreline should not show evidence of the pixels' location. This is relevant because the pixels' location is not precisely the same in all of the images. Therefore, their presence would introduce an error when comparing different shorelines.

To clarify, a smoothed vector that indicates the shoreline can be overlapped with shorelines obtained at different times in order to assess shoreline change.

The next paragraphs describe the process performed to the classified image to obtain a Satellite-Derived Shoreline (SDS) that can be further used in shoreline change studies. The steps involved are a raster to vector data type conversion, a manual edition and a smoothing process. A description of both data formats is provided here.

**Raster and vector data formats**

The conversion from raster to vector implies the use of a different format to represent the identified classes. Raster and vector formats are widely used in Geographic Information Systems and remote sensing. Whilst some features are better represented as vector than raster, both formats have their advantages and disadvantages.

Raster format is composed of columns and rows. In geographical analysis, these columns and rows can be used as matrices of data which allow algebraic calculations. They have the advantage of allowing calculations and mathematical operations over an area defined as a unit (pixel). Raster formats, however, need more storage space than vector formats. One disadvantage of raster formats is that they provide a broader representation of a line or sharp features. Raster formats are also not helpful for overlapping images of the same location.

Vector formats can be points, lines or polygons. They effectively mark linear features and the overlapping of several layers of information. Vector formats can also keep information from the vector in an attribute table without losing information from the columns and rows. In addition, vector formats have the advantage of requiring a small storage memory.

### Raster to vector conversion

The raster to vector conversion was executed in ArcMap using the conversion tools. The output is a vector line that goes along all the boundaries of the pixels in between both groups in the analysed image.

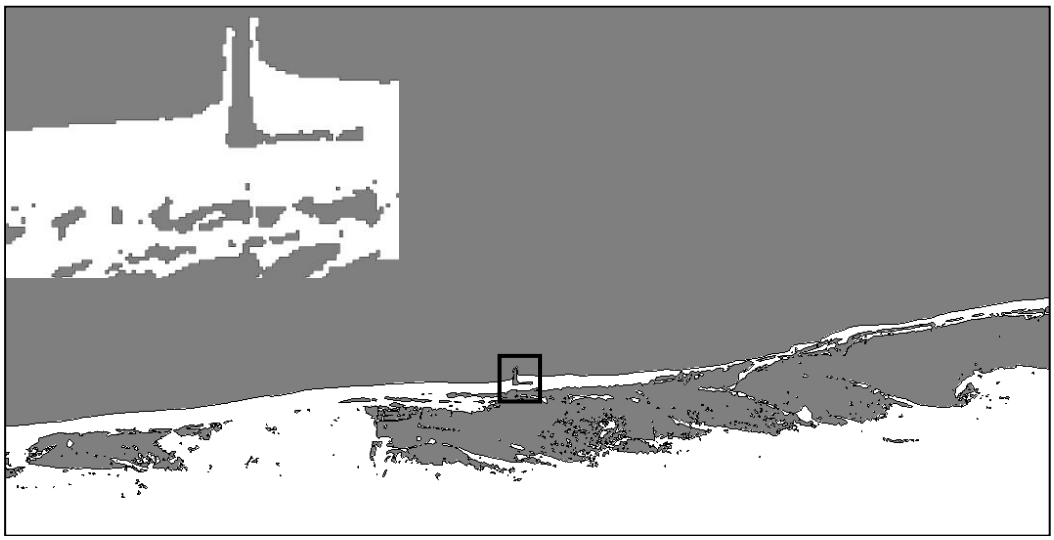

*Figure 3.24:* Extract of a classified image in sea (grey) and land (white) that has been vectorised, producing a stepped vector. The close-up is the area within the black square.

Figure 3.24 shows the resulting vector after the conversion. The output vector exhibits vector lines further inland, where sea features have been classified as water. The vector shows steps that coincide with pixels' locations in the raster image. The boundary that is of interest to this research is the one located in between the sea and the land.

### Editing process

The resulting vector requires a manual edit whereby the inland features not related to the shoreline are removed using ArcMap software. The output of this process is a stepped vector that follows the boundary between the pixels classified as sea and land.

### Smoothing

To perform the smoothing, it was necessary first to define where the shoreline is to be located within the pixel size. The stepped vector follows the boundary of the classified pixels as sea and land. Thus, the shoreline runs at half the classified pixel as sea and land (50 % each). Therefore, the smoothed shoreline was located at the midpoint of each step of the stepped vector, keeping equal proportions of sea and land. This approach to locate the shoreline beyond the pixel resolution was previously used by Foody (2002), showing that it increases the accuracy of the shoreline. However, even if a different location was chosen within the pixel, as long as the location was consistent and systematic no errors would be added into the shoreline location.

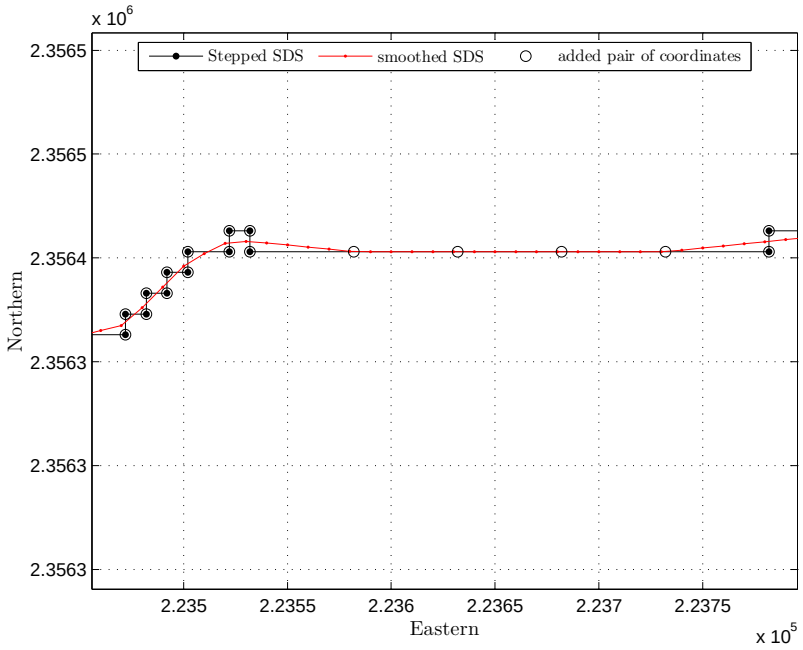


*Figure 3.25:* Smoothed vector (red line) and stepped raw vector (black line) that comes from the conversion of raster to polygon. The horizontal axis is the Eastern and the vertical axis is the Northen.

Figure 3.25 shows the smoothed vector at the chosen alongshore distance of 50 m, overlapped with the stepped raw vector. Figure 3.26 shows the different distances tested

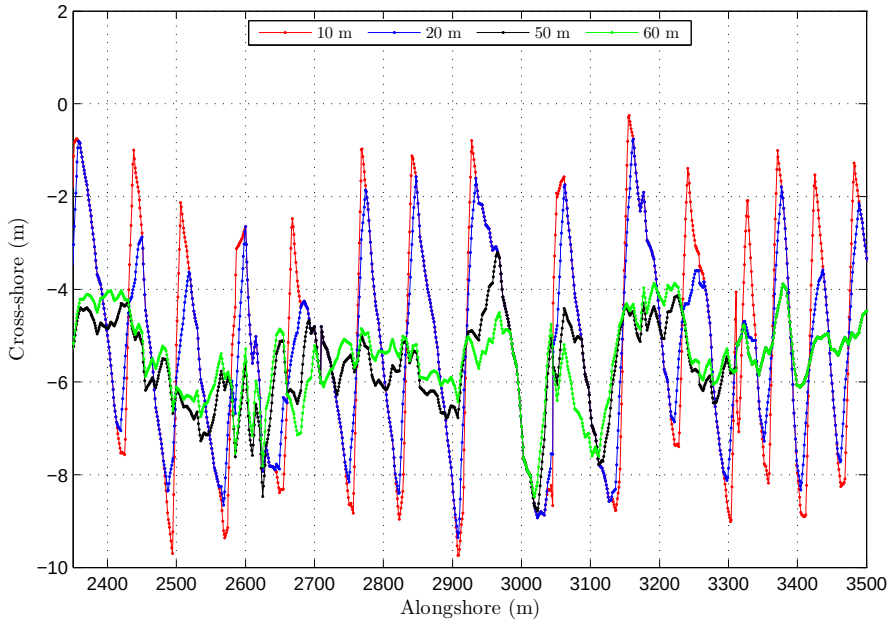


*Figure 3.26:* Smoothed SDS at alongshore distance of 10, 20, 50 and 60 m in Progreso, Yucatán, México (see chapter 4 for study area description.).

(10, 20, 50 and 60 m) and the difference in the cross-shore and alongshore from *in situ* shoreline measurements (see chapter 5 for further details about the validation of SDS). The cross-shore difference results in a negative number because the SDS is further North than the *in situ* shoreline measurements. To clarify, the SDS is seawards located in relation to the *in situ* shoreline measurements.

The smoothed SDS with alongshore distances of 10 m and 20 m retain a jagged shape in the alongshore, showing abrupt changes ranging between -10 and -1 m, whereas smoothed SDS with a distance of 50 and 60 m range between -10 and -4 m, reducing the change in the cross-shore by almost half the magnitude. This decrease in the cross-shore variability improves the accuracy detection of the SDS at higher resolution than the actual pixel size permits. The smoothed SDS at 60 m, despite having a similar shape to the SDS smoothed at 50, does not follow the slope of the smoothed SDS at a

smaller alongshore distance. This could be an indication that with a distance of 60 m the SDS degrades its resolution from the original stepped vector. This shows that the use of a distance of 50 m is adequate for this study area because the smoothed SDS at a distance of 50 m shows a significant reduction in the jagged shape, without degrading the resolution from the stepped raw vector.

The alongshore distance determined here is specific to the shoreline of Progreso, Yucatán. This is a location where the shoreline is mainly straight and does not show large oscillations and the few oscillations present in this area are well captured by the SDS. Chapter 4 provides further details from the case study area.

In chapter 5 it was found that the smoothed shoreline does not have random errors and, furthermore, that the pixel effect has been successfully removed.

## 3.7 Discussion

**Tested parameters**

The tested parameters were useful to specify the parameters providing the best definition of the shoreline, as well as to identify the steps that are not required for shoreline identification. For example, using sample sites (mask) degrades the difference between the sea and land with the shorter wavelengths (green), whilst the longer wavelegths do not show any improvement in the contrast between sea and land. This is interesting because other research found it useful to define a threshold based on an extract of the image to analyse (Liu et al. 2007), rather than using the whole image. However, here the results show that the mean of the groups does not accurately denote the groups to identify when a narrow region is used to classify the sea and land.

The test of the spectral bands shows that although all the spectral bands exhibit a decrease in intensities over the sea (see section 3.3), the NIR gives the largest difference in intensities between the sea and the land, even in presence of suspended sediment in

the nearshore. Furthermore, this test shows that there is a better contrast between sea and land using MS images with 10 m pixel size than PN 2.5 m pixel size images. Moreover, the use of longer wavelengths has been suggested by Frouin (1996) and White and El-Asmar (1999) to avoid the high reflectance due to the surf in the breaker zone. The use of the transfomed divergence is useful to quantify the difference between the identified groups and to estimate the classification of the groups' accuracy, as well as the visual assessment of the intensities identified as sea and land, that allows observation of the similarities and differences in intensities with shorter and longer wavelengths. Their information would not be replaced by the visual examination of the classification results.

The tests that involved a visual interpretation of the shoreline using satellite optical images show that shoreline identification seems to be more complex in this instance than the interpretation of aerial photographs. However, previous research that used a visual interpretation (Li et al. 2003; Shaghude et al. 2003; Chu et al. 2006) does not mention any difficulty in shoreline identification. This may be because their results were not contrasted with other methods to identify the shoreline. The tests show that differences much larger than the pixel size can occur, particularly in the presence of high suspended particles concentration in the nearshore region.

The use of a soft classification avoids the definition of a specific threshold to identify the sea and the land as has been defined in other methods (Foody et al. 2003; Liu and Jezek 2004). In contrast, soft classification considers the inherent differences in intensities within an image, ensuring that the groups identified have the greatest difference that is possible.

The tests using low or very high convergence thresholds in the soft classification give different classification results. A zero threshold, although it gives a broader identification of sea and land, shows relatively good results. A more precise selection of pixels

belonging to sea or land groups occurs from the first to the second iteration. However, no differences with further iterations was found. The highest threshold possible to achieve takes place in only 12 iterations. This suggests that from iteration to iteration the same pixels are constantly identified as part of the same group and that the pixels' membership is clear. In this research a high convergence threshold (95 %) was defined, ensuring that several iterations took place without restricting the pixels from changing their membership.

**The developed method**

The developed method for shoreline identification includes several steps. Although the methods used for shoreline identification are based on algorithms previously used, the series of steps proposed here is part of the developed method to identify a shoreline that can be further applied in shoreline change studies covering large spatial scales. Each step of the developed method has been defined through testing different parameters, ensuring the highest accuracy possible for the shoreline identification and for the study of shoreline change using SDS.

The geometric correction of the satellite image, although it is a common process in remote sensing, it is very important to keep high precision and to use *in situ* GCP rather than using another source as a reference. The classification performed with the NIR will produce a higher classification accuracy between the sea and the land even in the presence of suspended particles in the nearshore region. The vectorisation of the shoreline and the smoothing process are very important steps to remove the jagged pattern from the original raw vector, thus improving the spatial resolution of the shoreline within the pixel size using a systematic approach which will produce a SDS that can be further used in shoreline change studies.

Although the method developed to identify the shoreline in this thesis does not run automatically, the manual processes do not require a judgment that could add a subjective

error into the method. For the purpose of this research, a semi-automatic approach does not represent a limitation. It is recomended, however, that the SDS is visually assessed using the original satellite image and the classified image. This will allow the detection of errors in the identification of the sea and land, or during the vectorisation and smoothing process.

The current method could be improved to produce a more accurate shoreline location by predicting its location within the pixel size, rather than systematically locating the shoreline position within the pixel size. However, the location of the shoreline with a higher accuracy might not be relevant for the spatial scale covered with 10 m pixel size satellite images, taking into consideration that the range of positions that the shoreline can have due to the wave run-up may be even larger than the pixel size. Chapter 5 discussess the differences between the SDS and *in situ* shoreline measurements, considering the water levels. Moreover, the satellite-derived shorelines are suitable to make further comparisons with other shorelines of the same nature and for its application in shoreline change studies.

Although the proposed method is providing good results with the images tested in this thesis, it is possible that the shoreline identification in beaches with ample swash and shallow beach slopes would prove particularly difficult to study and further refinement of the method may be required.

The developed method locates the shoreline position in two dimensions. However, the incorporation of tidal levels when the image was taken enables the location of the shoreline with a more accurate position than the SDS.

The SDS extracted with the proposed method was validated using quasi-simultaneous *in situ* shoreline measurements (see chapter 5). This comparison, helped to define the differences between the SDS and the *in situ* shoreline measurements, as well as the confidence bounds.

## 3.8 Chapter summary

This chapter firstly assesses the capability of satellite optical images to distinguish between sea and land. Secondly it explores different techniques (edge detection, high pass filter, visual interpretation and soft classification) to determine which is suitable for shoreline identification. Thirdly, it defines the parameters to ensure the most accuracy in the shoreline identification. Fourthly it outlines the steps of the developed method and the parameters defined to identify the sea from the land in the unsupervised classification and describes the editing and smoothing process required to extract the shoreline using satellite optical images.

There is an abrupt decrease in intensities between land and sea from one pixel to the next, with all the spectral bands. Visual interpretation can have a much larger error than the pixel size when detecting the shoreline, even with high resolution images (2.5m). The soft classification or unsupervised classification accurately distinguish the sea and the land.

The NIR spectral band can distinguish sea and land even in the presence of suspended particles in the nearshore. However, all the spectral bands achieve separation of sea and land without the presence of suspended particles in the nearshore region. The developed method permits the shoreline identification as a line within the pixel size and it can be used to assess shoreline change. It is recommended that the SDS is visually examined using the classified image and the original satellite image.

The extracted SDS requires an estimation of the water level when the satellite image was taken otherwise its further application in shoreline change studies is not possible. The validation of SDS is addressed in chapter 5.

## 3.9 Conclusions

1. The NIR spectral band (0.78-0.89 $\mu$m) from satellite optical images, 10 m pixel size, can successfully separate pixels as sea and land without overlapping the intensities of each, even in the presence of suspended particles in the water column.

2. Images with a smaller pixel size (2.5 m) that do not include the NIR wavelengths, cannot successfully separate the sea and the land. Therefore, the NIR band is appropriate for shoreline identification, providing a consistent approach and producing a classification whose accuracy is as high as possible.

3. A method has been developed to identify the shoreline from satellite optical images, applying a soft classification, using the NIR spectral band (95 % convergence threshold and no mask) to separate the sea and land, followed by a vectorisation process (see section 3.6.2). The resulting shoreline indicates the boundary of the pixels classified as sea and land in the image.

4. The identified SDS does not show a pixel effect, allowing their comparison and calculation of shoreline change with other SDSs, without introducing an error related to the pixels' location.

5. The estimated accuracy of SDS extracted with the developed method is estimated to be within the pixel size (10 m).

6. The extracted SDS requires accurate estimation of water levels when the satellite passed for further application in shoreline change studies.

# Chapter 4

# Case study area and available data

## 4.1 Foreword

This chapter introduces the case study area and the available data. The case study area is used in chapter 5 to test the satellite derived shoreline (SDS), and in chapter 6 to assess the shoreline change using SDSs. This chapter describes the bathymetry, tides, winds, waves and beach slope within the region and, specifically, in Progreso. All of this information is required for the interpretation of shoreline change.

The region does not have long systematic data time series, however an extensive dataset has been compiled for the description of the case study, including data gathered during fieldwork. The compiled data comprises a few years of sparse measurements from different geographic locations within the region. The region is fairly homogeneous so it has been assumed that variations within different locations are fairly small. The data used here to describe the case study area is the best available data from the region.

This chapter is divided into three main sections. The first section gives a general overview of the region, and the location used to test the SDS is introduced. The second section describes the available SPOT images to assess shoreline change and the ancillary data. The wave and wind behaviour throughout the year is described using the compiled information. The third section assesses the tidal measurements obtained from the Mexican Navy (SM) with predicted tides. The SM tidal measurements are the

longest tidal records in Progreso. The aim was to select the most consistent and reliable tidal information that will be further used to estimate the tidal levels for each SDS.

Figure 4.1 summarises the chapter structure.

## 4.2 Introduction

The case study area is located in Yucatán Peninsula, México. This location combines different characteristics making it very interesting to test SDS and explore shoreline changes.

Most of the Yucatán shoreline has erosion problems, it extends about 1,700 km and is sparsely populated. Moreover, due to its location, between the Gulf of México and the Caribbean Sea, it experiences hurricanes every year (Figure 4.2). Coastal research in the region has only recently begun, regardless of the erosion problems. The beach morphology has been poorly surveyed, and considering its extent, monitoring of the shoreline on a regular basis requires a practical approach. The use of Yucatán as a case study area to validate the SDS using *in situ* shoreline measurements, might allow the exploration of shoreline change over a 6.5 year period. The shoreline change assessed in chapter 6 will contribute to the coastal knowledge in the locality. Finally, the use of this case study area as an example to study shoreline change using SDS could be further applied to implement a shoreline monitoring programme in places like Progreso.

Due to its geographical location, Yucatán remains relatively protected from incoming hurricanes and is fetch-limited, reducing the development of waves of large periods. Yucatán is surrounded by the Florida Peninsula (about 900 km to the NE), the Bahamas, and Cuba (about 1,000 and 500 km respectively to the East) and the Alacranes coral reef (located about 100 km to the North). However, tropical storms coming from the Caribbean Sea or tropical storms developed within the Gulf of México can have a direct impact on Yucatán.

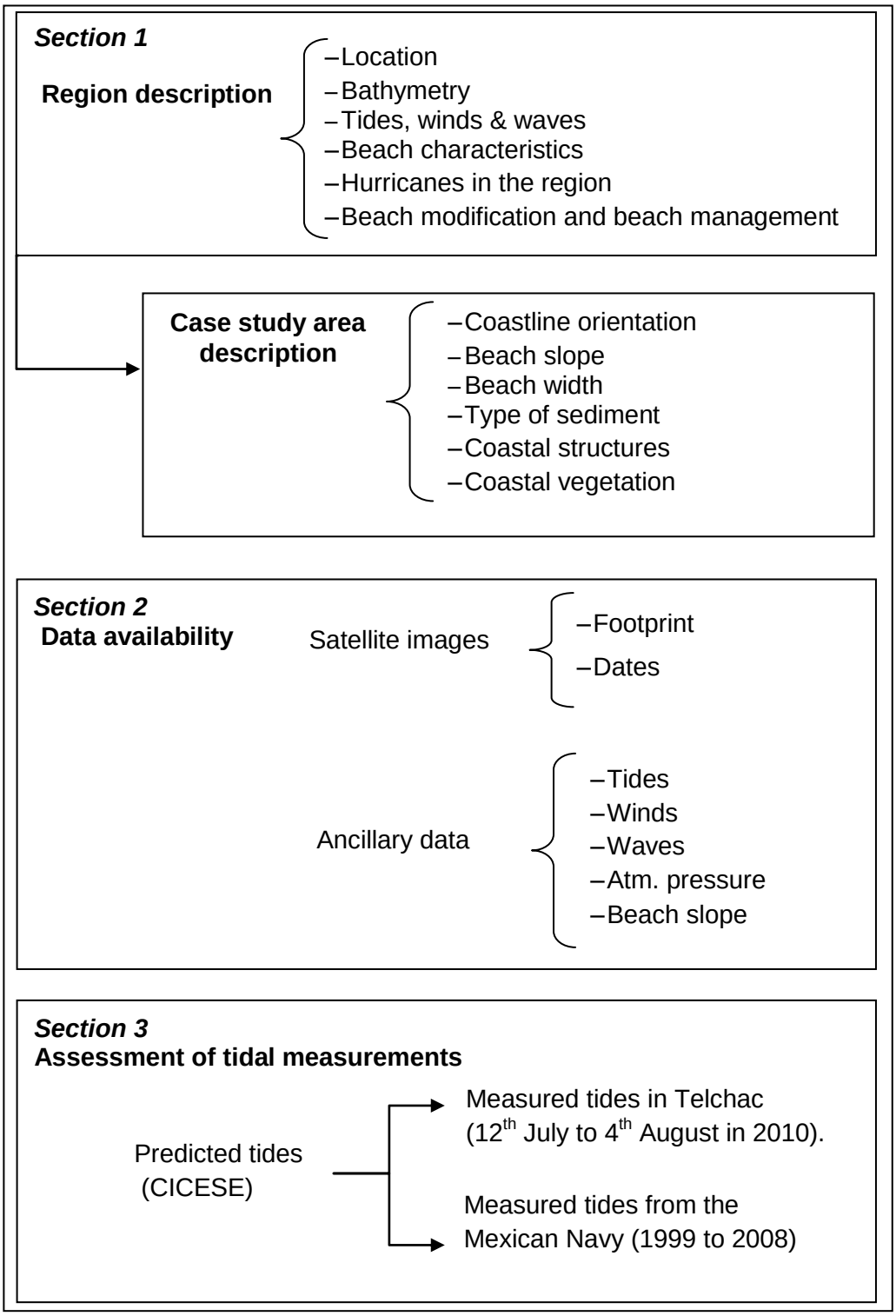


*Figure 4.1:* Chapter 4 structure summary.

The impact of a hurricane in Yucatán would produce an effect not only on the shores, but also on the inland villages. The largest cities: Merida, Campeche, Cancun and Chetumal, lie within 50 km of the coast (INEGI 2006), at no higher topographic level. So the floods can reach inland, potentially affecting 90 % of the population (1,818,948 inhabitants) living in inland and coastal counties.

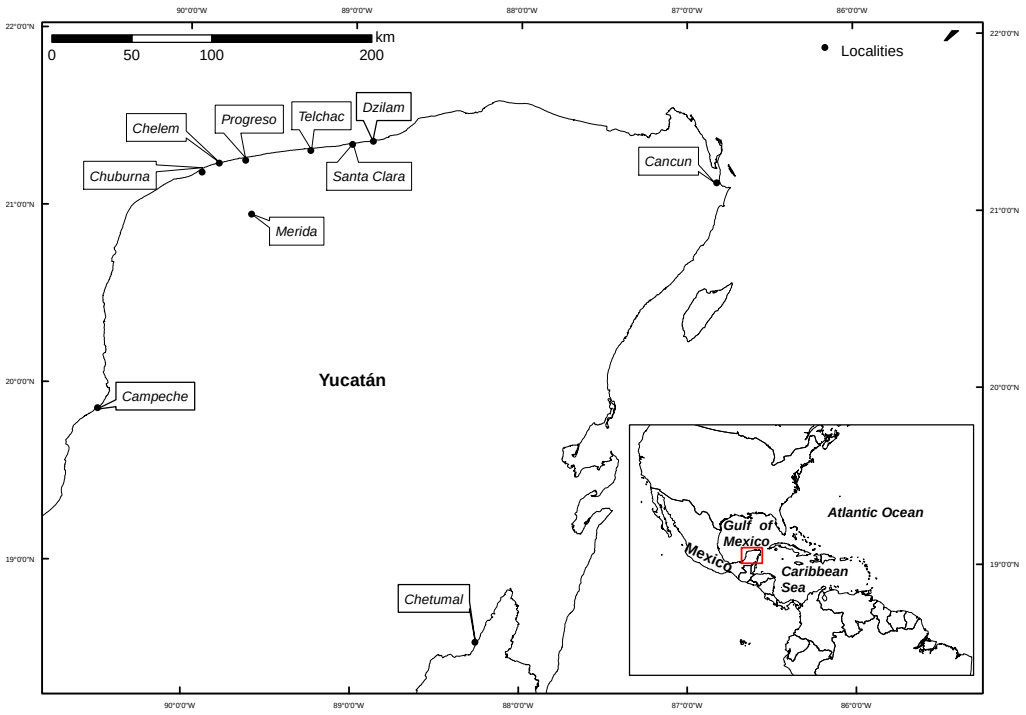


*Figure 4.2:* Geographic location of Progreso, Yucatán, México. The lower box shows the location of Yucatán within the continent.

## 4.3 Physical setting: General overview

This section gives a general overview of the Yucatán shoreline, considering the environmental factors that modify the beach morphology.

The environmental factors described here are: bathymetry, winds, waves, tides, longshore transport and hurricanes. Sections 4.4.2 and 4.5 in this chapter provide detailed information on the winds, waves and the assessment of tidal information.

### 4.3.1 Bathymetry

Knowledge of the bathymetry is essential to understand how the waves might approach the shore and which coastal processes can potentially take place at the shoreline.

Figure 4.3 shows the bathymetry of the region. It is typically shallow with a wide continental shelf, exceeding 100 km. The deeper depths (3,500-4,000 m) are found 300km north of Yucatán. The depth steadily decreases at an approximate slope of 1:1,000. Moreover, coral cays and shallow water features are found at depths of between 5 and 40 m depth. The offshore cays form a barrier for large waves coming from the north, whereas the onshore cays are sparsely located, potentially diffracting and refracting the waves approaching the shore. Such a shallow bathymetry dissipates the wave energy, reducing the wave height and aligning the approaching waves to the depth contours. In addition, Yucatán is limited to the north by the Gulf of México, where swell waves are not common. However, the effect of the bathymetry on the waves will depend on the wavelength. For example, a long wave of 11 second period coming from the north will start shoaling at 94 m depth, 160 km offshore. The depth contours are orientated NE-SW. Therefore, the wave rays will be diverging from each other and travelling towards the east. Further interaction with the cays in shallower waters bends the rays and breaks the waves while travelling onshore, producing an overall loss of energy from the waves. Alternatively, a relatively a small wave of five second period will be shoaling about 25km offshore at 19 m depth. The waves, while travelling onshore over 25 km distance, will align to the depth contours, mostly travelling parallel to the shoreline. Therefore, either large or small waves will be attenuating energy when travelling onshore (Section 4.4.2 provides more details about the decrease in the wave height in deep and shallow water). The effect of the wind in such a shallow bathymetry has to be considered. Wind-generated waves, when travelling onshore, will follow the wind direction, this is reviewed in the next section.

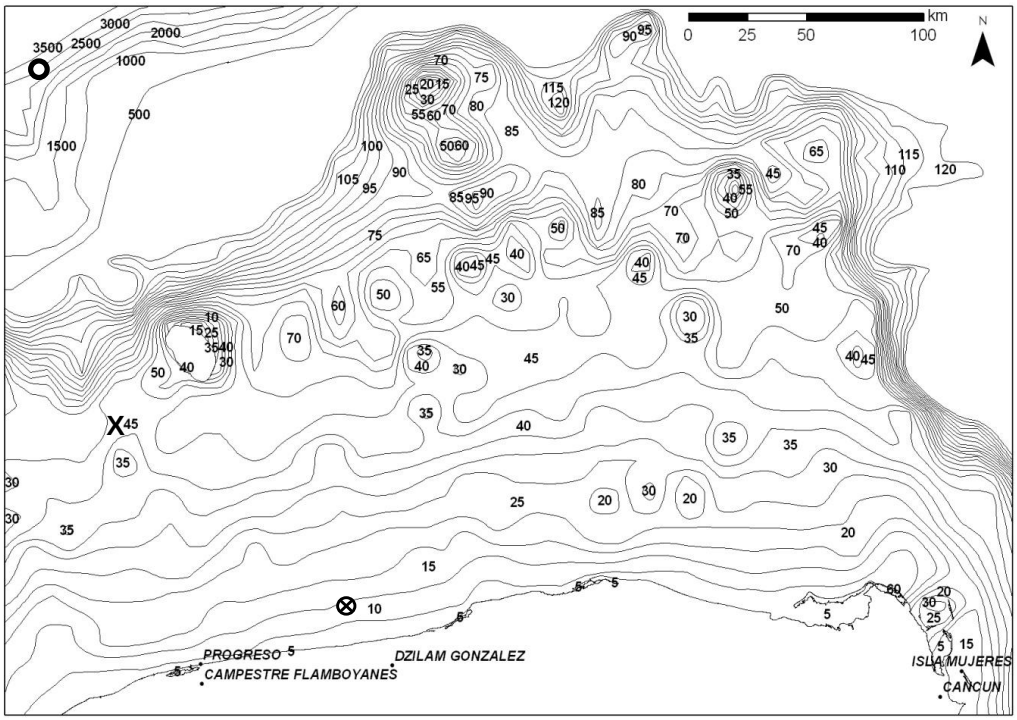


*Figure 4.3:* Bathymetry of the Northern coast of Yucatán. The contours are depth in metres. From SEMARNAT and SEDESOL (2009). The location of the NOAA wave buoy (42001) (⚬), modelled waves (×) and measured waves at Telchac (⊗) are marked (further mentioned in section 4.4.2.)

### 4.3.2 Winds and waves

The wind direction in Yucatán is dominated by the Trade winds, mainly coming from the NE during the year. The direction of the waves travelling onshore over such a shallow bathymetry are likely to be mainly driven by the wind force. The wave and wind direction is similar, with a dominant direction through the year from the E-NE although with some variations in winter and summer.

Waves approaching the shore will determine the direction of the longshore drift, in particular in this region, where the waves at the shoreline typically have a short period (see section 4.4.2).

The seasonality is not very strong. However, it is possible to identify three main sea-

sons in terms of wind directions, while the wave heights on average remain very similar (see section 4.5.2, Table 4.7). A calm season, from March to April, has easterly winds and significant wave height (Hs) of 0.6 m and a significant period (Ts) of 4 s (at 10m depth). A hurricane season, from June to November, has east winds with sudden changes in their direction when there is a hurricane, Hs of 0.6 m and Ts of 4.6 s (at 10m depth). A winter season, from December to February, has SE-NE winds, Hs of 0.7m and Ts of 5.3s at 10 m depth (Mariño-Tapia *pers. comm.*). The difference on the waves approaching into the shore will have an effect on the longshore transport and the gradients of sand and the coastal processes taking place in the case of study.

The wave behaviour in the region is episodic, characterised by small wave heights of about 0.15 to 0.3 m reaching the shore and maximum wave heights larger than a metre occurring during hurricane or winter seasons (Table 4.7).

### 4.3.3 Tides

Table 4.1 and figure 4.4 show the main tidal constituents amplitude (M2, S2, N2, K2, K1, O1, and P1). The tide in the study area is diurnal, it has a form factor (F) larger than 3 (4.8), indicating that the diurnal constituents are more important than the semidiurnal constituents (Pugh 2004). The tidal range is considered to be microtidal, with a maximum tidal range of 0.9 m during spring tides and less than 0.2 m during neap conditions. Section 4.5 provides more information about the tides and the local tidal measurements.

The datum used as a reference is the MLLWL (BMI). The BMI definition has been changing depending on the length of the time data series, and it is closer to the MWL rather than the MLLWL. Section 4.5 provides an assessment of the tidal record and further details about the vertical datum.

*Table 4.1:* Main tidal components and their amplitude and phase (°).

| Tidal components | H | Phase(°) |
|---|---|---|
| M2 | 0.06 | 97.3 |
| S2 | 0.012 | 86.1 |
| N2 | 0.020 | 75.8 |
| K2 | 0.002 | 76.9 |
| K1 | 0.179 | 298.6 |
| O1 | 0.168 | 297.9 |
| P1 | 0.053 | 300.5 |

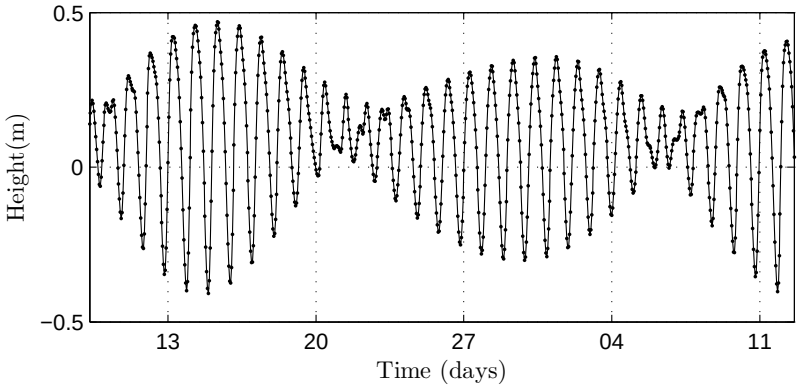


*Figure 4.4:* Predicted tide in Progreso, Yucatán, México. The datum of reference is the local BMI (MLLWL).

### 4.3.4 Longshore transport

The longshore transport will depend on a number of factors ranging from oceanographic processes, climate variability and engineering practices (Komar 1998; Masselink and Hughes 2003). However, one major factor is the approaching waves to the shore (Komar 1998). The usual scenario is wind generated waves of short period (<5s) approaching from NE, driving a westward longshore transport. Regardless of the lack of direct field measurements of the longshore transport, the wind direction provides a good indication of its direction, particularly in this region, where waves of short period typically occur. Field observations show constant accumulation of sand east of the groynes, suggesting a westward dominant drift direction that agrees with the dominant

wind direction. This section assumes the functioning of the longshore transport based on field observations and ancillary data, acknowledging the inherent difficulties with the understanding, measurement and observation of the longshore drift (Cooper and Pilkey 2004).

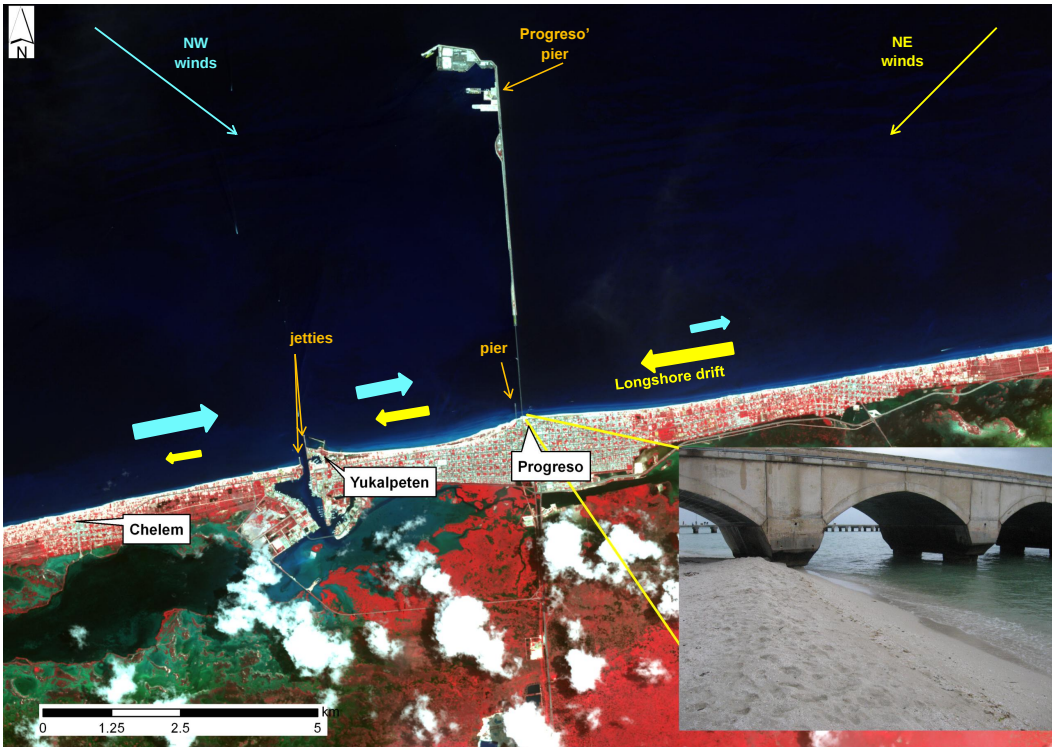


*Figure 4.5:* Direction of the alongshore transport in Progreso with NE (yellow arrows) and NW (blue arrows) winds. The length of the arrows denotes the assumed amount of sediment transport. The photograph is of Progreso' pier.

Figure 4.5 shows the assumed longshore drift given observations in the field and exploration of the ancillary data. The longshore transport in the study area is driven by wind generated waves, with winds from the NE (the dominant direction) and with winds from the NW, which occur in the presence of storms. The longshore transport, therefore, would be likely to be westwards during the year and eastwards in the presence of storms. The length of the arrows denote the estimated amount of sediment transport.

The study area has two man-made structures that can modify the alongshore gradients of sand. There is one pier (Progreso pier) that extends offshore for 6 km, with a shore-

parallel solid structure at its seaward end of 2 km long. The pier is not a solid structure, however, its presence would produce a significant reduction in the alongshore gradients of sand, while the shore-parallel structure is a barrier for easterly winds, reducing the wind generated waves towards the inmediate western side of the pier. These two effects by the pier result in deposition of sand, showing that the reduction of wind driven waves is a very important factor in the observed shoreline change in the case of study. Moreover, approximately 110 m west of Progreso pier there is another pier that is 285 m long. Both piers cause a decrease in the westwards longshore transport, making it difficult to move sand from the east of the pier to the west. Further down in Yukalpeten, approximately 4 km west, there are jetties, that are solid structures of approximately 200 m long. Therefore, the alongshore gradients of sand will be further decreased.

Local fishermen, questioned during our fieldwork in 2010, said that they have noticed a change in the beach width over the last 30 years. The western side close to the pier is getting wider, by as much as 100 m, while the beach slope is getting shallower and the breaking of the waves is further seawards than it was before, with erosion further west. This suggests that the pier attenuates the wave height, producing deposition of the sand in the nearshore zone and making a wider beach. This observation is in agreement with the shoreline change found in this research (see chapter 6).

The longshore sediment transport or littoral drift ($Q_1$) can be predicted by the following equation (Komar 1998; Masselink and Hughes 2003):

$$Q_l = \mathrm{K}P_1 = \mathrm{K}P_1 = \mathrm{K}(ECn)_b \sin\alpha_b \cos\alpha_b$$

where $Q_l$ is the volumetric transport rate in $\mathrm{m}^3\mathrm{day}^{-1}$. K is a proportionality coefficient that approximates to 0.7 in sand-sized sediments. This coefficient can vary but overall a 0.7 value provides a good fit (Komar 1998). $P_l$ is the longshore component of the wave flux, $(ECn)_b$ is the wave energy flux at the breaker point, and $\alpha_b$ is the angle of

the incident breaking wave.

The wave energy flux is a function of the breaking wave height ($H_b$) and the water depth. This equation can be simplified by using $\rho_s$=2,650 kgm$^{-3}$ for quartz-density sand and $\rho$=1,020 kgm$^{-3}$ for the seawater density. $H_br$ is the root-mean-square wave height.

$$Q_l = 1.1\rho g^{\frac{3}{2}} H_b r^{\frac{5}{2}} \sin\alpha_b \cos\alpha_b$$

This equation, although it applies to quartz-density sand, shows the relationship between the wave conditions and the resulting rates of longshore sediment. However, this relationship is not a function of the grain-size. Moreover, the sediment transport is assumed to result solely from waves breaking at an angle to the shore. To clarify, this equation is not applicable to the longshore sediment transport that occurs when the cell circulation, tides or the wind contribute to the magnitude of the longshore current, and thus the sediment transport (Komar 1998).

In the study area, locally generated waves of short periods will not generate strong longshore currents. However, during storms or hurricanes waves may approach at high angles. The amount of sand transported in this region will increase with the wave height and incidence angle. For example, applying the equations described above, the longshore transport with a $H_br$ of 0.25 m and with an hypothetical incidence angle ($\alpha_b$) of 25° will produce an amount of 3,317 m$^3$day, whereas an $\alpha_b$ of 15° will reduce the amount of sand per day to 2,165 m$^3$. Alternatively, an $\alpha_b$ of 25° with a $H_br$ of 0.5 m will increase the amount of sand to 6,634 m$^3$day.

Another factor not considered in the sediment transport estimation is the availability of sand. Particularly in Yucatán, the sandstone is at no more than 10-20 cm from the surface. The largest amounts of sand are only found next to artificial barriers of sediment. Thus, the availability of sand is a limiting factor for the total longshore

sediment transport.

The alongshore gradients in the transport of sediment, as well as the cross-shore transport, modifies the shoreline. However they have different time scales. The cross-shore transport is significant in short periods, during storms and hurricanes, taking sand offshore (Komar 1998). In contrast, the longshore transport occurs during longer time scales.

### 4.3.5 Beach modification and beach management

The beach modification in Yucatán started in 1947 with the construction of Progreso pier. Initially, the pier was 2 km long but it later had two extensions: the first to 4 km and the second to 8 km, as it remains today (Figure 4.5).

*(a)* *(b)*

*Figure 4.6:* *(a)* Aerial photograph from 2002, taken four kilometres east from Progreso pier. *(b)* Location in Chelem where a protection system is being implemented in 2010.

The setting and removal of groynes is commonplace. During the 1990s, an uncontrolled number of groynes were set by householders in an attempt to retain the beach in front of their properties, without considering the consequences to the vicinity. An aerial survey in Progreso from 1984 shows the presence of 178 jetties along 8.8 km of shoreline (Meyer-Arendt 2001). Due to a large number of groynes set in an anarchic way, by

2005 the local council removed all groynes due to increased erosion. Instead, geotextile and reefballs were installed to protect vulnerable areas from further retreat. After five years, the expected beach recovery has not occurred (AXIS 2008).

Recently, the local council has tried to organise the setting of coastal structures to avoid the excessive use of groynes that cause downstream erosion, affecting neighbouring beaches. Figure 4.6 shows the sediment barriers set parallel and perpendicular to the shore in Chelem to capture the sediment moved by the cross-shore and alongshore transport.

Moreover, the buildings in Yucatán are located very close to the shoreline, creating a continuous boundary of buildings built on the top of the dunes, thus removing the coastal vegetation and dunes. The coastal dunes and vegetation are the natural protection of the beach (Komar 1998), so their removal makes the beaches even more vulnerable in the event of a storm or a hurricane (Figure 4.11 *(c)*).

### 4.3.6 Hurricanes

The potential for hurricanes in the case study area is a constant threat. Although it is not possible to predict whether hurricanes will pass close to the study area or not, the analysis of long records of hurricane tracks gives an estimate of which months have a higher likelihood of occurrence.

The hurricane season in the Atlantic extends from June to November. The National Hurricane Center (NHC) of the National Ocean and Atmospheric Agency (NOAA) monitors hurricanes and tropical storms. Their hurricane database is open to the public and they have records from 1958 to date of hurricane tracks, wind velocities and surges.

Table 4.2 shows the Saffir-Simpson Hurricane Scale (SSHS) which is used to classify the events according to wind velocity, linking the wind velocity and the damage produced in populated locations (NHC 2010). The SSHS can be used to get a broad es-

timation of surge levels, however this scale does not consider important variables such as the system size and local bathymetry. Therefore, it is recommended by the NHC (2010) to use the estimated surge levels with caution.

*Table 4.2:* Saffir Simpson scale (SSHS), which relates wind velocity and surge to a hurricane category number (NHC 2010).

| Hurricane category | Wind velocity in mph ($kmh^{-1}$) | Associated surge in ft (m) |
|---|---|---|
| H5 | >156 (>250) | >18 (> 5.5) |
| H4 | 131 to 155 (210 to 249) | 13 to 18 (4.0 to 5.5) |
| H3 | 111 to 130 (178 to 209) | 9 to 12 (2.7 to 3.7) |
| H2 | 96 to 110 (154 to 177) | 6 to 8 (1.8 to 2.4) |
| H1 | 74 to 95 (119 to 153) | 4 to 5 (1.2 to 1.5) |
| | Additional categories | |
| Tropical Storm | 39 to 73 (63 to 117) | 0 to 3 (0 to 0.9) |
| Tropical Depression | 0 to 38 (0 to 62) | 0 (0) |

Figure 4.7 shows statistics from 1944 to 2002 in the Atlantic basin. It indicates that the hurricane activity increases from June to August. September experiences the highest hurricane activity of the year. The mean of events per year is 10, of which 2.5 have an intensity of H3 or higher, three will develop into hurricanes, and four will remain as named systems (Table 4.2).

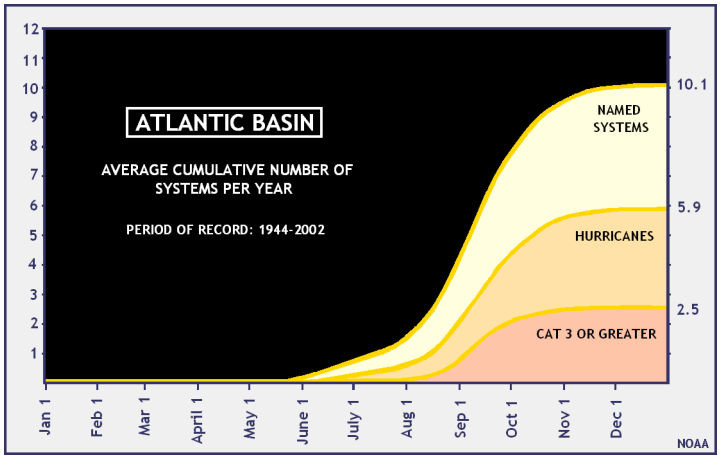


*Figure 4.7:* Acumulative average of hurricane frequency in the Atlantic basin per year, over a period of time from 1944 to 2002. Figure from NOAA-NHC (NHC 2010).

Figure 4.8 shows hurricane tracks that occurred in the Atlantic Ocean between 1954

and the present day. Typically, in a year there are frequent events of low intensities and a few very intense events. The few intense events can cause significant change in the beach morphology. In Yucatán the probability of a hurricane with intensity larger than four is highest in September.

The next paragraphs review two hurricanes that caused considerable damage to Yucatán beaches: Hurricanes Gilberto and Isidore.

Figure 4.8 highlights the tracks of Hurricanes Gilberto and Isidore. These two hurricanes had a direct impact on Yucatán, producing considerable damage to the area.

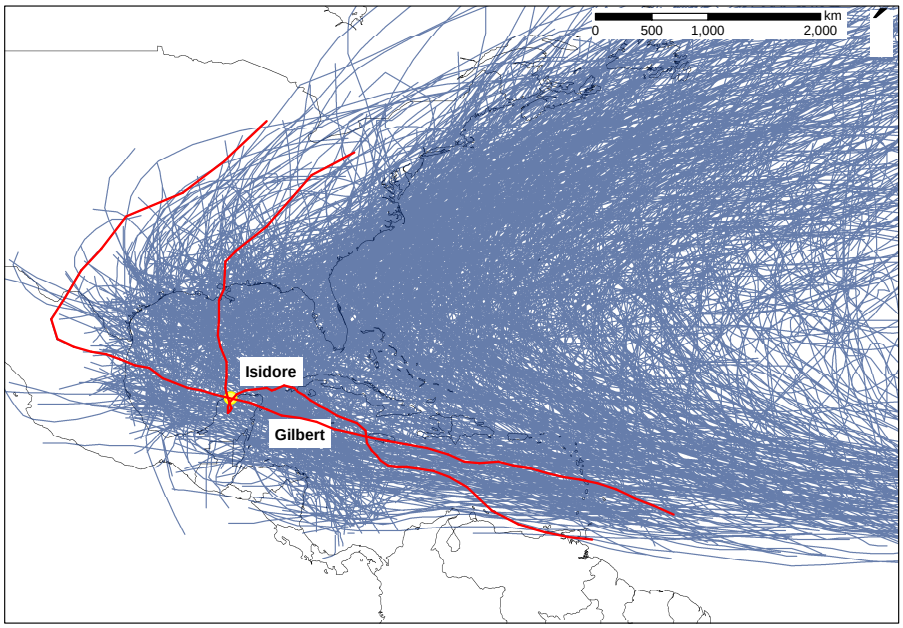


*Figure 4.8:* Hurricane tracks in the Atlantic basin since 1854 to date. The red line is the track of hurricanes Gilbert (1988) and Isidore (2002). The yellow circle highlights Progreso and its surroundings.

Hurricane Gilbert, H5, crossed the Yucatán Peninsula from east to west, passing over Telchac. The estimation of the surge levels was between four and six metres at the immediate coast near the hurricane. Two hundred people were reported dead and over 60,000 houses were damaged in the country. The main landfall was in Yucatán (NHC 1988). Local households said that all the properties located on the shore were totally

destroyed.

Hurricane Isidore, H3, remained in Yucatán for a few days, producing a storm surge of up to six metres in the southeast of Yucatán (NHC 2010). Local people from Progreso believe that after hurricane Isidore all the beaches have been greatly modified and may still not yet have recovered.

Figure 4.9 shows one of the inlets opened by Hurricane Isidore. Before its impact, the beach was in front of the house, which is now in ruins. During fieldwork for the current research project carried out in 2008 and 2010, it was observed that several inlets had remained opened since the hurricane. It is estimated that Hurricane Isidore produced a shoreline retreat of more than 50 m width in Santa Clara and Chelem, on the evidence of satellite optical images.

*Figure 4.9:* Location where Hurricane Isidore did direct impact in 2002 at Santa Clara, Yucatán. The photograph is from 2008.

The presence of hurricanes in the study area is relevant, especially because the typical waves are very small. However, during storms and hurricanes, larger waves from various directions will approach the shore, modifying the shoreline. Although the hurricane tracks are random, most of the hurricanes approach from the South and the Southeast,

moving either westwards and/or northwards, producing NE winds in Yucatán.

## 4.4 Case study description

This section describes the case study area used to validate SDS and to assess shoreline change in this research. The beach characteristics were assessed using images, *in situ* beach profiles and shoreline measurements carried out during fieldwork for this research project (see section 5.2.2 to 5.2.4 for further details of the *in situ* measurements).

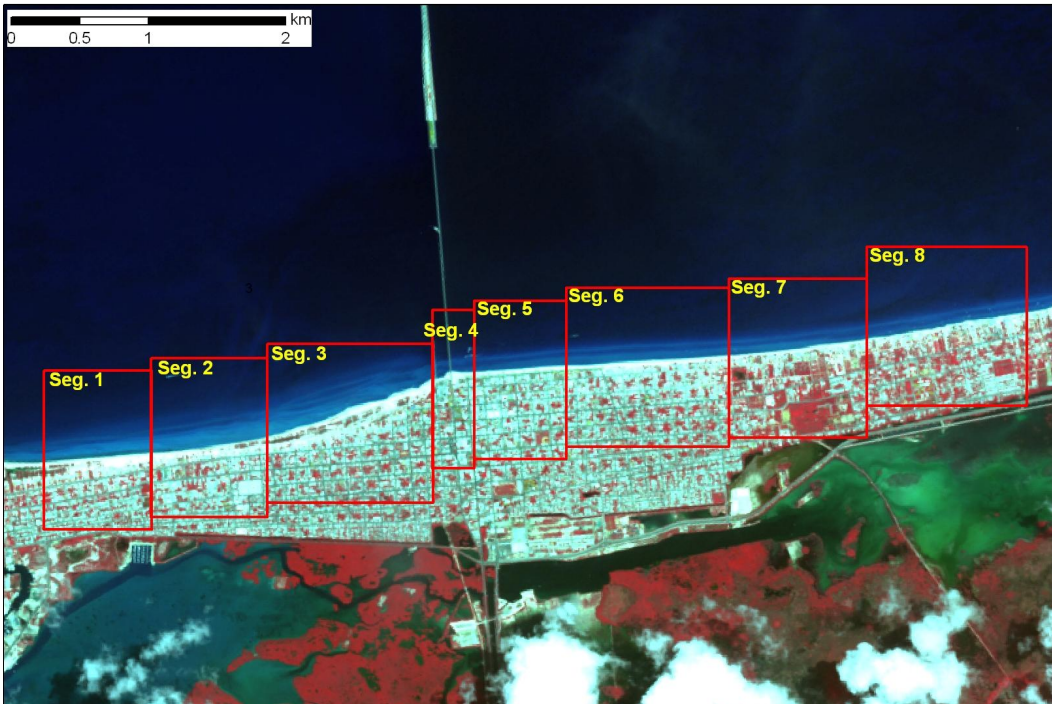


*Figure 4.10:* Shoreline segments on which the case study area was divided. The image is from July 12, 2010.

Figure 4.10 shows the case study area, located in Progreso, covering 8 km of shoreline. For the purpose of this study, the shoreline has been divided into eight beach segments according to morphology, rather than by their length.

### 4.4.1 Beach segments description

Table 4.3 shows the beach characteristics for the beach segments identified in Progreso. The beach segments can broadly be divided into two groups in terms of its relative

location to Progreso pier, with beach segments east and west of the pier. Segment 4 includes the two piers from Progreso, one 8 km long and the other 2 km. Segments 3 and 5, located next to the pier, are directly influenced by the pier. The differences within the east and west beach segments are mostly related to their distance from the pier (Figure 4.10).

*Table 4.3:* Beach characteristics of the beach segments from Progreso, the case study area. $\alpha$ is the shoreline orientation (Figure 4.12), $\beta$ is the beach slope in degrees.

| | West | | | | East | | | |
|---|---|---|---|---|---|---|---|---|
| | Seg.1 | Seg.2 | Seg.3 | Seg.4 | Seg.5 | Seg.6 | Seg.7 | Seg.8 |
| $\alpha$ (°) | 5 | 8 | 18 | 27 to -2 | 3.1 | 3.7 | 6.8 | 9.7 |
| $\beta$ (°) | 3 | 5 | 5 | 9 | 6 | 6 | 5 | 5 |
| Beach width (m) | 80 | 50 | 178 | 15 | 30 | 52 | 25 | 23 |
| $\bar{X}$grain size (mm) | 0.22 | 0.26 | 0.24 | 0.61 | 0.34 | 0.28 | 0.52 | 0.84 |
| Coastal vegetation | Yes | Yes | Yes | No | No | No | No | No |
| Coastal structures | No | No | No | Yes | No | No | No | No |
| Length (m) | 810 | 810 | 1,300 | 310 | 680 | 1,185 | 1,000 | 2,280 |

The beach characteristics for each beach segment are related to the pier located in the middle of the beach segments. The nearshore bathymetry for all of the eight segments is very shallow, with two metres depth at 100 m offshore. The approaching direction of the waves and wave height are similar along the eight beach segments. However, the coastal orientation, beach slope and beach width are different for the east and west beach segments, probably due to the alongshore sediment transport and cross-shore sand movements, making each segment different.

The presence of coastal structures and coastal vegetation is different between the east and west beach segments. The presence of coastal vegetation indicates how much a beach has been modified and is a guide to the vulnerability of a beach segment if a

storm or hurricane occurs.

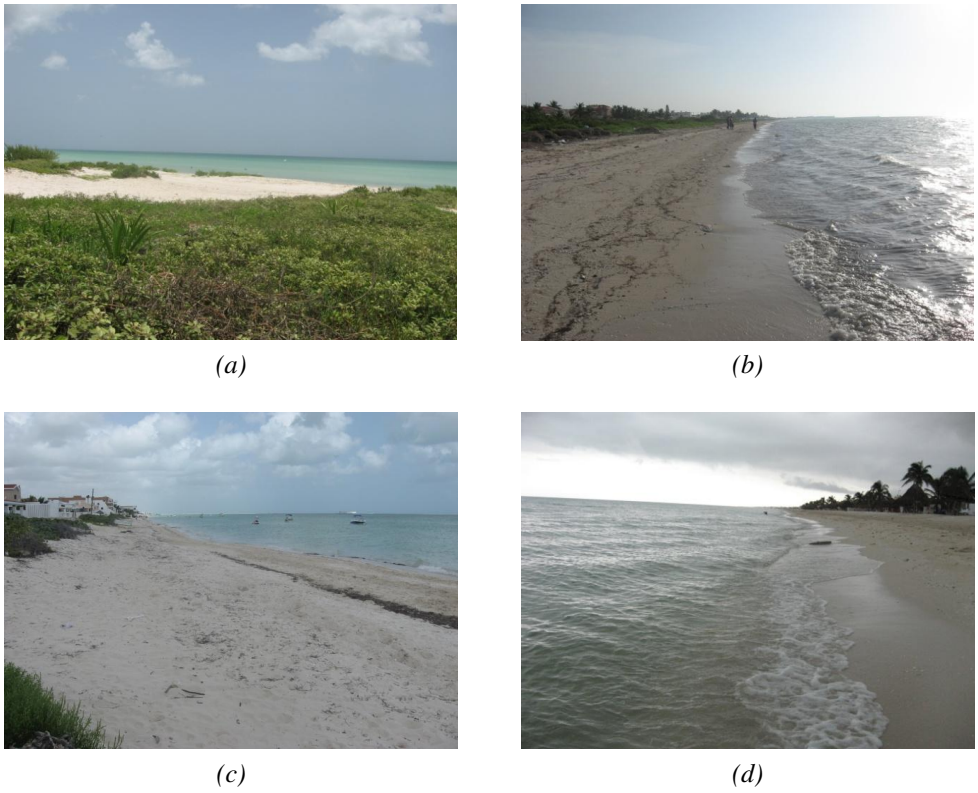

*(a)* *(b)*

*(c)* *(d)*

*Figure 4.11:* Photographs from segment 3 (a and b), segment 5 (c) and segment 8 (d).

Figure 4.11 shows photographs for the east and west beach segments. The west beach segments (1 to 3) have coastal vegetation and wider beaches ranging from 50 to 178m. Their beach slope is similar, ranging from 3° to 5°, with a mean grain size from 0.22 to 0.24mm. The coastal houses in these beach segments are not as close to the shore as they are in the east beach segments (5 to 8). Segment 4 is the shortest of the beach segments, it also includes two piers and it has the steepest beach slope (9°) and a narrower beach width (15 m). For the validation of SDS and shoreline change interpretation this beach segment has been kept separate, due to the presence of the piers and its abrupt change in the shoreline orientation. The east beach segments do not have coastal vegetation and their beach width is narrower, ranging between 30 and 52 m. The east beach

segments have houses very close to the shore, on the top of the dunes. Their beach slopes range between 5° and 6°, with a mean grain size between 0.28 and 0.84 mm. The mean sediment size has an alongshore gradient, the east beach segment has the largest grain size and the west beach segment has the smallest grain size, which is in agreement with a westward dominant longshore drift direction (see section 4.3.4).

### 4.4.2 Coastline orientation

The coastline orientation was estimated using a SPOT image from July 2010. The coastline orientation is relevant because it will affect the approaching waves to the shore and thus the littoral currents, which will modify the beach shape alongside other factors.

Figure 4.12 shows the measured angle ($\alpha$) to calculate the coastline orientation for each shoreline segment.

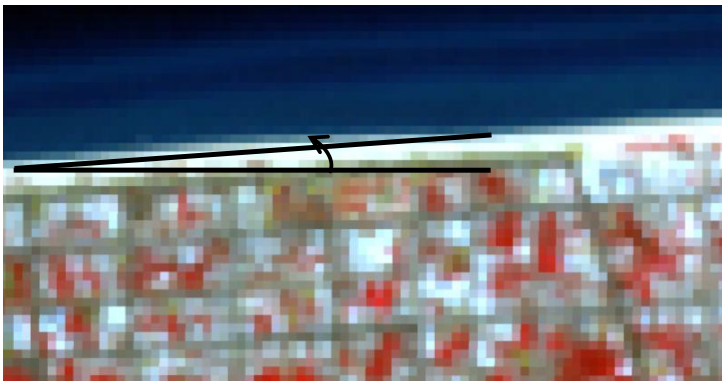

*Figure 4.12:* Schematic showing the angle measured to estimate the coastline orientation ($\alpha$) of each beach segment.

The coastal orientation changes from each beach segment in relation to its distance from the pier. The further the beach segment is from the pier, the larger the coastline orientation. Segments 3 and 4 show the largest effect of the pier. Segment 4 has two piers and an abrupt change in the shoreline orientation rotating from 27° (W facing) to -2° (E), it also has the steepest beach slope of all the segments. Segment 3 has the

largest overall coastline orientation of 18° (Table 4.3).

### 4.4.3 Type of sediment

The type of sediment on a beach is part of its general description. Sediment samples were taken from each of the eight beach segments within the inter-tidal zone. The mean grain size was estimated by the settling velocity of the sediment, measured in a settling tube. The samples were measured in triplicate for each shoreline segment and the mean grain size was determined using the method described by Ferguson and Church (2004). Table 4.3 shows the type of sediment found for each beach segment. The mean grain size corresponds to medium sand. The western beach segments have the finer sand (0.22 to 0.26 mm), whereas the eastern beach segments have medium sand to coarse sand (0.28 to 0.84 mm).

### 4.4.4 Beach slope and beach width

The beach slope is required to estimate the shoreline location at a given tidal level. In this research, the beach slope used to estimate the shoreline location is the inter-tidal slope, which is the slope in between the high and low water shoreline level in spring tide conditions. Different inter-tidal slopes will move the shoreline location either landwards or seawards. On shallow beach slopes, shoreline locations will reach shorewards in high tide conditions. In contrast, steeper beach slopes will have a smaller shorewards extent in high tide conditions.

Figure 4.13 shows the main components on a beach profile. It shows the location of an inter-tidal beach slope used to describe each beach segment from the case study area. Typically, beach profiles are steepest at the shore and the slope decreases progressively as the water depth increases in the offshore direction (Komar 1998).

The beach slope and beach width was estimated from *in situ* beach profiles measured on July $13^{th}$, 2010. One beach profile was surveyed for each shoreline segment. There-

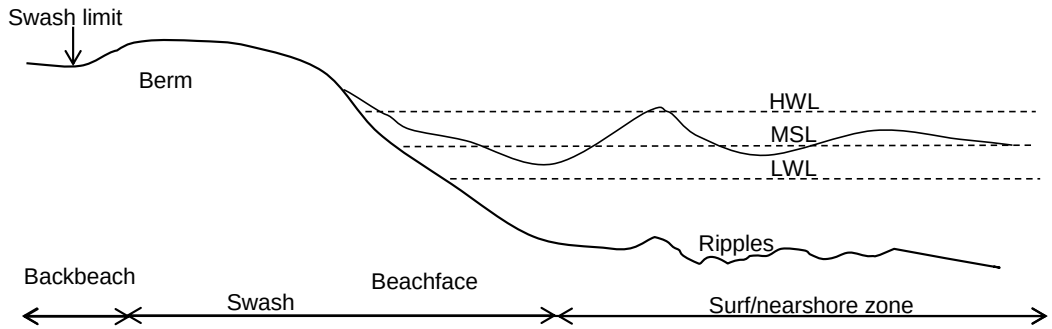


*Figure 4.13:* Diagram showing the main components of a beach profile.

fore, it was assumed that the inter-tidal beach slope is homogeneous within each beach segment. The low and high tides during spring tide conditions were used as a reference to calculate the beach slope of the inter-tidal region.

Table 4.3 shows the beach width and beach slope of the different beach segments. The beach profiles (see appendix) from segments 1 and 2 are very similar in shape. However, segment 1 has a better developed dune vegetation and shallower inter-tidal beach slope (3°), whereas segment 2 shows a deteriorated dune vegetation and a steeper inter-tidal beach slope (5°). Segment 3, although it has the wider beach, it has a shallow height (-13 m, see appendix) at the top of the beach, which is the result of the human modification for the development of houses next to the beach. The beach profile from segment 4, which has the two piers, is the narrowest (15 m) from all the beach segments. Furthermore, it does not have any dune vegetation, and the beach slope is the steepest (9°) from all the surveyed beach profiles. The beach profiles located towards the east of the pier show similarities. These beach profiles does not have any dune vegetation, the inter-tidal beach slope is similar (5° to 6°), and the houses are very close from the shoreline (< 50 m). Interestingly, the beach profile from segment 6 has the widest beach in relation to the rest of the eastern beach segments. However, this beach segment does not have coastal dunes, so, this could be probably the effect of a local convergence of the nearshore currents.

### Inter-tidal beach slope variability

The beach morphology shows changes over time. It is well demonstrated that the change of the beach slope has a strong relationship with the grain size and the wave condition. Furthermore, the beach slope responds to long-term trends due to decadal changes in the beach morphology (Komar 1998). In a location such as Progreso, where there is not a strong seasonality affecting the wave height and the approaching waves to the shore, the observed changes in the beach profile will be mostly driven by hurricanes and storms rather than by seasonal changes.

This section includes an estimation of the associated horizontal excursion, that could have occur with a variation of the inter-tidal beach slope over the year, considering the previously found difference (5 cm) between the measured tides and the predicted tides (see Figure 4.23).

Table 4.4 shows the shallowest estimated inter-tidal beach slope, using as a reference the estimated *in situ* beach slope. Because the beach profiles were carried out in July, where the meteorological and oceanographic conditions were calmed, is expected that the beach slope it was very close to the steepest point over the year. And, that the beach slope would reach their shallowest point in presence of hurricanes and storms.

*Table 4.4:* Observed *in situ* and estimated shallowest inter-tidal beach slope, and the associated horizontal excursion of 5 cm of difference between the predicted and measured tidal levels (see Figure 4.23.)

| Seg. | *In situ* beach slope ($\frac{dx}{dy}$) | Est. beach slope ($\frac{dx}{dy}$) | Horiz. excursion (m) | |
|---|---|---|---|---|
| 1 | $\frac{1}{19}$ | $\frac{1}{22}$ | 0.9 | 1.1 |
| 2 | $\frac{1}{11}$ | $\frac{1}{15}$ | 0.5 | 0.7 |
| 3 | $\frac{1}{11}$ | $\frac{1}{15}$ | 0.5 | 0.7 |
| 4 | $\frac{1}{6}$ | $\frac{1}{8}$ | 0.3 | 0.4 |
| 5 | $\frac{1}{9}$ | $\frac{1}{11}$ | 0.4 | 0.5 |
| 6 | $\frac{1}{9}$ | $\frac{1}{11}$ | 0.4 | 0.5 |
| 7 | $\frac{1}{11}$ | $\frac{1}{15}$ | 0.5 | 0.7 |
| 8 | $\frac{1}{11}$ | $\frac{1}{15}$ | 0.5 | 0.7 |

### 4.4.5 Section summary

The case study location is in Progreso, Yucatán (Figure 4.2). The coasts are sparsely populated, are subject to hurricanes every year (on average 10 per year) and exhibit shoreline erosion. Moreover, the shorelines have been highly modified and only a few locations have coastal dunes and vegetation.

The tides are diurnal (F=4.8) with a maximum range of 0.9 m. The bathymetry is very shallow with a wide continental shelf (> 100 km). Hence, the typical waves are wind generated with short periods (< 5 s), and when moving onshore the waves will align towards the wind direction.

The dominant wind direction (NE) does not significantly change through the year, except during storms and hurricanes. The wave behaviour in the region is episodic, with small wave heights reaching the shore (0.15 to 0.3 m) for most of the year and maximum wave heights, as large as one metre in height, during storms and hurricanes. The estimations from the alongshore drift suggests a westward direction, however local changes of its main direction may occur.

The case study area from Progreso was divided into eight segments based on their beach characteristics, such as shoreline orientation, beach slope, beach width, presence of coastal vegetation and structures (Table 4.3).

## 4.5 Data availability

This section describes the available satellite imagery and ancillary data for the region that will be used for further interpretation and analysis of SDS. The compiled data is the result of an extensive search using a number of resources, including online public domain archives and direct contact with researchers in charge of taking local measurements. Moreover, fieldwork data has been collected to understand the study area and the conditions of the tidal gauge in Progreso.

### 4.5.1 Satellite imagery available for Yucatán

The satellite images used in the current research have two main objectives. First, to validate SDS using simultaneous *in situ* shoreline measurements, and second to assess shoreline change in the case study area using SDSs.

To synchronise fieldwork with a satellite image, two images were programmed as close as was possible to the fieldwork conducted in 2008 and 2010. The providers of SPOT images give a window of time within 3 to 4 weeks to acquire an image of the study area. However, the precise time when an image is taken will depend on the weather conditions. The programmed images were directly bought from SPOT using funds from the University of Plymouth and funds from this project supported by the Consejo Nacional de Ciencia y Tecnologia (CONACYT), which is the Research Council of Science and Technology in México.

Access to historical imagery from the case study area was through the co-operation of Dr Ismael Mariño Tapia from the Physics Oceanographic department in Centro de Investigación y de Estudios Avanzados (CINVESTAV), the Research Centre of Advance Studies. CINVESTAV has open access for SPOT images thanks to an agreement with the Mexican Navy (SM), which allows the use of SPOT images of 10 m pixel size (MS) free of charge as long as the images are used for research purposes. Two

other images were acquired through the kind support of the Comisión Nacional Forestal (CONAFOR), the Forest Ministry of México, in aid of the development of the current research.

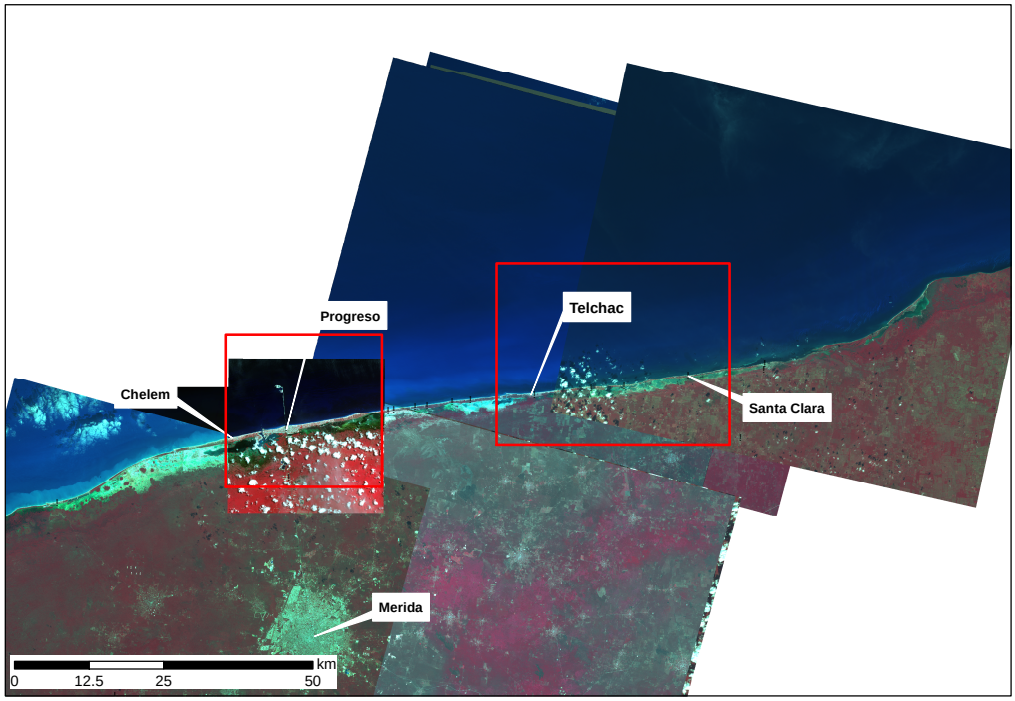


*Figure 4.14:* The largest number of available SPOT images for Yucatán are within the red square. The location of Progreso has 13 images and the location of Telchac have 10 images.

Figure 4.14 shows the location of the acquired images, which are the result of an extensive search in the SPOT archives. They were not taken at regular intervals over time, many of them are from the hurricane and storm season, and they also have slightly different spatial geographic locations.

Progreso and Telchac locations have the largest number of images in Yucatán. Progreso has 13 images and Telchac 10. Table 4.5 details their dates. The dates for the images in Progreso are better spaced, particularly for the years 2004 and 2005, whereas the images from Telchac will only allow the examination of 2004 in detail and sparse images in 2005, 2006 and 2007. In addition, Progreso has several man-made structures that are

*Table 4.5:* Dates of the available images in Progreso and Telchac, Yucatán.

| Dates | |
|---|---|
| Progreso | Telchac |
| 12/07/2010 | |
| 20/09/2008 | |
| 05/09/2007 | 05/09/2007 |
| 06/02/2006 | 06/06/2006 |
| 30/07/2005 | 17/07/2005 |
| 17/07/2005 | 11/01/2005 |
| 04/04/2005 | |
| 20/03/2005 | 23/12/2004 |
| 15/11/2004 | 21/10/2004 |
| 27/09/2004 | 11/09/2004 |
| 25/06/2004 | 17/04/2004 |
| 20/05/2004 | 09/01/2004 |
| 23/12/2003 | 04/01/2004 |

very likely to have an effect on the shoreline location. The analysis of Progreso might involve larger shoreline change, whereas Telchac might exhibit such a small shoreline change that it is not detected using SDS. The temporal spacing of the archived SPOT images is random and it depends on the previously requested images by users. These images are all the available images in Yucatán from the SPOT satellite.

The chosen case study area (Progreso) has 13 images overlapping each other, covering a time-span of 6.5 years. The years from 2004 and 2005 have more than one image per season, which allowed the exploration of the intra-annual shoreline change. In contrast, the years from 2006 to 2010 have only one image per year from the hurricane or winter season, with exception for year 2009, which allowed the assessment of inter-annual shoreline change (see chapter 6).

The exploration of these images during this time-span offers the possibility of assessing shoreline change in a place where there are no other studies covering this geographic area and time scale.

### 4.5.2 Ancillary data

This section introduces the ancillary data, the location where the measurements were taken, the type of measurements and the time-spans that they cover. The ancillary data was also examined to describe the case study area in more detail. The second section assesses the tidal measurements using predicted and *in situ* measurements.

Ancillary data is required for the interpretation of shoreline location and shoreline change over time. The data included as ancillary data are: winds, waves, tides, hurricanes, bathymetry, beach profiles and surge levels.

Table 4.6 shows a summary of the ancillary data. The ancillary data is from different sources therefore each data source has different characteristics. They also originate from different locations within the region. Some of the data is available in the public domain, whereas some has been provided for the purpose of this research.

**Wind**

There are two data sources for the wind. The first of these is from the CINVESTAV at Merida and at Telchac, which are measurements with the highest temporal resolution (approx. every 10 mins). These measurements started in 2008 and they are available in the public domain. The other data source is from Progreso pier, with measurements from 2003 to 2008. This time series has hourly measurements, however the time series is not complete. The years from 2005 and 2006 have the longest record, with hourly spacing (Table 4.6).

The calm season occurs predominantly between March and May. The main direction is from the northeast and east with velocities up to 20 $\text{kmh}^{-1}$ with an average of 10 $\text{kmh}^{-1}$ (in 2005-2006).

The hurricane season, from June to November, is when most of the rainfall takes place in the region. The main direction is from the northeast and east with velocities up to

*Table 4.6:* Summary of the available data of the existing ancillary data from the study area, the time-span covered and a description.

| | Period of time | Description |
|---|---|---|
| **Waves** | 2008 (from Apr. to Jul., Oct. to Dec.)<br>2009 (Jan. to mid Feb.) | Acoustic wave and current profiler (AWAC) at 10 m depth at Telchac. |
| | Nov. 2003, 7-19 May 2004, 7-19 Sept. to Dec. 2006 | Progreso harbour data at 5 m depth. |
| | 1997 to date | NOAA buoy (42001) at 3,365 m depth. |
| **Modelled waves** | 1947 to 2007 | Wave prediction model considering cyclones (WAM/HURAC). |
| **Tides** | June 1999 to date | Predicted tides from CICESE<br>Measured tides from SM at Progreso pier (4 km offshore). |
| **Winds** | 2008 to date | Telchac and Merida, meteorological station from CINVESTAV. |
| | Dec. 2003 to 2008 | Measured at Progreso harbour, they are not a complete time series. Years 2005 and 2006 are the most complete. |
| **Hurricanes** | 1958 to date | Wind velocity, track, atmospheric pressure, Saffir-Simpson category. |
| **Bathymetry** | Charts from 1993, 2001, 2005, 2009 from Progreso | Covering the vicinity of the pier |
| | Bathymetry covering the south from the Gulf of México to Yucatán | Contours each 200 m, interpolated every 50 m. |
| **Storm surge** | Probabilities model (NHC 2010), for the north of the Gulf of México. | Probabilities geographically solved. |

25 $kmh^{-1}$ and an average of 7 $kmh^{-1}$ (in 2005-2006). However, the wind velocity and direction can vary during a hurricane. The average of the winds shown here does not represent well the sudden change of direction and velocities that the winds can have

when a hurricane is in the region.

During the winter season, from December to February, incoming low pressure systems from the Gulf of México produce storms. Without the presence of storms, the winds come from the east and eastnortheast but in storm conditions the direction changes towards the north. The velocities are up to 20 $kmh^{-1}$ and an average of 8 $kmh^{-1}$ (in 2005-2006).

### Waves

There are waves measured from deep water conditions (3,365 m depth) and shallow water conditions (10 and 5 m) from sparse periods of time. Moreover, there are waves modelled in deep water conditions throughout the period between 1947 to 2007 (Table 4.6).

The measured waves in deep water and shallow water conditions are not simultaneous in time. However, the available data includes different seasons through the year, allowing assessment of how the significant wave height (Hs) varies with depth (Table 4.6).

The next paragraphs describes the Hs and significant wave period(Ts) through the year using the measured wave record.

### Waves in deep water conditions

NOAA has a network of buoys in deep waters of the Gulf of México, which have been recording wave data since 1996. The closest buoy to Yucatán (No. 42001) is at 25° 53' 16.8" N and 89° 39' 28.8" W, at a depth of 3,365 m and at more than 200 km offshore from Progreso. It has been gathering information since 1996. The modelled waves are from a grid point (21° 30' N and 90° W), with a temporal resolution of one minute, covering a footprint of 1 $km^2$, at an approximate water depth of 45 m, about 50 km offshore. Figure 4.3 shows the geographical location of this data.

Figure 4.15 *(a)* and *(b)* shows the range of Hs and Ts respectively, as measured by the NOAA station since 1996. The largest Hs and Ts within a year is from October to March, with a range between 0.5 and 2.2 m and with Ts between 4 and 6 s. Although waves with Ts larger than 8 s have been recorded, these events are not frequent.

The waves measured offshore confirm that the overall wave climate is episodic, characterised by an overall small Hs and short Ts, with the presence of large waves during storms and hurricanes. The hurricane season demonstrates the largest Hs and Ts

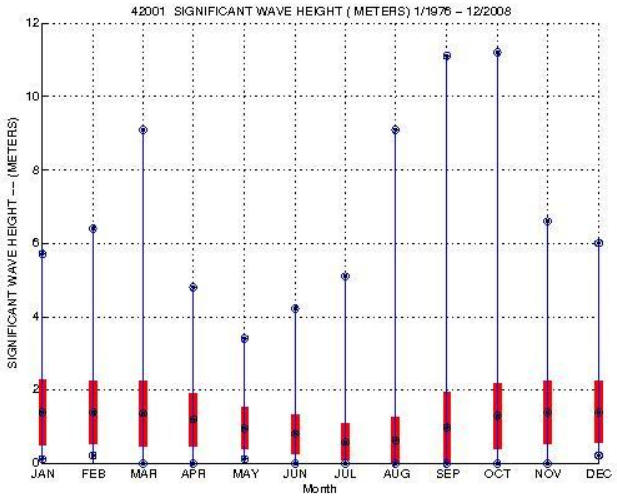


*(a)*

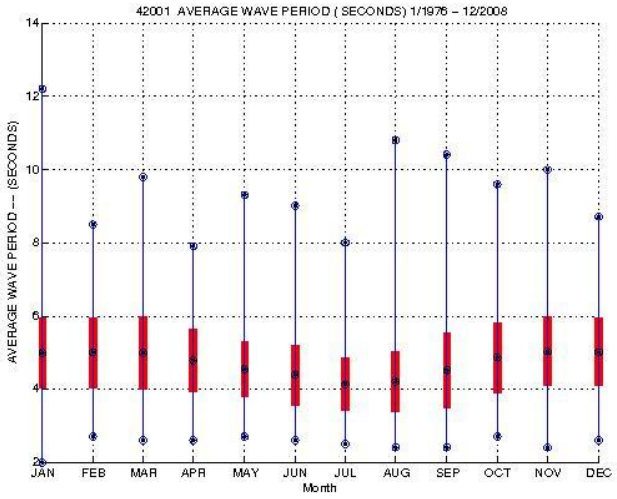


*(b)*

*Figure 4.15:* Hs(a) and Ts (b) from the buoy 42001 from 1976 and 2008. The $\bar{X}$ and SD (red bars) and max. and min. recorded heights (blue). Figure from NOAA (2011)

variability, whereas during winter large waves regularly occur. The modelled waves indicate that the dominant direction of the waves is between NNE and E.

### Waves in shallow water conditions

Waves in shallow water conditions were measured in 5 and 10 m depths. The measurements at 10 m depth are from Telchac at about 8 km offshore. Figure 4.3 shows the geographical location of the measurements. The measurements from five metres depth are from Progreso at about four kilometres offshore from the pier. The measurements from Progreso and Telchac include measurements from winter, hurricane and calm conditions (Mariño-Tapia 2010).

Table 4.7 shows the minimum, mean and standard deviation of Hs and Ts at 5 m and 10m depth in different seasons. The main direction of the incoming waves is from NNE to NE, which matches the direction of the offshore waves and the winds, showing that the wind direction can indicate the wave direction of wind generated waves.

*Table 4.7:* Statistics of the measured waves in shallow water conditions at 5 and 10m depth in Telchac and Progreso respectively. Data from Ismael Mariño-Tapia.

| Depth (m) | | | Calm | Hurricane | Winter |
|---|---|---|---|---|---|
| | | | March to Jul. | Jun. to Nov. | Dec. to Feb. |
| 10 | Hs, Ts | Min | 0.2, 1.67 | 0.08, 1.42 | 0.19, 1.97 |
| | | Max | 1.37, 9.63 | 2.1, 10.89 | 1.83, 11.5 |
| | | $\bar{X}$ | 0.6, 3.82 | 0.58, 4.64 | 0.71, 5.33 |
| | | SD | 0.19, 1.15 | 0.29, 1.7 | 0.29, 1.96 |
| 5 | Hs | Min | 0.18 | 0.17 | 0.17 |
| | | Max | 0.35 | 0.57 | 0.54 |
| | | $\bar{X}$ | 0.25 | 0.31 | 0.33 |
| | | SD | 0.04 | 0.08 | 0.07 |

Figure 4.16 highlights the difference in wave heights in deep water and shallow water conditions. The waves in shallow water are much smaller than in deep water. This is due to the wide shelf in Yucatán and because the waves reaching the shore are mostly wind generated. The shoaling coefficient from deep waters to 10 m depth is between 0.5 and 0.6 and the waves decrease in height from 5 to 10 m depth, with a shoaling coefficient of 0.41 to 0.58 from 10 to 5 m depth. A shoaling coefficient of this magnitude

fits with the shallow bathymetry in Yucatán and with wave measurements recorded in other regions of the Gulf of México, with waves of 1.8 m height at 3,474 m water depth and waves 0.68 m height at less than 10 m water depth (Defne et al. 2009).

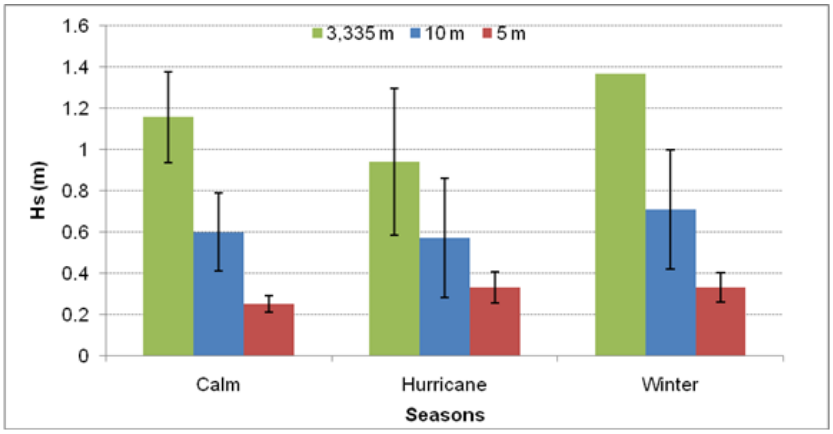


*Figure 4.16:* Wave height in deep water conditions (3,335 m) in the Gulf of México and in shallow water conditions, at 10 m and 5 m, in Telchac and Progreso respectively. Data from NOAA and (Mariño-Tapia 2010)

During the wave measurements from July 2008, three tropical storms took place Bertha, Dolly and Cristobal (see appendix). Tropical storms Bertha and Dolly passed too far away from Telchac to detect a change in the water levels. Tropical Storm Dolly, in contrast, crossed Yucatán on July $21^{st}$, 2008 at about 6-7 am (local time), with a wind velocity of 83 $kmh^{-1}$ and an atmospheric pressure of 1005 hPa (Figure 4.17).

Figure 4.18 *(a)* and *(b)* show that on the $20^{th}$ at about 3 pm, the Hs increased from 0.44m to 0.94 m with a Ts of 4.4 s. By the $21^{st}$ (9 am) longer period waves had developed, increasing from 5 to 10.8 s, with Hs of 0.65 m. The relatively large waves only lasted for 6 hours, showing that the waves from hurricanes dissipate in a short period of time.

The presence of large waves in storms and hurricanes is characteristic of this region. Therefore, it is not clear whether the shoreline retreat is due to the presence of storms and hurricanes or man-made coastal structures. The shoreline change assessed using SDSs (chapter 6) considers both factors to deduce the processes involved. It is impor-

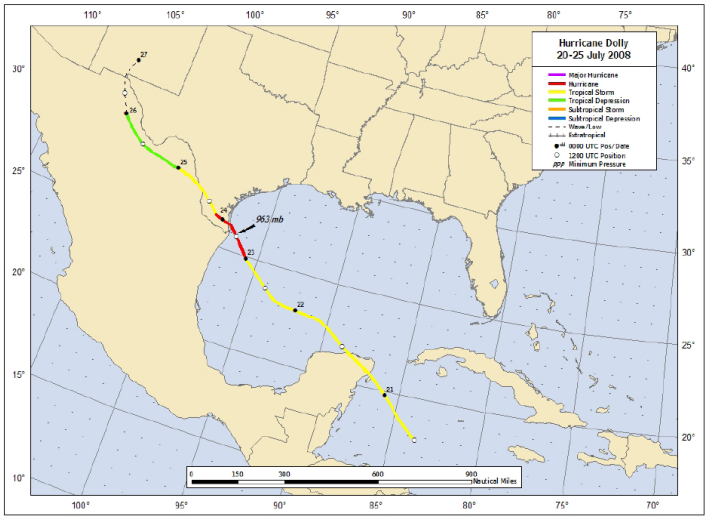


*Figure 4.17:* Track of Hurricane Dolly (20-25 July, 2008) (NHC 2010).

tant to mention, however, that the value of the available data about waves is limited, with no long time series of wave measurements close to the shore during the same periods as the assessed shoreline change.

## 4.6 Assessment from the measured tides

The estimation of the tidal level of the SDSs is important in this research. In Yucatán there are no long systematic tidal measurements available in the public domain. However, the Mexican Navy is attempting to produce a systematic record of the tides. Their measurements were compared against independent measurements carried out for this research in Telchac and against predicted tides to assess their value for further use in this research.

This section first describes the three tidal records. Secondly, the Mexican Navy tidal record is examined in terms of datum changes, failures of equipment, or any other indications of inconsistencies in the record. Thirdly, the measured tides from Telchac are compared against the predicted tides. This comparison gives information about the quality of the tidal predictions and tidal measurements by the Mexican Navy. This

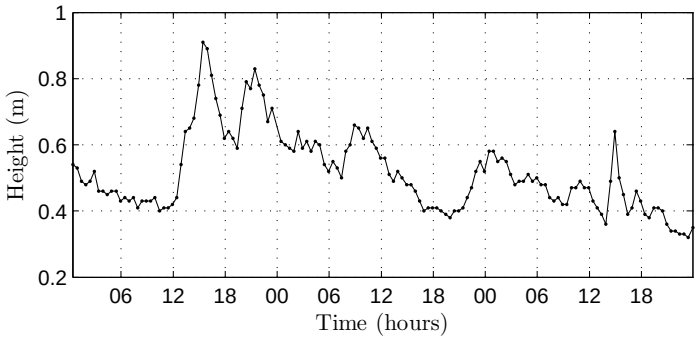


*(a)*

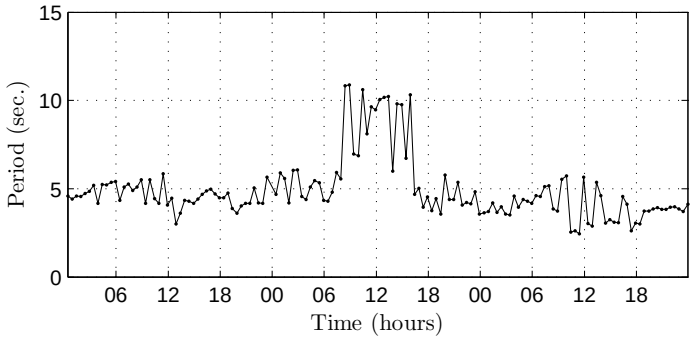


*(b)*

*Figure 4.18:* Measured wave height (a) and period (b) in July 20 - 22, 2008, at 10 m depth in Telchac. Data from Ismael Mariño-Tapia.

comparison allows assessment of the best tidal record to use in terms of consistency and accuracy in order to assess the tidal levels in SDSs.

### 4.6.1 Measured tides in Progreso

Figure 4.19 shows the equipment used by the Mexican Navy to record the tides. The tidal gauge is located on Progeso pier at 21° 18' 11.2" N, 89° 39' 59.13" W at 8 m depth, using a pressure sensor and a data logger model 3624M Aaderaa. Measurements are taken hourly. The equipment has been adapted to compensate for the atmospheric pressure by using a balloon, in an attempt to measure the hydrostatic pressure rather

than the total pressure.

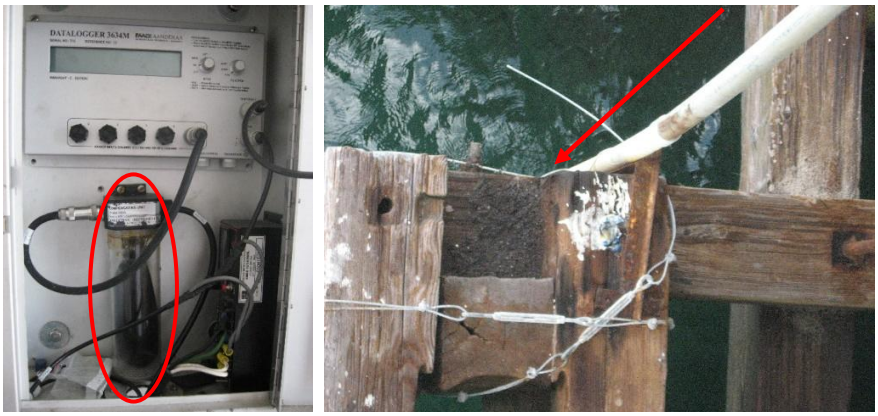

*Figure 4.19:* Left:Datalogger model 3624M Aanderaa. The red circle shows the balloon used to compensate for the atmospheric pressure. Right: Location of the sensor fixed to Progreso pier.

### 4.6.2 Measured tides in Telchac

The measurements collect from Telchac as part of the current study were carried out using a data logger RBR model TWR-2050, recording total pressure every 10 mins between July $12^{th}$ and August $4^{th}$ 2010, measuring the tide over spring and neap tides. The sensor was installed on the leg of a pier. Its position was recorded using the DGPS in a static mode. Its position is at lat. 21° 20' 26.4" N and at long. 89° 18' 27.8" W and at a height referred to the ellipsoid (WGS84) of -15.25 m, deployed at 1.6 m water depth below the HWL.

The instrument was deployed at that location to ensure the safety of the equipment. Figure 4.20 shows where the instrument was deployed. There is a 40 km distance between Progreso and Telchac however, due to the homogeneity of the region and the large spatial scale of the tide (> 100 km), no changes in the tide are expected to occur between Progreso and Telchac, apart from a local effect related to the harbour.

*Figure 4.20:* Location where the datalogger was deployed in Telchac harbour (red spot).

### 4.6.3 Predicted tides

The predicted tides are processed by González et al. (2010) from the research centre Centro de Investigaciones Científicas y de Estudios Avanzados de Ensenada (CICESE). The predictions are available in the public domain. The predicted tides are calculated using input data measurements from Universidad Autónoma de México (UNAM) and the Mexican Navy, collected over 20 years.

### 4.6.4 Results

**Progreso measurements assessment**

Figure 4.21 shows the measured tides overlapped with the predicted tides from 1999 to 2008. Both records use the same tidal datum as a reference, the MLLWL (known locally as BMI), but the local BMI has been estimated using different time series. Therefore, there is a difference of approximately four centimetres between the BMI from the Mexican Navy and the predicted tides. The estimated BMI from the predicted tides is at a lower water depth than the measured tides. This difference could be an error due to the constant change of the equipment and the attempt of the Mexican Navy to remove the atmospheric effect from the observed water level.

Both tidal records agree on tidal phase during spring tides and, overall, their tidal range is about the same magnitude. However, the measurements are larger than the predicted tide.

The assessment of measured tides shows that the tidal record has several offsets of different magnitudes, failures in the equipment, as well as plenty of gaps lasting from a few days to several months.

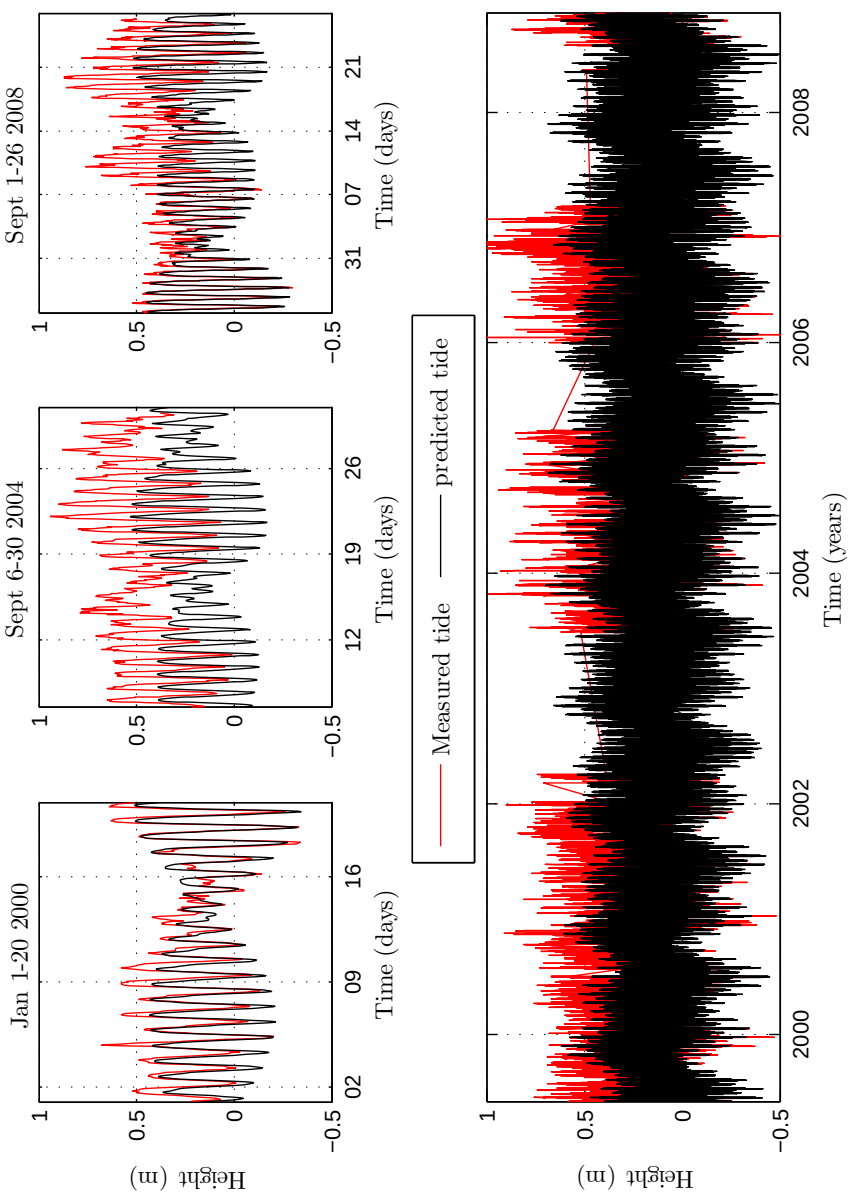


*Figure 4.21:* Measured and predicted tide in Progreso from 1-20 January 2000 (a), 6-30 September 2004 (b), 1-26 September 2008 (c).

Figure 4.22 shows a histogram of the tidal residual between the measured tide and predicted tide at Progreso. The mean difference between the measured tide in Progreso and the predicted tide is 14 cm, with a SD of 11 cm and with maximum residuals of 80 cm and minimum of -39 cm. The magnitude of the residuals is much larger than the tidal range at Progreso.

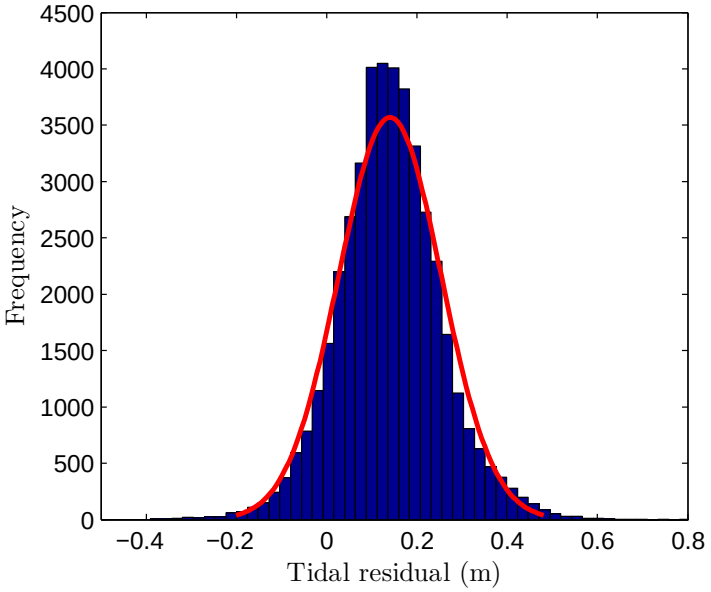


*Figure 4.22:* Histogram of the tidal residuals between the measured tide in Progreso and the predicted tide. The red line adjusts to normal distribution ($p<0.01$).

The differences identified between the measured and predicted tides are the result of failures in the equipment and meteorological effects. The failures in the equipment are revealed by isolated abnormal data (sudden jumps), offsets and progressive differences. Stable offsets could be, in principle, possible to correct. However, the offsets change in magnitude over time. The progressive difference between the measured and predicted tides has to be interpreted by considering their length in time, in order to differentiate whether the progressive difference is due to a failure in the equipment or to a surge. Surges do not occur for longer than one to two days and they occur with a change in

the atmospheric pressure. Therefore, the examination of changes in the atmospheric pressure and their duration gives guidance on whether the difference is due to a surge or to a failure in the equipment.

Figure 4.21 (a), (b) and (c) show some examples with the most common types of offset detected in the tidal measurements, spanning from 1-20 January 2000, 6-30 September 2004 and 1-26 September 2008 respectively.

From 1-20 January 2000 there is an overall good fit between both measurements, although there is a 10 cm difference between the measured and predicted tides that remains constant, as well as abrupt changes, for example of 20 cm on the $5^{th}$ in spring tide conditions and on the $12^{th}$ in neap tide conditions. The offset between the records might be related to a difference in the datum used as a reference, which can be corrected. However, the sudden jumps in the measurements, occurring in spring and neap tides, suggests that the difference between both records is related to a failure in the equipment which cannot be corrected and is not related to a real change in the water levels (Figure 4.21 (a)).

From 6-30 September 2004 there is a gradual increase in the measured tides. Moreover, the measured tides show an offset of approximately 25 cm from the predicted record. The gradual increment is between 0.15 and 0.50 m, over a period of 24 days. During that time, Hurricane Ivan (see appendix) was passing over the Gulf of México, from the $2^{nd}$-$24^{th}$. However, the gradual increment in the measured tide is slightly longer (2 days) after Hurricane Ivan was in the Gulf of México. Moreover, Hurricane Ivan was relatively close to Yucatán from the $12^{th}$-$16^{th}$ and by the $16^{th}$ Hurricane Ivan was further inland towards the north of Florida. Therefore, the increase in the observed tides related to Hurricane Ivan and lasting from the $6^{th}$-$30^{th}$ seems unlikely. However, the difference observed from the $12^{th}$-$16^{th}$ might be the result of a surge. The inverse barometer effect explains up to 20 cm of this difference, a magnitude that could in-

crease when considering the wind effect over a surge. Unfortunately, the difference between the measured and predicted tides is a mix of a failure of the equipment and the likely occurrence of a surge. There is no indication of how to correct the measured data because the observed difference between both records has a different magnitude than the 10 cm previously found. Therefore, the quantitative use of this measurement as reference would not be reliable, considering that the difference between the measured and predicted tide is not a constant offset but shows a variation with time (Figure 4.21(b)).

Overall from 1-26 September 2008 there is a good fit between the measured and predicted tide but with a further increase in the measured tides after neap tides. Hurricane Ike (see appendix) was in the vicinity during the $9^{th}$-$12^{th}$. The difference between both records decreases and increases in synchrony when Ike was in the vicinity, with magnitudes of 40 cm and with a further decrease by the $15^{th}$, when Ike was further north suggesting that the difference between measured and predicted tides could be due to a surge related to Hurricane Ike. However, after the $15^{th}$ there is a progressive difference between both tidal records that does not agree with Hurricane Ike, suggesting that the latest observed difference is likely to be due to a failure in the equipment as observed in the previous example. The *in situ* shoreline measurements carried out on the $9^{th}$ suggest that the water depth at the shoreline level was three times larger than the predicted tides (see chapter 5), which agrees with the difference observed here between the measured and predicted tides. Moreover, a surge of about this magnitude (50 cm) was measured in Pensacola, Florida (NHC 2010), when Hurricane Ike was about the same distance from Yucatán (500 km) and this is further evidence that the first difference between the measured and predicted level is due to a surge (Figure 4.21 (c)).

The examples described here show that the measured tides exhibit differences from the predicted by as much as half of the tidal range in the study area due to changes in the datum and failures in the equipment. Some of the differences, however, could

be due to real changes in the water levels. Unfortunately the conclusion must be that the measured tides can only be useful qualitatively, even after taking into consideration atmospheric pressure, because their error can be as large as 50 % in the estimation of the water levels.

### 4.6.5 Predicted tide and measured tide in Telchac

This section compares predicted tides and measured tides from Telchac. This comparison allows identification of how well the predicted tides fit into tidal measurements, as well as the effect of meteorological conditions on the measured tides. Differences in height between measured and predicted tides could occur because the location of the datalogger was inside the harbour, where changes in tidal levels outside and inside the harbour could cause strong tidal currents. However, this is unlikely to occur in a location with microtidal conditions.

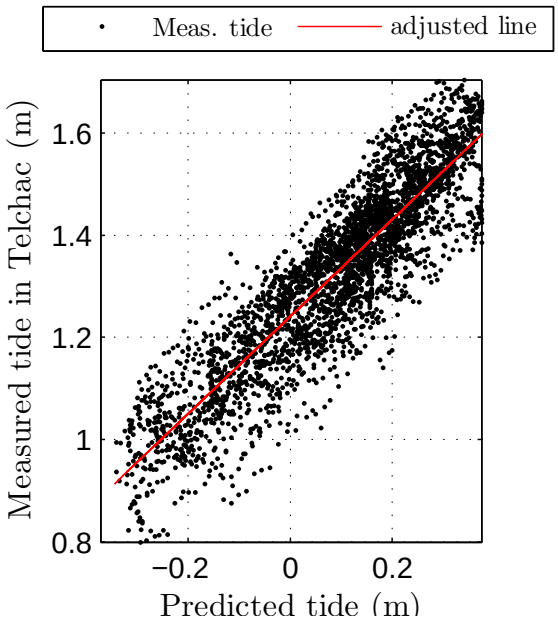


*Figure 4.23:* Predicted and measured tide in Telchac, Yucatán, México. The adjusted line (red) has a gradient of 0.95 and a constant of 1.24, with a $r^2$=0.8, df=3300.

Figure 4.23 shows the predicted against measured tide, which adjusts well into a line, with a gradient of 0.95, meaning that the measured tides are larger than the predicted tides by 5 %. The intercept of 1.24 m was used to overlap both records. This intercept indicates the difference between the datum from the predicted and measured tides.

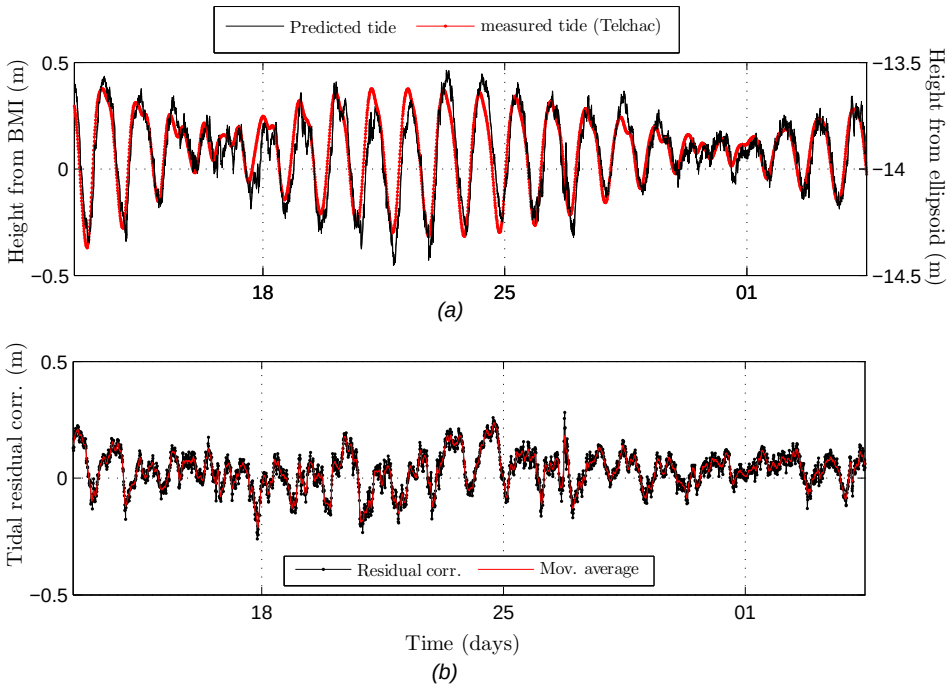


*Figure 4.24:* Measured tide in Telchac and predicted tide overlapped (a) Residual between measured tides in Telchac and predicted tides (b).

Figure 4.24 *(a)* shows that the predicted and measured tides fit well when considering phase, only showing small differences in the phase on the $18^{th}$. The predicted tides in spring tides are symmetrical and have a smaller tidal range, whereas the measured tides seem asymmetrical, during the $21^{nd}$ to $22^{nd}$ the low and high water level is smaller than predicted, particularly the low water level.

The measurements have been referred to the same datum as the predicted tides use for a reference (BMI). Furthermore, the height of the measured tides were estimated using

the DGPS measurements as a reference at the location of the datalogger, information that would allow comparison of the measured height *in situ* at the shoreline levels with the measured tide (see chapter 5). This comparison shows that the zero does not fit to the MLLWL. The BMI is very close to the mean water level rather than the MLLWL.

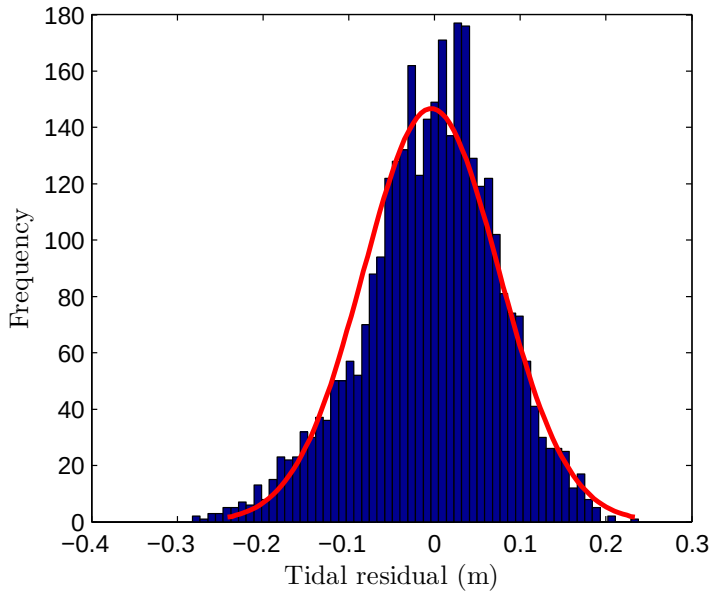


*Figure 4.25:* Histogram of the tidal residuals between measured tides in Telchac and predicted tides. The red line shows the fit into a normal distribution, with a p<0.01 and a k=0.42.

Figure 4.24 *(b)* shows the residual between measured and predicted tides corrected to a standard atmospheric pressure. Overall, the predicted and measured tides agree in the phase, following the same shape through the spring-neap cycle ($\bar{X}$=0.004, SD=0.079). However, there are residuals as large as 10 and 30 cm with a diurnal periodicity, suggesting that some diurnal constituents have not been considered in the tidal predictions or that their tidal amplitude underestimates the observed amplitude.

Figure 4.25 shows that the histogram of the residuals follows a normal distribution (k=0.42, p< 0.01). Most of the residuals (86 %) range between -11 and 13 cm in magnitude. The larger residuals (> 20 cm) are at low and high water levels. The mean

residual is positive, showing that overall the measured are higher than the predicted tides as has been previously discussed in this section.

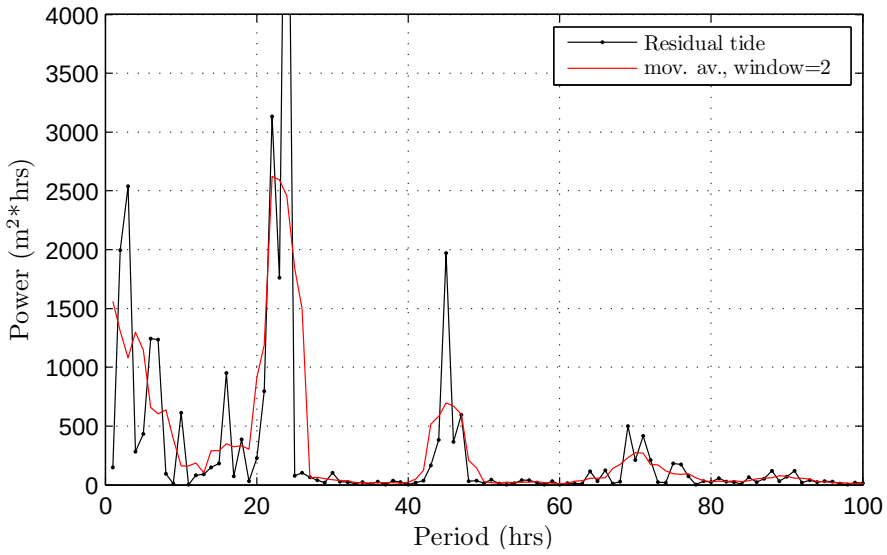


*Figure 4.26:* Fourier analysis of the tidal residuals between the predicted and measured tides in Telchac, Yucatán, México. The red line is a smoothing using the moving average with a window size of 4.

Figure 4.26 shows that the residuals have a periodic signal, with one peak between 22 and 25 hrs and another one between 44 and 47 hours. The first peak has a periodicity of a lunar diurnal constituent and the second peak can be related to a solar-lunar diurnal constituent, which are not considered in the tidal predictions. The Fourier analysis also shows the presence of high power in the lower frequencies, which could be associated with the lower pressure systems occurring during the measurement period. During the $18^{th}$ and from $21^{st}$ to $22^{nd}$ there is a negative residual. However, these dates does not agree with TS Two and Bonnie, both occurring on different dates in July (see appendix). Therefore, the negative residual could be due to a prevailing low pressure system in the region.

Comparing the measured tides (Progreso and Telchac) in relation to the predicted tides

shows that the measured tides from Telchac (min. -0.23, max.0.28 m) have a smaller difference than the measured tides from Progreso (min. -0.4, max. 0.8 m). The difference between measured tides in Progreso and predicted tides is as large as the tidal range. However, comparing the simultaneous record measured at Progreso shows that both measurements have the same phase but the measurements at Progreso are much larger in magnitude. The slope between the predicted and measured tides is 1.3, which is 30 % larger than the slope between predicted and Telchac measurements. This difference is very likely to be due to the balloon used in an attempt to measure hydrostatic pressure rather than total pressure. However, this balloon introduces a source of error in the measurements. It also does not allow systematic and consistent measurements in the water levels to be obtained because it constantly has to be replaced. This simultaneous measured record leads to the conclusion that, although the tidal measurements from the Mexican Navy show some improvement with time, the data still show inconsistencies, with differences due to the defined datum and general failures in the equipment.

The difference between measured tides in Telchac and predicted tides shows that predictions underestimate the tidal amplitude or that some diurnal tidal constituents have not been included in the predictions, as the high power at a diurnal frequency shows. However, although the predicted tides do not include all the diurnal constituents, the high and low tides are well phased and the largest difference in the predicted tidal amplitude with observed tides occurs at spring tides.

The most important feature is that the predicted tides do not have changes in their datum, therefore it is a systematic record in relation to the measured tides from Progreso. The tidal measurements from Progreso have to be considered cautiously. Their value is more qualitative than quantitative. Therefore the predicted tides is a better estimation of the tidal levels. The disadvantage of using predicted tides rather than measured tides is that the presence of surges would not be detected. However, the NHC provides

measurements and estimates from different locations with surges. Moreover, SDS that are likely to have the effect of a surge can be treated with appropriate caution, avoiding their use as much as is possible.

The tidal assessment allows for a number of recommendations that could improve the quality of measurements in the region. The recommendations are highlighted in section (4.7).

## 4.7 Recommendations

### 4.7.1 Tidal measurements and tidal predictions

**Tidal measurements**

The Mexican Navy needs to improve the tidal measurements in Progreso. Although the Mexican Navy have devoted time and resources to producing systematic tidal measurements, the current function of the tidal gauge at Progreso does not ensure systematic measurements. In order to achieve this it is recommended that:

1. The balloon should be removed from the pressure sensor. The balloon was installed to measure hydrostatic pressure rather than total pressure, however it produced non-systematic changes in the tidal range and drift in the mean pressure level. The atmospheric effects on the water level are possible to correct using direct atmospheric measurements, whereas the errors in the tidal measurements due to the balloon are not. Therefore, the use of the balloon produces an unfortunate loss of data.

2. The back up system has to be improved by investing in higher capacity data storage equipment to avoid data being re-written by the instrument or by taking measurements with a lower temporal resolution (e.g. 30 mins).

3. The removal of the equipment during cyclones should be carefully evaluated and, if possible, a tidal gauge should be installed which can continue to operate during hurricanes.

**Tidal predictions**

The tidal predictions from Progreso are mostly well phased in relation to measurements. However, the tidal amplitude under-estimates the observed tides, particularly during spring tides. Therefore, further development of accurate predicted tides is recommended, based on reliable tidal measurements.

## 4.8 Conclusions

1. Due to the problems with erosion seen since Hurricane Gilbert in 1988 and the annual occurrence of hurricanes, the case study area of Progreso is a good opportunity to explore shoreline change using satellite-derived shorelines, applying the method developed in this research.

2. The available satellite optical images (SPOT) in Progreso allow the exploration of shoreline change during a 6.5 year period.

3. The ancillary information (winds and waves, their direction and velocity), although not from a complete time series, act as a guide to estimate the approaching angle of the waves to the shore and therefore the direction of the alongshore transport.

4. The available information on waves in Yucatán, although it does not cover the same period of time as the available satellite images, allows an understanding of the waves in Yucatán. The waves in Yucatán are mostly wind generated, with short periods (< 5 s), approaching the shore with a height significantly smaller (min. 0.17 m and max. 0.57 m) than the height of offshore waves (min. 0.5 m and max. 2.2). Large waves (>1.5 m) with periods up to 11 s can occur in the presence of hurricanes, dissipating within two to three days.

5. The tidal measurements from Progreso are not systematic, showing differences from predicted tides (min. -0.4 and max. 0.8 m) larger than the tidal range (0.8 m). Moreover, the tidal differences have different temporal scales and they are of different magnitudes. Therefore, the measured tides are not a reliable source of data to estimate tidal levels.

6. The measured record from Telchac, when compared against predicted tides, shows overall a smaller tidal range, with differences on average of 15 cm. The difference between the measured and predicted record show periodicity, suggesting that the amplitude or some tidal consituents are not being considered in the predicted record.

7. The predicted tides, althought they underestimate the observed tide by 5 %, are a consistent and systematic reference to estimate the tidal levels for each SDS.

# Chapter 5

# Validation of Satellite-Derived Shorelines

## 5.1 Introduction

This chapter validates satellite-derived shorelines (SDS) extracted using the developed method described in chapter 3: using quasi-simultaneous inter-comparisons between *in situ* shoreline measurements and SDS. These inter-comparisons provide valuable information about the SDS location in relation to the *in situ* shoreline position. It allows confidence bounds to be defined for the SDS, which are further used to explore shoreline change. The case study area used to validate the SDS is Progreso, México, a location described in section 4.2.

The two inter-comparisons are from two different years: one quasi-simultaneous in 2010 with five hours of difference, and another with 11 days of difference in 2008. The water levels between the SDS and the *in situ* shoreline measurements were adjusted to equal levels using the inter-tidal beach slope from *in situ* beach profiles and the predicted tidal levels, assuming an homogeneous inter-tidal beach slope within each beach segment.

The difference between the SDS and the *in situ* shoreline measurements will change in the alongshore depending on the beach characteristics. The values presented here are

only valid for the case study area. However, this current research might be instructive as it shows which factors need to be taken into consideration when attempting to use SDS to study shoreline change in other locations.

Figure 5.1 summarises the contents of this chapter.

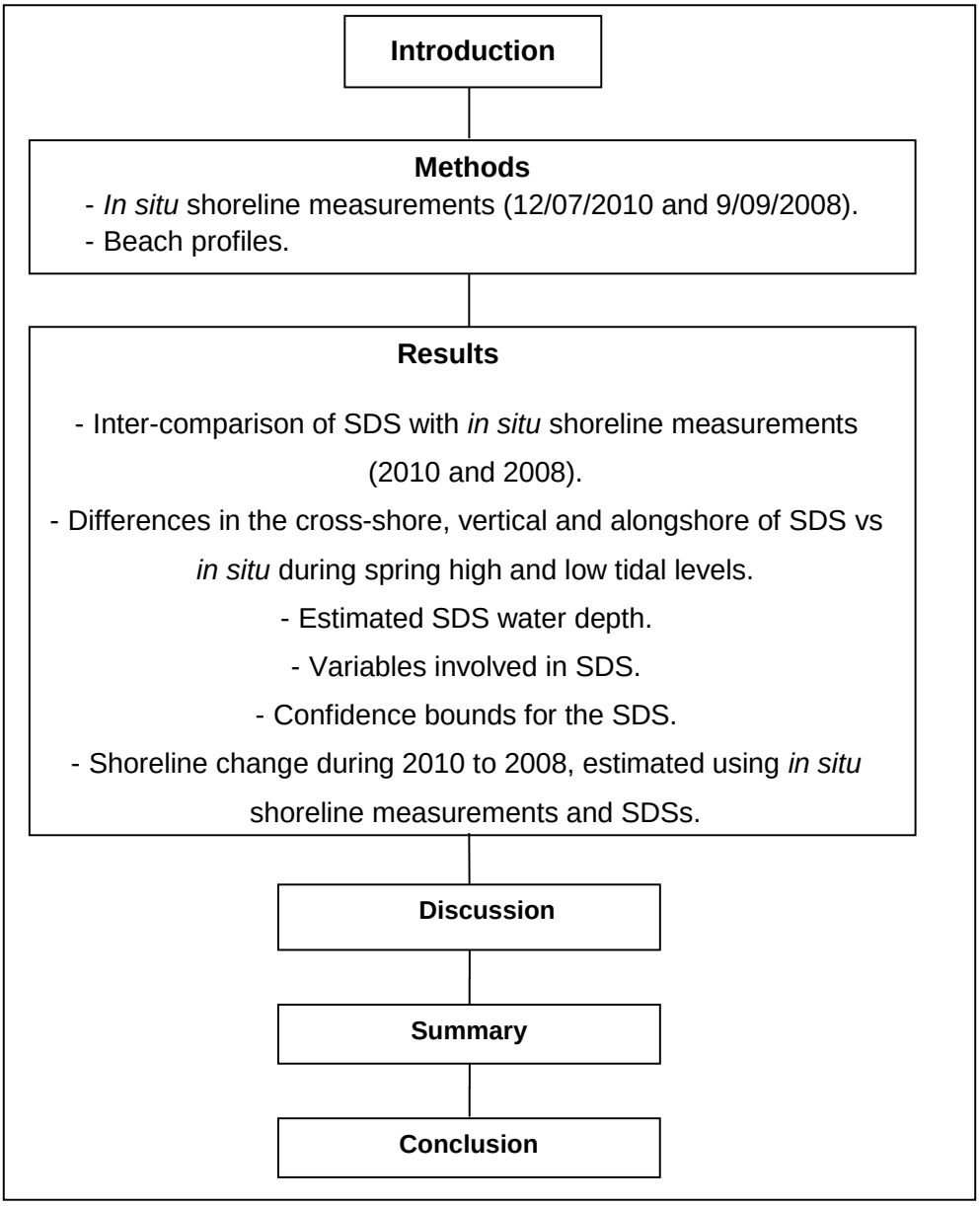


*Figure 5.1:* Chapter 5 structure summary.

Following this introduction, the methods used to obtain the *in situ* shoreline measure-

ments, the beach profiles, as well as the considerations to be taken into account prior to the inter-comparison are described. The results are divided into four main sections.

The first section describes the results from the 2010 inter-comparison, showing the differences between the SDS and the *in situ* shoreline measurements in the cross-shore and in the alongshore.

The second section shows the confidence bounds that have been defined based on the 2010 inter-comparison.

The third section describes the results of the 2008 inter-comparison both cross-shore and alongshore, as well as the effect of Hurricane Ike on the *in situ* shoreline measurements.

The fourth section compares the estimated shoreline change using SDSs in relation to *in situ* shoreline measurements, showing their similarities and differences. The results of this comparison are discussed in terms of the SDS capabilities in the study of shoreline change. The last part of this chapter provides a summary and conclusions.

## 5.2 Methods

This section describes the methods used to carry out the *in situ* shoreline measurements, beach profiles, as well as the adjustments of the *in situ* shoreline measurements to ensure that the inter-comparisons are at equal tidal levels.

### 5.2.1 *In situ* shoreline measurements in 2008 and 2010

This section describes:

1) The survey details for the two different surveys carried out in 2008 and 2010.

2) The required post-processing of the acquired data with the DGPS, and

3) The considerations that need to be taken into account prior to the inter-comparison

of the *in situ* shoreline measurements.

**Survey details**

Figure 5.2 shows an example of the *in situ* measured shoreline. The feature recorded in the field was the instantaneous shorewards extent of the wave run-up at a given time when walking along the beach. Therefore, the shorewards extent and the backwards extent of the wave run-up was noted. An alongshore distance of 8 km was covered, encompassing the beach segments described in section 4.3.7.


*Figure 5.2:* Example of the measured shoreline *in situ* in Progreso, Yucatán. The black solid line indicates the measured shoreline. The black dotted line shows the mark of the last high water.

The equipment used was a Leica Differential Global Positioning System (DGPS) in Post-Processing Kinematic (PPK) mode. The positions were recorded along the survey area every second, therefore each measurement is spaced approximately one and a half metres alongshore. The measurements were projected using a Universal Transverse Mercator (UTM) projection, zone 16 N, with the geoid reference WGS84. A planar projection adjusts effectively in places like Yucatán that are mainly flat. Moreover, working with UTM projection in the field is practical because the units are in metres with increasing northwards and eastwards values.

Figure 5.3 shows the physical location of the DGPS base station, fixed at a known location. The base station was settled in the middle of the surveyed beach at a benchmark. The mobile rover and the base station simultaneously receive the position from satellites. In 2010 and 2008, the mobile rover was carried using different equipment (Figure 5.4 *(a)* and *(b)*). In 2008 the antenna from the mobile rover was transported on a golf bag carrier, fixing the antenna in a vertical position at one metre height, whereas in 2010 a trolley was used and the antenna was set at two metres height. It required one person to keep it upright in a vertical position. The only disadvantage of using the trolley is that two people are required to carry out the survey. However, the system used in 2010 enabled better reception than the one used in 2008. If a slight movement in the vertical position of the antenna occurred in the 2008 and 2010 surveys, the associated error in the recorded height would be no larger than five centimetres.

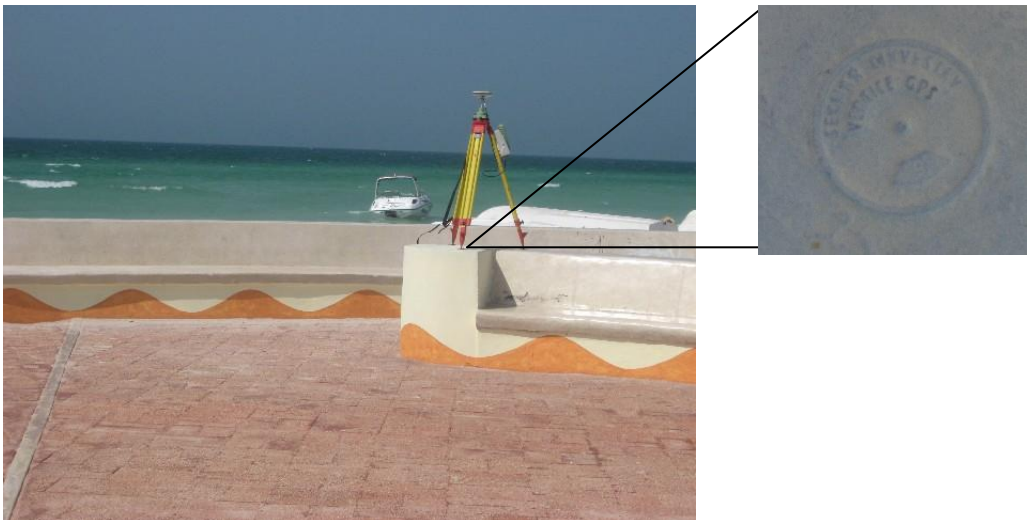

*Figure 5.3:* Location of the base station at the benchmark used for the shoreline measurement in Progreso, Yucatán.

The shoreline measurement was recorded as continuously as possible. However, the measurement was paused by the presence of ropes, piers and stones at the shoreline level.

In 2010, shoreline measurements were carried out during spring tides to capture the

*(a)* Equipment used in 2010.

*(b)* Equipment used in 2008.

*Figure 5.4:* Equipment used to carry out the shoreline measurement in 2010 (a) and 2008 (b).

range of locations that the shoreline can have in different tidal levels.

### Post-processing of *in situ* data

The post-processing of the data can be divided into three main steps. Firstly, positions with an accuracy of less than 95 % are discarded, which ensures that all the included data points have the best spatial accuracy that the equipment is capable of obtaining (< 5 cm in the horizontal position and < 10 cm in the vertical position). The accuracy is calculated by the equipment, depending on how well the two received signals from the

mobile and the base station are phased.

Secondly, the location of the base station is corrected using simultaneous measurements from the Merida GPS station. Once the location of the base station is corrected then the base station can be used as a reference to correct the location of the mobile rover measurements. After this post-processing, the accuracy of the data points is less than five and 10 cm respectively in the horizontal and in the vertical.

### 5.2.2 *In situ* shoreline measurement in 2008

The shoreline measurements were carried out on September $9^{th}$, with an outgoing tide, starting at 11:45 and ending at 13:33 (local time), from the eastern (seg. 8) to the westernmost (seg. 1) part of the beach. The predicted tide when the measurements started was 0.13 m and ended at -0.03 m (pred.) (Table 5.1).

### 5.2.3 *In situ* shoreline measurement in 2010

The shoreline measurements were carried out on July $12^{th}$, with an outgoing tide, starting at 15:39 and ending at 17:38 (local time), from the eastern to the westernmost part of the beach. The predicted tide level over the measurements fell from 0.14 m to -0.029 m (pred.) and the measured values were from 0.17 m to -0.013 m from the MLLWL (Table 5.1). The difference between the measured and predicted tides during the shoreline measurements shows a difference in the low water level, which was previously discussed in section 4.5.5.

The support of three people was required to carry out the measurements. Two were needed to record the shoreline and another one to look after the base station. In the middle of the survey, the person who was looking after the base station swapped places with the person who was keeping the antenna in a vertical position. The shoreline measurement was paused during this change.

#### *In situ* shoreline measurement in high tide conditions

Shoreline measurements during spring high tide conditions took place on July $13^{th}$ from 9:08 to 9:23 (local time), covering segment 3 (Figure 4.10 in section 4.1), located on the western side (seg. 3) of the pier, which has a shallower beach slope. During the time that the survey was undertaken, the change in the tidal level was not detectable. The tidal level of the SDS and the *in situ* shoreline are the same (0.38 m predicted and 0.45 m measured). Hence, tidal adjustment of the SDS and *in situ* shoreline measurements was not required.

#### *In situ* shoreline measurement in low tide conditions

The shoreline measurement during spring low tide conditions took place on July $12^{th}$ from 23:08 to 23:31 (local time), with a tidal level of -0.33 m (predicted) and -0.25 m (measured).

### 5.2.4 Beach profiles

Beach profiles were recorded covering all the beach segments in the case study area. The measurements were carried out using a DGPS in PPK mode on the $13^{th}$ of July 2010, only one day after the satellite passed over Progreso. To estimate the vertical resolution within the beach profile, each beach profile was repeated at least three times at the same location. In total, 35 profiles were recorded. The precise location of the beach profiles was determined by selecting a beach transect that describes each beach segement, e.g. the presence of dunes, vegetation and beach slope. Therefore, the beach profiles are not located at the middle of each beach segment (see appendix).

### 5.2.5 Considerations prior to the inter-comparison of *in situ* shoreline and SDS

Figure 5.5 shows a schematic of the difference between both shorelines and their adjustment in location prior to the inter-comparison. The *in situ* measurements and the

SDS aimed to detect the location of the shoreline but using different types of data. Each type of data, by its nature, captures a different shoreline position. Their differences are important to be aware of prior to the inter-comparison of both shorelines. The following paragraphs describe the main differences between each data type and the required adjustments.

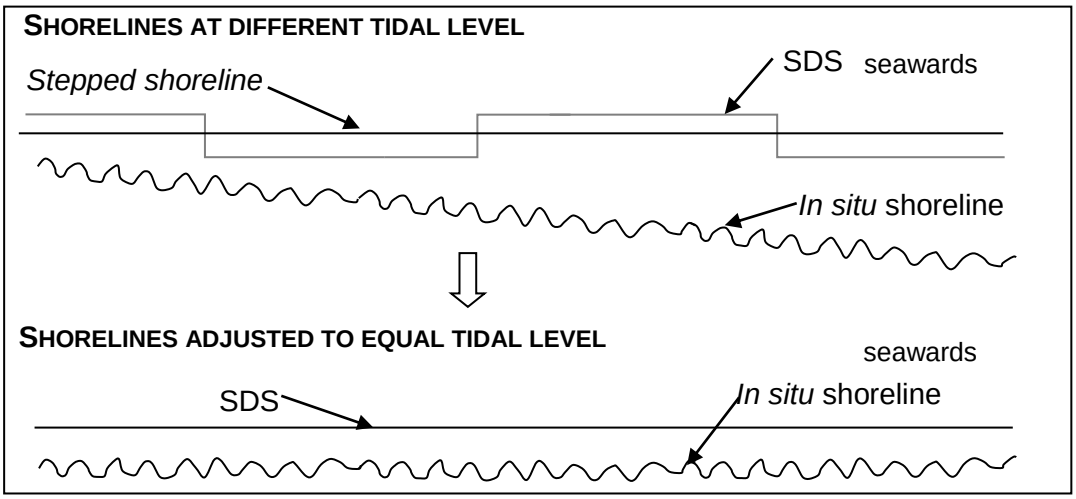


*Figure 5.5:* Diagram showing a plan view of the *in situ* shoreline (oscillating line) and SDS (flat line) before and after their adjustment to equal tidal levels.

### 5.2.6 Satellite-derived shoreline

Satellite images cover a large area simultaneously. Therefore, the whole shoreline included in the image has the same tidal level along the shore. The shoreline location, however, will change due to the instantaneous swash excursion, capturing the shorewards and backwards extent of the wave run-up along the shoreline.

The wave run-up in the region is between 0.2 and 0.4 m height. On a beach with a slope of 6°, that magnitude will cause a shorewards excursion between 2 m and 4 m. This magnitude is less than the pixel size and therefore is not expected to be detected by the satellite. However, in locations where the scale of the wave run-up is larger than the pixel size, it might be detectable with SDS.

### 5.2.7 *In situ* shoreline

The *in situ* shoreline recorded the instantaneous shorewards extent of the wave run-up when walking along the shore. Thus, it includes part of the wave run-up excursion, due to the constant backwash and shorewards extent of the wave run-up. Moreover, due to the outgoing tide during the measurements (> 1 hour), a progressive seawards movement on the shoreline position was measured.

The shorewards extent of the wave run-up and the tidal change occur at different spatial and time scales. Changes in the tidal height are detectable after covering a distance longer than 100 km and periods of time greater than half an hour, while the wave run-up varies within distances as short as one metre and in periods of time as small as a fraction of a second. Therefore, the change in height due to the tide and the wave run-up can be identified separately in the shoreline measurements. Thus, the variation of the *in situ* shoreline would include an important part of the range due to the wave run-up. However, for further analysis of shoreline change, the average shoreline position within each segment was used, so, the change of the shoreline position due to the wave run-up would be removed, whereas the wave set-up would still show an effect on the shoreline position.

The height measured during the *in situ* shoreline survey was verified with measured water levels (at Telchac) and tidal predictions. In this way it was possible to detect if any other factor could be involved in the shoreline location apart from the tides.

The *in situ* shoreline location was adjusted to an equal tidal level as the image. The inter-tidal beach slope and the difference in tide between the *in situ* shoreline measurement and the SDS was used to bring the shoreline position either seawards or landwards, depending on the tidal level of the image. Is important to emphasize that the adjustment of the shoreline assumed an homogeneous inter-tidal beach slope within each

beach segment. Because each beach segment was determined based on their geomorphological characteristics, this assumption seemed to be adequate to do the adjustment of the shoreline position. However, is recognised that local differences may occur particularly in the transitions of each beach segments. For example a 20 cm difference in the water level will produce a horizontal excursion ranging between 3.8 m to 1.2 m, with beach slopes of 3° to 9° (see Table 4.3). The largest difference in the beach slopes occurs from segment 1 to 2, segment 3 to 4 and 4 to 5. Given the example, the expected order of magnitude to occur in the segments transitions would be as large as 1.6 m from segment 1 to 2, and of 0.6 m from segments 3 to 4 and 4 to 5.

Table 5.1 shows the tidal levels during the *in situ* shoreline measurements in 2008 and 2010 and their associated horizontal excursion. The adjustment of the shoreline location in the inter-comparison of 2008 is small, with maximum seawards movements of 1.6 m in the easternmost part of the surveyed beach. The adjustment of the shoreline location in the inter-comparison of 2010 required a larger adjustment, with maximum landwards movement of up to 5 m on the easternmost part of the surveyed beach.

*Table 5.1:* Tide difference and associated horizontal excursion between the *in situ* shoreline measurements in 2008 and 2010 and the SDS. The predicted tide is referred to the local MLLWL. The measured tide is referred to the ellipsoid WGS84 and in brackets to the local MLLWL.

| Date | Local time (-6 GMT) | Tide | | | Horiz. exc. |
|---|---|---|---|---|---|
| | | Pred. | Meas. | Tide diff. | |
| 9/09/08 | 11:45 to 13:33 | 0.13 to -0.03 | – | 0.02 to 0.22 | up to 1.6 m (seawards) |
| 12/07/10 | 15:39 to 17:38 | 0.14 to -0.029 | -13.87 (0.13) to -14.04 (0.04) | -0.47 to -0.27 | up to 5 m (landwards) |

## 5.3 Results

This section shows the results of:

1) The two inter-comparisons in 2010 and 2008,

2) Their variations in the alongshore and cross-shore,

3) The variables involved in the location of the SDS in relation to *in situ* shoreline measurements, and

4) Defined confidence bounds for the SDS.

### 5.3.1 Inter-comparison in 2010

The inter-comparison between the SDS and the *in situ* shoreline of 2010 is an excellent opportunity to examine their differences quasi-simultaneously in the cross-shore and alongshore. This inter-comparison is also used to determine confidence bounds.

**Horizontal difference between the SDS and the *in situ* shoreline in the cross-shore**

The overall difference was calculated using observations by each pixel (10 m). The SDS is consistently seawards from the *in situ* shoreline. Overall, the SDS is -5.6m from the *in situ* shoreline over 8 km of surveyed shoreline, which is smaller than the pixel size (10 m).

Figure 5.6 shows the cross-shore distribution of the difference between the *in situ* shoreline and the SDS. The distribution is narrower than a normal distribution, 80 % of the values are between -6.9 and -4 m, with only 0.2 % of the values larger than the pixel size.

The seawards location of the SDS is probably best explained by the minimum water depth required to decrease the intensities from dry sand to sea. Lafon et al. (2002) show that the NIR spectral band is sensitive to changes in water depth of less than

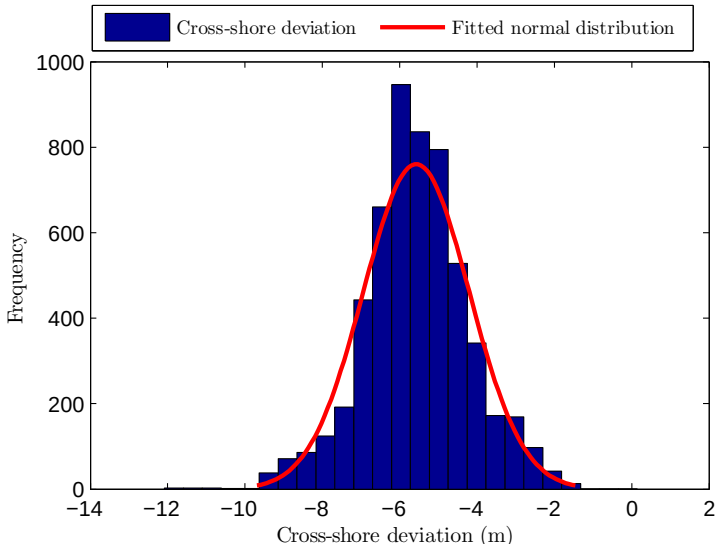


*Figure 5.6:* Histogram of the cross-shore distance between *in situ* shoreline measurements and SDS in 2010. The distribution fits into a normal distribution (k=0.979, c.v.=0.0182, n=709).

10 cm. Intensities from emerged sand to 10 cm water depth decrease by 15 %. The spectral response from the sea (see section 3.3.) includes intensities ranging between 20 and 180, whereas the typical intensities found on the shore are about 220. Intensities of about 180 can correspond to water depths as shallow as 10 to 20 cm, which have been detected by the satellite as sea. However, there are few pixels detected as sea with relatively high intensities (Figure 3.19), indicating that the satellite needed a deeper water depth to distinguish the sea from the land.

Table 5.2 shows the mean cross-shore difference between *in situ* shoreline measurements and SDS for each segment. Figure 5.7 shows the cross-shore difference along the shore. It is important to highlight that overall the mean distance between *in situ* shoreline measurements and SDS is similar in the alongshore. This suggests that there is a fairly constant displacement of the SDS from the wave run-up line of the magnitude of the overall mean (-5.6 m). This is also consistent with the fact that 80 % of the values are at one standard deviation from the mean.

*Table 5.2:* Cross-shore difference (m) of the SDS and *in situ* in 2010 and 2008 for each segment. $\alpha$ is the shoreline orientation and $\beta$ is the inter-tidal beach slope, both are in degrees. *Estimated water depth. The ellipsoid of reference is the WGS84.

| | 2010 | Mean=-5.57 m, SD=1.37 m | | | | | | |
|---|---|---|---|---|---|---|---|---|
| | Seg. 1 | Seg. 2 | Seg. 3 | Seg. 4 | Seg. 5 | Seg. 6 | Seg. 7 | Seg. 8 |
| Mean | -6.6 | -5 | -4.7 | -7.4 | -6 | -5.6 | -5.7 | -5.3 |
| Std. dev. | 1 | 0.8 | 1.6 | 1.9 | 1.1 | 1 | 0.9 | 1.4 |
| Range | 7.1 | 3.5 | 10.3 | 9.7 | 4.9 | 5.6 | 4 | 7.5 |
| | 2008 | Mean=-0.4 m, SD=2.2 m | | | | | | |
| Mean | 1.3 | -0.5 | 1.5 | 3.5 | -0.6 | -2.1 | -1.1 | -1.1 |
| Std. dev. | 1.2 | 1.5 | 2.8 | 3.9 | 1.1 | 1.05 | 1.4 | 1.7 |
| Range | 5.5 | 6.4 | 15.7 | 13 | 4.6 | 4.6 | 7.9 | 9.5 |
| $\alpha(^\circ)$ | 5 | 8 | 18 | 27 to -2 | 3.1 | 3.7 | 6.8 | 9.7 |
| $\beta(^\circ)$ | 3 | 5 | 5 | 9 | 6 | 6 | 5 | 5 |
| Water depth (m)* | 0.67 | 0.52 | 0.65 | 1.15 | 1.13 | 0.91 | 0.41 | 0.54 |

The largest difference between *in situ* shoreline measurements and SDS occurs in segments 4 and 3 due to abrupt changes in shoreline orientation. The mean difference is -7.4 m and -4.7 m, respectively. The large difference in segment 4 is explained by the rotation of the beach from -2° to 27°, due to the two piers located within this segment (see section 4.3.7). The standard deviation of segment 4 is the largest (1.9 m) in relation to the other beach segments. In contrast, segment 3 has a much smaller mean (-4.7 m) than segment 4, with a standard deviation as large as segment 4 (1.6 m). The large standard deviation is due to the changes in shoreline orientation. The change in shoreline orientation in segment 3 is explained by the accumulation of sand as a result of the eastwards longshore transport of sediment, which is reduced by the two piers located in segment 4 (Figure 5.7).

Segments 2, 5, 6 and 7 have a small range of difference between *in situ* shoreline measurements and SDS. Furthermore, their standard deviation is smaller than 1.1 m. These beach segments are mainly straight whereas the segments with the largest shoreline orientation have the larger difference. This shows that the standard deviation decreases

over a straight shoreline and increases with a largest shoreline orientation.

Figure 5.7 shows the cross-shore difference along the shore. There are rapid variations in the alongshore that are not explained by the shoreline orientation. Segment 8, for example, has a mostly straight shoreline and also has these rapid variations. These rapid variations are fluctuations in the shorewards extent of the wave run-up. Thus the differences in the fluctuations are also related to changes in the beach slope and the waves reaching the shore. However, overall the cross-shore difference between the SDS is consistently seawards from the *in situ* shoreline measurements. This shows that the SDS has a displacement from the wave run-up line. In a location such as Progreso this displacement is an approximate magnitude of the overall mean difference between the *in situ* shoreline measurements and the SDS over the 8 km of surveyed shoreline.

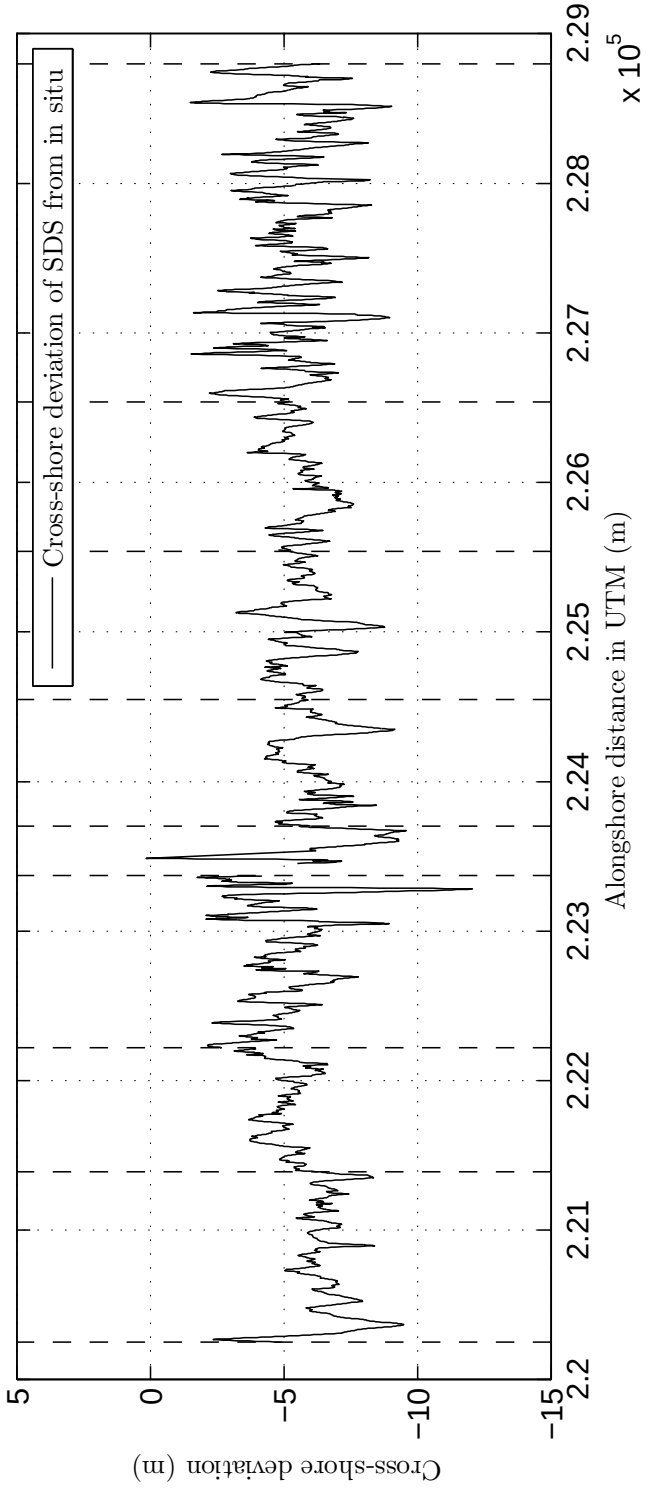


*Figure 5.7:* Difference in the cross-shore (m) between the SDS and *in situ* shoreline measurements in the alongshore, measured in 2010 at Progreso, Yucatán. Segments 1 to 8 are from left to right, divided by dashed lines. The horizontal axis is the eastern values, which increase towards the right. Progreso piers are located within segment 4 at the 2.238 m eastern.

Figure 5.8 shows visually the spatial location of the SDS in relation to the *in situ* shoreline measurements. Here are shown the cases where the cross-shore difference varies in the alongshore due to changes in the shoreline orientation. Differences larger than the pixel size (-12 m) are related to abrupt changes in shoreline orientation when the alongshore distance over which the change occurs is smaller than 50 m (Figure 5.8 b). When the shoreline orientation does not change or curves within an alongshore distance greater than 50 m then the difference of the SDS remains within the pixel size although the rapid variations remain (Figure 5.8 *a* and *c*).

An alongshore distance of 50 m was set in the SDS smoothing process (see section 3.6.2), which was found to be adequate to indicate the shoreline location. There are some specific locations where SDS does not adjust well to rapid changes in the shoreline orientation (Figure 5.8 b). However, these locations, are a small amount of the surveyed shoreline (0.2 %) and are spatially well identified.

*Table 5.3:* Measured *in situ* height (m) during the shoreline measurement in 2010 and 2008. The horizontal excursion was estimated by considering the tidal change of each beach segment and the beach slope ($\beta$).

| | 2010 | | | | | | | |
|---|---|---|---|---|---|---|---|---|
| | Seg.1 | Seg.2 | Seg.3 | Seg.4 | Seg.5 | Seg.6 | Seg.7 | Seg.8 |
| Range | 0.23 | 0.16 | 0.33 | 0.21 | 0.27 | 0.21 | 0.20 | 0.36 |
| Min | -14.15 | -14.13 | -14.12 | -14.01 | -13.95 | -13.95 | -13.97 | -14.01 |
| Max | -13.92 | -13.97 | -13.79 | -13.79 | -13.68 | -13.74 | -13.77 | -13.64 |
| Mean | -14.05 | -14.05 | -13.99 | -13.89 | -13.88 | -13.88 | -13.86 | -13.82 |
| SD | 0.04 | 0.03 | 0.07 | 0.05 | 0.04 | 0.03 | 0.03 | 0.04 |
| Horz. exc. | 4.4 | 1.8 | 3.8 | 1.3 | 2.6 | 1.9 | 2.3 | 4.1 |
| | 2008 | | | | | | | |
| Range | 0.13 | 0.2 | 0.29 | 0.35 | 0.24 | 0.36 | 0.55 | 0.35 |
| Min | -14.1 | -14.1 | -14.15 | -14.0 | -13.98 | -13.96 | -13.97 | -13.85 |
| Max | -13.97 | -13.89 | -13.86 | -13.62 | -13.74 | -13.6 | -13.43 | -13.5 |
| Mean | -14.05 | -14.01 | -13.97 | -13.85 | -13.9 | -13.85 | -13.85 | -13.74 |
| SD | 0.03 | 0.04 | 0.05 | 0.08 | 0.03 | 0.06 | 0.07 | 0.07 |
| Horz. exc. | 2.47 | 2.28 | 2.17 | 2.2 | 2.28 | 3.42 | 6.27 | 3.99 |

Table 5.3 shows the statistics of the measured height during the *in situ* shoreline measurement. The standard deviation of the height recorded during the *in situ* measurements ranges between 0.13m and 0.38 m, which corresponds to the observed shorewards extent of the wave run-up. The associated horizontal excursion with the deviation of the measured height is between 1.7 m and 3.2 m over the 8 km of surveyed shoreline.

The mean measured height at the shoreline level in 2008 and 2010 is very similar, with a difference of less than 10 cm. Furthermore, the mean measured height at the shoreline level has less than five centimetres difference in relation to the water depth measured in Telchac, which is of the expected order of magnitude for the wave set-up ($< 3$ cm) that could have be produced by breaking waves of 10 cm ($\gamma$=0.5) (Table 5.1). This agreement is a further confirmation that the correction done to the DGPS measurements using the base station and the station at Merida resulted in measurements with high resolution, that allowed to determine that the effect of the wave set-up is not relevant for the shoreline position.

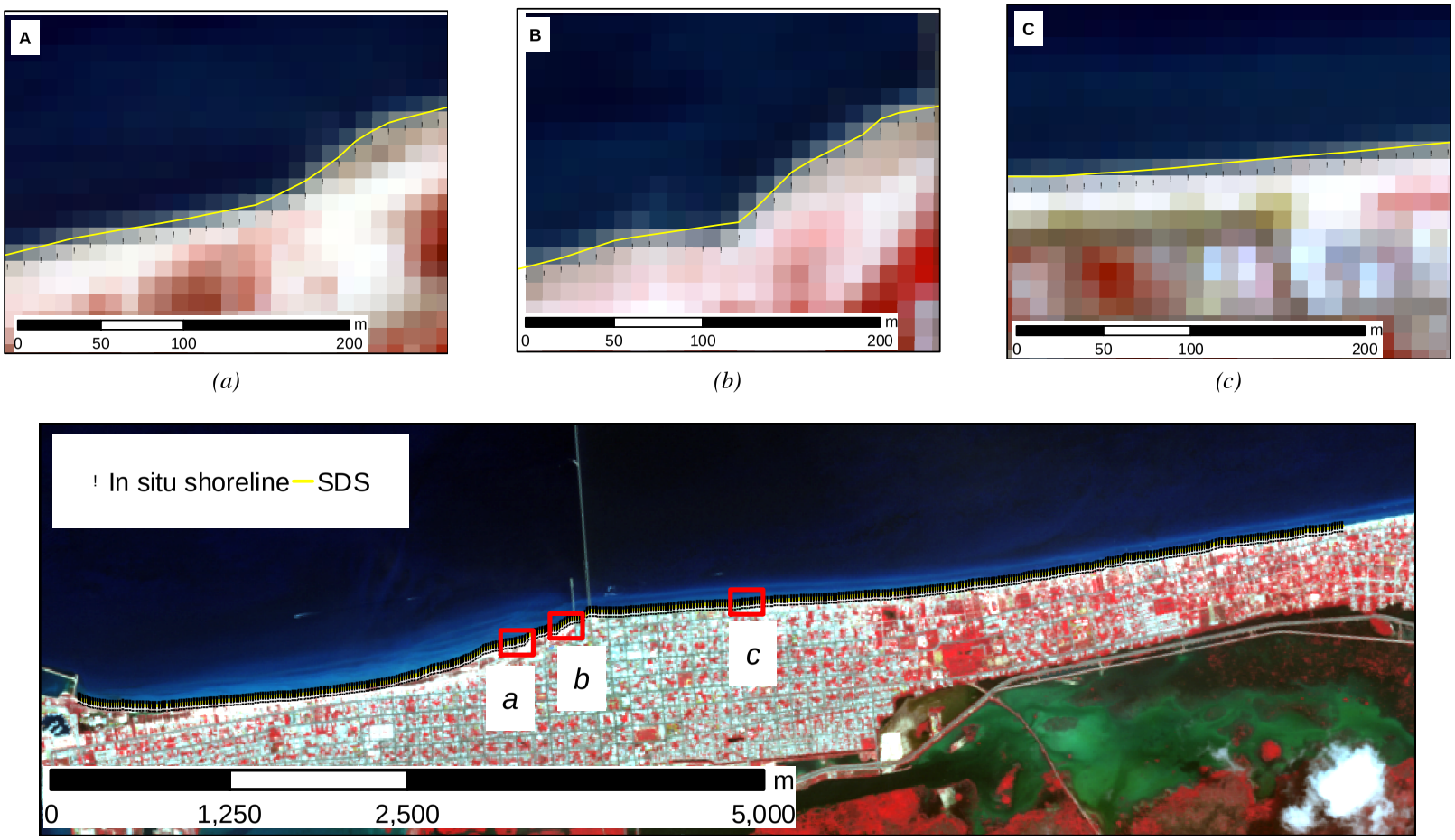


*Figure 5.8: In situ* shoreline measurements overlapped with the SDS and the satellite image in 2010 at Progreso, Yucatán, México. A, B and C are close ups within the red squares.

Figure 5.9 shows the Fourier analysis of the difference beween the *in situ* shoreline measurements and the SDS. The power is located in the longer wavelenghts, showing a brown or red type of noise in the extracted SDS.

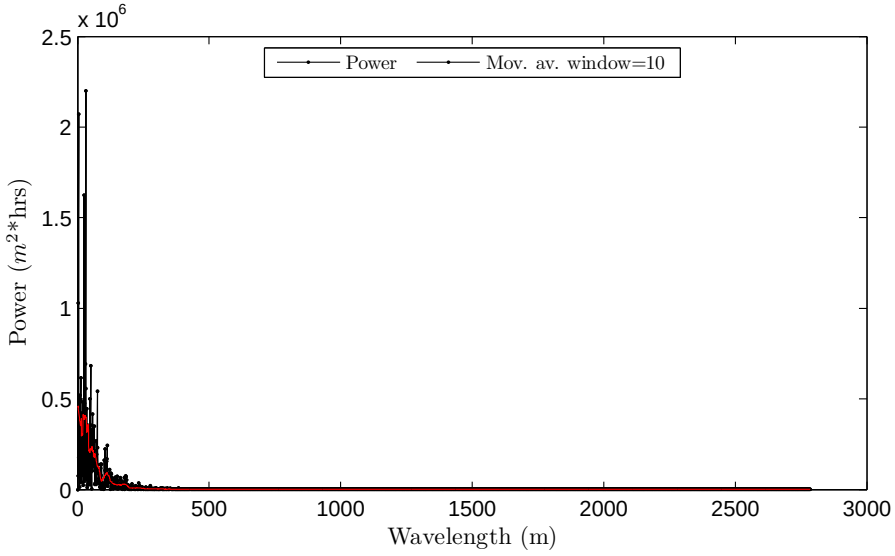


*Figure 5.9:* Fourier analysis of the difference between the *in situ* shoreline measurements and the SDS. The SDS (black) and the smoothed signal (red) using a moving average with a window of ten.

### 5.3.2 *In situ* shoreline measurements in spring tides

Figure 5.10 shows the histograms of the cross-shore difference between the SDS and the *in situ* shoreline measurements during the spring high and low tide conditions in segment 3, which has an abrupt change in shoreline orientation (see Figure 5.8 b). The mean difference between the SDS and the *in situ* shoreline during low tide conditions is 2.55 m with a standard deviation of 1.76 m. Their difference is landwards and much smaller than the displacement found in the inter-comparison in 2010. This is because the *in situ* shoreline measurements are in low tide conditions thus the shoreline moved further seawards than the SDS.

The shoreline measurements in high tide conditions have an equal tidal level to the

SDS (0.38 m pred.) and have a mean difference of -5.87 m and a standard deviation of 1.95m. The magnitude of this displacement is very similar to the displacememt of the SDS from the wave run-up line in the inter-comparison in 2010 (see section 5.2). This suggests that the displacement, when assessing different optical satellite images from Progreso, would be of approximately the same magnitude. Furthermore, this displacement is well explained to be due to the optical requirement of the NIR spectral band to distinguish a pixel as sea or land.

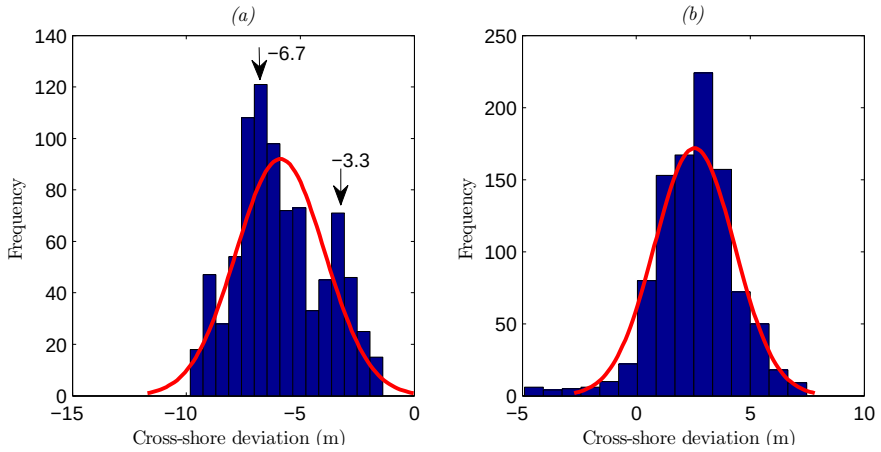


*Figure 5.10:* Histogram of difference in the cross-shore between the SDS and the *in situ* shoreline measurements in spring high (a) and low (b) tide conditions at Progreso, Yucatán. The black arrows indicates the central value of the two crests.

The distribution of the cross-shore difference in high tide conditions shows two crests, at -6.7 m and -3.3 m. The difference in the cross-shore seems to be related with the pier, which is located towards the east. Figure 5.11 shows that the differences between -4 m and -2 m, associated with the crest at -3.3 m, are closer to Progreso pier (east); whereas the values with differences between -8 m and -5 m, associated with the crest at -6.7 m, are farther away from the pier (see Figure 4.10). The section of shoreline that is closer to Progreso pier is sheltered by the easterly winds, reducing the wind-generated waves and, the shorewards extent in the wave run-up. This suggests that the cross-shore

difference decreases with a smaller wave run-up and vice versa.

Furthermore, the observed difference between the *in situ* shoreline measurements in low tide have a similar difference in the alongshore. This could be explained by the calm conditions during the survey, with almost no waves, and therefore a very reduced wave run-up along the whole surveyed beach segment. This suggests that the wave run-up could be an important factor explaining the total difference found between the *in situ* shoreline measurements and the SDS. However, it has to be taken into consideration that although the DGPS measurements showed to be accurate, in order to determine the change in the shoreline position due to the wave run-up, the use of other techniques such as a RTK system would be more suitable.

Table 5.4 shows the difference between the SDS and the *in situ* shoreline in low and high tide conditions, as well as the measured height during the survey. Interestingly, the measured elevation of the shoreline during high and low tide conditions is of the same magnitude as the measured height during low and high tide conditions in Telchac (see section 4.5), showing that the water depth measured at the shoreline was not affected by the wave set-up. Overall, the vertical displacement in the wave run-up was smaller in low tide conditions (0.17 m) than in high tide conditions (0.28 m). The associated horizontal excursion of the wave run-up in a beach slope of 5° is between 1.3 and 2.15m respectively in high and low tide conditions.

*Table 5.4:* Difference between SDS and *in situ* shoreline measurements in low and high tide conditions, and the measured height at the shoreline level during the survey. The height is referred to the ellipsoid (WGS84).

| Tidal level | Difference (m) | | Elevation (m) | | |
|---|---|---|---|---|---|
| | $\bar{X}$ | SD | $\bar{X}$ | SD | range |
| Low tide | 2.55 | 1.76 | -14.45 | 0.095 | 0.17 |
| High tide | -5.87 | 1.95 | -13.6 | 0.065 | 0.28 |

Figure 5.11 also shows that the difference between the SDS and the *in situ* shoreline in

the alongshore have a similar shape. The largest difference occurs at the same location no matter what the tidal level is. This suggests that the largest distance is related to an abrupt change in the shoreline orientation, due to the shorewards extent of the wave run-up. Overall, the difference between the SDS and the *in situ* shoreline in low and high tide conditions shows that the SDS extracted from an image in high tide conditions remains within the inter-tidal zone, closer to the *in situ* shoreline surveyed in low tide.

The conclusion of this comparison is that the displacement between the *in situ* shoreline and the SDS is of similar magnitude to that previously found in the 8 km of surveyed shoreline. In addition it was found that a smaller shorewards extent of the wave run-up can decrease the difference between the *in situ* shoreline and the SDS. However the displacement of the SDS remains within the range of magnitude covered by the horizontal excursion of the wave run-up. Finally, the wave set-up is not relevant in the overall difference between the *in situ* shoreline and the SDS.

*Figure 5.11:* Difference in the alongshore between the SDS and the *in situ* shoreline measurements during high and low tide conditions in segment 3 at Progreso, Yucatán, México.

### The water depth of the SDS

This section assesses the water depth of the SDS using the measured height during the *in situ* beach profiles. The water depth of the SDS was estimated using the measured height at the intersection of the beach profiles with the SDS position. It was assumed that the SDS water depth was the result of the difference between the measured height at the shorewards extent of the wave run-up and the measured height at the intersection point of the SDS and the beach profile.

Table 5.5 shows the water depth of the SDS at each beach segment. These are independent measurements to the previous inter-comparison. Furthermore, the beach profiles were measured only one day after the satellite image passed Progreso. The estimated water depth at the locations of the beach profiles shows that the satellite requires, at the very minimum, half a metre to distinguish intensity values between sea and land.

*Table 5.5:* Measured height at the SDS and *in situ* shoreline in 2010 (height referred to the ellipsoid WGS84). The horizontal excursion was estimated considering $\beta$ for each beach segment.

| | Height (m) | | | |
|---|---|---|---|---|
| | SDS | *In situ* | SDS water depth | Horiz. excursion |
| Seg. 1 | -14.27 | -13.6 | 0.67 | 12.8 |
| Seg. 2 | -14.16 | -13.62 | 0.52 | 5.9 |
| Seg. 3 | -14.23 | -13.58 | 0.65 | 7.4 |
| Seg. 4 | -14.65 | -13.5 | 1.15 | 7.3 |
| Seg. 5 | -14.63 | -13.5 | 1.13 | 10.8 |
| Seg. 6 | -14.45 | -13.54 | 0.91 | 8.7 |
| Seg. 7 | -13.95 | -13.54 | 0.41 | 4.7 |
| Seg. 8 | -14.07 | -13.53 | 0.54 | 6.2 |

The beach segments can be divided into three groups (eastern, middle and western), in terms of the SDS water depth. The eastern and western segments (1 to 3 and 7 to 8) have the shallowest water depths (-13.95 to -14.27 m). The segments from the middle have the deepest water depth (-14.45 m to -14.65 m).

The SDS water depth at the location of the beach profiles has a range between 0.5m and one metre depth, showing that the classification does not differentiate between these range of water depths to identify a pixel as sea. Therefore, the SDS includes a range of water depths rather than a fixed depths.

The difference between the *in situ* shoreline and the SDS is probably best explained by the water depth required by the satellite to identify a pixel as sea, although is recognised that the concentration of suspended particles could be an important factor too. The required water depth correspondes with the displacement previously found of the SDS and the wave run-up line. This also shows that the displacement of the SDS can be larger when the study area has a shallower beach slope and can be smaller in a steeper beach slope.

### 5.3.3 SDS confidence bounds

**Cross-shore**

The confidence bounds have been determined using the difference in position between the SDS and the *in situ* shoreline measurements. The displacement of the SDS from the *in situ* shoreline measurements seems to be related to the optical requirements of the satellite (see section 3.3) needed to distinguish the sea. Thus, is expected that every satellite image will include a displacement from the *in situ* shoreline which is fairly constant in the alongshore. In the case of study the deviation around the displacement is less than 3 m (Figure 5.7). In a normal distribution 34.1 % of the values are at distance of one standard deviation from the average. In addition, the difference between the SDS and the *in situ* shoreline measurements has a narrower distribution (Figure 5.6), where 40 % of the values are at a distance of one standard deviation from the average. Which indicates that this displacement is constant and of about the same magnitude all over the surveyed shoreline. Thus, it has been assumed that this displacement will have a

similar magnitude in different SDS extracted using this method at the case of study. As a result, the displacement will be disregarded when comparing different SDS and was not considered to define confidence bounds.

Table 5.6 shows the differences between the SDS and the *in situ* shoreline for the studied beach segments using one observation every pixel (10 m). The standard deviation of *in situ* shoreline position is much smaller than the displacement and its magnitude corresponds to the cross-shore extent of the wave run-up that occurred during the *in situ* shoreline measurement. Furthermore, this deviation would be different when comparing different SDS. Thus it would be appropriate to use the deviation as a confidence bound for the SDS to include the variation of the wave run-up.

The fact that the standard error (SE) is very small (< 6 cm), confirms that the difference between the *in situ* and the SDS does not have a large variation within each data point, and is a further confirmation of the high accuracy of the SDS.

*Table 5.6:* Upper and lower confidence bounds defined for the SDS. They were defined using the cross-shore difference ($\bar{X}$, SD, SE) between *in situ* and horizontal excursion of the wave run-up (see Table 5.2).

| | Cross-shore dev. | | | Bounds | | | Run-up |
|---|---|---|---|---|---|---|---|
| Seg. No. | $\bar{X}$ | SD | SE | Upper | Lower | $\beta$ | Horiz. exc. |
| 1 | -6.6 | 1 | 0.04 | -7.6 | -5.6 | 3 | 4.4 |
| 2 | -5.0 | 0.8 | 0.03 | -5.8 | -4.2 | 5 | 1.8 |
| 3 | -4.7 | 1.6 | 0.06 | -6.3 | -3.1 | 5 | 3.8 |
| 4 | -7.4 | 1.9 | 0.2 | -9.3 | -5.5 | 9 | 1.3 |
| 5 | -6.0 | 1.1 | 0.05 | -7.1 | -4.9 | 6 | 2.6 |
| 6 | -5.6 | 1.0 | 0.04 | -6.6 | -4.6 | 6 | 1.9 |
| 7 | -5.7 | 0.9 | 0.03 | -6.6 | -4.8 | 5 | 2.3 |
| 8 | -5.3 | 1.4 | 0.03 | -6.7 | -3.9 | 5 | 4.1 |
| All seg. | -5.6 | 1.4 | 0.01 | -7 | -4.2 | | |

**Alongshore resolution**

The SDS was extracted from 10 m pixel size satellite images, and its resolution allows detection of changes from one pixel to the next. However, the smoothing applied to

the SDS (see section 3.5) is sampled taking into account transitions at each 50 m of the alongshore. Thus, when the smoothing removed the jagged pattern it also removed abrupt transitions in the alongshore but overall the shoreline shape was successfully captured.

**Vertical resolution**

The SDS is at a water depth of between 0.41 m and 1.13 m (Table 5.2), with a range of depth of 0.72 m. This water depth estimation is based on the beach profiles of each beach segment. It is possible that this water depth might change when more beach profiles are considered as part of the estimate.

The vertical resolution of the SDS will depend on the depth variation, suspended particles in the water column, and probably the presence of small ripples on the sea surface. The change in intensity values due to the previously mentioned factors has not been fully explored in this research. The range of water depth estimated in this research is within the order of magnitude (0.5 m) that Lafon et al.(2002(a)) determined when deriving bathymetry from optical satellite images at the Banc d'Arguin, France.

The change of intensities in relation to the water depth is a topic that requires further research to determine the water depth variation using optical satellite images, particularly because it does affect the accuracy of the SDS. However, for shoreline change purposes, although this would be helpful information it is not required to identify the shoreline. This is because there is a clear drop between the intensities of the land and the sea.

### 5.3.4 Inter-comparison in 2008

The inter-comparison of 2008 has 11 days of difference between the *in situ* shoreline measurement and the SDS. Hurricane Ike was in the vicinity during the *in situ* shoreline measurements. The difference between the SDS and the *in situ* shoreline measurements

was affected by the presence of a storm surge produced by Hurricane Ike. The conference included in the appendix gives further details of this inter-comparison.

Table 5.2 shows the overall displacement from the SDS and the *in situ* shoreline (-0.4m), which is much smaller than the displacement in the inter-comparison from 2010 (-5.6 m). The fact that the inter-comparison between *in situ* shoreline and SDS in 2008 is so small can be attributed to the presence of a negative storm surge during the *in situ* measurements, moving the measured shoreline seawards.

Figure 5.12 shows spatially the differences between the *in situ* shoreline measurements and SDS. The *in situ* shoreline measurements began at the eastern side of the pier and then moved to the western side. During this period the tide level was falling, with a predicted drop of around 17 cm between the start and end of the measurement period. To see whether this drop is detectable, separate means and standard deviations have been calculated for the eastern and the western sides of the pier, adjusting both to equal predicted tidal levels. The mean for the eastern side is 1.2 m with a standard deviation of 1.3 m whilst the mean for the western side is -1.5 m with a standard deviation of 2.3 m. A positive mean indicates that the *in situ* shoreline is landward of the SDS. So, the drop in the mean from east to west is qualitatively consistent with a drop in sea level over the measurement period, which is not explained by the fall in the predicted tidal levels. Interestingly, the measured vertical elevations of the *in situ* shoreline measurements also provide some independent evidence that the actual drop in mean water level was considerably larger than the tide prediction.

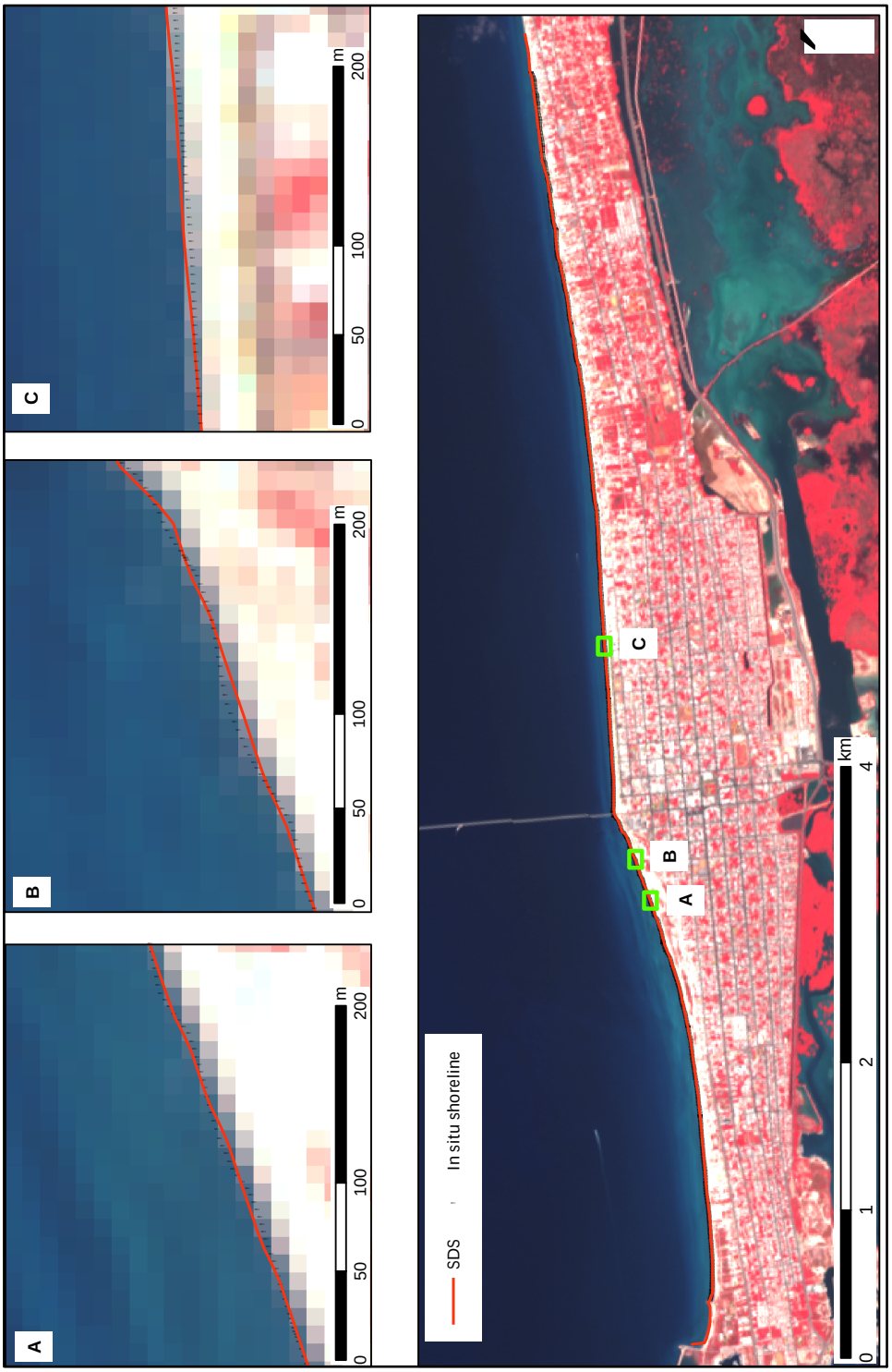


*Figure 5.12: In situ* shoreline measurements and SDS overlapped with the satellite image of 2008 in Progreso, Yucatán, México. A, B and C are close-ups within the green squares.

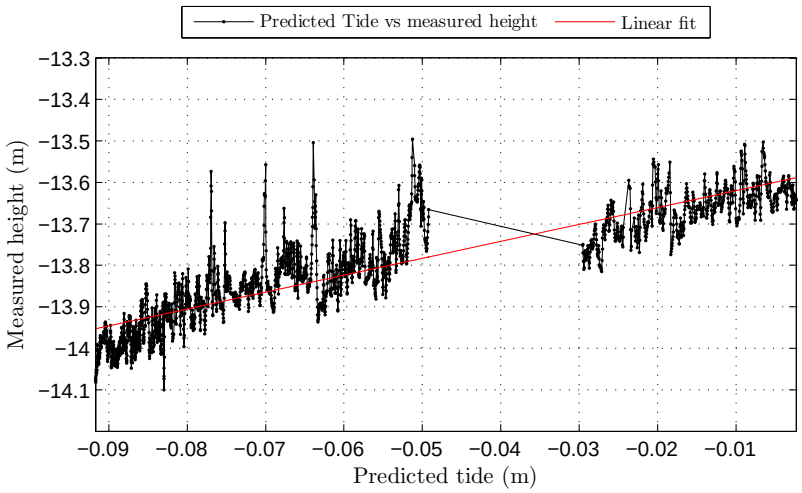


*Figure 5.13:* Measured height during the *in situ* shoreline measurements against the predicted tide in Progreso, Yucatán, México. The gradient is -4 and the intercept is -13.57, $r^2$=0.78.

Figure 5.13 shows a plot with the *in situ* measured height, corrected for atmospheric pressure variations, versus the predicted tide level. The rapid variations are fluctuations in the shorewards extent of the wave run-up but there is a longer term slope that fits a linear trend with a high correlation ($r^2$=0.8). The slope of this trend is four times greater than expected, suggesting a drop in sea level of almost 35 cm. Moreover, the intercept is at an elevation of 0.43 m, which is very close to the HWL (see section 4.5.5), whilst the predicted levels indicate a tidal level of 0.14 m, which is 25 cm from the HWL. This indicates that the measured elevation at the shoreline level was at a higher elevation than predicted and this difference is not explained by the wave set-up. The wave set-up does not produce an elevation of this magnitude, as was observed in the in *in situ* shoreline measurements of 2010. The equivalent horizontal shoreline excursion of 25 cm would be between 2.4 m and 4.8 m, as can be observed in the eastern and western side. Thus, the observed difference between the inter-comparison in 2008 produces an overall *in situ* shoreline measurement very close to the position of the SDS and five times smaller

than the difference in 2010, when no cyclones took place.

Figure 5.14 shows the *in situ* measured elevation at the shoreline level, the predicted tides, and the winds and atmospheric conditions during the *in situ* shoreline measurements. The offshore winds have velocities between 15 and 22 $kms^{-1}$, contrary to the dominant westwards direction throughout the year (see section 4.2). The atmospheric pressure during the measurement period shows only 5 cm of difference to a standard atmospheric pressure (1013 hPa). The inverted barometer effect will only explain up to 5 cm of the water levels from the 30 cm observed.

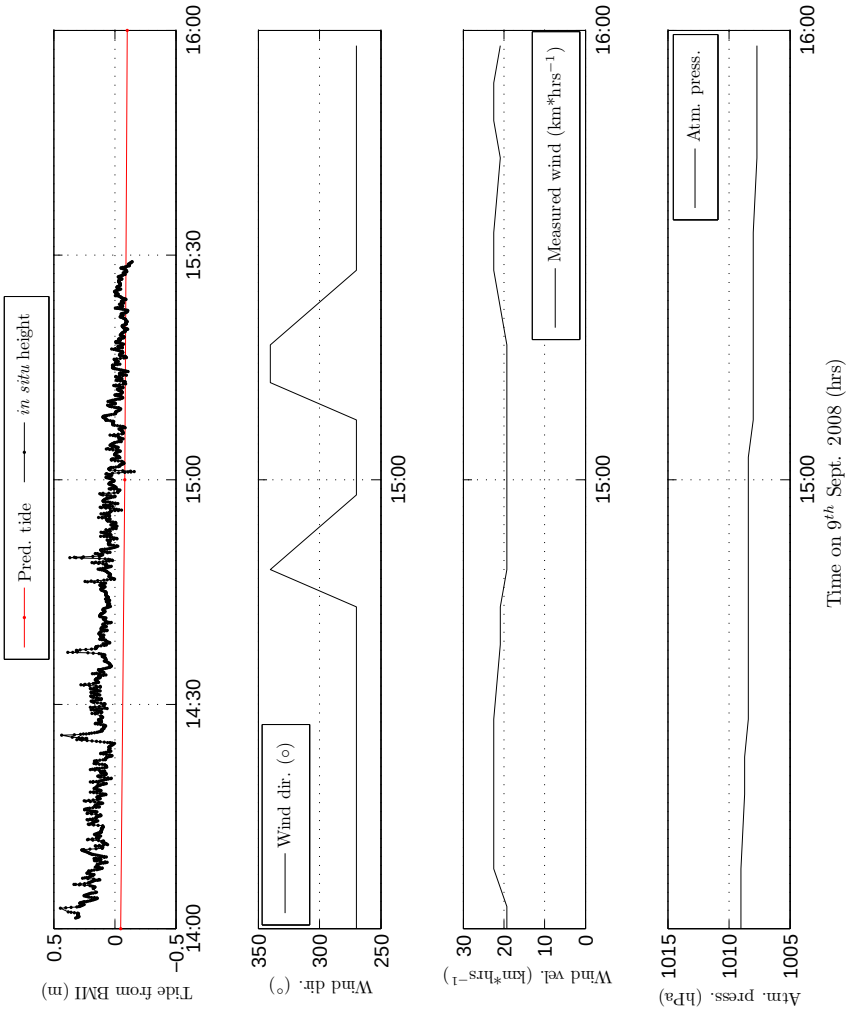


*Figure 5.14:* (Top) Measured water levels at the shoreline level with predicted tides overlapped. Wind direction (°), wind velocity ($kmh^{-1}$) and atmospheric pressure (hPa) on September $9^{th}$ 2008.

### 5.3.5 Shoreline change using *in situ* shoreline measurements and SDSs

This section compares the estimated shoreline change from two different years (2008 and 2010), using SDSs and *in situ* shoreline measurements. This comparison is useful to assess the capability of SDS to detect shoreline change. The previous sections have been focused on the capabilities of the SDS to identify the shoreline, whereas this section assesses its capability to assess shoreline change. The estimated shoreline change with the SDS included the confidence bounds as defined earlier in this chapter.

Figure 5.15 (a) shows the shoreline change found using the SDS and the *in situ* shoreline measurements. The shoreline change found using the *in situ* shoreline is overall within the estimated range of change estimated using the SDS, given the defined confidence bounds. This shows that the SDS estimates a range of shoreline change similar to measured by *in situ* shoreline measurements. Is interesting to note that the shoreline change found using *in situ* shoreline measurements is much closer to the maximum shoreline change than the minimum shoreline change. Furthermore, although segment 4 shows a change of 33 m and an abrupt change in shoreline orientation, the estimated shoreline change remains within the defined confidence bounds, showing the capabilities of the SDS to identify shoreline change at shorelines with an abrupt shoreline orientation change.

Figure 5.15 (b) shows the difference in the estimated shoreline change using the SDS and the *in situ* shoreline measurements. The estimated shoreline change using the *in situ* shoreline measurements is between 5 and 10 m larger than SDS. Moreover, there is a difference of a magnitude between 3 and 5 m that remains fairly constant along the whole shoreline surveyed. This offset can be related to the uncertainties of tidal levels in the shoreline measurements in 2008. Therefore, due to the use of predicted tides, it would be adequate to add the associated horizontal excursion to the uncertainty of predicted tides into the confidence bounds (Figure 4.23).

The average difference (15 cm) in height between predicted and measured tides will produce a horizontal excursion of 1.6 m in a beach slope of 5°. This horizontal excursion in a seawards and landwards direction will produce an overall horizontal excursion of 3.2 m. Adding this range of magnitude to the confidence bounds will produce a better fit for the *in situ* shoreline measurements into the estimated shoreline change using SDSs.

Overall, the shoreline changes assessed with SDSs have similar shapes in relation to the shoreline changes found with *in situ* shoreline measurements. However, the shoreline change estimated with *in situ* shoreline measurements detected changes smaller than 5 m, which were not detected by the SDSs (e.g. segments 2, 7 and 8, Figure 5.15 (a)). This shows that assessments by SDSs, although they cannot detect small shoreline changes, will provide a good estimation of the shoreline change that took place in a determined location. This is particularly valuable in locations with no *in situ* shoreline measurements or few records of the shoreline position to study shoreline change. A discussion is given in chapter 7 in section 7.5 considering beaches with different characteristics. It has to be taken into consideration the application of the developed technique can encounter difficulties in beaches with a very wide swash region and a shallow beach slope.

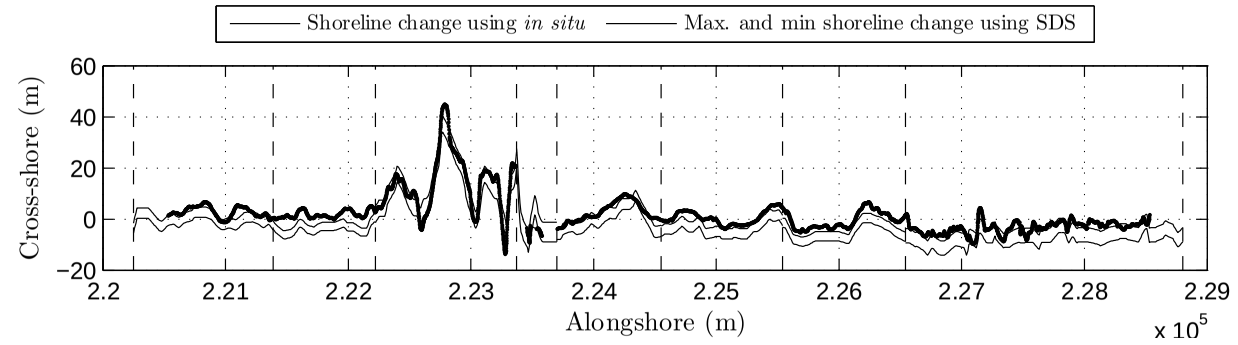


*(a)*

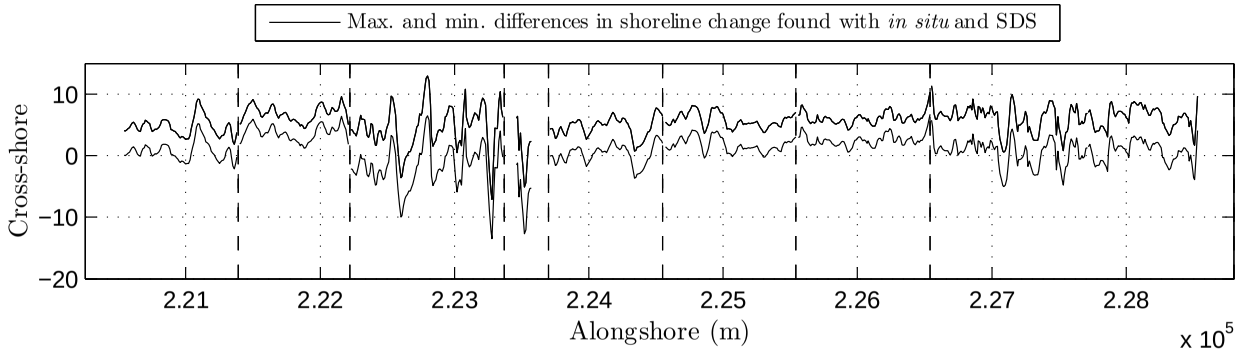


*(b)*

*Figure 5.15:* (a) Shoreline change from September 2008 to July 2010 estimated using *in situ* shoreline measurements and SDSs. (b) Difference in the shoreline change estimated using *in situ* shoreline measurements and SDSs. The dashed lines are the limits of each beach segment. Progreso pier is located within segment 4 at the 2.238 eastern.

*Table 5.7:* Shoreline change found with SDS and *in situ* shoreline measurements between September 2008 and July 2010.

| Seg. no. | Shoreline change (m) | | | | Diff. |
|---|---|---|---|---|---|
| | *in situ* | | SDS | | |
| | $\bar{X}$ | SD | $\bar{X}$(SDS) | SD | |
| Seg.1 | 2.76 | 2.15 | 0.05 | 1.66 | 2.7 |
| Seg.2 | 1.77 | 1.45 | -3.48 | 1.46 | -1.7 |
| Seg.3 | 14.05 | 11.43 | 12.4 | 9.63 | 1.6 |
| Seg.4 | -5.54 | 1.75 | -1.48 | 7.13 | 4.1 |
| Seg.5 | 2.72 | 3.85 | 0.17 | 4.12 | 2.5 |
| Seg.6 | 0.59 | 2.66 | -2 | 2.33 | -1.4 |
| Seg.7 | -0.67 | 3.32 | -4.91 | 2.94 | -5.6 |
| Seg.8 | -3.32 | 2.42 | -6.56 | 2.03 | -3.2 |
| | | | | | ($\bar{X}$) -1.13 |

Table 5.7 shows the shoreline change found by the *in situ* shorelines and the SDSs. The difference between both shoreline change estimations is smaller than -5.6 m and the overall average difference is -1.13 m. This is much smaller than the pixel size and is in part related to the uncertainty in the water levels during the *in situ* shoreline measurements in 2008, also, the shoreline change estimation with SDS includes the inherent uncertainty of the technique. The difference between them shows that the estimated shoreline change using SDSs is of a similar magnitude to the estimated shoreline change using *in situ* shoreline measurements, allowing the estimation of erosion and accretion by using this technique.

Overall, the shoreline changes found using the SDSs and *in situ* shorelines are similar in magnitude. The shoreline change from 2008 to 2010 is small. Segment 3 is the exception, showing a maximum seawards movement up to 40 m in a two-year period. In contrast, the western part of segment 8 moved landwards by between three and five metres (Figure 5.15).

This comparison shows the capabilities of SDSs to detect shoreline change. Moreover,

it confirms that the use of SDS is possible as another resource to explore shoreline changes covering large spatial scales and that its future application to assess longer periods of time is possible.

## 5.4 Discussion

The definition of the *in situ* shoreline used in this research was adequate to compare the instantaneous shoreline location that the satellite could detect. This allowed the assessment of the factors that determine the accuracy of the SDS.

The simultaneous measurements of the tides and the shoreline location allowed a link to be made between the measurements, a tidal vertical datum, and the ellipsoid. This is important for the future comparison of the shoreline location of SDS with different data types, such as charts and other GPS surveys.

The inter-comparisons assessed in this chapter were helpful to investigate the differences between SDS and *in situ* shoreline measurements. The validation also highlighted the relevance of adjusting, both *in situ* shoreline and SDS, to equal water levels, even when the location has microtidal conditions and the horizontal excursion of the swash remains within the pixel size. The *in situ* shoreline measurements from 2008 were influenced by Hurricane Ike, moving the shoreline position seawards, by approximately one metre. Although the shoreline was adjusted to equal tidal levels, the shoreline from 2008 is further seawards than it should be during typical conditions. As a result, the shoreline change observed by using *in situ* shoreline measurements is relatively larger by approximately 1 to 3 metres than would be expected when using observed water levels to adjust both shorelines to equal tidal levels. This underlines the importance of avoiding analysing images when cyclones are in the vicinity because of the possible presence of a surge.

### 5.4.1 Validation of SDS

The inter-comparisons between SDS and *in situ* shoreline measurements allowed validation of SDS and an understanding of the factors involved in shoreline identification. Although there are a number of research projects that have previously used satellite optical images for shoreline identification, no validation has been carried out using quasi-simultaneous *in situ* shoreline measurements. Therefore these inter-comparisons are a first indication of the differences between a shoreline identified by optical satellite images in relation to *in situ* shoreline measurements.

The SDS is located in between the classified sea and land at half the pixel magnitude. This approach was followed by Foody (2002) in their earlier research to develop super-resolution methods. Although the precise location of the shoreline within the pixel is not known, that does not restrict its use for shoreline change studies. The validation revealed that the pixels classified as land might correspond to the swash region.

The extracted SDS in a location such as Progreso has a displacement from *in situ* shoreline measurements of -5.6 m. This displacement is related to the optical requirements of the NIR spectral band to detect a pixel as sea. This is in agreement with the previous research of Lafon et al.(2002(a)) concerning the properties of NIR to go through the water column. Moreover, the assessment of the capabilities of the spectral bands (chapter 3) indicates that the NIR is, in fact, the band that provides the best differentiation between sea and land. Furthermore, the estimated water depth of the SDS is in agreement with the seawards displacement and the NIR capabilities, which is a further confirmation that the displacement is an inherent characteristics of the satellite images.

The relevance of this displacement is that when extracting the SDS, it will be located at a lower elevation than the tidal level (by approx. 0.5 m to 1 m) when the satellite passed the study area. As a result, the SDS is located further seawards than the *in situ*

shoreline. So, when attempting its use for coastal management applications, it could decrease the assessment of vulnerability of coastal areas to flooding. Moreover, the horizontal distance will vary depending on the slope of the inter-tidal region. Thus, the displacement can be associated with a horizontal distance larger than the one found at Progreso in shallower (<3°) slopes (Figure 5.11).

When applying the SDS for estimating shoreline change it has been assumed that the displacement is the same over different images. When substracting the shoreline positions of different SDSs the displacement was disregarded. This is the main reason why it has not been used to determine confidence bounds.

Besides the displacement, the extracted SDS has a deviation (< 3 m) that is similar in magnitude to the cross-shore excursion due to the wave run-up. This deviation will be different in each SDS. Therefore, the use of the standard deviation to define confidence bounds was found to be adequate.

### 5.4.2 Accuracy of SDS

The accuracy of the shoreline extracted is the result of the developed methods and the accuracy of the geometric correction. Few studies correct satellite images geometrically using *in situ* GCP. The use of maps is widely used to correct images geometrically rather than *in situ* GCP (Robinson 2004; Lillesand et al. 2008). Studies such as White and El-Asmar (1999); Lafon et al.(2002(a)); Chu et al. (2006); Dinesh-Kumar et al. (2007) have corrected images using mostly GCP from *in situ* and from maps when *in situ* GCP is not available. In this way it is possible to achieve a geometric correction with an error less than the pixel size of the image. Hence, when the developed method is applied to images with an error in the geometric correction that is larger than the pixel size, the results could be different than those presented here.

The methods of Muslim et al. (2006); Foody et al. (2005) were found to offer the

greatest accuracy for shoreline detection. However, the estimated total RMS (3.2 m) was achieved using 16 m pixel size images that were originally 1 m pixel size. Thus, it would be difficult to achieve the same RMS using an image of 20 m pixel size. Their accuracy is twice as high as the accuracy achieved in this research. However, the comparison between both methods is not straightforward because the data referenced as true measurements was another image of 1 m pixel size, rather than *in situ* shoreline measurements as was the case in this research.

In contrast, the error found by Wang et al. (2010) of 87.3 m, using images of 30 m pixel size, is nearly three times larger than the pixel size. In contrast the maximum difference found between SDS and *in situ* shoreline measurements in this research is not larger than the pixel size. However, the reference used to assess the accuracy was not specified by Wang et al. (2010). Their accuracy is of the same order in magnitude as White and El-Asmar (1999) estimated (72 m) using the same pixel size images. Their research suggests that this is the order of accuracy that it is possible to achieve when using 30 m pixel size images for shoreline detection.

The uncertainty of the water depth found in this research, demonstrates a similar level of accuracy as that found by Lafon et al. (2002(a)) for deriving the bathymetry using a similar type of data (20 m pixel size images). Considering the pixel size, the uncertainty is less than the uncertainty in the water depth of the SDS identified here. However, the research from Lafon et al. (2002(a)) is focused on deriving the bathymetry, whereas this research has been focused on assessing the shoreline change and shoreline location.

Comparing the accuracy obtained with optical satellite images with other types of data, it has been found that the displacement between SDS and *in situ* shoreline is very close to the horizontal accuracy found with LIDAR images, with an error of 4.5 m (95 % c.i). This estimated error has a superior accuracy to shorelines extracted from traditional aerial photography (Liu et al. 2007). This shows that the difference in shoreline position

assessed with optical satellite images and LIDAR are comparable in their magnitudes.

The difference in tidal level when the image was taken does not have an effect on the ability to identify the SDS, as can occur with SAR images (Mason et al. 1995), due to the wet sand present in low tide conditions. The inter-comparisons assessed here reveal that the SDS extracted from an image in low tide conditions (2008) do not have any difficulties in the extraction, showing similar differences between *in situ* shoreline measurements and SDS.This suggests that the presence of wet sand in low tide conditions does not affect the ability to distinguish the shoreline using satellite optical images. However, this is a consideration that could be important in areas where the tidal range is larger than the pixel size and where the sediment on the beach can retain more water.

### 5.4.3 Validation of the SDS

The difference between the SDS and the *in situ* shoreline measurements varies depending on the beach characteristics, mainly due to the inter-tidal beach slope, shoreline orientation, and shorewards swash extent, demonstrating that the SDS does not show a random location. This was confirmed by the FFT analysis, which detected a red type of noise. Other factors that can affect the shoreline location include the nearshore bathymetry and suspended particles in the water column. However, the effect of these factors would not be as significant when using the NIR wavelength (Frouin 1996; White and El-Asmar 1999; Robinson 2004).

The differences between SDS and *in situ* shoreline measurements depend on the characteristics of the beach and the local conditions in terms of the water levels. The tides, surges and the atmospheric pressure can modify the accuracy of the SDS extracted from an image.

The use of optical satellite images, 10 m pixel size, provides a good spatial resolution

when using the method proposed in this research. The use of images with smaller pixel size might provide a smaller difference between SDS and *in situ* shoreline measurements. However, the overall difference will depend on the beach type and the local conditions of the study area. The optical capabilities of the satellite imagery are not going to vary with a smaller pixel size (see section 3.3.4).

### 5.4.4 Shoreline change using SDS

The comparison betwen the shoreline change found using *in situ* shoreline measurements and SDSs shows that the SDSs can identify shoreline changes larger than 5 m. Furthermore, the shoreline change assessed with SDSs is smoother in relation to the estimated shoreline change using *in situ* shoreline measurements.

The developed method could potentially underestimate rather than overestimate shoreline change. The presence of high concentrations of suspended particles and the shallowness of the bathymetry might move the SDS further seawards from *in situ* shoreline measurements. In addition, the presence of a large shorewards excursion of the wave run-up can move the *in situ* shoreline measurements further landwards from the SDS.

Locations with significant swash (1 m) over an inter-tidal beach slope of 6° will produce a shorewards extent as large as 13 m. Therefore, the confidence bounds would be about a pixel and a half when analysing 10 m pixel size images, which could reduce the capability of SDS to identify shoreline change. One possible approach to reduce the confidence bounds would be the use of a different definition of the *in situ* shoreline that does not involve the swash excursion, such as the vegetation line (Chen and Rau 1998; Shaghude et al. 2003; Fromard et al. 2004).

For coastal management applications, where the place of interest of study has large and rapid shoreline change (> 20 m), or the shorewards extent of the wave run-up is narrower than the shoreline change expected, the use of SDS can be useful to determine

coastal management actions appropriate to the estimated shoreline change rates using SDS.

## 5.5 Chapter summary

This chapter validates SDS using quasi-simultaneous *in situ* shoreline measurements. Two inter-comparisons are assessed from two different years, 2010 and 2008, with different tidal conditions. The SDS from 2010 was used to define confidence bounds, due to the presence of a cyclone in the vicinity during the *in situ* shoreline measurements in 2008.

The SDS is consistently seawards in relation to the *in situ* shoreline measurements, with an overall displacement of -5.6 m over 8 km of shoreline. This magnitude agrees with the measurements carried out in high tide conditions. This displacement of the SDS is related to the optical requirements of the satellite needed to distinguish intensity values as either land or sea. The deviation between *in situ* shoreline measurements and SDS ($\pm$ 1.4 m) is associated to the horizontal excursion of the wave run-up.

The comparison of the tidal predictions and the *in situ* measured height suggests the presence of a negative surge (30 to 40 cm) during the *in situ* shoreline measurements in 2008. This negative surge explaines the overall small mean difference (0.4 m) found between the SDS and *in situ* shoreline measurements.

Confidence bounds were determined for the SDS using the standard deviation between the *in situ* shoreline and the SDS, which is related to the wave run-up.

The shoreline change detected by SDS corresponds well to the shoreline change found using *in situ* shoreline measurements, with differences as large as 3.6 m from the upper limit of the determined confidence bounds.

## 5.6 Conclusions

1. The SDS identified with satellite optical images (see section 3.3) is located seawards with a mean cross-shore difference of -5.6 m and a standard deviation of 1.4 m over 8 km of shoreline. This difference was assessed using quasi-simultaneous *in situ* measurements, over a five hour period, both adjusted to equal tidal levels.

2. The identified SDS has an alongshore resolution of 50 m in relatively straight shorelines (see section 3.6.2). Therefore, abrupt changes in shoreline orientation along a shore smaller than 50 m long would not be identified by the SDS. For example, segments showing a relatively large orientation (18°, seg. 3) have a difference between -12 and -1.7 m, whereas straight segments, such as segments 1 and 2, have a difference ranging between -9 and -2 m.

3. The confidence bounds for the SDS are within the pixel size, even when the deviation and the associated horizontal uncertainty due to the difference between predicted and measured tide have been included (3.2 m). The deviation is associated with the shorewards extent of the wave run-up.

4. The shoreline change estimated with SDS, given the confidence bounds, is of the same magnitude as the shoreline change estimated with *in situ* shoreline measurements, showing its capability to assess shoreline change during longer periods of time.

5. Shoreline change calculated with SDS would not detect changes in the shoreline position smaller than 5 m in the horizontal.

# Chapter 6

# Assessing shoreline change using SDSs

## 6.1 Introduction

This chapter shows the capability of SDSs to detect shoreline change over a 6.5 year period, from December 2003 to July 2010, using Progreso, Yucatán as a case study area (see chapter 4). The shoreline change found here gives an indication of the local coastal processes and their relationship to the winds and waves.

The SDSs used in this chapter to describe shoreline change were extracted using the previously developed methods (section 3.3), which were validated using quasi-simultaneous *in situ* shoreline measurements. The shoreline change presented here considers the upper and lower limits of confidence bounds for the SDS determined in relation to *in situ* shoreline measurements (see chapter 5).

Progreso is located in the path of cyclones, faces coastal erosion and has little information about its shoreline change, and is therefore an interesting location to apply the developed method to explore shoreline change using SDSs.

The SDSs analysed here are from different seasons and different years. Inter-seasonal and inter-annual shoreline change was detected using SDSs, as well as the overall change in shoreline location over time.

The observed shoreline change is interpreted by considering the environmental factors

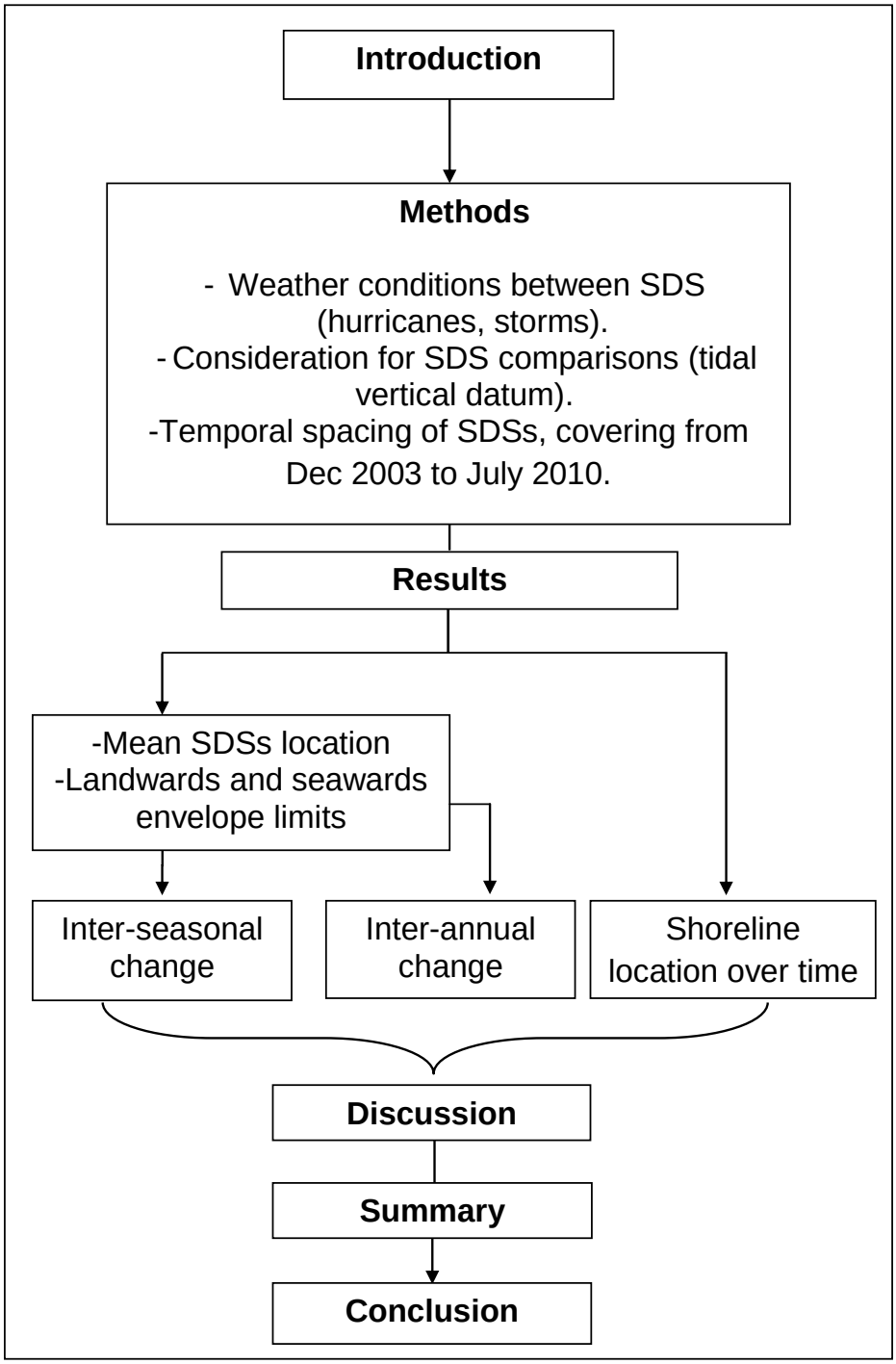


*Figure 6.1:* Chapter 6 structure summary.

such as storms, winds, waves, and artificial barriers of sediment (groynes, piers) to deduce which processes may be involved.

Figure 6.1 summarises the contents of this chapter. In this chapter, after the introductory section, methods are described with considerations for further calculation of shoreline change. The meteorological conditions that took place between SDSs are also described in this section. The results section is divided into three parts. The first part assessess inter-seasonal shoreline changes. The second part assess the inter-annual shoreline change. The third part explores the overall shoreline change over time. The section of discussion integrates the results with the environmental factors and the local processes that could have been involved in the shoreline change. The last two sections give a summary and conclusions for the chapter.

## 6.2 Methods

The SDSs are referred to the same vertical datum as the predicted tides (MLLWL, see section 4.5). The shoreline position was adjusted using the estimated inter-tidal beach slope for each beach segment in July 2010 (see section 5.2.4) and the predicted tidal levels (see chapter 4). The fact that all the SDSs were adjusted using a fixed inter-tidal beach slope when is known that the beach profile changes over time adds an error into the adjustment. This approach was possible to follow for the case of study, because it does not have a strong change over the seasons, and thus, their variability is not significant (see section 4.4.4).

### 6.2.1 Temporal spacing

The SDSs used in this chapter comprise a variety of seasons, covering a time span of 6.5 years. The SDSs from 2004 and 2005 are more frequent, with four images per year, whereas from 2006 to 2010 there is one SDS per year and for 2009 there is no SDS available. The temporal spacing was considered for the interpretation of shoreline change as well as the 'typical' shoreline change for Progreso. Therefore the analysis of the SDSs from 2003 to 2005 might allow an estimate of the seasonality of shoreline

change to be proposed.

The SDSs from 2004 and 2005 were used to calculate the mean annual SDS position and the envelope of shoreline change over different seasons.

The SDSs between 2006 and 2010 are during the hurricane season. Therefore, their shoreline locations do not describe 'typical' conditions (Crowell et al. 1991; Leatherman and Douglas 2003) in the region, their position are interpreted within the envelope of shoreline change with reference to the earlier SDSs.

**Inter-seasonal shoreline change**

The inter-seasonal shoreline change, as well as the seaward and landward envelope limits of the shoreline, were estimated using the SDSs from December 2003 to July 2005. This time span includes a minimum of two SDSs per season. The SDS of different seasons is then compared to the mean shoreline position.

**Inter-annual shoreline change**

The inter-annual shoreline change was calculated using the mean SDS position. Although the mean SDS does not correspond to the assessed period of time, it showed to be an useful reference to compare the different SDS positions.

**Shoreline change over time**

The mean shoreline position of each beach segment was adjusted into a line to find whether there was a negative or positive gradient over time. A negative gradient corresponding to erosion was found for all beach segments, with the exception of segments 3 and 6 for which there was a positive gradient. Rates of change were estimated using the slope of the adjusted line for each beach segment.

### 6.2.2 Spatial resolutions

The shoreline change was estimated by considering the upper and lower limits in shoreline position for each SDS (see section 5.4). So, the shoreline change has a maximum and a minimum shoreline change that could have occurred between two SDSs.

The shoreline change was estimated using the average shoreline change for each beach segment. The shoreline change is analysed taking into consideration the beach characteristics such as the coastal orientation, beach slope, groynes and piers. The average shoreline change does not consider the variations in the alongshore. However, the plots of the change in the alongshore show the variation within each beach segment.

### 6.2.3 Meteorological conditions for the SDSs

Table 6.1 summarises the meteorological conditions prevailing in between the different SDSs assessed, including the season, the occurrence of storms, hurricanes and corresponding measurements from the previous SDS date.

During the 6.5 years of shoreline change, cyclones, storms as well as calm conditions occurred. The spacing of SDSs is random and it does not include an SDS before and after a cyclone or a storm. Between each SDS a number of events occurred, which makes it difficult to investigate the effect of a specific event on the shoreline location. However, it is possible to estimate the overall conditions during the period in terms of wind velocity and direction, offshore waves and the track of hurricanes. Within the time span studied, the 2005 hurricane season was the most active on record in the Atlantic (NHC 2010). However, the more significant hurricanes in terms of strength and distance from Yucatán are Hurricane Ivan (2004), Hurricane Emily (2005) and Hurricane Ike (2008).

## 6.3 Results

### 6.3.1 Inter-seasonal shoreline change using SDSs (Dec. 2003-2005)

This section firstly shows the shoreline positions of the SDSs from 2003-2005. Secondly, five inter-comparisons are used to describe inter-seasonal shoreline change: two inter-comparisons from winter, one from a calm period and two from the hurricane season.

The shoreline change that occurred in the inter-comparisons is related to waves and winds. Although the waves from deep water conditions and shallow water conditions are different, they were included to assist the interpretation of shoreline change and to estimate the number of storms in the case study.

**Envelope of shoreline positions (Dec. 2003-Jul. 2005)**

Figure 6.2 shows the shoreline position of all the SDSs in relation to a mean shoreline (N=9). Each beach segment has a range of change of about 20 m, with the exception of segments 3 and 8, which have a range of up to 150 m and 30 m respectively.

Beach segments 3, 6, 5 and 4 are the beach segments showing the largest shoreline change respectively. Segments 7 and 8 show rapid changes, moving as much as 30 m within months. In contrast, segments 1 and 2 show the smallest movement in shoreline location.

*Table 6.1:* Environmental conditions within the SDS used to assess shoreline change limited to the available data. See appendix for further details from hurricanes.

| SDS date | Δt(yrs) | Season | Environmental conditions |
|---|---|---|---|
| 12/07/2010 | 1.8 | Hurricane | The 2009 hurricane season was not very active. One hurricane passed close to Yucatán from Nov. 4 to 10. On the $8^{th}$ it was at its closest to Yucatán (approx. 370 km), holding winds of 160 $kmh^{-1}$ and atm. pres. of 976 hPa. |
| 20/09/2008 | 1 | Hurricane | H Ike passed close to Yucatán at approximately 500 km NE, with intensity as cat. 1, with winds of 56 $kmh^{-1}$ and 957 hPa of atm. press. on the $10^{th}$ of September, then moved north to Galveston, Texas, where it had its main landfall. |
| 5/09/2007 | 1.5 | Hurricane | TS Alberto passed close to Yucatán on Jun. 8, 2006. In 2007, H Dean crossed Yucatán from the eastern to the western coast with an intensity of cat. 2, with winds of 168 $kmh^{-1}$ and 950 hPa of atm. press. |
| 6/02/2006 | 0.6 | Winter | The 2005 hurricane season was the most active on record. Four cyclones passed close to Yucatán: H Rita, H Wilma, H Stan and H Katrina. H Rita passed at approx. 500 km, with intensity of cat. 5, winds of 264 $kmh^{-1}$ and atm. press. of 914 hPa. H Wilma passed at approx. 280 km, on Oct. 22, with intensity of cat. 2, winds of 160 $kmh^{-1}$ and atm. press. of 957 hPa. H Stan passed at approx. 80 km, as TS, holding winds of 64 $kmh^{-1}$ and atm. pres. of 1004 hPa. H Katrina passed at approx. 544 km with intensity of cat. 4, winds of 230 $kmh^{-1}$ with atm. press. of 955 hPa. |
| 30/07/2005 | 0.08 | Hurricane | Hurricane Emily passed at approx. 90 km from Yucatán as cat. 2, winds of 160 $kmh^{-1}$ and an atm. press. of 975 hPa. |

*Table 6.1 continued...*

| SDS date | Δt (yrs) | Season | Environmental conditions |
|---|---|---|---|
| 17/07/2005 | 0.25 | Hurricane | Hurricane Arlene passed at approx. 540 km from Yucatán, winds of 72 $kmh^{-1}$ with atm. press. of 1000 hPa. |
| 04/04/2005 | 0.085 | Calm | There is no evidence of any storm taking place. |
| 20/03/2005 | 0.37 | Calm | There is no evidence of any storm. |
| 15/11/2004 | 0.12 | Winter | No hurricanes passed close to Yucatán. |
| 27/09/2004 | 0.25 | Hurricane | TS Bonnie, approx. 240 km from Yucatán, with winds of 72 $kmh^{-1}$ and an atm. press. of 1007 hPa. H Charley, approx. 800 km from Yucatán with intensity of cat. 2 with winds of 168 $kmh^{-1}$ and atm. press. of 975 hPa. A surge of 3.9 m in Playa Cajio, Cuba was reported on Sept. 13 (NHC 2010). H Ivan, approx. 256 km from Yucatán on Sept. 14, with intensity of cat. 5 with winds of 256 $kmh^{-1}$ and atm. press. of 924 hPa. |
| 25/06/2004 | 0.083 | Hurricane | No hurricanes passed close to Yucatán. |
| 20/05/2004 | 0.41 | Calm | The wave record from Dec. $30^{th}$ to May $19^{th}$ has a mean Hs of 0.26 m, with max. of 0.35 m measured in Progreso, 4 km offshore. |
| 23/12/2003 | | Winter | Hs of 0.32 m and max. of 0.57 m measured in Progreso, 4 km offshore from the pier, from Nov. $11^{th}$ to Dec. $20^{th}$ |

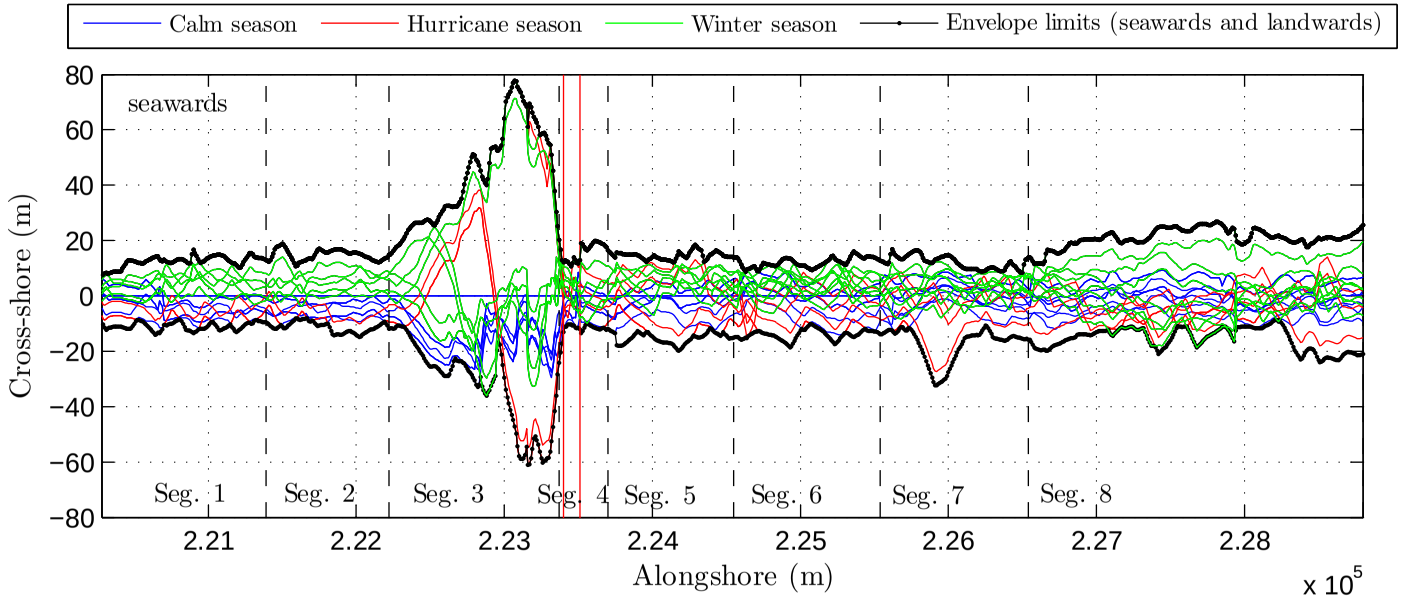


*Figure 6.2:* SDSs from Dec. 2003 to Jul. 2005, showing the seaward and landward envelope limits, in relation to the mean SDSs in Progreso, Yucatán. The SDS position for each date considers their landward and seaward position due to their confidence bounds. Positive values are seawards and negative values are landwards. SDSs from the same season have the same line colour, blue for calm season, red for hurricane season and green for winter season. The beach segments' order increases from west to east (dashed lines). The vertical red lines indicate the position of the two Progreso piers (see section 4.3.7).

### Winter

The SDSs from the winter season are from December 23, 2003; May 20, 2004; November 15, 2004, and March 20, 2005. The spacing of the SDSs allows assessment of the shoreline change occurring in two different winters.

### November 2004 to March 2005

The SDSs from November and March mark the start and the end of the winter season. Figure 6.3 shows the storms that occurred in this period. The stronger events are on December 25 to 26, January 13 to 16, February 28 to March 6 and March 17 to 19, making a total of 17 days. Generally the storms show western winds, the opposite direction to the dominant winds, and offshore Hs larger than 1.5 m. When travelling onshore the waves will approach aligned to the wind direction and with a smaller Hs than in offshore conditions (see section 4.3). Offshore waves between 1.5 and 2.5 m height might decrease their height to less than 0.5 m, with an approaching angle driven by a wind direction of 140° with NW winds. The changes in their approaching angles reverses the alongshore transport and turns the sand movement towards the east.

Figure 6.4 shows the shoreline change in relation to the mean SDSs. It is important to highlight that the SDS from November had some recovery after the hurricane season in 2004, during which time three cyclones passed close to Progreso (Figure 6.9). The SDS from November is at the seaward envelope limit whereas the SDS from March is landward by approximately 10 m in relation to the SDS from November (segments 1 to 2 and 5 to 7). Segment 7 has some overlap between both SDSs and has an abrupt landward movement of approximately 10 m on its western side, which seems to be related to a groyne. Segment 3 shows that the SDS from March moved landwards on its western side and seawards on its eastern side. This landward movement is consistent with the presence of storms with opposite wind direction (west). In addition, modelled

waves with Hs of 1.5 m offshore took place one day before the SDS from March.

Table 6.2 shows that the overall shoreline change was landward, between 3.4 (seg.3) and -18.6 m (seg.8). The most eastern beach segment (seg.8) and the segment in the middle (seg. 4) show an overall landward movement of up to -18.6 m and -18.3 respectively. The landward movement of segment 4 could be explained by the two piers. The waves, when interacting with the pier, can produce undertow currents thus eroding the nearshore bottom and producing erosion at the shoreline level. In contrast, the landward movement of segment 8 might be related to cross-shore transport, because there is no presence of coastal structures close to this segment, which therefore allows the sand to move in the alongshore and cross-shore directions. This is in agreement with the presence of storms, where the cross-shore transport is larger than the alongshore transport (Komar 1998; Masselink and Hughes 2003).

**December to May (2003-2004)**

The shoreline change observed from December to May shows an overall landward movement. The mean shoreline change has smaller magnitudes than those previously observed between November and March, ranging between -0.7 m and -4 m, which can be explained in principle because this inter-comparison evaluates a smaller period of time and the SDS from December is landwards in relation to the SDS from November. Segment 8 has the largest shoreline retreat, as was observed between November and March (Table 6.2).

Figure 6.5 shows that six storms ocurred from January to May, over a total of 16 days. Five of these events occurred simultaneously with offshore waves larger than Hs 1.5m. The shoreline change between December and May is of a smaller magnitude than the shoreline change from November to March, even though more storms could have occurred between December and May. However, the SDS from May is three weeks after the last storm, whereas the SDS from March is one day after the last storm. Some

recovery of the beach may have taken place between the last storm and image of May 2004 but this could not be identified by the SDS. Moreover, December to May SDSs include part of the calm season, where the storms are less frequent and Hs is smaller than 1.5 m whereas November to March SDSs had Hs larger than 1.5 m one day before the satellite passed over Progreso.

Given the temporal spacing the two inter-comparisons from November 2004 to March 2005 and December to May 2004 show consistency in their overall landward movement, which is of a similar magnitude. Moreover, both inter-comparisons agree that segment 8 had the largest landward movement. Their consistency provides an element of confidence that they are showing a consistent seasonal effect.

*Figure 6.3:* Wind direction, wind velocity, Hs (offshore) and Ts, during Nov. $15^{th}$, 2003 to March $20^{th}$, 2004. The winds were measured at Telchac and the waves are modelled in deep water (see section 4.4.2).

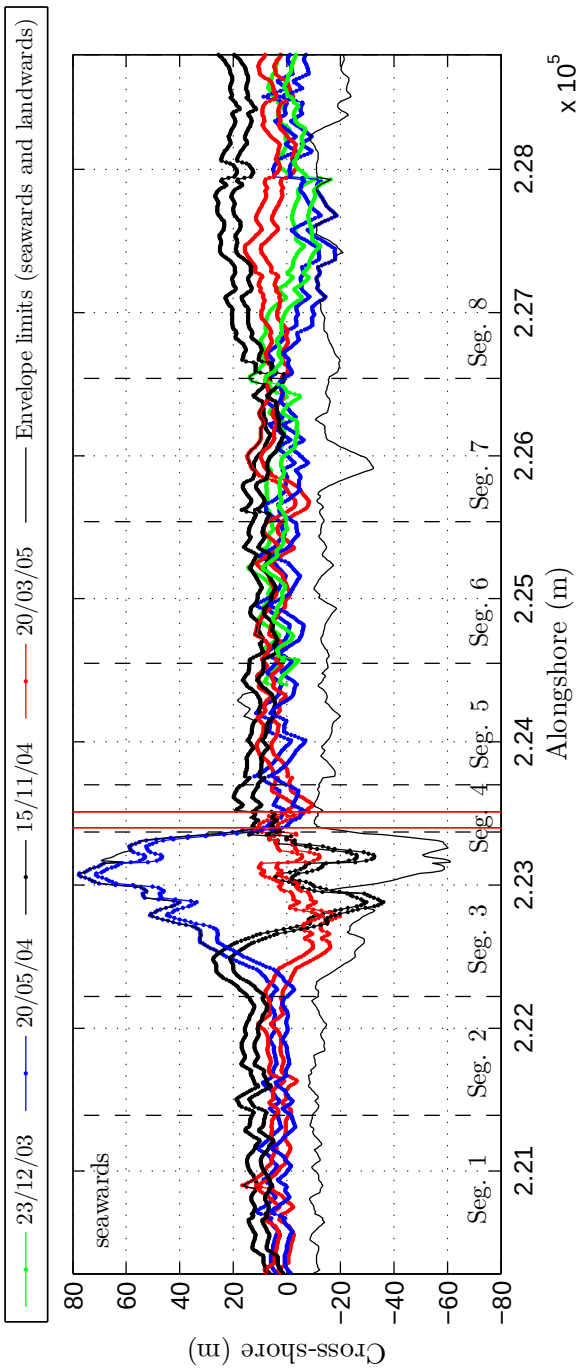


*Figure 6.4:* Shoreline change on the 15/11/04, 20/03/05, 23/12/03 and 20/05/04. SDSs in relation to the mean SDS in Progreso, Yucatán, México. The SDS position for each date considers their landward and seaward position due to their confidence bounds. Positive values are seawards and negative values are landwards. The beach segments' order increases from west to east (dashed lines). The SDS from 15/11/04 only covers part of segments 5 to 8. The vertical red lines indicate the position of the two Progreso piers (see section 4.3.7).

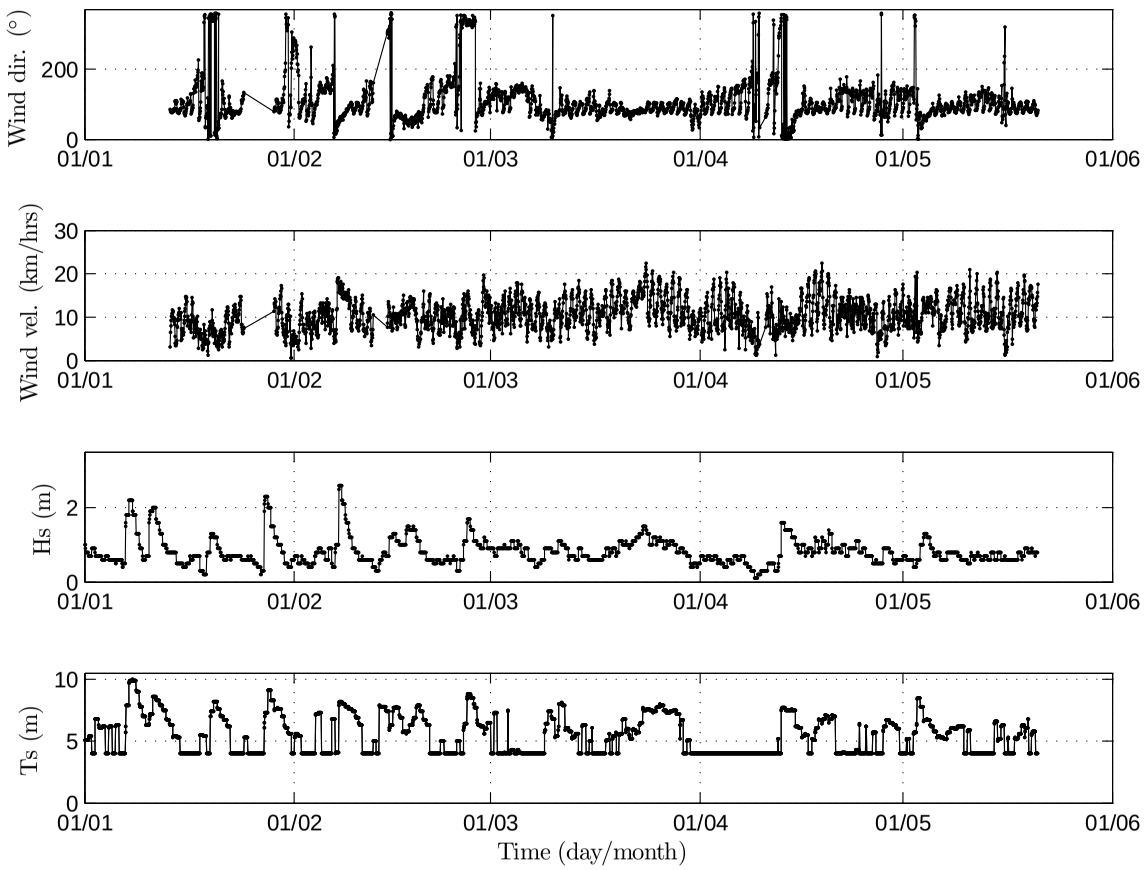


*Figure 6.5:* Wind direction, wind velocity, Hs (offshore) and Ts, during Jan $1^{st}$ to March $20^{th}$, 2004 in Progreso. The winds were measured at Telchac and the waves were modelled in deep water (see section 4.4.2).

*Table 6.2:* Overall inter-seasonal shoreline change for each beach segment (min, max and mean) in Progreso.

| Date (d/m/y) | | Seg.1 | Seg.2 | Seg.3 | Seg.4 | Seg.5 | Seg.6 | Seg.7 | Seg.8 |
|---|---|---|---|---|---|---|---|---|---|
| 15/11/04 to | min | -11.1 | -13.4 | -9.4 | -18.3 | -10.4 | -9.6 | -8.6 | -18.6 |
| 20/03/05 | max | -0.7 | -3.8 | 3.4 | -4.4 | 0.4 | 0.7 | 1.4 | -6.6 |
| | $\bar{X}$ | -5.9 | -8.6 | -3 | -11 | -5 | -4.5 | -3.6 | -13 |
| 23/12/03 to | min | | | | | -6.1 | -8.9 | -6.9 | -10 |
| 20/05/04 | max | | | | | 4.7 | 1.4 | 3.1 | 1.9 |
| | $\bar{X}$ | | | | | -0.7 | -3.8 | -1.9 | -4 |
| 20/03/05 to | min | | | | | | | -14 | -16 |
| 04/04/05 | max | | | | | | | 1.9 | 1.2 |
| | $\bar{X}$ | | | | | | | -6.5 | -7.6 |
| 20/03/05 to | min | -27.4 | -20 | -3.93 | -26.9 | -22.5 | -25.1 | -19.8 | -21.7 |
| 17/07/05 | max | -0.3 | 0.07 | 3.8 | 8.3 | -3.5 | 3.3 | 7.2 | 0.2 |
| | $\bar{X}$ | -10.9 | -10.4 | -12.9 | -7.7 | -11.9 | -11.2 | -8.21 | -10.1 |
| 20/05/04 to | min | | | | -14.3 | -11.2 | -21.7 | -13.8 | -11.4 |
| 25/06/04 | max | | | | 18.6 | 18.7 | 8.5 | 8.9 | 19.1 |
| | $\bar{X}$ | | | | 2.7 | 4 | -1.1 | -0.6 | 2.6 |
| 20/05/04 to | min | -20.3 | -19.9 | -132 | -44.4 | -30.5 | -28.3 | -32.9 | -32.7 |
| 27/09/04 | max | 1.7 | 1.7 | -0.5 | 1.1 | -2.5 | -2.7 | -2.9 | 18.8 |
| | $\bar{X}$ | -9.6 | -10.7 | -45.5 | -10.1 | -12.2 | -11.2 | -15.6 | -4.6 |
| 20/05/04 to | min | -8.16 | -2.16 | -86.1 | -16.3 | -6.8 | -4.7 | -6.1 | -5.9 |
| 15/11/04 | max | 17.7 | 20.6 | 22.5 | 25.5 | 21.6 | 18.6 | 20.9 | 44.1 |
| | $\bar{X}$ | 6.3 | 9.6 | -36.5 | 10.5 | 8.1 | 8.2 | 7.4 | 22.9 |

**Calm**

The SDSs from the calm season are from March 20, April 4 and July 17, 2005. The SDS from March is from the start of the calm season. Therefore it serves as a reference for the shoreline location. The SDS from April is 15 days later than the earlier shoreline. Therefore, it would not be expected to detect many changes in such a short period of time. The shoreline from July 17 includes a month and a half of the hurricane season period when TS Arlene (see appendix) passed approximately 500 km east of Yucatán,

from June 10 to 11, with winds of 72 $kmh^{-1}$ and an overall NNW movement. As a result, the shoreline change might have been affected by TS Arlene. So, the temporal spacing of the available SDS would not allow assessment of shoreline change in the calm season.

Figure 6.6 shows the wind and waves from March to July. The winds were from NE-NEE directions, with velocities between 10 and 20 $kmh^{-1}$. During the last week of March and the first two weeks of April the winds changed direction from NE to NW, with offshore Hs as large as 2 m. A storm in early April is out of the storm season and it might have produced an effect on the SDS in April.

Figure 6.7 shows that during the 15 days from March to April the shoreline effectively moved landwards. The SDS from April is approximately 10 m seaward from the mean SDS. This shoreline change seems to be due to a storm out of season in Progreso. Table 6.2 shows that the overall shoreline change from March was -7.6 m. The eastwards segment 8 had the largest movement (-16 m).

Figure 6.7 shows that the SDS from July is located landwards between 20 and 27 m from the March SDS, at a similar location to the April SDS. The upper and lower limits overlap in segments 7 and 8, suggesting that no change took place in segments 7 and 8 from April to July. Interestingly, the SDS is further seawards in the westward beach segments, at the envelope limit. This might be related to westward alongshore transport, which is reduced by the pier. This inter-comparison does not allow measurement of the effect of TS Arlene on the SDS from July, particularly because a considerable time occurred between TS Arlene and the SDS date.

The inter-comparison of this season shows that the shoreline position did not recover in 2005, remaining closer to the landward envelope limit rather than the seaward envelope limit, which could leave it more vulnerable to shoreline retreat during the hurricane season. However, the SDS from March is seawards of the mean SDS shoreline position,

suggesting some recovery in the shoreline position after the winter season.

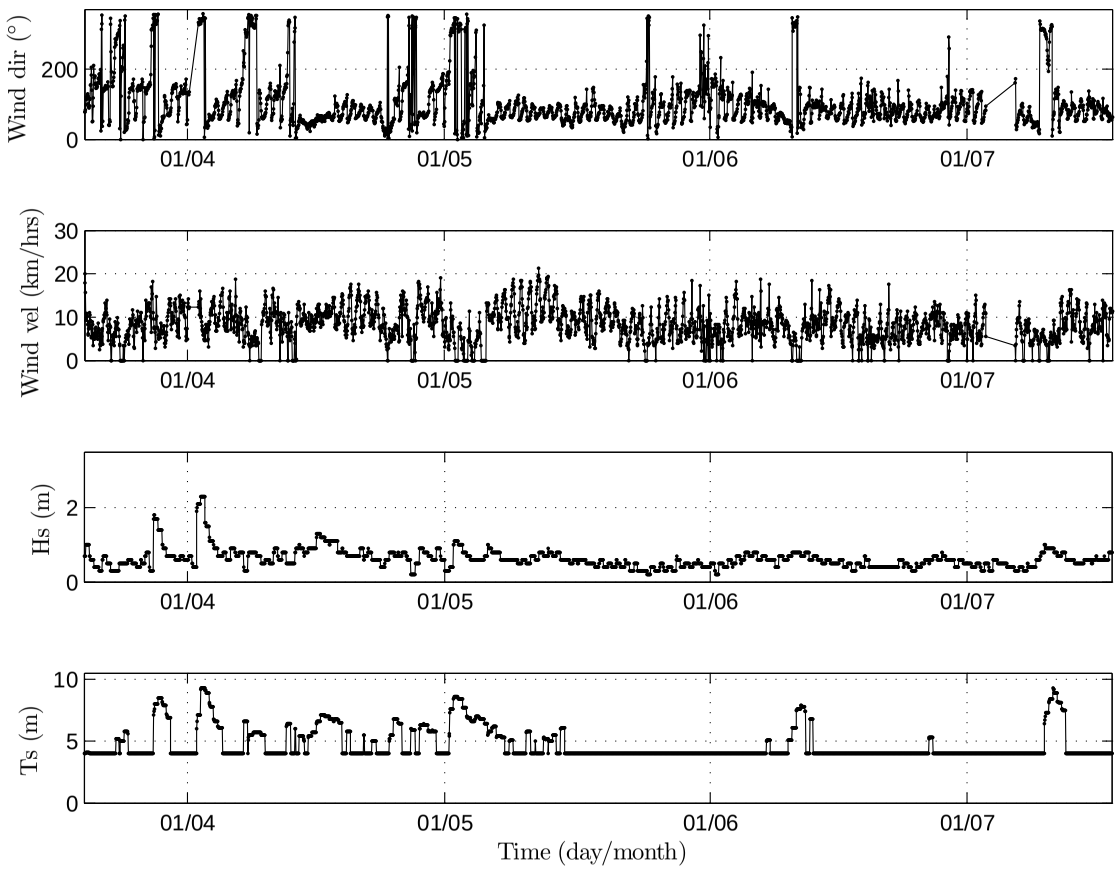


*Figure 6.6:* Wind direction, wind velocity, Hs (offshore) and Ts, from March $20^{th}$ to July $17^{th}$ 2005. The winds were measured at Telchac and the waves were modelled in deep water (see section 4.4.2).

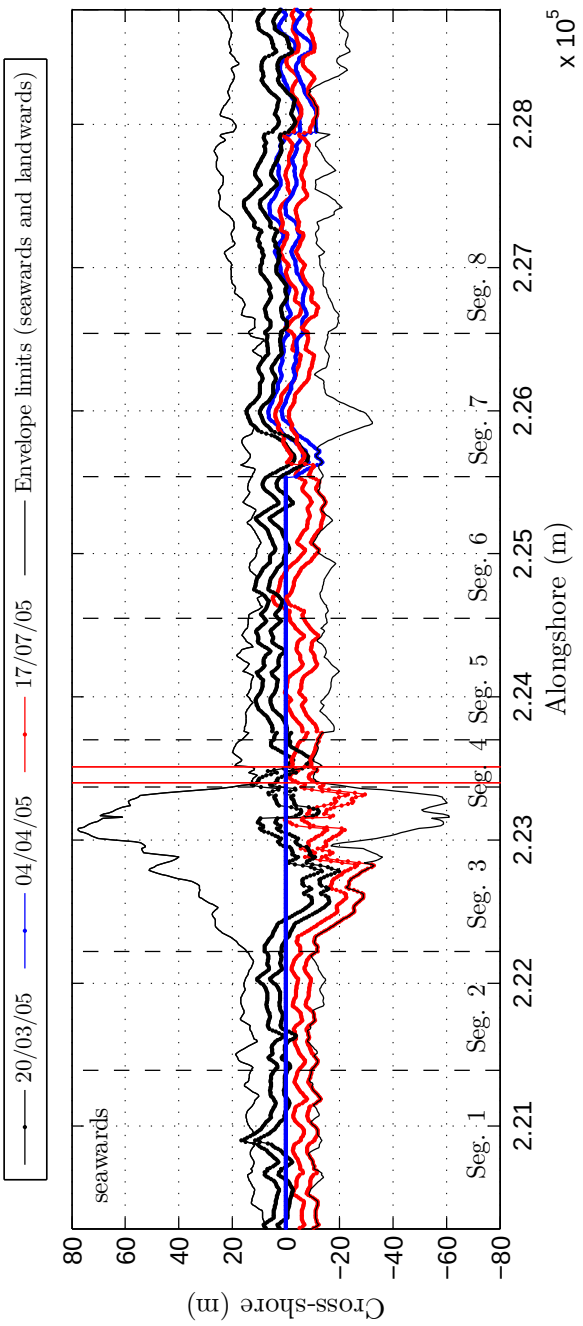


*Figure 6.7:* Shoreline change from March $20^{th}$ 2005 to July $17^{th}$ 2005. SDSs in relation the mean SDS in Progreso, Yucatán, México. The SDS position for each date considers the landward and seaward position due to the confidence bounds. Positive values are seawards and negative values are landwards. The beach segments' order increases from west to east (dashed lines). The vertical red lines indicate the position of the two Progreso piers (see section 4.3.7).

### Hurricane

The SDSs from the hurricane season are from June 25 and September 27. Their spacing allows assessment of the shoreline change at different stages within the hurricane season. During June-July and October-November, the hurricane activity is typically small, and during August-September the hurricane season has higher activity (see section 4.3.5, Figure 4.7). The shoreline change of these SDSs is analysed in relation to the shoreline from May 20, 2004, rather than using the mean SDS. This is because the SDS from May is from late within the calm season, and can be used as a reference of the shoreline location before the hurricane season starts. However, the plots include the mean SDS and the envelope limits used as a reference.

Figure 6.8 shows the wind and wave heights from late May to November. The wind records do not cover the whole period. However, the existing data shows that from late May to June there was no presence of cyclones, the wind had overall low velocities (5-20 $kmh^{-1}$) with NE-SE wind directions and Hs smaller than one metre, reaching the shore at less than 0.5 m, with an approaching angle between 80 and 120° from the north, mostly parallel to the shore. Therefore, the longshore transport would have been reduced, hence, little change in the shoreline location was expected to occur. However, H Ivan, TS Bonnie and H Charley took place in August, therefore, September SDS could have been modified by their effects.

### June in 2004

Figure 6.9 shows that the shoreline from May to June remained at the same location. The upper and lower limits of the SDSs overlap. The SDS from June 25, 2004 only covers part of segment 3 to 8 due to the availabily of the satellite imagery.

Table 6.2 shows that the mean shoreline change is smaller than 5 m. Segment 5 has the largest change, of 4 m seawards, whereas the rest of the segments had a smaller

shoreline change. The small change observed agrees with the overall calm conditions from May to June, when the hurricane activity is small. In addition, it provides further evidence that the SDS reproduces the same results when the shoreline has not changed its position.

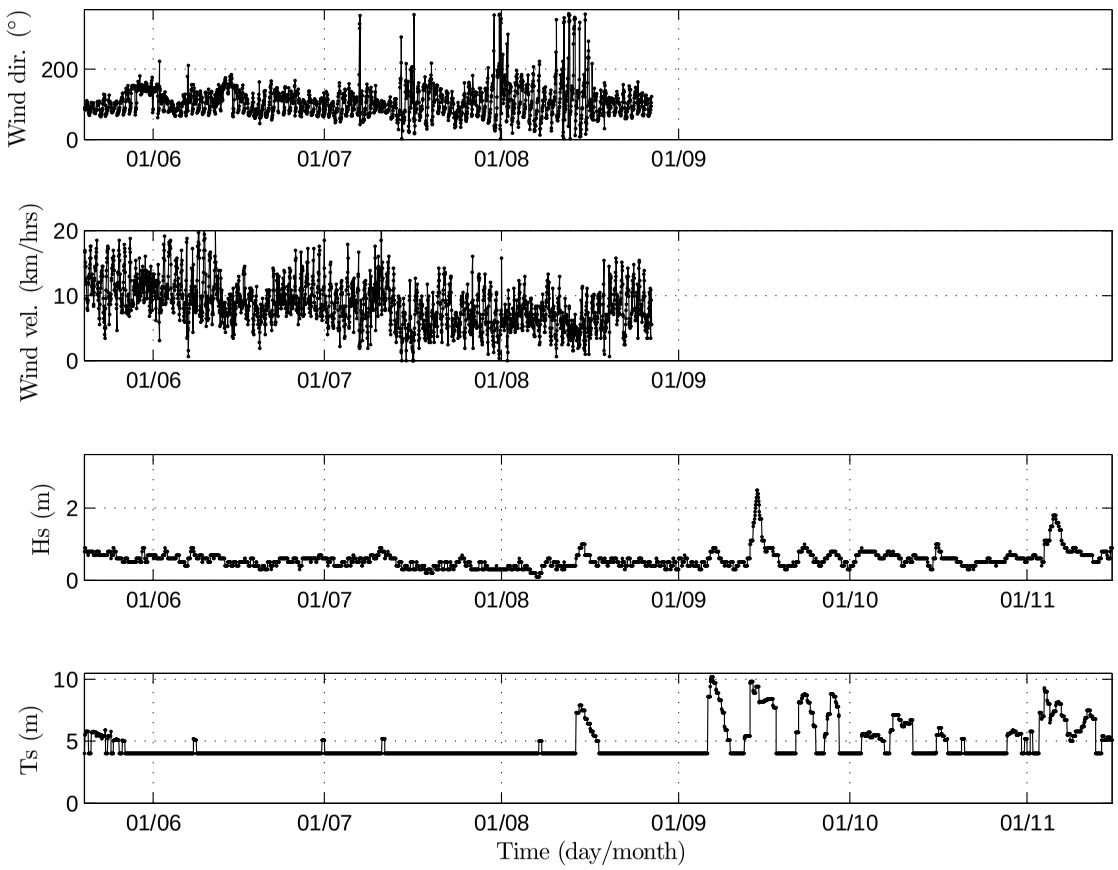


*Figure 6.8:* Wind direction, wind velocity, Hs (offshore) and Ts, from May $20^{th}$ to June $25^{th}$ in 2004. The winds were measured at Telchac and the waves were modelled in deep water (see section 4.4.2).

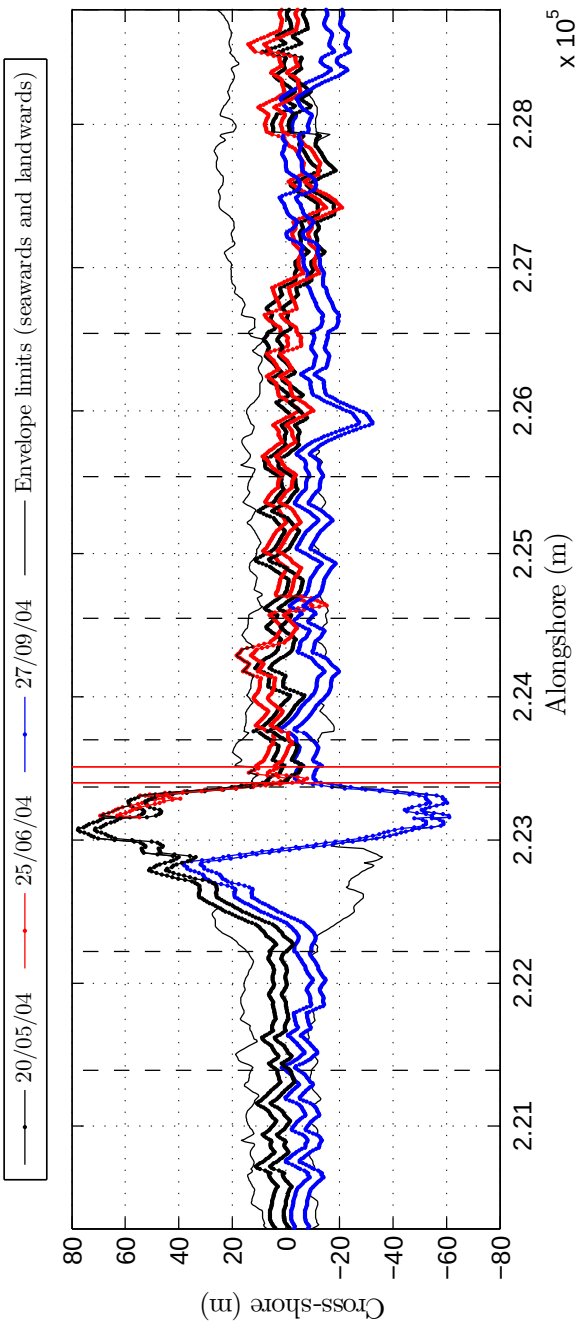


*Figure 6.9:* Shoreline change from May $20^{th}$ 2004 to September $27^{th}$ 2005 in Progreso, Yucatán, México. The SDS from 25/06/04 only covers part of segment 3 to 8. The SDS position for each date considers their landward and seaward position due to their confidence bounds. Positive values are seawards and negative values are landwards. The beach segments' order increases from west to east (dashed lines). The vertical red lines indicate the position of the two Progreso piers (see section 4.3.7).

**September 2004**

Figure 6.9 shows that the upper and lower limits of the SDSs from May and September are clearly distant from each other. The SDS from September moved landwards at least 10 m, remaining at the landward envelope limit. The large shoreline change can be explained by the presence of three hurricanes that passed close to the area: TS Bonnie, H Charley and H Ivan. TS Bonnie and H Charley occurred during the first two weeks of August (see appendix), while Ivan took place 13 days before the SDS from September.

Table 6.2 shows that all the beach segments moved at least 10 m landwards, with maximum possible changes of 130 m. Eastern beach segments show larger landward movement (from 28 to 44 m) than the western beach segments (20 m). Segment 3 had the largest landward movement (up to 130 m), along 300 m of shoreline.

The wind velocities in July and August remained within the typical ranges ($< 12\,\mathrm{kmh}^{-1}$, E-SE direction). Hurricane Ivan was the closest to Yucatán on the $14^{th}$ September (Figure 6.10). The offshore waves during a hurricane can be as large as 2.5 m in height and when travelling onshore they will approach at different angles according to the hurricane track. There are no wave records in shallow water depths to estimate how large and in which direction the waves reached the shore during Hurricane Ivan. The existing measurements (see section 4.3) were used to estimate the Hs that Hurricane Ivan could have produced.

H Ivan, category 5 intensity, could generate even larger waves than those measured during category 2 H Dolly. Technical reports from Pensacola, Florida (Wang and Enfield 2006) show that H Ivan caused changes along 300 km of shoreline leading to an erosional elevation of between 2 and 5 m height, with severe backwash erosion. However, the effect of H Ivan over Progreso was much smaller than in Pensacola, primarily because H Ivan had a direct impact on the shore of Pensacola, whereas H Ivan passed at approximately 450 km from Yucatán. At such a distance, large wave attenuation will

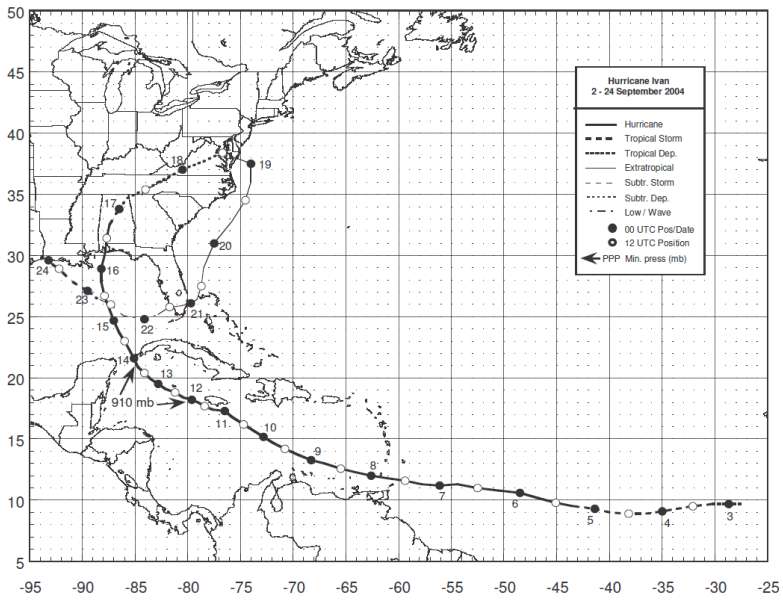


*Figure 6.10:* Track of Hurricane Ivan. The image is from NHC (2010).

have occurred. For example, waves of 12 m were recorded in the hurricane eye at Pensacola, while 150 km offshore the waves were only 5 m in height. Hence, the waves reaching the shore in Progreso were likely to have been less than one metre in height. Secondly, Hurricane Ivan made its main landfall in Florida and after a few hours its maximum storm surge was recorded (2 m), producing an extensive overwash. Moreover, the measured tides on the $14^{th}$ show a 0.5 m residual during neap tides (see section 4.3). This residual is probably due to a real surge. Although, the precise magnitude of this surge is unknown due to the lack of confidence in the tidal record. A surge of 30 to 50 cm magnitude would be possible, considering the surge produced by Hurricane Ike (see Figure 5.13).

### 6.3.2 Inter-seasonal shoreline change summary

The different inter-comparison assessed here show that the shoreline changes observed by using SDS are consistent, thus allowing estimation of seasonal shoreline change in Progreso and confirming the relationship between the observed shoreline change

and wind, waves and cyclones. In winter evidence was found of consistent landward movement of 4 m to the east and 6 m to the west of the pier. Moreover, Hurricane Ivan produced landward movement of at least 10 m and up to 45 m near Progreso pier.

It is important to mention that due to the random spacing of the SDS, the assessment of a single storm was difficult. However, the observed shoreline change was useful to estimate the range of change during the year.

### 6.3.3 Inter-annual changes in shoreline position

This section assesses the differences in shoreline position of SDSs from February 6, 2006; September 7, 2007; September 20, 2008 and July 12, 2010, in relation to the mean SDS calculated using the SDSs from December 2003 to July 2005 and the seaward and landward envelope limits calculated from December 2003 to July 2005. Although the mean used as a reference does not correspond to the period of time of the assessed SDSs, its use allows comparison of the differences in shoreline position over different seasons. The use of this mean is the best reference possible to explore longer periods of time, given the SDS spacing.

**February 2006**

Figure 6.11 shows the difference in shoreline position from February 2006 in relation to the mean SDS. The shoreline difference is within the envelope limits, close to the mean SDS, with magnitudes of change smaller than 5 m. Table 6.3 shows that the overall shoreline difference had maximum magnitudes landwards and seawards between -13.5 m (seg.3) and 1.2 m (seg.5) respectively. It is interesting that there is consistency in the mean relative shoreline position between eastern and western beach segments, with the exception of segment 8, despite the mean difference being very small. Segments 1 to 3 and 8 moved landwards, and segments 4 to 7 moved seawards. This difference is in agreement with a western longshore transport of sediment and Progreso pier.

Figure 6.12 shows the wind and wave conditions in January. Two storms took place, from the $6^{th}$ to $8^{th}$ and from the $17^{th}$ to $20^{th}$, which simultaneously had Hs > 2 m (offshore) and wind coming from the west. The SDS is two weeks after the last storm, during a period where some recovery could have occurred, and therefore cannot be expected to detect the immediate effects of these storms on the shoreline location, particularly using the mean SDS as a reference.

The relative shoreline location from March 2004 and February 2006 (Figure 6.4) is very similar and is close to the mean SDS. This shows a consistent shoreline location in SDSs at approximately the same period of time within the year.

*Table 6.3:* Difference in shoreline position (min., max. and $\bar{X}$) for February 2006, September 2007, September 2008 and July 2010, in relation to the mean SDS of the period of December 2003 to July 2005 in Progreso.

| Date | | Seg.1 | Seg.2 | Seg.3 | Seg.4 | Seg.5 | Seg.6 | Seg.7 | Seg.8 |
|---|---|---|---|---|---|---|---|---|---|
| 06/02/06 | max. | -5 | -5.2 | -13.5 | -3.05 | 1.2 | 0.9 | -1.7 | -7.5 |
| | min. | 0.2 | -0.3 | -7.1 | 3.9 | 6.6 | 6.1 | 3.2 | -1.5 |
| | $\bar{X}$ | -2.4 | -2.8 | -10.3 | 0.4 | 3.9 | 3.5 | 0.7 | -4.5 |
| 07/09/07 | max. | -6.3 | -5.7 | 3.1 | -6.8 | -10.8 | 2.8 | -6.7 | -12.8 |
| | min. | -1.1 | -0.9 | 9.5 | 0.2 | -5.4 | 8 | -1.7 | -6.8 |
| | $\bar{X}$ | -3.7 | -3.3 | 6.3 | -3.3 | -8.1 | 5.4 | -4.2 | -9.8 |
| 20/09/08 | max. | -8.3 | -8.8 | 4.4 | -7 | -7.6 | 3.9 | -7.7 | -10.9 |
| | min. | -3.1 | -4 | 10.8 | -0.1 | -2.2 | 9.2 | -2.6 | -4.9 |
| | $\bar{X}$ | -5.7 | -6.4 | 7.6 | -3.5 | -4.9 | 6.6 | -5.1 | -7.9 |
| 12/07/10 | max. | -8.3 | -12.3 | 15.6 | -10.4 | -8.6 | -0.4 | -12.9 | -18.2 |
| | min. | -3.1 | -7.5 | 21.9 | -3.5 | -3.2 | 4.8 | -7.9 | -12.2 |
| | $\bar{X}$ | -5.7 | -9.9 | 18.8 | -6.9 | -5.9 | 2.2 | -10.5 | -15.2 |

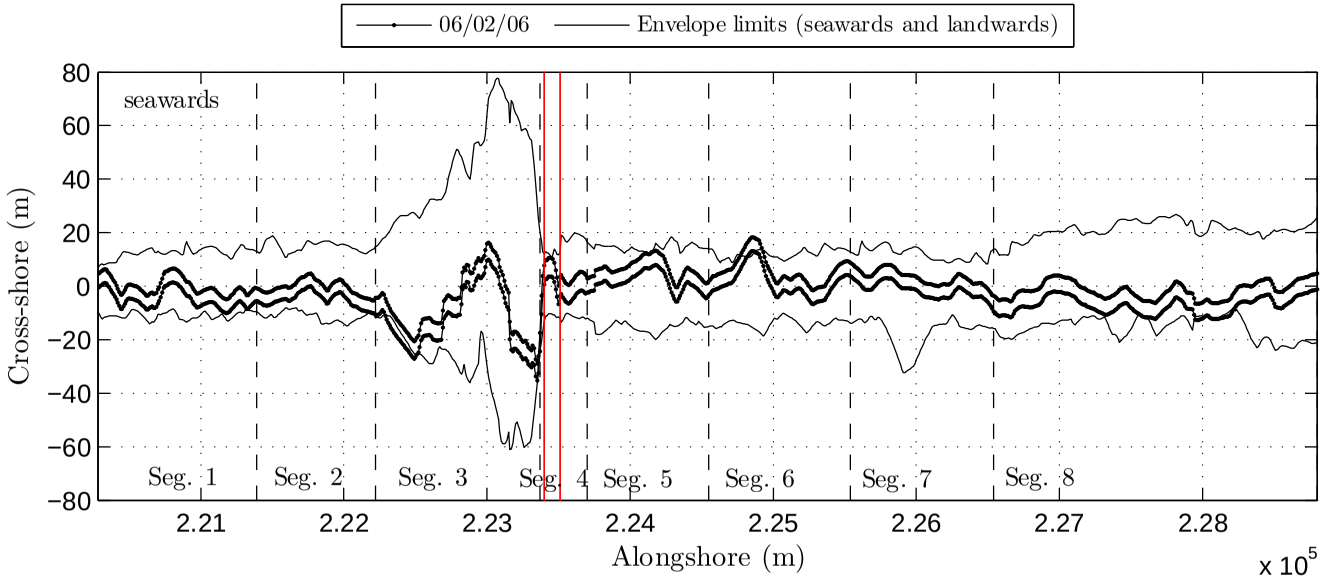


*Figure 6.11:* Difference in shoreline position from February $6^{th}$, 2006 in relation to the mean SDS. The SDS position considers the landward and seaward position due to the confidence bounds. Positive values are seawardS and negative values are landwards. The beach segments' order increases from west to east (dashed lines). The vertical red lines indicate the position of the two Progreso piers (see section 4.3.7).

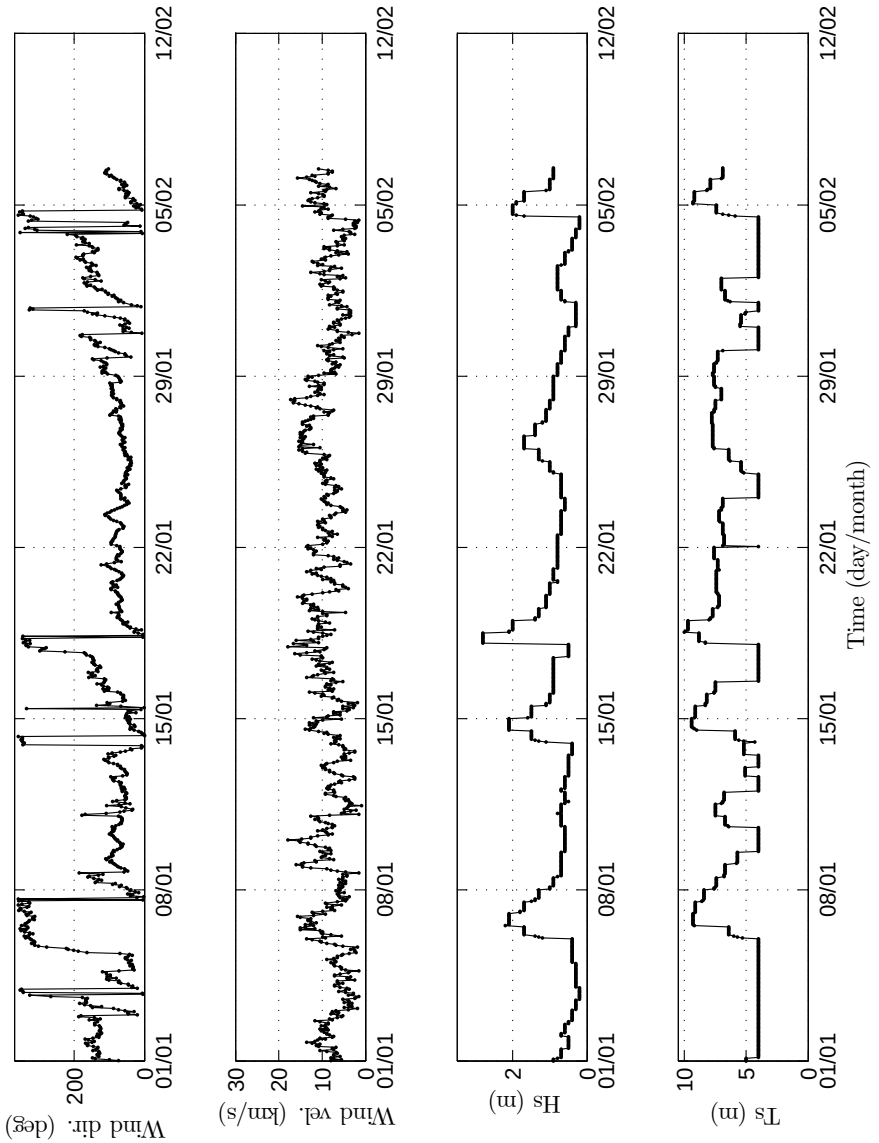


*Figure 6.12:* Wind direction, wind velocity, Hs (offshore) and Ts, in January 2006. The winds were measured at Telchac and the waves were modelled in deep water (see section 4.4.2).

### September 2007

This SDS was taken 14 days after Hurricane Dean (see appendix), which had a direct impact on the eastern coast of Yucatán ($21^{st}$ Aug.), and was a category 5 storm. Its effect was predominantly over the eastern coast of Yucatán. Besides Hurricane Dean, no other cyclone reaching the hurricane category was closer to Yucatán or could have had an effect on the shoreline change observed in this SDS.

Figure 6.13 shows the change in shoreline position of the SDS from September 2007 in relation to the mean SDS. The change in shoreline position is within the envelope limits. Segments 1, 2, 5 and 8 are closer to the landward envelope limit, whereas segments 3 and 6 are closer to the seaward envelope limit.

The relative shoreline position is similar to the SDS from 2006, although both are from different seasons. They show differences in segments 3, 5 and 8. Segments 3 and 5 are further seaward and segment 8 is further landward than the SDS in 2006.

Table 6.3 shows that all the beach segments have a mean relative landward position between 3 m and 10 m (seg. 8) except segments 3 and 6, which show a mean seaward relative position of 6 m and 5 m, respectively. Segments 3 and 5 have the largest difference in 2006 and 2007, with 16.3 m seaward and 12 m landward respectively.

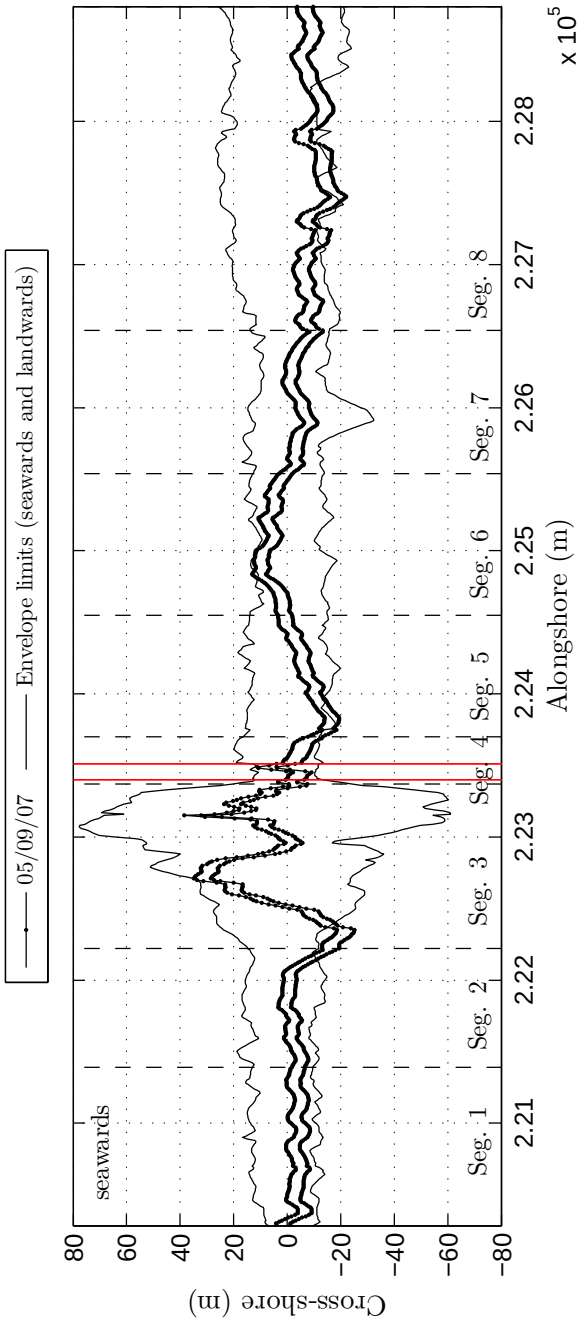


*Figure 6.13:* Difference in shoreline position from September 7, 2007 in relation to the mean SDS. The SDS position considers the landward and seaward position due to the confidence bounds. Positive values are seawards and negative values are landwards. The beach segments' order increases from west to east (dashed lines). The vertical red lines indicate the position of the two Progreso piers (see section 4.3.7).

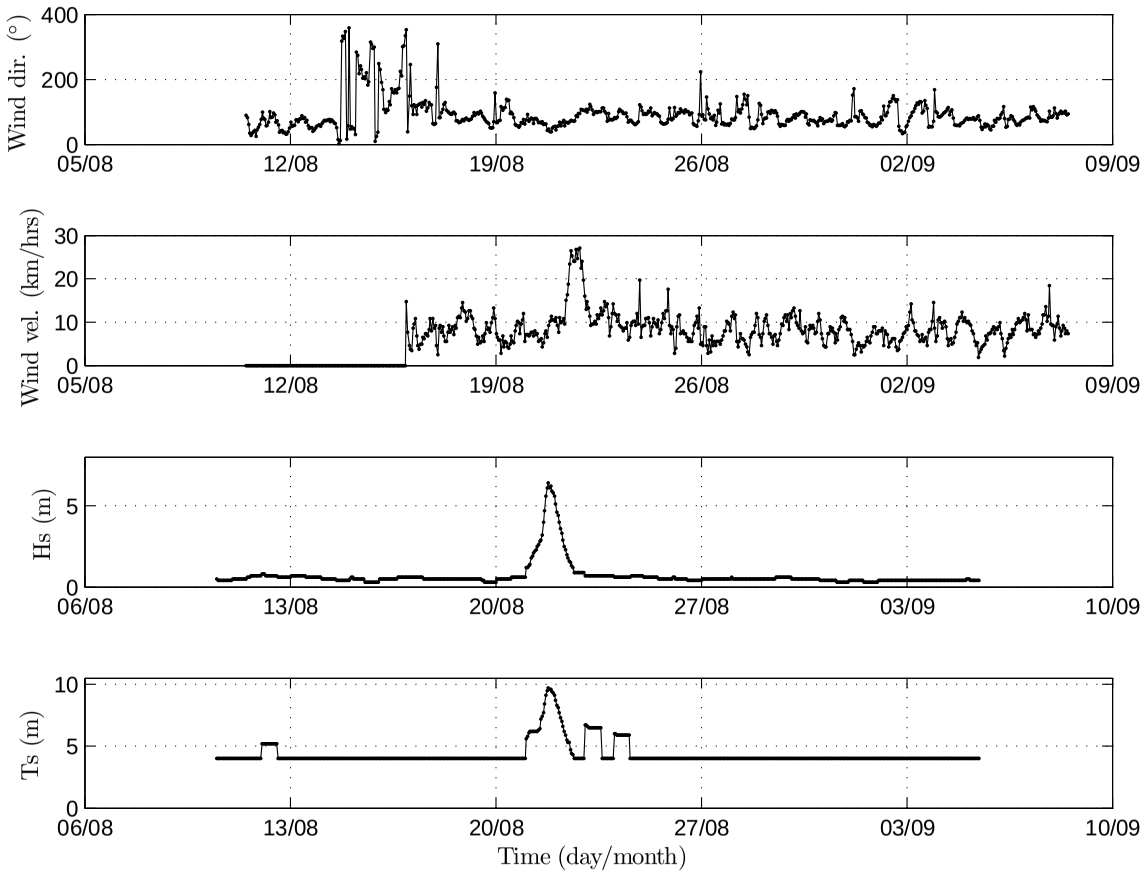


*Figure 6.14:* Wind direction, wind velocity, Hs (offshore) and Ts, from August $10^{th}$ to September $5^{th}$ 2007. The winds were measured at Telchac and the waves were modelled in deep water (see section 4.4.2).

### September 2008

Figure 6.15 shows the difference in shoreline position of the SDS from September 2008 in relation to the mean SDS. The difference in shoreline location of this SDS and the SDS from 2007 of the same month is remarkably similar, with differences overall in shoreline position smaller than 2 m (Table 6.3). This shows consistency between shoreline positions at similar times of the year, as previously observed in the inter-seasonal changes in the latest months from the winter season (February 2006 and March 2004) and early in the hurricane season (May and June 2004).

The SDS from 2008 is 20 days after Hurricane Ike passed, approximately 500 km NE (see appendix) from Yucatán. However, no large changes in the wind direction and velocity that could have produced a significant movement in the relative shoreline position. It is important to mention that besides Hurricane Ike, no other cyclones took place. Therefore, it is likely that the shoreline position from 2007 did not greatly change. Unfortunately, the available SDS does not allow exploration of the inter-seasonal changes in shoreline position in 2007.

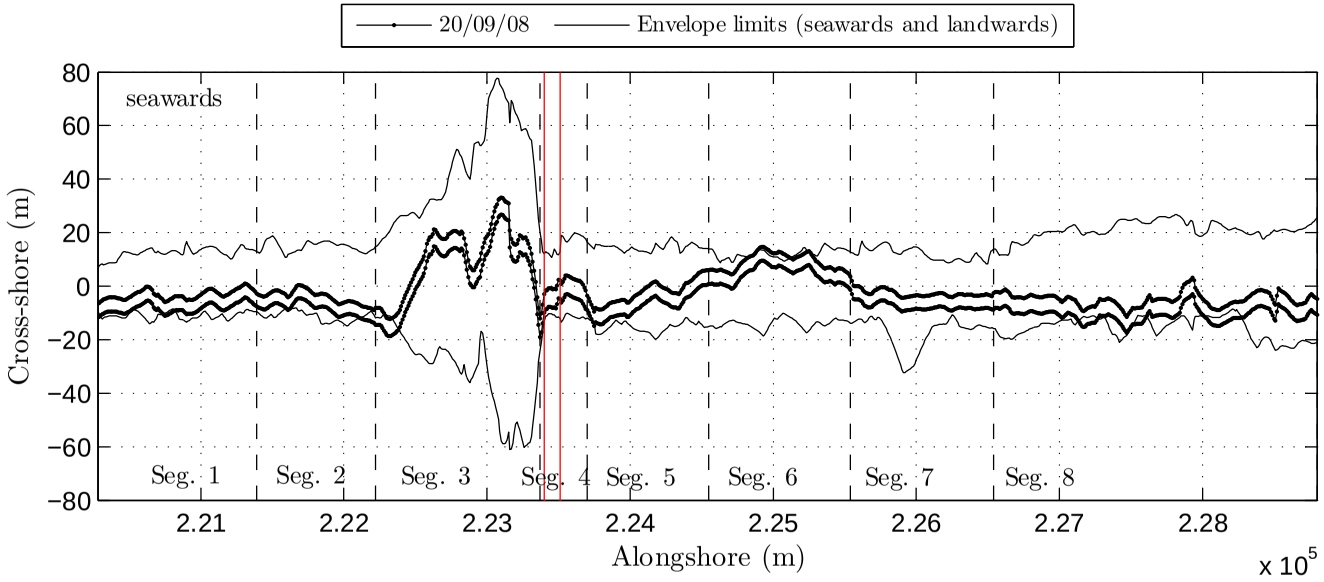


*Figure 6.15:* Difference in shoreline position from September 20, 2008 in relation to the mean SDS. The SDS position considers the landward and seaward position due to the confidence bounds. Positive values are seawards and negative values are landwards. The beach segments' order increases from west to east (dashed lines). The vertical red lines indicate the position of the two Progreso' piers (see section 4.3.7).

### July 2010

Figure 6.16 shows the difference in shoreline position of the SDS from July 2010 in relation to the mean SDS. The relative shoreline position is overall similar to the SDSs of 2007 and 2008, which are within the hurricane season (Table 6.2).

The most evident difference is in segment 3, which is further seawards than in 2007 and 2008. The seaward position is to be expected considering that the SDS is early in the hurricane season, when the hurricane activity is small. In contrast, the SDS from 2007 and 2008 come from the most active month of the hurricane season, suggesting that segment 3 moves landwards when cyclones are in the vicinity. Segments 2, 4, 5 and 7 moved landwards between 3 m (Seg. 4) and 7 m (Seg. 8). Segment 6 shows a relatively seaward movement on its shoreline position of approximately 11 m.

Interestingly, the shoreline location in segment 8 is further landwards (< 5 m) of the envelope limits. This SDS is from early in the hurricane season and the 2009 hurricane season had an activity below the average (NHC 2010), without cyclones passing close to Yucatán. This suggests that in the presence of cyclones segment 8 might reach a further landward location over time.

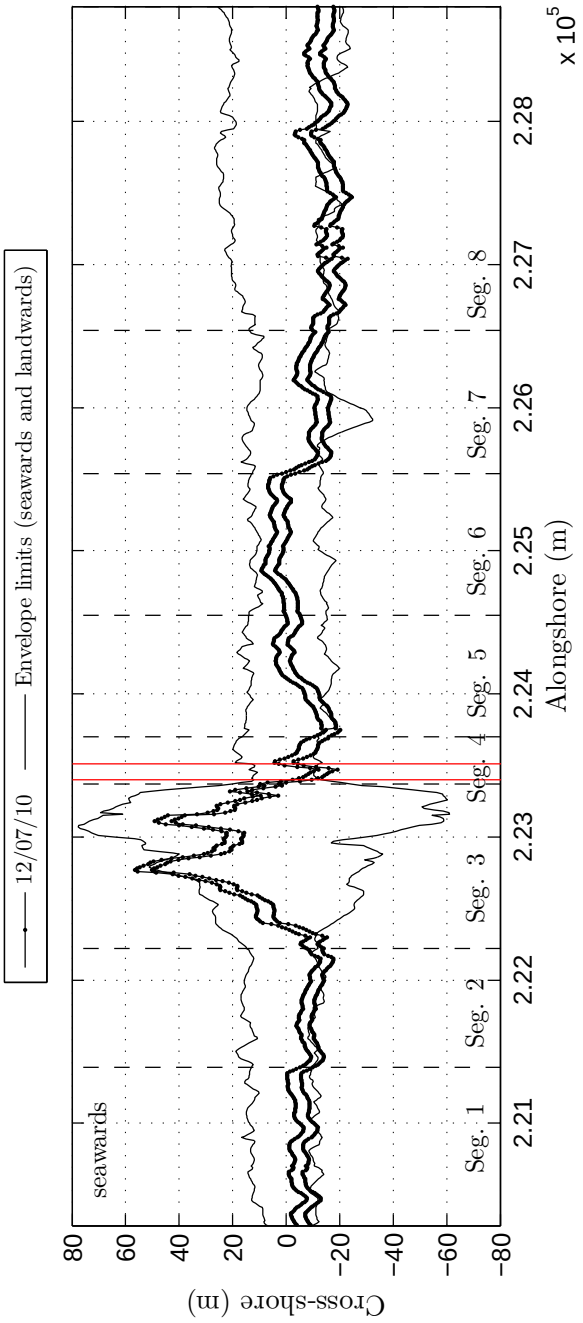


*Figure 6.16:* Difference in shoreline position from July $12^{th}$ 2010 in relation to the mean SDS in Progreso, Yucatán, México. The SDS position considers the landward and seaward position due to the confidence bounds. Positive values are seawards and negative values are landwards. The beach segments' order increases from west to east (dashed lines). The vertical red lines indicate the position of the two Progreso piers (see section 4.3.7)

The different SDSs analysed reveal consistency in their location. Furthermore, the relative shoreline change observed agrees with the season of the studied SDSs, showing that SDS can be reliable when exploring differences in shoreline position.

The exploration of the relative shoreline position over time would provide valuable information about predominant landward shoreline movement, allowing identification of beach segments showing progressive changes on their location over a 6.5 year period.

### 6.3.4 Shoreline location over time

This section explores the mean shoreline location for each beach segment over time. This would allow assessment of progressive movement of the shoreline position either landwards or seawards.

Figure 6.17 shows the overall change in shoreline position that occurred at each beach segment over time. Positive values refer to seawards shoreline position relative to the mean SDS and vice versa.

The effect of winter storms and cyclones on the shoreline location is possible to detect. The largest changes took place between 2004 and 2005, related to winter storms and particularly to Hurricane Ivan. Changes as large as 70 m occurred (segment 3), when all eight beach segments are examined. However, without considering segment 3 the shoreline change decreases to 25 m. Late in 2004, some recovery of the shoreline location took place in all beach segments, which moved seawards by approximately 20m, with the exception of segment 3, which experienced a 5 m seaward movement. This can be interpreted as if the sand from segment 3 moved offshore, distributing sediment into the other segments and contributing to their seawards movement.

The overall shoreline position of all the beach segments from late 2004 to early 2005 shows a landward movement of approximately 10 m to 20 m, which is related with the end of the winter season and storms. Later on July 2005 a landwards movement that

is likely to be related to TS Arlene, showing a slight effect on the shoreline location in relation to the landward movement observed with Hurricane Ivan. The overall change in shoreline location was less than 30 m, returning to the same range of magnitude observed in 2004, with the exception of segment 3.

In 2005 the shoreline position remained landwards, and does not show the seaward position that was observed in 2004. This might be related to the unusually high hurricane activity in 2005.

Considering the overall change in shoreline position in 2004 and 2005, it is possible that range of change in shoreline location of approximately 30 m typically occurs during the year. In addition, that the accumulation of sand for segment 3 takes several years, showing a slow recovery after cyclones and storms.

The overall change in shoreline position from 2006 to 2008 onwards, shows less variation than was observed in 2004 and 2005. This could be due firstly to the spacing of the available SDS, with the existing data it is not possible to know whether the inter-seasonal changes between 2006 and 2010 were of the same range in magnitude. Secondly, the hurricane seasons in 2004 and 2005 were significantly more active than in 2006 to 2007 (see appendix).

The shoreline position in all the beach segments remains within the same range of magnitude. However, they show a slow overall landwards movement, with the exception of segment 3, which exhibits a seawards movement. Segment 3 has moved seaward approximately 20 m, from -20 to -10 m to 0 to 10 m. It is likely that the further seawards shoreline location of segment 3 is recovered after several years of accumulation of sand. In contrast, of all the beach segments, segment 8 has moved furthest landwards by approximately 10 m, from 0 to 10 m, to -5 to -12 m. If this landward movement continues in segment 8, it will increase the vulnerability of this segment to shoreline erosion and the safety of the coastal buildings.

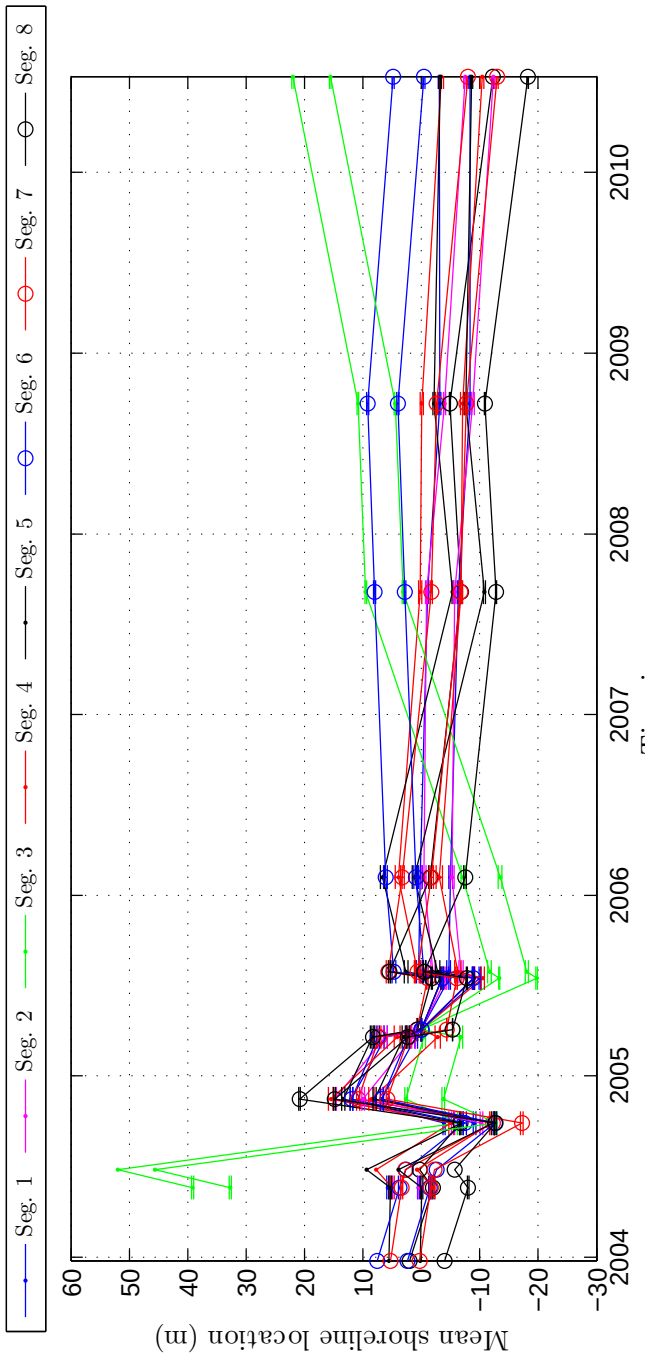


*Figure 6.17:* Change of the mean shoreline location for each beach segment over time.

It is interesting to note the large range of shoreline locations between beach segments in 2010. Segment 3 is the furthest seawards, at approximately 20 m, and segment 8 is located the furthest landwards at approximately -15 m. This segment moves consistently landwards over time, in particular after 2006. This suggests that the sand is being accumulated in beach segments 3 and 6, whereas the rest of the beach segments do not have sand to recover the earlier seaward shoreline position. The sand seems to be mostly located at beach segment 3, which might be redistributed to the other beach segment when a cyclone takes place, moving the sand offshore as observed in 2005 during Hurricane Ivan.

Table 6.4 shows the estimated rate of shoreline change for each beach segment, showing a landward rate between -1.2 myr$^{-1}$ (Seg. 1 and 4) and -2.4 myr$^{-1}$ (Seg. 8) for segments 1, 2, 4, 5, 7 and 8. Segments 3 and 6 show a positive rate of change, suggesting that the shoreline is moving seawards between 0.3 myr$^{-1}$ and 0.6 myr$^{-1}$ respectively.

*Table 6.4:* Estimated rate of change (myr$^{-1}$) for each beach segment according to the gradient of the adjusted line. *Variation with 95 % confidence interval.

| Beach seg. | Rate of change (myr$^{-1}$) | Gradient, constant | Variation of gradient* |
|---|---|---|---|
| Seg.1 | -1.2 | -1.2, 2543.8 | -2.9, 0.5 |
| Seg.2 | -1.8 | -1.8, 3615.0 | -3.7, 0.3 |
| Seg.3 | 0.3 | 0.3, -482.1 | -2.9, 0.4 |
| Seg.4 | -1.2 | -1.2, 2521.5 | -3.0, 0.6 |
| Seg.5 | -1.6 | -1.6, 3330.0 | -1.1, 0.03 |
| Seg.6 | 0.6 | 0.6, 1317.0 | -1.1, 2.35 |
| Seg.7 | -1.6 | -1.6, 3188.3 | -3.3, 0.28 |
| Seg.8 | -2.4 | -2.4, 4763.3 | -4.5, 0.01 |

Figure 6.18 shows the identified locations with the largest landward and seaward shoreline movement. Some of these locations have experienced rapid changes in the presence of storms, such as segment 3, while others show slow but constant movement, such as segment 8. Segment 7, although it did not exhibit changes as large as segment 3, within two months had an overall change as large as 22 m by 13 days after Hurricane Ivan in

2004.

The identification of both types of areas is important for coastal management. In the presence of a change in the sea level and large waves, the segments showing the largest rates of erosion, narrower beach and smoother top of the beach slope, would be more vulnerable to floods and overwash.

For instance, with the analysed SDSs, segment 8 is the most vulnerable of the beach segments. This segment also has the narrowest beach width, with no coastal dunes or coastal vegetation, which increases its vulnerability to erosion during storms.

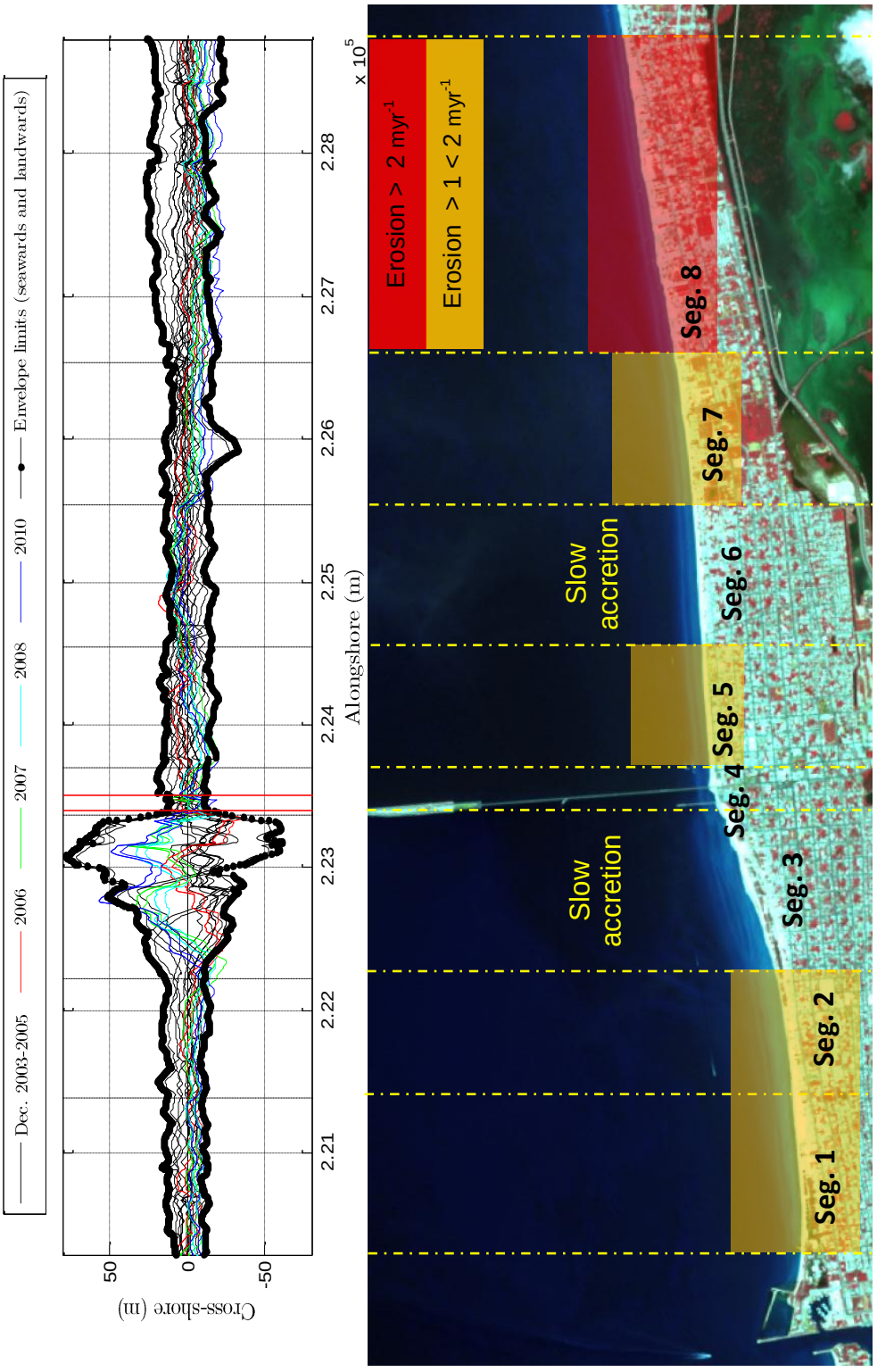


*Figure 6.18:* Top: Difference in shoreline position observed in relation to the mean for all the beach segments over the 6.5 yrs studied. Bottom: Diagram showing the beach segments and their relative change in shoreline position over time in Progreso, Yucatán.

## 6.4 Discussion

The results show the capabilities of the SDS to detect changes in the shoreline within periods as short as one month after cyclones have passed by, allowing in addition the assessment of the change in the shoreline over time, as the research of Maiti and Bhattacharya (2009) show.

### 6.4.1 Intra-annual comparisons

The inter-annual shoreline change has been assessed, allowing detection of the effect on the shoreline location due to winter storms occurred in winter and cyclones identifying beach segments showing the largest shoreline change. Although the spacing of the SDSs was not ideal to assess the effect on the shoreline before and after a specific storm, it was possible to assess the overall effect in different seasons and to estimate a mean shoreline location through the year, as well as the seaward and landward limit on the shoreline position within the year. Such information becomes very useful to interpret SDS from different years and for coastal management actions.

Because the obtained shoreline change is relative to the mean SDS, thus, the estimated mean shoreline location can be an important limitation to detect shoreline change. The mean SDS was estimated using SDSs from different seasons and different years, four SDSs within the hurricane season, two SDSs from the winter season and three SDSs from the calm season. It is recommended when studying shoreline change to include shoreline positions from all the year (Leatherman and Douglas 2003; Moore et al. 2006). However, although shoreline locations from different seasons are included, because of long-term meteorological and oceanographic factors, always it remains the possibility that the estimated mean shoreline position has not be fully represented. This can have an effect on the estimated shoreline change. For example, the assessment of shoreline change using a mean shoreline position which mostly includes extreme

events, will be located further landwards than the mean shoreline position. Thus, the shoreline change would under estimate the landwards movement due to storms, and over estimating the seawards movement of the shoreline in summer.

The changes detected here are consistent with a landward shoreline movement after the winter. The SDSs later in the winter are landward in relation to the earlier SDSs from the same season. The time between the SDS and a specific storm can result in different shoreline locations, as was found in November to March 2005 and December to May 2004 comparisons. Although all the segments mostly have a landward movement of about the same magnitude (10 m), segments 4 and 8 had the greatest shoreline movement (-18 m). These changes might be related to the cross-shore transport rather than the alongshore gradients of sand. This agrees with the effect of storms in winter. The change in segment 4 may be due to the position between two piers, where relatively strong undertow currents could be produced. The large change in segment 8, in contrast, may be due to the alongshore gradients of sediment transport and the reduced availability of sand in the region, leading to erosion of the beach at the shoreline level.

It was not possible to assess the calm season in Progreso. The earliest and latest shoreline location within the season were only a few weeks apart, at the start of the calm season, and there was the additional the effect of a storm out of season. The other SDSs include the effect of a hurricane, since the SDS is from the early part of the hurricane season. So, it was not possible to detect movement in the shoreline position after the calm season.

The SDSs analysed during the hurricane season show that there is a difference within the months and the track of the hurricanes observed. The September 2004 SDS, when Hurricane Ivan passed, caused a significant landward movement in the shoreline, whereas Hurricane Dean did not produce a significant effect on the shoreline position.

The most landward shoreline position in segment 3 is consistent with the observation

of local people that the beach is getting wider, shallower and that wave heights have decreased in the last few years. Which could be the effect of the accumulation of sediment produced by the decrease of the alongshore transport due to the pier, and a recovery process that is continuing after Hurricane Ivan.

A very active hurricane season took place in 2004 and 2005, the latter being the strongest on record with the largest number of cyclones ever recorded. Consequently, the seaward and landward envelope limits are likely to be larger than the range of seaward and landward limits that the shoreline would have had with a less active hurricane season. However, the defined envelope limits are a good reference to compare the shoreline change of SDSs.

Although the changes in the winds and waves in the region are small over the year, the shoreline location shows large changes in its shoreline position. The comparisons in 2004 and 2005 show an overall shoreline change of the order of 10 m, with some segments showing changes of up to 20 m, indicating that Progreso has a dynamic shoreline in spite of its relatively low wave heights.

Assessing the 2003 to 2005 SDSs has also allowed observation of the jagged shape of the earlier shorelines. This could be related to the groynes that were removed in 2005 in Progreso. The SDS of the following years might show differences in the shoreline location after the removal of these groynes.

### 6.4.2 Inter-annual comparisons

The SDSs analysed here are not as frequent over the year, with only one image per year and for 2007 and 2009 there were no SDS available. However, although 10 from 13 SDSs were from the hurricane or winter storm season, not all the SDS from the hurricane season immediately followed a hurricane. This is not ideal to study shoreline change (Leatherman and Douglas 2003; Moore et al. 2006). However, these SDSs were

the images of the region available.

The SDS from 2006 to 2010 remains within the envelope limits defined using the shoreline position from December 2003 and 2005, showing that the location is within the previously observed shoreline locations, indicating that the intra-annual shoreline change is larger than the inter-annual shoreline change. The use of the seaward and landward envelope limits enabled consideration of the seasonal and inter-annual variation when interpreting shoreline change during different years. Although the calculated mean SDS does not describes the 'real' mean shoreline location, because a few SDS from different seasons and years are included mixing seasonal with inter-annual variations, it was needed to further assess earlier SDSs. However, even if more SDSs had been considered to calculate a mean SDS, the mean shoreline location would depend on a temporal scale.

The overall SDSs show that erosion is taking place in Progreso. This observation has been previously found in other locations within Yucatán, as it occurs in Cancun. Diez et al. (2009) found that the erosion problems in Cancun, located on the eastern coast of the Yucatán Peninsula, are not due to the presence of hurricanes. The origin of the shoreline retreat in Cancun is due to the occupation and settlement of the coastal barrier. Cancun, as well as Progreso, has the same karstic formation as the rest of Yucatán and is also a barrier. Therefore, it is possible that the erosional observations made from Progreso have a strong influence by the human modification.

The shoreline location over time shows negative gradient erosion from segments 1 to 2, 4 to 5, and 7 to 8 during the 6.5 year period.

Segment 8 shows a consistent landward movement over time (10-20 m), which might be related to several factors such as its narrowness, lack of coastal dunes, coastal vegetation (see section 4.2), as well as the limited availability of sand in the region. The limited availability of sand could be related to an extension in the breakwater of Pro-

greso pier five years ago, traping the sediment in segment 3. This segment has a smaller coastal orientation thus the waves will approach at lower angles, reducing the alongshore transport of sand in relation to the other segments, that have a larger coastal orientation. In addition, the closeness of the urban area at a low elevation level makes the coastal houses which are located in front of the sea more vulnerable to the direct impact of a hurricane.

If the shoreline position continues moving landwards at the estimated rate of change, the properties in front of the sea will be at high risk of damage by the sea action during storms or hurricanes. However, it is not clear if the landward movement is related to the cross-shore or the alongshore transport. There are no groynes further east or west from segment 8, suggesting that the landward movement could be due to a negative gradient of sand and the cross-shore transport during storms. However, the volumes of sand in alongshore transport might be much larger in magnitude than the cross-shore transport. The cross-shore transport occurs during storms with large waves, whereas the alongshore transport occurs during the whole year, with variations in its intensity.

Segments 3 and 6 are the beach segments with an overall seaward movement, in contrast to the rest of the beach segments. However, their estimated rate of change is much smaller (0.9 myr$^{-1}$) in relation to the landward rate of change of the rest of the segments (9.3 myr$^{-1}$), suggesting that there is an overall loss of sand in Progreso. The estimated landward rate of change is 10 times larger than the seaward rate of change. However, this is a gross estimation, which could be underestimating (see section 5.4) the shoreline retreat and therefore more detailed research *in situ* should be carried out to provide a more precise estimation.

The rates of change estimated in this research are within the range of rates reported for other locations within the Gulf of México, where erosion rates of -1.5 m per year were found in Florida (Morton et al. 2005), while other locations like Lousiana have erosion

rates as large as -12 m per year. The relevance of this comparison is not the magnitude of change but the fact that shoreline retreat is also observed in other locations within the Gulf of México and within Yucatán and that this is of a regional magnitude.

After the removal of the groynes in Progreso in 2005 a clear seaward movement of the shoreline has not been detected over time, showing that the sand has been widespread along the shore. However, a considerable amount of sand could still be retained by the breakwater from Yucalpetén, affecting Chelem beaches located downdrift (see section 4.1). Interestingly Chuburná, which is further west (downdrift), apparently has few problems with shoreline erosion. This may be as a result of the sand coming from other sources, as well as the presence of coastal dunes and coastal vegetation on the shore.

### 6.4.3 Physical interpretation of shoreline change

This subsection has the purpose of discussing which coastal processes could have been involved on the observed shoreline change.

**Intra-annual comparisons**

**Winter**

The range of shoreline change for segments 3, 4 and 5 is larger than the variability of any other possible source of error such as the inter-tidal beach slope, wave set-up or concentration of suspended sediments (see section 4.3.4). The results suggest that the observed change is related with the cross-shore and the alongshore transport of sand. The cross-shore or the alongshore transport of sediment would be a more important factor driving the landwards movement of the shoreline according to the location of each beach segment. The presence of piers in segment 4 affects the observed shoreline change of the eastern and western beach segments. The alongshore drift decreases to the west of the pier, producing an accumulation of sand to the east and depletion to the west of the pier with winds from the NE, the dominant direction. However,

the largest accumulation occurs towards the west, in segment 3, the segment with the largest shoreline change of all.

The shoreline change of segment 3, seems to be related to the 2 km long shore-parallel structure of the pier. The shore-parallel structure is a barrier for the wind, and because the waves of the region are mostly wind-driven, the wave height that approaches into the shore is reduced. So, deposition of sand can take place in this segment, but also the sand seems to remain overall in the western segments, and not moved eastwards, even during storms. As a result, the changes observed in segments 1 and 2 are of a smaller magnitude in relation to segment 3, beach segment where the largest amount of sand is accumulated.

The shoreline change from segment 6, in contrast, seems to be related to the cross-shore transport rather than the alongshore transport. The rapid changes can be related to storms or cyclones, which produce a change in the 'typical' conditions, producing relatively large waves moving the sand offshore.

**Hurricane**

The observed shoreline change during hurricanes suggests that the cross-shore transport and the presence of surges can produce significant change in the shoreline position. The shoreline change observed in the hurricane season shows that the presence of surges is an important factor that drives shoreline change. For example, the landwards movement of the shoreline occured during Hurricane Ivan could be explained with a positive surge of 0.5 m. The top of the beach slope in segment 3 is very shallow; only the rise in the sea level, without considering the wave set-up, could produce an overwash of at least 150 m. In contrast the rest of the segments, with a steeper top of the beach slope, had a landward movement of approximately 20 m.

Segment 8 had a seaward and a landward movement, which might be related to cross-

shore transport that could have occurred during Hurricane Ivan.

**Inter-annual comparisons**

The observed shoreline change over different years suggests an overall progresive erosion, particularly in segment 8 (Table 6.4). The erosion seems to be the effect of different factors. Firstly, the cross-shore transport of sand during storms is a significant factor that can move sand further seawards. Secondly, the frequent presence of surges increase the water levels, allowing the overwashing. Thirdly, the significant human modification in the case of study (e.g. removal of coastal dunes and vegetation, urbanisation very close to the shoreline and presence of piers) have changed the gradients of sand. Finally, the region does not have large amounts of available sand, the sandstone is very close to the surface, and the sediment supply is limited to marine sources. All these factors added together result in overall erosion in Progreso. The erosion observed in segment 8 might be due to negative gradients of sand and the cross-shore transport. The shoreline further east of Progreso is formed mostly by sandstone with limited sand (see chapter 4). Therefore, the available sand could be moved offshore during extreme events, as the landwards movement of the SDS of November 2004 indicates.

The erosion of segments 1, 2, 5 and 7 seems to be part of the regular distribution of sand within the region, which constantly moves either seawards or landwards depending on the number of storms and cyclones in the region. The eastern and western beach segments are likely to have a reduced exchange of sand due to the barrier that Progreso pier is for the alongshore gradients of sediment, partially dividing the eastern and western segments. However, during storms or hurricanes the accumulated sand in segment 3 can be moved offshore and be distributed into the rest of the beach segments as occurred with Hurricane Ivan.

Segment 3 and 6 have the highest stability in their shoreline location, which might be

explained by their relative distance from the pier, providing shelter from the approaching waves. This is mainly the case for segment 3, however segment 6 is in between two beach segments that showed overall erosion, and therefore the constant movement of sand maintains this segment in a similar position over time.

### 6.4.4 Coastal management

The assessment of shoreline change over a 6.5 year period in Progreso, supports evidence for the recommendations listed below to decrease the erosion found at the beach segments 1, 2, 5, 7 and 8 (Figure 6.18).

1. Progreso pier influences the accumulation of sand in segment 3, thus the dredging of sand and its distribution towards the eastern segments might reduce the observed progressive erosion of segment 8.

2. Segment 3 is the segment that has the shallowest top of the beach ($< 3^{\circ}$) and therefore the highest vulnerability to flooding during a surge. The rehabilitation of the coastal dunes and native vegetation would be useful to increase the beach slope and minimise the damage caused by water during a surge.

3. The rates of change obtained in this research might change when a longer period of time and better spaced images are analysed. Therefore, it is advisable to continue with the monitoring of the changes in the shoreline position.

The assessment of the shoreline change using satellite images at other locations can be improved by using frequent images covering the whole year and by constant monitoring over the long-term. It is also important to include as much as possible satellite images during the calm periods, as well as satellite images before and after storms and hurricanes. For example, the consideration of at least two images before and after a specific storm and the acquisition of further images spaced fortnightly following a storm over

a suggested period of two months, could provide information regarding the effect on the shoreline position and the recovery of the shoreline after a storm. Such spacing is suggested to capture the effect of the storm on the shoreline, however each location has to be sampled depending on their specific characteristics, such as the strength and frequency of storms. Including at least two images during the calmest period, spaced approximately two months apart, can give very good guidance about the variability of the shoreline during the year.

This will allow estimation of the most seaward shoreline position and most landward shoreline position. These limits are important to consider for coastal management actions and to define set-back distances to ensure the safety of people living close to the shore. Furthermore, estimation of the seasonal movement of the shoreline during the year and monitoring over the long-term (> 10 years) can provide valuable information necessary to estimate the shoreline movement in energetic events and to forecast the shoreline position over a large length of shoreline (> 5 km).

## 6.5 Chapter summary

This chapter explores the application of SDSs to identify shoreline change using Progreso as a case study area, whose location is described in chapter 4. The comparisons between 13 different SDSs covers a period of 6.5 years. The assessment of the SDSs covering the higher temporal resolution (2003 to 2005) allows a mean SDS to be estimated as well as the most seaward and landward limit of the shoreline location. This information is further used to evaluate each SDS.

From the intra-annual SDSs assessed it was possible to estimate the changes in the shoreline during the winter and hurricane season. However during the calm season it was not possible to assess overall change due to the lack of availability of SPOT images for Progreso. The seasonal shoreline change is much larger than the inter-annual shoreline change. The largest shoreline change found was associated with Hurricane Ivan (2004), which is likely to have produced a storm surge of half a metre, resulting an overwash of at least 100 m in a beach slope as shallow as segment 3. It has resulted in a maximum landward movement of -132 m and a mean landward movement between -15 to -5 m in the rest of the segments.

The inter-annual shoreline change is within the seaward and landward envelope limits. However, the SDSs tend to remain landwards of the mean SDS, even though the SDSs were from early in the hurricane season, suggesting a recurrent landward trend in shoreline position, in particular for segment 8. The adjusted line of the mean shoreline change shows that all the segments, with the exception of segments 3 and 6, have a landward movement with time. The estimated rate of change is between -2.4 and -1.2m per year, whereas segments 3 and 6 have an estimated accretion rate between 0.3 and 0.6 m per year, which in total is a landward rate of change of 9.3, almost ten times larger than the seaward (0.9) rate of change, suggesting a deficit of sand in Progreso.

## 6.6 Conclusions

1. The use of SDSs has proved to be very valuable to assess shoreline change, allowing identification of seasonal changes, the effect of hurricanes and inter-annual changes, given the spacing of the SDS was not ideal.

2. The shoreline location of SDS from the same season but from different years is consistent, giving confidence that the interpretation of different positions of SDS shows real changes between seasons.

3. Overall landward shoreline change is found by the end of the winter season to be larger towards the east (approximately 9 m) and smaller towards the west (5 m).

4. The calm conditions could not be assessed due to the temporal spacing of the SDS. However, the SDS from May to June (2004) remained at a similar shoreline location, which agrees with the calm conditions during that period of time.

5. Hurricane Ivan (2004) produced a landward movement of at least 10 m and up to 45 m near the pier due to a reversal in the alongshore drift transport.

6. The beach located west of the pier (segment 3) has the largest and rapid changes in shoreline position associated with Hurricane Ivan. However, the recovery of this segment show to be very slow and reaching the seaward position of 2003 may take several years.

7. Segment 8 shows a consistent landward position, with no recovery on its shoreline location during December 2003 to July 2010. In addition, the shoreline location of 2010 is further landward than the landwards envelope limit. Therefore, the monitoring of this beach segment is recommended to identify whether this erosion continues over time.

8. The estimated magnitude of the shoreline rates of change (-2.4 to 0.6 myr$^{-1}$) seem reasonable considering the observed shoreline change. However, it would be preferable to include better spaced and a longer record of SDS.

# Chapter 7

# Discussion

## 7.1 Introduction

This chapter discusses the topics developed in this research within the context of the existing published work on shoreline change and shoreline identification using optical satellite images. In this chapter the advantages of this research over previous work is demonstrated and the process involved is evaluated.

Following the introductory section, this chapter is divided into the sections listed below:

1. The first section (7.2) gives a summary of the key findings of the current research, and its relation to the defined aim.

2. The second section (7.3) explains how the developed research bridges the gap between the existing published work concerning an accurate shoreline identification and shoreline change studies.

3. The third section (7.3.1) shows specific examples of contributions made by this research in the context of the previous work within the field. These examples support the statement of section two and highlight, for example, the methods followed to identify the shoreline and their approach to inherent difficulties (e.g. water levels, different wavelengths) when identifying the shoreline and assessing shoreline change.

The contents of these three sections address the objective 'To develop a method to identify the shoreline from optical satellite images'.

4. The fourth section (7.5) discusses the accuracy of the shoreline identified by optical satellite images. This section includes the validation of the SDS using *in situ* shoreline measurements, the water levels and the beach slope. Furthermore, other considerations about the accuracy of the identified shoreline are also discussed in this section.

   The contents of this section address the objective 'To validate satellite-derived shorelines (SDS)'.

5. The fifth section (7.6) describes the application of the method developed in this research at different types of beaches.

6. The sixth section (7.7) discusses the main findings and the difficulties involved in the estimation of shoreline change by using the method developed in this research. This section contains a discussion of the importance of the temporal spacing of the available satellite images in order to estimate the shoreline position.

   The contents of this section address the objective 'To assess and to interpret shoreline change using SDSs in the case of study of Progreso, Yucatán, in relation to environmental factors'.

7. The seventh section (7.8) outlines future research to improve the current understanding of the extraction of the shoreline and an assessment of shoreline change using optical satellite images.

## 7.2 Summary of key findings

This research demonstrates that optical satellite images can produce accurate estimations (< 10 m in the horizontal) of shoreline change covering large spatial scales in the alongshore (> 5 km), as well as short (< 1 year) and long (> 5 years) temporal scales, using Progreso as a case study. This research also provides an interpretation of the satellite-derived shoreline identified by the developed method using *in situ* shoreline measurements as a reference, and considers the application of the method at other locations.

The aim of this research was focused on the application of optical satellite images for shoreline change studies. This aim is subject to two assumptions: first, that a reliable shoreline identification is possible from optical satellite images and that the accuracy of the identified shoreline allows shoreline change detection. Both of these assumptions have been demonstrated in this research.

## 7.3 Combining shoreline identification and shoreline change studies

The published work about shoreline change and shoreline identification using optical satellite images is divided into two general areas. One is focused on the development of the methods to accurately locate the shoreline beyond the pixel size (Foody et al. 2003, 2005; Muslim et al. 2006; Li et al. 2008; Chen and Chang 2009; Wang et al. 2010), and the other, on the assessment of shoreline change (Blodget et al. 1991; Chen and Rau 1998; White and El-Asmar 1999; Fromard et al. 2004; Trebossen et al. 2005; Chu et al. 2006; Zakariya et al. 2006; Ekercin 2007; Dinesh-Kumar et al. 2007; Hanamgond and Mitra 2008; Kumar and Jayappa 2009; Kuleli et al. 2011).

The previously developed methods for shoreline identification with accuracies beyond

the pixel size are not used in shoreline change studies. In contrast, studies in this area applied techniques that, in principle, might be successful when identifying the shoreline, such as filters and classification techniques. These techniques have been tested in this research to assess their suitability for shoreline detection, finding that their results require further analysis to identify the shoreline and that their results do not give a clear definition of where the shoreline is. However, the research regarding shoreline change does not specify the methods followed to identify the shoreline or to assess shoreline change. This is possibly a result of the implicit complexity of the methods of shoreline detection, and due to the fact that there are many methods available, from which there is no clear optimum method.

This research, therefore, focused on shoreline identification and its accuracy, prior to the assessment of shoreline change. This research also bridges a gap between shoreline change studies and refined methods in shoreline identification, giving evidence and an explanation of the methods necessary to achieve reliable shoreline identification.

The next section (7.3.1) discusses the methods followed by previous work in shoreline change, showing the advantage of the current research due to the different parameters tested for the development of the method for shoreline identification.

The main purpose of testing different parameters in this research was the identification of the shoreline, ensuring the clearest difference between sea and land. Once the clearest possible shoreline location had been achieved, the estimation of the shoreline change and shoreline rates of change could begin.

### 7.3.1 Some previous work on shoreline change studies

The potential of optical satellite images for shoreline change studies is clear (White and El-Asmar 1999; Foody et al. 2003, 2005; Muslim et al. 2006; Zakariya et al. 2006; Ekercin 2007; Dinesh-Kumar et al. 2007; Liu et al. 2007; Chen and Chang 2009; Wang

et al. 2010; Kuleli et al. 2011). However, there is a lack of consensus over the different parameters to use for shoreline identification. For example, for multispectral images there is not a general agreement about which spectral band to use. Blodget et al. (1991) and White and El-Asmar (1999), are two initial studies assessing shoreline change with optical satellite images and they use the SWIR and NIR respectively because of their short penetration into the water column. However, apart from those mentioned above, there are few studies that mention the physics behind the use of a particular range of wavelengths. The most recent research does not provide a clear explanation of the significance of choice of spectral bands.

In this research, all the spectral bands were assessed in order to find which one gave the best definition of the shoreline. It was found that the NIR has the largest difference between sea and land intensity values. Moreover, it was found that the appropriate application of a wavelength for shoreline identification is more relevant than using images with a smaller pixel size (chapter 3). For example, Li et al. (2008) extracted 3-D shorelines from panchromatic images, disregarding the fact that visible wavelengths go deeper into the water column in relation to longer wavelengths (Morel 1974). Comparisons between multispectral and panchromatic images (see Table 3.1 to find the difference between panchromatic and multispectral images) carried out in this research showed that errors as large as 30 m can occur when identifying the shoreline from 2.5m pixel size panchromatic images. Meanwhile, 10 m pixel size images covering the NIR spectral band from multispectral images show errors smaller than 10 m. This error is related to the deeper penetration of wavelengths from the visible spectrum in relation to the NIR. As a result, panchromatic images are more likely to detect higher intensity values in the nearshore region due to a high amount of total suspended particles or bars. The case of study have bars in the western beach segments. However, the methodology did not encounter any difficulty to identify pixels as sea, inspite of their higher intensity

values (see Figure 3.14). This is a further confirmation that the classification technique is robust and its application could be possible in locations with nearshore bars when using the NIR spectral band.

Previous studies related to the assessment of shoreline change do not provide sufficient description of the methods followed to identify the shoreline and to calculate shoreline change. For example, Zakariya et al. (2006) mention the use of a sample site (mask) to classify the sea and land followed by a digitisation to locate the shoreline. However, no details are provided about the parameters used to classify the sea and land and the criteria in the digitisation.

This research provides an indication of which parameters could be used for shoreline identification (chapter 3). The results highlighted that the use of a sample site or a mask does not improve the classification results when using longer wavelengths. Interestingly, when using shorter wavelengths, the use of a sample site can reduce the contrast between sea and land. As a result, the use of different paremeters such as a sample site and the use of short and long wavelengths can result in a different classification of sea and land. Therefore, the specification of how the shoreline was extracted is relevant for the reliability of the estimated shoreline change.

Equally, Dinesh-Kumar et al. (2007) and Kumar and Jayappa (2009) calculate erosion and accretion by subtracting the classified pixels without providing an estimation of the errors involved when using the pixel as a unit of analysis. In this research, it was clear that when analysing different images the precise location of the pixels randomly change from image to image. Thus, the use of the pixel as a unit of analysis would introduce an error in the estimated shoreline change.

There are some shoreline change studies that disregard water levels, without providing a broad estimation of the tidal range (Zakariya et al. 2006; Ekercin 2007; Kuleli et al. 2011). As this research shows, the lack of certainty in water levels affects the further

interpretation of the shoreline change in terms of a fixed elevation.

When assessing long-term shoreline changes with optical satellite images, the seasonal change and the temporal spacing of the available images is not explicitly taken into consideration (Fromard et al. 2004; Trebossen et al. 2005; Zakariya et al. 2006; Ekercin 2007; Kuleli et al. 2011). In this research, it was shown that it is possible to estimate the seasonal shoreline change using SDS covering the different seasons within the year. Therefore, when assessing long-term shoreline change using SDS the assessment of satellite images from different seasons should be taken into consideration as much as possible in order to estimate the variability of the shoreline during the year.

This research also indicates that the shoreline accuracy can vary at different locations. The earlier research has been applied in estuaries, rivers and beaches (e.g. Amazon, Egypt, Yellow river in China, French Guiana, Malaysia, Sagar island and Mangalore in India, the coast of Taiwan). However, the accuracy of shoreline identification in relation to the characteristics of the location has not been discussed, nor have the required modifications on their techniques when applied at different locations been explored. This will be considered later in this chapter when applying the developed method to different types of beaches.

## 7.4 Accuracy of the shoreline identified by optical satellite images

There are uncertainties that have to be addressed to ensure the accuracy of the shoreline location. The most important consideration is the water level when the satellite passed over the study area. When the extracted shoreline is not related to a water level or when only a broad estimation of the water level is provided, the shoreline location cannot be referred to a specific vertical tidal datum. Thus, as a result, its further application for shoreline change studies is limited.

In previous research by Chen and Rau (1998), the difference in the tidal levels between

different images was used as an advantage to develop an inter-tidal bathymetry. They identified the shoreline at different tidal levels during a short period of time. However, our results show that the SDS is consistently seawards from the *in situ* wave run-up line, at an approximate water depth of half a metre and at a metre depth below the tidal level of the image. This is discussed further in the section on validation of SDS. However, it is interesting to note that the extracted shorelines from different tidal levels, following Chen and Rau (1998) methods, provide an indication of the nearshore bathymetry rather than the inter-tidal bathymetry.

In other research, the uncertainty of water levels of the extracted shoreline was addresseded by analysing images with similar tidal conditions or by studying locations with microtidal conditions (White and El-Asmar 1999; Chu et al. 2006). This approach is reasonable but it has the disadvantage of reducing the available images to use for shoreline identification. The approach followed by Chen and Chang (2009) used estimates of water levels and beach slopes, which provided a better definition of the shoreline considering a vertical tidal datum and that allowed the study of shoreline change.

The results of this research show that uncertainties due to water levels degrade the accuracy of shoreline location, even at locations with microtidal conditions. The implication of this is that satellite images alone cannot be a resource for shoreline identification, even when it is assumed that the difference in water levels is not relevant. The lack of water level and beach slope estimations, limits the accuracy of shoreline identification and shoreline change studies.

This research also highlights that the use of *in situ* Ground Control Points (GCP) is important to achieve a high precision in shoreline detection, as advised by White and El-Asmar (1999). The precision of the geometric correction is inherent to the analysis of images and it requires an accuracy of a minimum of half the pixel size (Lillesand

et al. 2008). The *in situ* GCP used in this research have an accuracy smaller than half a metre making it possible to achieve a geometric correction of approximately 2 to 5 m as a maximum. In contrast, when the acquisition of *in situ* GCP is not possible, it has to be considered that the shorelines extracted will have an error of about the same magnitude of the image used as a reference to perform the geometric correction. The error can significantly increase, reaching values larger than 20 m.

The validation of the SDS inherently includes the error of the geometric correction and this error is not related to the observed differences between the *in situ* shoreline measurements and the SDS. This is because the geometric correction of the images was performed using the same GCP and their consistency was verified from all the images assessed in this research. Thus, if an image had an offset due to the geometric correction it would have been identified.

The proposed method was tested using Progreso as a case study area; a location with microtidal conditions and a small shorewards extent of the wave run-up. It proved to be a very good scenario to test SDS, detecting the shoreline with high accuracy (<10 m). Although the use of predicted tides still leaves an uncertainty of approximately 5 to 15 cm (vertical) in the surveyed beaches with relatively steep beach slopes (5° of 6°), it produced a horizontal excursion of approximately 1.5 m. Furhermore, the small breaking waves in the region (< 20 cm) produced a narrow swash excursion. Thus, the confidence bounds (< 3 m) for the SDS were relatively narrow.The developed method, although not automatic, is not time consuming and all the steps involved are objective. This is relevant for further application of our method where relatively large numbers of images need to be analysed.

### 7.4.1 Validation of the satellite-derived shoreline

The validation of the SDS using quasi-simultaneous *in situ* shoreline measurements (2008 and 2010) revealed a constant seawards displacement from the wave run-up line and indicated that the SDS does not randomly change its location. Although the displacement was different in 2008, this could be attributed to a negative surge due to the effect of Hurricane Ike in the vicinity (chapter 5) during the *in situ* shoreline measurements and not to the capability of the SDS to identify the shoreline.

When the SDS and the *in situ* shoreline measurements are at equal tidal levels, the SDS is located seawards, with an overall value of 5.6 m over 8 km of shoreline at Progreso. The displacement is better explained by the optical requirement that the satellite images need to detect the sea. The NIR spectral band has a clear drop in intensity values of almost three times (e.g. from 105 to 38) from the land to the sea. As a result, the SDS is consistently located seawards from the *in situ* wave run-up line.

There was a small proportion (< 1 %) of the surveyed shoreline with a larger difference than the overall mean displacement. However, this was due to the presence of piers and not to a change in the optical capability of the satellite images.

The validation also revealed a small standard deviation between the wave run-up line and the SDS. The deviation is a result of differences between instantaneous images of the shoreline and *in situ* shoreline measurements. *In situ* shoreline measurements provide the full extent of the wave run-up excursion, while an instantaneous image provides a point example of the wave run-up. Our results confirm that the difference between *in situ* shoreline measurements is constant in the alongshore and fluctuates in the cross-shore direction due to wave run-up. Furthermore, it was observed that the difference between the *in situ* shoreline measurements and SDS decreases from 6.7 m to 3.3 m when there is a smaller wave run-up (Figure 5.3 (a)). For the shoreline survey in

beach segment 3, which is partially sheltered from the dominant wind direction by the 8 km long pier, the breaking wave height in the sheltered section was of approximately 5 cm, while the exposed segment had heights of 15 cm. Therefore, since the wave run-up of 15 cm wave height would be of approximately 0.16 m, thus the horizontal excursion in the exposed segment would be of approximately 1.7 m in a beach slope ($\tan\beta$) of 0.09. This would suggest that a difference of 3.3 m seawards of the wave run-up line is the result of the optical properties of the satellite image, while the 2 m difference is the result of the shorewards extent of the wave run-up. Together, the displacement and deviation explain the overall mean of this segment (- 5.8 m), which is of similar magnitude than the previously found over 8 km of shoreline.

Both the displacement and deviation have implications when estimating shoreline change using SDS. The optical displacement is assumed to be constant and thus is disregarded. Furthermore, the effect of the wave set-up in the displacement is not significant. The deviation, on the other hand, which is associated to the wave run-up, varies in magnitude. Therefore has to be taken into account for each SDS. The magnitude of the deviation was found to be adequate to cover the horizontal wave run-up excursion. Such a consideration when measuring shoreline change with SDS has not been considered in previous shoreline change studies.

One advantage of the beaches surveyed in Progreso is their narrow swash that allowed recording of the approximate backwash and shorewards excursion of the wave run-up in the field, providing a good estimation of the cross-shore range of the wave run-up. For example, waves of 0.5 m height with 4 s period over a beach slope ($\tan\beta$) of 0.1 would produce an estimated elevation of 30 cm, which might be exceeded in only 2 % of the observed cases (Masselink and Hughes 2003). This elevation would produce then a horizontal excursion of approximately 3 m over the beaches surveyed in Progreso. This magnitude agrees with the magnitude of the confidence bounds (2 times the standard

deviation), confirming that the confidence bounds cover the deviation of the SDS.

### 7.4.2 Data availability

Shoreline change analysis using optical satellite images requires data to be available, such as water levels and beach slope.This section outlines the approaches taken in this research to use available data and the problems encountered related to data quality and availability.

#### Water level

An estimation of water levels is required for an accurate shoreline identification. Where locations have unreliable tidal measurements, water levels can be estimated using predicted tides.

In the case study of Progreso, although there were measured tides, they were not consistent. So, the best available data to estimate water levels was predicted tides. Our own short term measurements using a pressure sensor have shown that the predicted tides underestimate the tidal range by 5 % (approx. 5 cm). An underestimation of this magnitude, given the beach slope of the study area (5°) would have a horizontal excursion small (< 1 m) enough to remain within the pixel size. Therefore, the predicted tides were useful for the estimation of water levels from SDS.

Aside from the water level estimation, the inter-tidal beach slope is required to adjust satellite-derived shorelines to a common tidal vertical datum. In studies such as Chen and Chang (2009), the beach slope was estimated from digital elevation models. In this research, the beach slope was obtained from beach profiles measured *in situ* on one day. It was assumed that the inter-tidal beach slope was approximately the same within each beach segment, although it is possible that small variations within each beach segment occur (Table 4.4). However, in general the inter-tidal beach slope is similar between beach segments, ranging from 5° to 6° with the exception of segment 1, with a beach

slope of 3°, and segment 4 with a beach slope of 9°. Therefore, it is not expected that differences in beach slope of larger than 1° will occur within each beach segment. A difference like this would not produce a significant change in the shoreline location (approx. 1 m horizontally). Thus factors such as surges and the inverted barometer effect would be expected to be more relevant than small variations of the inter-tidal beach slope within each beach segment.

Changes in water level due to surges and the inverted barometer effect are particularly relevant for locations where hurricanes are common, such as Progreso. The surge level (typically 0.5 m) can be as large as the tidal range of the study area (< 1 m), which would produce a horizontal excursion larger than 10 m on a beach slope shallower than 3°. Thus, the capability to assess shoreline change over time would be significantly reduced. As a result, it is advisable to avoid analysing images that could show the effect of a surge.

## 7.5 Application of the method to different locations

The application of SDS to explore shoreline change on different types of beaches requires a definition of confidence intervals. Confidence intervals can be based on *in situ* shoreline measurements or on accurate estimations of the shorewards extent of the wave run-up and the beach slope. Because these factors vary at different locations, the confidence bounds can increase for some beach types, reaching a magnitude at which the shoreline change detection would not be possible in extreme cases. The following section outlines further considerations when applying the developed method to different types of beaches.

### 7.5.1 Beaches with steep slope, microtidal conditions, and narrow swash

Beaches with a steep inter-tidal slope, microtidal conditions and narrow swash would show small confidence bounds of the SDS, potentially even smaller than the confidence

bounds from Progreso (< 3 m) (chapter 5). Therefore, shoreline change assessment by SDS should not be difficult.

A steep beach slope would reach the water depth required to identify the shoreline in a shorter horizontal distance than at Progreso. Furthermore, the microtidal conditions and relatively small waves would produce a narrow tidal range, shortening the horizontal distance between the SDS and the shorewards excursion of the wave run-up. This type of beach could be found at places with a narrow continental shelf and fetch-limited waves. Places like this can be found at lower latitudes, for example in Manakau Harbour, New Zealand, Como beach in Western Australia, the southeast coast of México, the south coast of the USA and Mozambique (Pilkey et al. 2009).

### 7.5.2 Beaches with shallow slope, microtidal conditions, and narrow swash

Beaches with a shallow inter-tidal beach slope, microtidal conditions and narrow swash would have confidence bounds of the SDS similar in magnitude to those found in Progreso (< 3 m). Therefore once the tidal level of the SDS is estimated, the shoreline change assessment of SDS should be achievable, with an accuracy within the pixel magnitude.

### 7.5.3 Beaches with steep slope, macrotidal conditions, and narrow swash

The application of our method to beaches with macrotidal conditions but with small shorewards extent of the wave run-up (< 3 m in the horizontal), may allow the location of the shoreline within the pixel magnitude, as long as there are accurate water level estimations. Otherwise, the errors involved in the SDS location could be as large as the pixel size. For example, in a beach as steep as 10° with breaking waves of 0.8m, and breaker criterion ($\gamma$) of 0.78, the wave set-up would produce an elevation ($\eta$) of 0.08 m. This $\eta$ would then produce a horizontal excursion that could reach 0.4 m. Equally, an uncertainty in the tidal levels as large as 1 m would produce a horizontal

uncertainty of 5 m. Adding both uncertainties would produce an overall uncertainty in the shoreline location of 6 m, which is small enough to remain within the pixel size. An uncertainty about this magnitude and even slightly larger (< pixel magnitude) would allow assessment of shoreline change with our method.

Beaches with these characteristics can be found at higher latitudes, which have fetch-limited waves and a narrow or relatively narrow continental shelf, for example in North France and Eastern Canada (French and Burningham 2011).

### 7.5.4 Beaches with shallow slope and wide swash

Beaches with shallow beach slopes and wide swash regions (> 20 m), regardless of their tidal range, might not be suitable for the application of the developed method for assessment of shoreline change. The shoreline position will vary greatly due to the shorewards extent of the wave run-up. Therefore, estimation of the water levels based on the tidal range is not enough to produce an accurate estimation of the water levels.

For these locations, it would be necessary to first estimate the magnitude of the shorewards extent of the wave run-up, as well as the magnitude of the shoreline change expected to be detected. When the cross-shore range of the shorewards extent of the wave run-up is larger than the shoreline change, or when both are of similar magnitude, this method would not be suitable to assess shoreline change.

In the cases where the SDS is suitable to assess shoreline change, it would be desirable to carry out *in situ* shoreline measurements to estimate the inter-tidal beach slope and the shorewards extent of the wave run-up.

For locations where SDS is not suitable to assess shoreline change, the use of the vegetation line could be useful to assess shoreline change. The use of field surveying techniques, such as beach profiles, could provide estimations of the changes in the geomorphology taking place on the beach. It is important to mention that the use of other

types of images to assess shoreline change will have similar difficulties to the use of optical satellite images.

### 7.5.5 Other considerations

The magnitude of the mean difference between SDS and *in situ* shoreline could vary due to the presence of suspended particles in the water column and the beach slope in the nearshore region. High concentrations of suspended particles in the water column might displace the SDS further seaward away from the *in situ* shoreline. The suspended particles increase the reflected intensity values. Therefore, the image may require a deeper water depth to measure a reduction in the intensity values sufficient to be identified as sea.

In this research it was assumed that the mean difference between SDS and *in situ* shoreline is constant from image to image. Thus, estimation of shoreline changes can be made in spite of this difference. However, in the case that the water depth changes from image to image, due to temporal variations in suspended particles for example, it would be necessary to estimate the magnitude of any such change. Therefore, the confidence bounds would require the addition of a correction factor.

To estimate the range of the mean difference between SDS and *in situ* shoreline due to different concentrations of suspended particles in the water column, further simultaneous inter-comparisons between *in situ* shoreline measurements and SDS would be required. There is existing research on this topic by Teodoro et al. (2007, 2008), who found that there is not a linear relationship between the reflectance and the total suspended particles in the water column. Moreover, the difference in reflectance changed by less than 8 % with concentrations between 14 and 449 $mgL^{-1}$ of total suspended particles in the water column. A magnitude of this order is not expected to produce a significant effect on the shoreline location.

## 7.6 Shoreline change using SDS

### 7.6.1 Data availability

#### Optical satellite images

The availability of satellite images at a given time and position is a fundamental limitation when assessing shoreline changes at remote locations. While looking for the availability of images in Yucatán, it became evident that for locations such as the USA shoreline, or heavily populated regions, the availability of images is higher, whereas at remote locations and scarcely populated areas, the availability of images significantly decreases. As a consequence, further assessment of shoreline change at remote locations would not be possible without available images.

For example, the available images from Yucatán cover over 200 km of shoreline. The locations of Progreso and Telchac have images for different seasons during several years. The temporal spacing of images from Progreso was better than for Telchac, allowing estimation of intra-annual shoreline change based on the two years which show the highest frequency of images (see chapter 6). This demonstrates that although locations may not have large numbers of images within a year, the assessment of seasonal shoreline change and the exploration of longer periods of time may still be possible.

The comparison of two different dates is valuable for estimation of relative shoreline change during a specific period of time, when there is no other information available. The assessment of shoreline change in this research allowed the estimation of shoreline change during the hurricane season, winter storms and relatively calm conditions, using images that do not have a surge effect. The result of this assessment revealed that an overall landwards movement of the shoreline occurs after storms in winter (November to March 2004) of approximately 3 to 13 m. Furthermore, on average changes as large as 40 m can take place over a shoreline 300 m long, 13 days after Hurricane Ivan

(category 4). In addition, no changes in the shoreline location were found when the overall conditions were calm (March to June 2004). These observations in the shoreline changes would not be identified when comparing widely spaced SDSs, demonstrating the value of doing comparisons between two SDS within a short time period (< 1 year).

The study of relatively widely spaced SDSs is also useful for the estimation of changes in the shoreline position in the long-term. However, estimation of the seasonal shoreline change at the location under investigation is also important (Crowell et al. 1991; Leatherman and Douglas 2003). Otherwise, it is not possible to determine when the shoreline moved further away from the usual limits within the year. Our results highlight that it is possible to estimate rates of change using a combination of widely spaced and frequent images. A progressive movement in the shoreline position was determined using the average shoreline position over time, allowing the estimation of the rate of change within the studied time span.

Although our results revealed a generalised shoreline retreat in Progreso, it remains possible that the shoreline retreat is due to the fact that most of the assessed SDSs (10 of 13) are from the hurricane and storm season. However, disregarding the spacing of the SDSs, this highlights the potential use of our method to estimate rates of shoreline change and the forecasting of shoreline change, when there are better spaced SDSs, for coastal management purposes.

Remote locations that are scarcely populated and with little available coastal information are likely to be limited on tides, waves, meteorological data and available satellite images as well. These kind of locations require the development of systematic and accurate tidal measurements and tidal predictions. Although tidal predictions for most of the coastal locations are available, the predictions will have some uncertainty in relation to tidal measurements, which has to be taken into account. This is particularly true when the magnitude of the expected shoreline change is similar to the uncertainties due

to the tidal levels.

It is also important to mention that the random availability of archived optical satellite images appears to be a disadvantage in relation to other types of data such as LIDAR, radar and SAR sensors, where the specific times are specified by the user. However, the possibility that optical satellite images offers for the assessment of shoreline change in the long-term, using archived images, is an advantage, particularly at locations where there is no other type of data available to assess shoreline change. Furthermore, the cost per kilometre of optical satellite images is significantly less expensive than LIDAR images. Satellite images cost approximately £1.30 for archived images between 1986 and 2006 and £20 for recent images, while LIDAR images cost £230 (Table 2.1 in section 2.4).

## 7.7 Estimation of shoreline change

In this research, the data available to interpret the shoreline change allowed explanation of the observed shoreline change based on environmental factors, showing consistency with SDS from similar seasons. For example: the SDS from February 2006 and March 2004, both from late winter are at a very similar shoreline location. The SDS from May 2004 and June 2004 both have very similar shoreline location, explained by the prevailing calm conditions. The SDS from September 2008 and September 2007 are very close in their shoreline location. These results suggests a seasonal movement of the shoreline over the year, where the shoreline location is at an approximately similar shoreline position at similar times during the year. It is also important to mention that within the relatively consistent location of these shorelines, a progressive landwards movement in the shoreline position was detected.

It was also found that the observed shoreline change overall agrees with the westwards dominant direction of the longshore drift, and that the cross-shore transport of sediment

is significant in high energy events. Furthermore, Progreso pier reduces the alongshore transport of sand, producing accumulation of sand in segment 3.

The wind data had the longest time series of the available ancillary data, providing information that was valuable to estimate the longshore drift direction. The available measured wave data for Yucatán was from a NOAA buoy located 200 km offshore from Progreso. Moreover, modelled wave data was developed to reconstruct wave time series for the Gulf of México (Betancourt-Quiroga 2007). This information, although valuable to the understanding of the wave behaviour in the region, does not describe the waves approaching the shore. However, the wave measurements in shallow waters at Telchac and at Progreso (Mariño-Tapia 2010) were valuable to confirm the contrasting behaviour of waves in shallow water (0.2 m<Hs<0.8 m) and deep water (1 m<Hs<5m) conditions over the year. Such data also allowed the estimation of the number and frequency of storms that occurred during the evaluated period of time in winter.

The results obtained by the application of our method show that it is valuable to study shoreline change on large geographical scales. The assessment of SDS was relevant for estimation of the processes involved in shoreline change. For example, the results suggest that segment 8 is eroding at a higher rate than the other segments. This might be related to several factors such as the longshore direction of the sediment transport, the limited availability of sand in the region, and the presence of coastal buildings located very close to the shoreline. All these factors may contribute to a progressive landwards movement of the shoreline. However, more detailed studies considering higher spatial scales would be useful for the understanding and verification of the processes involved in this shoreline retreat.

The information gathered using this method can be further used for the development of coastal management actions. For example, the assessment of SDSs at Progreso revealed that most of the shoreline exhibits overall erosion over a 6.5 year period, with

estimated rates of between -2.4 and -1.2 myr$^{-1}$ (Figure 6.18). This information would not be found without SDS. However, it is recognised that the calculation of rates of shoreline change should be done cautiously, including as many and as well-spaced SDSs as possible during the studied period of time.

Optical satellite images have also been applied to the assessment of floods (Klemas 2009), showing their value when monitoring floods caused by Hurricane Katrina. In the present research the effect of Hurricane Ivan in 2004 and Hurricane Ike in 2008 was detected, producing a surge of approximately half a metre in height, thus demonstrating the value of optical satellite images to study shoreline change in short periods of time.

Although the types of data to monitor the shoreline and coastal disasters are vast, the use of optical satellite images provides large amounts of information by visual assessment. In contrast, images from SAR and LIDAR require the scheduling of a flight, besides the further processing of the data. Aerial photographs depend on the climatic conditions, besides requiring extensive post-processing to map a surface as large as the optical satellite images. The analysed optical satellite images had different tidal levels and none of them had difficulties when extracting SDS. In contrast, SAR images have difficulties with the shoreline extraction from images in low tide conditions (Mason et al. 1995). The possibility of using optical satellite images for any tidal level for shoreline identification is a significant advantage of the type of data and our technique.

## 7.8 Future research

This section suggests further research related to topics addressed in this research for the development of optical satellite images for coastal applications.

### 7.8.1 Vectorisation and shoreline smoothing

The accuracy achieved in the developed method is within the pixel size, allowing shoreline change assessment. However, the accuracy of the SDS location could be improved by refining the smoothing process. For example, abrupt changes in the shoreline orientation within an alongshore distance of 50 m are not as effectively captured as shorelines with gentle changes in orientation. Therefore, future development of the shoreline extraction method could improve the accuracy of the SDS.

### 7.8.2 Assessment of satellite optical images for coastal research

Further understanding of the change in intensity values over different types of beaches is required using *in situ* verification. For example, variables such as the beach slope, shorewards extent of the wave run-up, type of sediment, suspended particles in the water column, and a sea surface with ripples can modify the water depth needed to identify the shoreline. Therefore, to extract the best possible information from optical satellite images, calibration is required based on *in situ* measurements of the effect of all the previously mentioned factors.

The exploration of the accuracy of SDS using images with a pixel size smaller than 10 m would be interesting. It is possible that the higher spatial resolution does not imply higher accuracy on shoreline detection and that with a higher resolution other difficulties in shoreline detection could occur as was found, for example, in the use of panchromatic images.

### Cross-shore range in the extent of the swash

The inter-comparisons indicate that the mean difference between SDS and *in situ* shoreline measurements is fairly constant and that is associated with the optical requirements of images to identify a pixel as water. However, it would be of interest to perform further simultaneous measurements to confirm that the mean difference between SDS and *in situ* shoreline measurements is indeed relatively constant between images, and identify conditions in which this assumption might break down.

### Shoreline change detection on barred beaches

The investigation of shoreline change linked to the presence of nearshore bars could be addressed by the use of optical satellite imagery. There are previous studies (e.g. (Lafon et al. 2002)) that addressed the movement of bars using satellite imagery. Therefore, by the application of the methods developed here, it would be possible to study shoreline change and their feedback with bars in the nearshore region covering large geographical scales.

### Shoreline change in Yucatán

For further research the completion of the analysis of shoreline change using all the available optical satellite images in Yucatán would be of great value. There are other locations, such as Telchac, that have some available optical satellite images. In this location an inlet was opened when Hurricane Isidore (see chapter 4) passed. Therefore, the study of the shoreline change would provide a better understanding of the coastal processes taking place and the magnitude of the shoreline change during extreme events in Yucatán.

# Chapter 8

# Conclusions

Optical satellite images can produce accurate estimations (< 10 m) of shoreline change covering large spatial scales (> 15 km), as well as short (< 1 year) and long (> 5 years) temporal scales. Furthermore, rates of change can be estimated, demostrating their utility for shoreline change studies, as this research shows using Progreso as a case of study.

The case study of Progreso was chosen due to erosion problems, paucity of coastal information and yearly presence of hurricanes and storms, characteristics that made it a challenging and interesting location to evaluate shoreline change with SDS. The fact that this location has microtidal conditions and a small shorewards extent of the wave run-up, allowed shoreline identification with high accuracy (< 10 m) and the estimation of intra-annual and inter-annual shoreline change.

The aim and objectives defined in this research outlined an approach to gain a better understanding of the capabilities of optical satellite images to assess shoreline change. The main conclusions of this study are listed below and matched to the corresponding objectives.

## 8.1 To develop a method to identify the shoreline from optical satellite images

This objective is addressed in chapter 3, by the assessment of different spectral bands over the cross-shore profile and different techniques to extract the shoreline. The conclusions related to this objective are listed below:

1. A method has been developed to extract the shoreline from optical satellite images, which ensures the clearest difference between the classified sea and land, by using the NIR alone. The method does not require the use of a sample site (mask) of the study area. It systematically locates the shoreline as a line between the classified sea and land, with an accuracy half the pixel magnitude (5 m). The use of a sample site and different spectral bands in the classification can result in a different location of the shoreline. Thus, these parameters were tested to produce the clearest difference between sea and land.

   (a) The use of a sample site of the study area does not improve the classification results when using longer wavelengths. Furthermore, when using shorter wavelengths the use of sample site (mask) reduces the contrast of the intensity between sea and land. For example, the mean intensity of the pixels classified as sea increased from 20 to 80 with the narrower sample site, and the mean intensity of the pixels classified as land decreased from 220 to 140. Thus the use of the whole image, without the application of a mask, provides better contrast in the intensity values needed to distinguish between sea and land.

   (b) The use of the NIR provides the largest differentiation between sea and land, even in the presence of suspended particles in the water column. Comparisons between multispectral and panchromatic images (see Table 3.1 for

their description) carried out in this research showed that errors as large as 30 m can occur when identifying the shoreline from 2.5 m pixel size panchromatic images. Using the NIR spectral band, 10 m pixel size multi-spectral images show errors smaller than 10 m. This error associated with panchromatic images is related to the deeper penetration (> 10 m, Lafon et al. (2002)) of wavelengths from panchromatic images in relation to the NIR spectral band. As a result, panchromatic images are more likely to classify the nearshore region as land rather than sea. Thus, the sole use of the NIR is recommended for shoreline identification.

(c) The extracted shoreline systematically locates the boundary between the classified sea and land at half the pixel magnitude (5 m) and smoothes the shoreline in the alongshore at a maximum distance of 50 m. This value was found to be adequate in order to represent the classification results successfully and to remove the jagged pattern caused by the pixels' location (Figure 3.26). This process ensures that the extracted shoreline could be further used to assess shoreline change.

(d) The extracted SDS using the developed method must consider the water level when the satellite passed the study area. The use of inter-tidal beach slope over beach segments with similar characteristics is recommended to adjust the SDS to a specific vertical tidal datum, assuming that the inter-tidal beach slope is constant within each beach segment.

## 8.2 To validate satellite-derived shorelines (SDS)

This objective is addressed in chapter 5 and required the development of contents in chapter 4 to take into consideration the characteristics of the study area, such as water levels and beach slope. The validation of the SDS was based on inter-comparison from 2010 with quasi-simultaneous SDS and *in situ* shoreline measurements with five hours of difference. The two measurements had different tidal levels, however for the validation, the *in situ* shoreline measurements and the SDS were adjusted to an equal tidal level. The conclusions about this objective are listed below:

1. The validation revealed that the SDS has a seawards displacement and a deviation from the *in situ* wave run-up line. In a region such as Progreso, these had an overall value of 5.6 m and 1.4 m respectively, over 8 km of shoreline.

   (a) The displacement between the *in situ* shoreline measurements and the SDS is due to the required water depth (approx. 0.5 to 1 m) of optical satellite images to distinguish the sea. The NIR spectral band has a clear drop in intensity values of almost three times (e.g. from 105 to 38) from the land to the sea. This explains the seawards position of the SDS and the water depth required to distinguish the reflected intensity as sea. Moreover, this displacement is fairly constant in the alongshore, with 80 % within one standard deviation, between the values of -6.9 and -4 m (Figure 5.6).

   (b) The SDS has a deviation between the *in situ* shoreline measurements because the image instantaneously captured the location of the shoreline, recording the backwash and shorewards excursion of the wave run-up. The magnitude of the standard deviation in Progreso (1.4 m) agrees with the estimated wave run-up given a wave height smaller than 0.5 m and beach slope of 3° to 6°. The standard deviation between *in situ* shoreline measurements and

SDS provided a good estimation of the confidence bounds of the SDS.

(c) The assessment of shoreline change from 2008 and 2010 with SDS over determined beach segments with similar characteristics, have differences 3.6 m smaller than *in situ* shoreline measurements. In addition, it should also be noted that the analysis of a beach segment gives a better estimation than specific point beach locations. For example, using SDS the estimated shoreline change from 2008 to 2010 in segment 3 using SDS is seawards between 9 m and 16 m. The estimated change found with *in situ* measurements is 14 m (seawards), which is within the estimated range of SDS. However, the measured change at a specific location within segment 3 can be slightly (<5 m) out of the estimated range of change produced by the SDS.

(d) The application of our method at locations where the confidence bounds are of the same order of magnitude as the expected shoreline change would not be successful. The expected amplitude of the wave run-up provides a clear limit of the accuracy of the SDS and of the minimum shoreline change that can be detected.

## 8.3 To assess and to interpret shoreline change using SDSs in the case study of Progreso, Yucatán, in relation to environmental factors.

This objective is addressed in chapter 6, by applying our method to the available satellite optical images in Progreso, Yucatán (December 2003 to July 2010), considering the presence of man-made structures, as well as winds and wave data. The conclusions about this objective are listed below:

1. The assessment of SDS demonstrated its capability to assess shoreline change in short (< 1 year) and long (> 5 year) temporal scales, achieving an estimate of the mean SDSs position and the envelope of shoreline positions during 2004 and 2005, as well as detection of a progressive shoreline retreat over a 6.5 year period. Moreover, the observed shoreline change can be linked to the overall environmental conditions (seasons, storms and hurricanes). For example:

   (a) The SDS from late winter (March 20, 2004) is landwards in relation to the SDS in early winter (November 11, 2003), by approximately 5 m to 9 m. The largest change occurs in the eastern beach segments, probably due to a high cross-shore transport of sediment during storms.

   (b) Overall the SDSs from the hurricane season are located at the landwards envelope limit during the year, with a shoreline change between -30 m to 15 m in relation to the mean SDSs over the year.

   (c) An overall landward movement of at least 10 m and up to 45 m in segment 3 (west of the pier) was found in an image 13 days (September 27, 2004) after Hurricane Ivan (2004) was at its closest to the study area. This change is not expected to happen with the dominant western direction of the longshore

drift, suggesting it may be related to the cross-shore transport of sediment during Hurricane Ivan.

(d) An overall seawards movement of the shoreline during calm conditions could not be assessed due to the temporal spacing of the SDS. However, the SDS from May to June (2004) remained at a similar shoreline location, which agrees with the calm conditions during that period of time.

2. The assessed SDS positions over a 6.5 year period suggests a progressive landwards movement of the shoreline (Figure 6.18) over approximately 6 km with an overall estimated rate between -2.4 to -1.2 myr$^{-1}$. Segments 3 and 6 are the exceptions, showing low overall accretion rates (0.3 to 0.6 myr$^{-1}$).

3. Beach segments (3, 4 and 5) located approximately 500 m from Progreso piers exhibit the largest changes after high-energy events, such as storms and hurricanes (e.g. Hurricane Ivan in 2004). In contrast, segments located further from the piers exhibit smaller shoreline change in the presence of storms and cyclones indicating that the sand accumulated closer to the pier is moved offshore during high energy events.

# Appendix A

## A.1 Cyclone reports

This section includes reports that are open to the public domain in the webpage of the NHC (NHC 2010). The reports are in chronological order. They are listed below (to see the report press click):

1. Hurricane Camile (1969)

2. Hurricane Isidore (2002)

3. Hurricane Ivan (2004)

4. Tropical storm Arlene (2005)

5. Hurricane Emily (2005)

6. Hurricane Wilma (2005)

7. Hurricane Dean (2007)

8. Hurricane Ike (2008)

# Appendix B

## B.1 Beach profiles carried out in Progreso in 2010

This section shows the spatial location of the beach profiles carried out for each beach segments and each beach profile.

Figure B.1 shows the spatial location of the beach profiles for each beach segment.

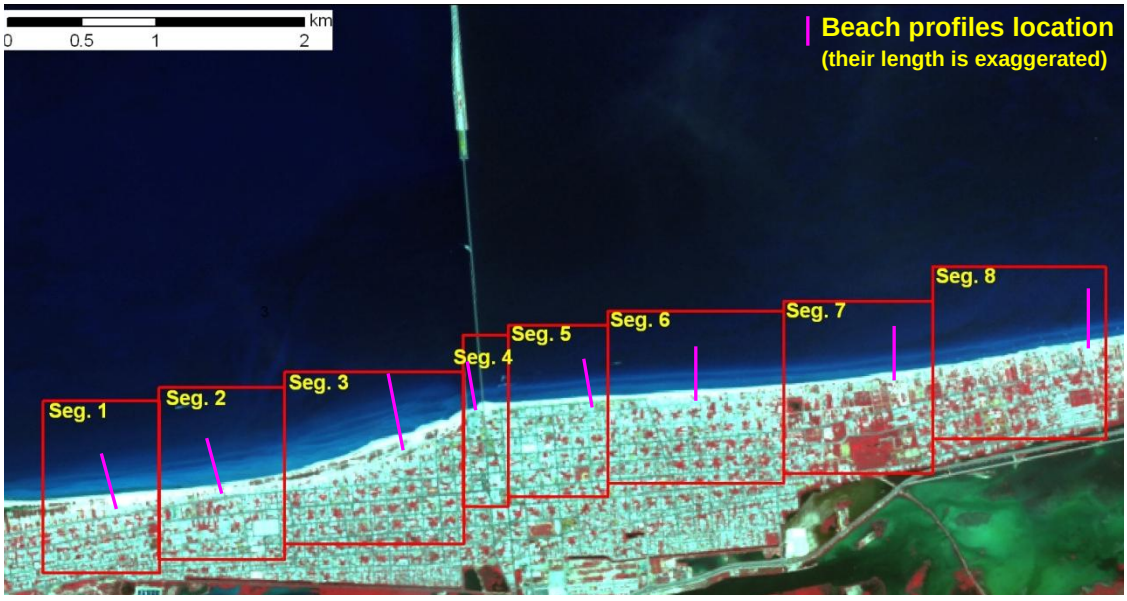


*Figure B.1:* Location of the beach profiles carried out in 2010.

Figures B.2, B.3, B.4. B.5 show the beach profiles for each beach segment.

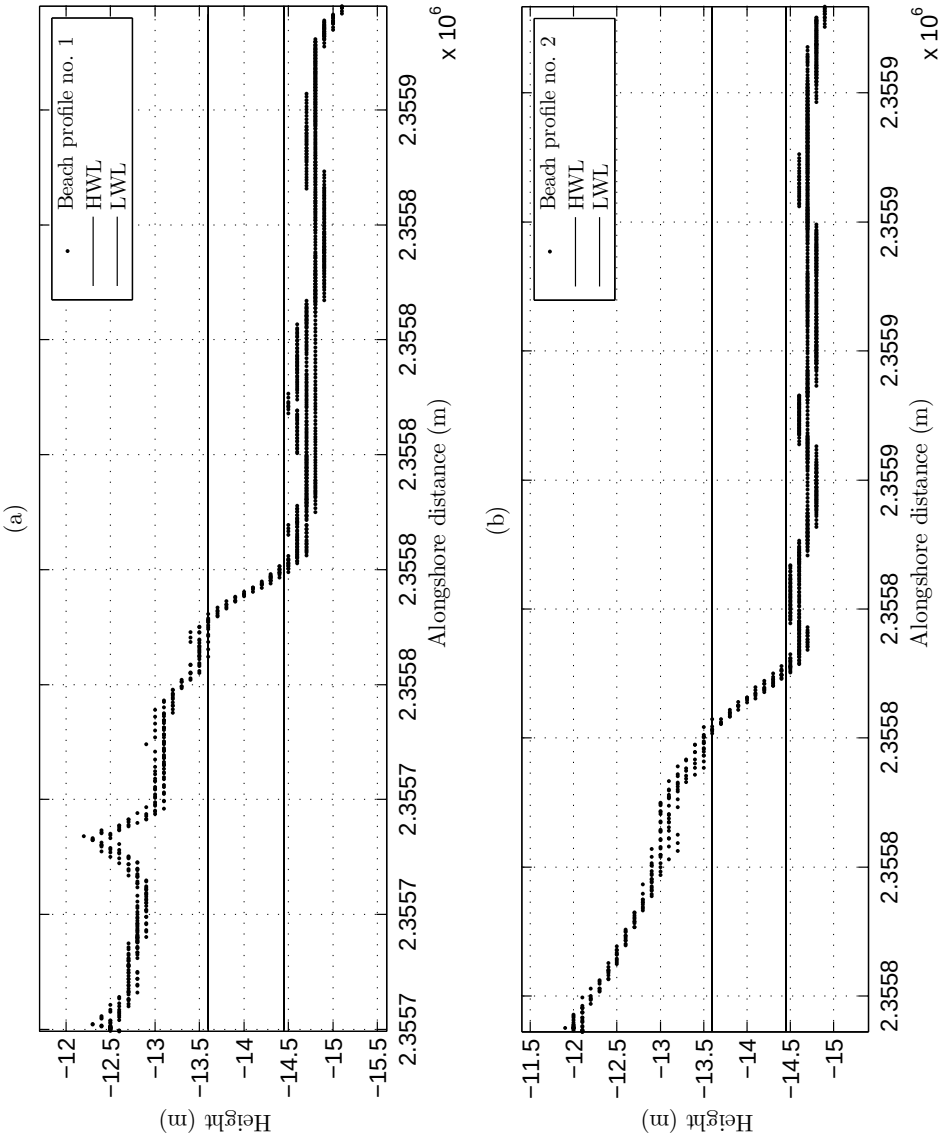


*Figure B.2:* Beach profiles 1(a) and 2 (b).

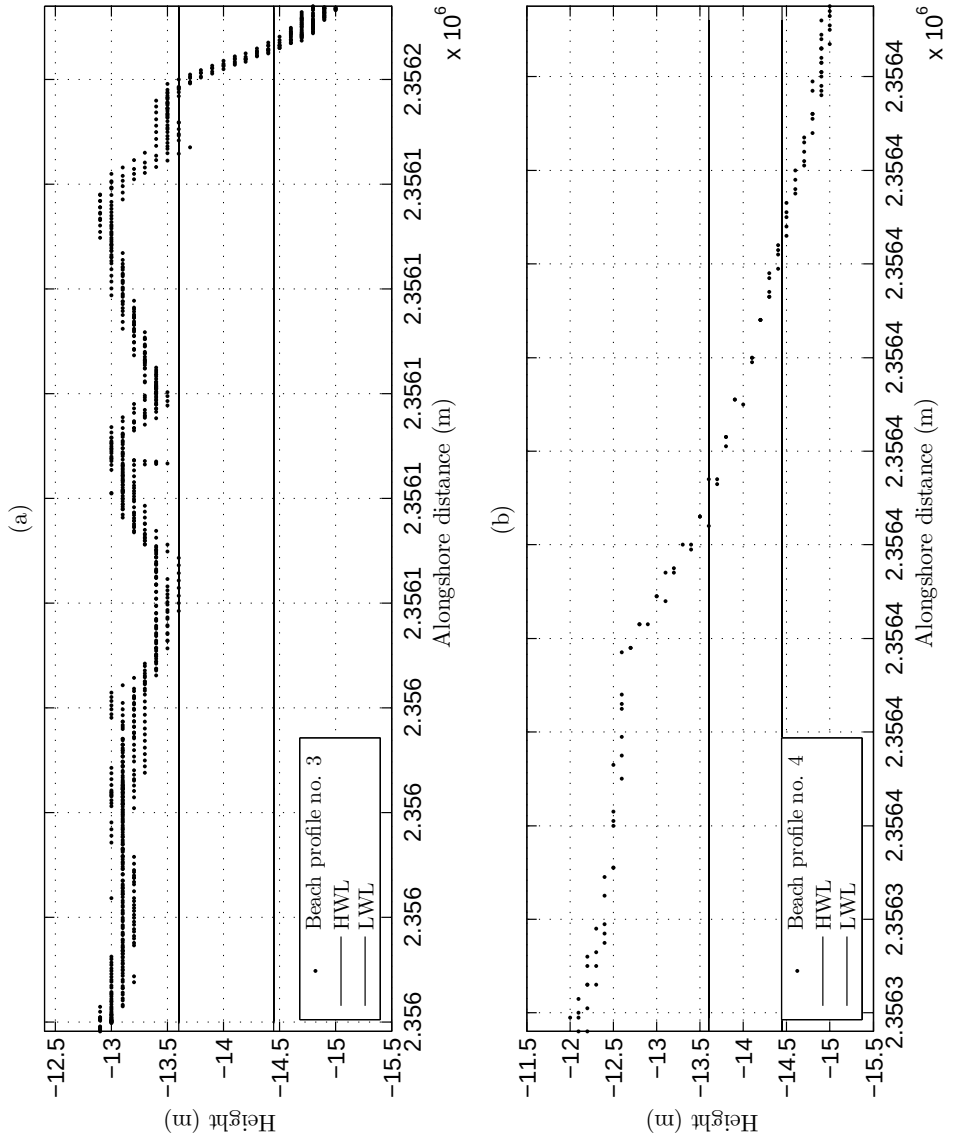


*Figure B.3:* Beach profiles 3(a) and 4 (b).

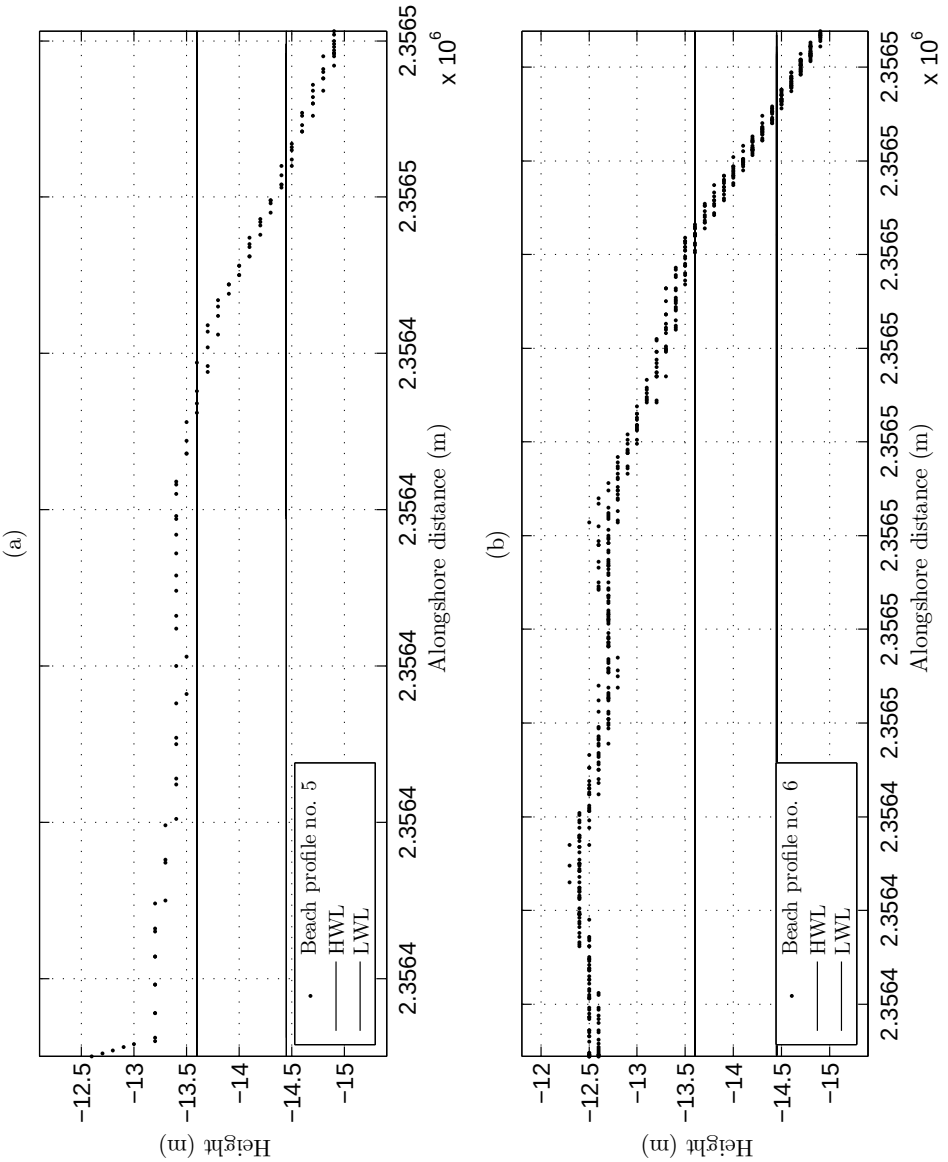


*Figure B.4:* Beach profiles 5(a) and 6 (b).

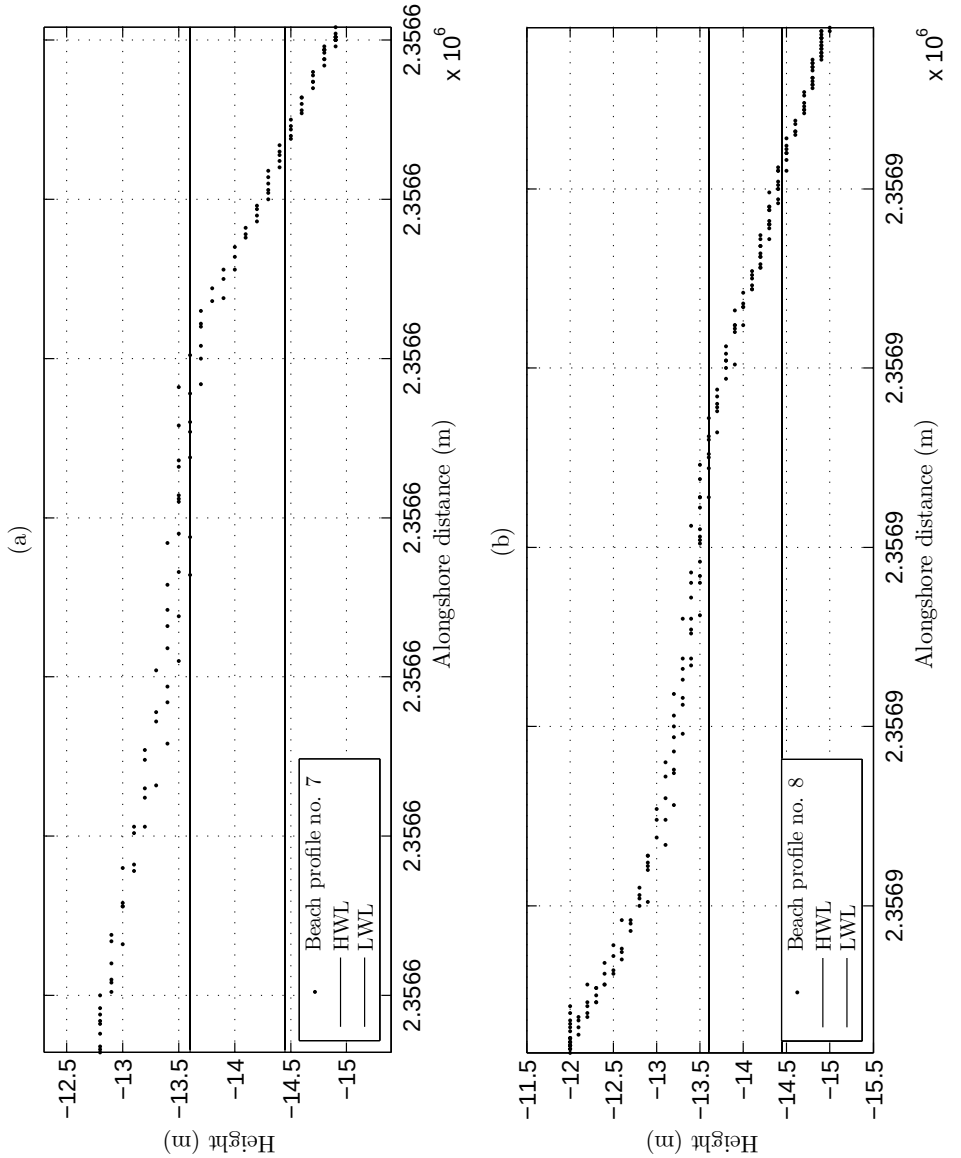


*Figure B.5:* Beach profiles 7(a) and 8 (b).

# Appendix C

## C.1 Conference paper presented in Coastal Dynamics (2009)

This section includes the conference paper presented in the Coastal Dynamics 2009 Conference held in Tokyo, Japan. The paper is titled: Shoreline identification using satellite images

# List of references

Aarninkhof, S. (2003), Nearshore bathymetry derived from video imagery, PhD thesis, Delft University, Delft University of Technology, Netherlands.

Anders, F. J. and Byrnes, M. R. (1991), 'Accuracy of shoreline change rates as determined from maps and aerial photographs', *Shore and Beach* **59**(1), 17–26.

Armaroli, C., Ciavola, P., Balouin, Y. and Gatti, M. (2004), 'An Integrated Study of Shoreline Variability using GIS and ARGUS techniques', *Journal of Coastal Research* **SI 39**, 473–477.

AXIS (2008), Reporte de resultados de las campañas de monitoreo realizadas como parte del programa de seguimiento del proyecto: "Estabilizacion de la duna costera mediante tubos geotextiles, para industria salinera de Yucatan, S.A de C.V., en las Coloradas, Yuc.", Technical report, AXIS.

Betancourt-Quiroga, O. (2007), Determinacion del clima maritimo en zonas costeras, PhD thesis, Engineering.

Blodget, H. W., Taylor, P. T. and Roark, J. (1991), 'Shoreline changes along the Rosetta-Nile promontory monitoring with satellite observations', *Marine Geology* **99**, 67–77.

Boak, E. H. and Turner, I. L. (2005), 'Shoreline definition and detection: A review', *Journal of Coastal Research* **21**(4), 688–703.

Campbell, J. B. (1996), *Introduction to Remote Sensing*, Vol. 2nd, The Guildford Press.

Chen, L. and Rau, J. Y. (1998), 'Detection of shoreline changes for tideland areas

using multi-temporal satellite images', *International Journal of Remote Sensing* **19**(17), 3383–3397.

Chen, W. and Chang, H.-K. (2009), 'Estimation of shoreline position and change from satellite images considering tidal variation', *Estuarine, Coastal and Shelf Science* **84**, 54–60.

Chu, Z. X., Sun, X., Zhai, S. and Xu, K. (2006), 'Changing pattern of accretion/erosion of the modern Yellow River (Huanghe) subaerial delta, China: Based on remote sensing images', *Marine Geology* **227**, 13–30.

Cooper, J. A. G. and Pilkey, O. H. (2004), 'Longshore drift: Trapped in an expected universe', *Journal of Sedimentary Research* **74**(5), 599–606.

Cracknell, A. P. (1999), 'Remote sensing techniques in estuaries and coastal zones-an update', *International Journal of Remote Sensing* **19**(3), 485–496.

Crowell, M., Leatherman, S. P. and Buckley, M. K. (1991), 'Historical shoreline change: Error analysis and mapping accuracy', *Journal of Coastal Research* **7**(3), 839–852.

Defne, Z., Haas, K. A. and Fritz, H. M. (2009), 'Wave power potential along the Atlantic coast of the southeastern USA', *Renewable Energy* **34**, 2197–2205.

Diez, J., Esteban, M. and Paz, R. (2009), 'Cancun-Nizuc Coastal Barrier', *Journal of Coastal Research* **25**(1), 54–68.

Dinesh-Kumar, P. K., Gopinath, G., Laluraj, C., Seralathan, P. and Mitra, D. (2007), 'Change Detection Studies of Sagar Island, India, using Indian Remote Sensing Satellite 1c Linear Imaging Self-Scan Sensor III Data', *Journal of Coastal Research* **23**(6), 1498–1502.

Dolan, R., Hayden, B. P. and Heywood, J. (1978), 'A new photogrammetric method for determining shoreline erosion', *Coastal Engineering* **2**(1), 21–39.

Douglas, B., Kearney, M. S. and Leatherman, S. P., eds (2001), *Sea Level Rise: History and Consequences*, Vol. 75, International Geophysics Series.

Ekercin, S. (2007), 'Coastline Change Assessment at the Aegean Sea Coasts in Turkey Using Multitemporal Landsat Imagery', *Journal of Coastal Research* **23**(3), 691–698.

ESSA (1969), Hurricane Camille August 12-22, 1969, Technical report, U.S. Department of Commerce.

FitzGerald, D. M., Fenster, M. S., Argow, B. and Buynevich, I. V. (2008), 'Coastal impacts due to sea-level rise', *Annu. Rev. Earth Planet. Sci.* **36**, 601–647.

Foody, G. (2002), 'The role of soft classification techniques in the refinement of estimates of ground control point location', *Photogrammetric Engineering and Remote Sensing* **68**, 897–903.

Foody, G. M., Muslim, A. M. and Atkinson, P. M. (2003), 'Super-resolution mapping of the shoreline through soft classification analyses', *IEEE Transactions on Geoscience and Remote Sensing* pp. 3429–3431.

Foody, G. M., Muslim, A. M. and Atkinson, P. M. (2005), 'Super-resolution mapping of the waterline from remotely sensed data', *International Journal of Remote Sensing* **26**(24), 5381–5392.

French, J. R. and Burningham, H. (2011), 'Coastal geomorphology', *Progress in Physical Geography* **35**(4), 535–545.

Frihy, O. and Lotfy, M. F. (1997), 'Shoreline changes and beach-sand sorting along the northern Sinai coast of Egypt.', *Geo-Marine Letters* **17**, 140–146.

Fromard, F., Vega, C. and Proisy, C. (2004), 'Half a century of dynamic coastal change affecting mangrove shorelines of French Guiana. A case study based on remote sensing data analyses and field surveys', *Marine Geology* **208**, 265–280.

Frouin, R. (1996), 'Spectral reflectance of sea foam in the visible and near-infrared: In situ measurements and remote sensing implications', *Journal of Geophysical Research* **101**(C6), 14361–14371.

Galal, E. M. and Takewaka, S. (2008), 'Longshore Migration of Shoreline Mega-Cusps Observed with X-Band Radar', *Coastal Engineering Journal* **50**(3), 247–276.

Gens, R. (2010), 'Remote sensing of coastlines: detection,extraction and monitoring', *International Journal of Remote Sensing* **31**, 1819 –1836.

González, J. I., Morales, A. and Ochoa, J. L. (2010), Prediccion de Mareas en México, http://oceanografia.cicese.mx/predmar/.

Gutierrez, B. T., Plant, N. G. and Thieler, E. R. (2011), 'A bayesian network to predict coastal vulnerability to sea level rise', *Journal of Geophysical Research* **116**, 1–15.

Hanamgond, P. and Mitra, D. (2008), 'Evolution of Malvan Coast, Konkan, West Coast of India: A Case Study Using Remote Sensing Data', *Journal of Coastal Research* **24**(3), 672–678.

Holman, R. A. and Stanley, J. (2007), 'The history and technical capabilities of Argus', *Coastal Engineering* **54**, 477–491.

INEGI (2006), *II Conteo de Población y Vivienda 2005*, Instituto Nacional de Geografia y Estadistica.

Intergovernmental Panel on Climate Change (1990), "Policymaker's: Summary of the Potential Impacts of Climate Change" report from working group ii to the intergov-

ernmental panel on climate change., Technical report, Intergovernmental Panel on Climate Change.

Kingston, K. (2003), Applications of complex adaptative systems, approaches to coastal systems, PhD thesis, University of Plymouth, Plymouth.

Klemas, V. V. (2009), 'The Role of Remote Sensing in Predicting and Determining Coastal Storms Impacts', *Journal of Coastal Research* **25**(6), 1264–1275.

Komar, P. D. (1998), *Beach Processes and Sedimentation*, Vol. 2nd, Prentice-Hall, United States of America.

Kuleli, T., Guneroglu, A., Karsli, F. and Dihkan, M. (2011), 'Automatic detection of shoreline change on coastal wetlands of Turkey', *Ocean Engineering* **38**, 1141–1149.

Kumar, A. and Jayappa, K. S. (2009), 'Long and Short-term Shoreline Changes Along Mangalore Coast, India', *Int. J. Environ. Res.* **3**(2), 177–188.

Lafon, V., Dupuis, H., Howa, H. and Froidefond, J. (2002), 'Determining ridge and runnel longshore migration rate using SPOT imagery', *Oceanologica Acta* **25**, 149–158.

Lafon, V., Froidefond, J., Lahet, F. and Castaing, P. (2002(a)), 'SPOT shallow water bathymetry of a moderately turbid tidal inlet based on field measurments', *Remote Sensing of Environment* **81**, 136–148.

Leatherman, S. and Douglas, B. (2003), 'Sea level and coastal erosion require large-scale monitoring', *EOS, Transactions, American Geophysical Union* **84**(2), 13–20.

Leatherman, S. P. (1983), 'Shoreline mapping: a comparison of techniques', *Shore and Beach* **51**, 28–33.

Li, R., Deshpande, S., Niu, X., Zhou, F., Di, K. and Wu, D. (2008), 'Geometric integration of aerial and high-resolution satellite imagery and application in shoreline mapping', *Marine Geodesy* **31**, 143–159.

Li, R., Di, K. and Ma, R. (2003), '3-D Shoreline Extraction from IKONOS Satellite Imagery', *Marine Geodesy* **26**, 107–115.

Lillesand, T., Kiefer, R. and Chipman, W. (2008), *Remote Sensing and Image Interpretation*, 6 edn, John Wiley & Sons, Inc., United States of America.

Liu, H. and Jezek, K. (2004), 'Automated extraction of coastline from satellite imagery by integrating Canny edge detection and locally adaptive thresholding methods', *International Journal of Remote Sensing* **25**(5), 937–958.

Liu, H., Sherman, D. and Gu, S. (2007), 'Automated Extraction of Shorelines from Airbone Light Detection and Ranging Data Accuracy Assessment based on Monte Carlo Simulation', *Journal of Coastal Research* **23**(6), 1359–1369.

Maiti, S. and Bhattacharya, A. K. (2009), 'Shoreline change analysis and its application to prediction: A remote sensing and statistics base approach.', *Marine Geology* **257**, 11–23.

Mariño-Tapia, I. (2010), pers.comm., CINVESTAV-Merida, Researcher from Oceanography Physics in CINVESTAV-Merida.

Mason, D. C., Amin, M., Davenport, I. J., Flather, R., Robinson, G. and J.A.Smith (1999), 'Measurement of Recent Intertidal Sediment Transport in Morecambe Bay using the Waterline Method', *Estuarine, Coastal and Shelf Science* **49**, 427–456.

Mason, D. C., Davenport, I. and Flather, R. (1997), 'Interpolation of an Intertidal Digital Elevation Model from Heighted Shorelines: a Case Study in the Western Wash', *Estuarine, Coastal and Shelf Science* **45**, 599–612.

Mason, D. C. and Garg, P. K. (2001), 'Morphodynamic Modelling of Intertidal Sediment Transport in Morecambe Bay', *Estuarine, Coastal and Shelf Science* **53**, 79–92.

Mason, D., Davenport, I. J., R.A.Flather, Gurney, C., Robinson, G. and J.A.Smith (2001), 'A sensitivity analysis of the Waterline Method of Constructing a Digital Elevation Model for Intertidal Areas in ERS SAR scene of Eastern England', *Estuarine, Coastal and Shelf Science* **53**, 759–778.

Mason, D., Davenport, I. and Robinson, G. (1995), 'Construction of an inter-tidal digital elevation model by the water-line method', *Geophysical Research Letters* **22**(23), 3187–3190.

Masselink, G. and Hughes, M. G. (2003), *Introduction to Coastal Processes & Geomorphology*, Arnold.

May, S., Dolan, R. and Hayden, B. P. (1983), 'Erosion of the US shorelines', *EOS* **64**(35), 521.

McBeth, F. (1956), 'A method of shoreline delineation', *Photogrammetric Engineering* **22**(2), 400–405.

Meyer-Arendt, K. J. (2001), 'Recreational development and shoreline modification along the north coast of Yucatan, Mexico', *Tourism Geographies* **3**(1), 87–104.

Miller, T. L. and Fletcher, C. H. (2003), 'Waikiki: Historical analysis of an engineered shoreline', *Journal of Coastal Research* **19**(4).

Moore, L. J. (2000), 'Shoreline mapping techniques', *Journal of Coastal Research* **16**(1), 111–124.

Moore, L. J., Ruggiero, P. and List, J. H. (2006), 'Comparing Mean High Water and High Water Line Shorelines: Should Proxy-Datum Offsets be incorporated into Shoreline Change Analysis?', *Journal of Coastal Research* **22**(4), 894–905.

Morel, A. (1974), *in* 'Optical Aspects of Oceanography', Academic Press, pp. 1–24.

Morton, R. A. (1991), Accurate shoreline mapping: past, present and future, *in* 'Coastal Sediments', Seattle, Washington, pp. 997–1010.

Morton, R. A., Miller, T. L. and Moore, L. J. (2004), National Assessment of Shoreline Change: Part 1 Historical Shoreline Change And Associated Coastal Land Loss Along the U.S.A. Gulf of Mexico, Technical report, US.

Morton, R. A., Miller, T. and Moore, L. (2005), 'Historical Shoreline Changes Along the US Gulf of Mexico: A Summary of Recent Shoreline Comparissons and Analyses.', *Journal of Coastal Research* **21**(4), 704–709.

Morton, R. and Speed, F. M. (1998), 'Evaluation of shorelines and legal boundaries controlled by water levels on sandy beaches', *Journal of Coastal Research* **14**(4), 1373–1384.

Muslim, A. M., Foody, G. M. and Atkinson, P. M. (2006), 'Localized soft classification for super-resolution mapping of the shoreline', *International Journal of Remote Sensing* **27**(11), 2271–2285.

Muslim, A. M., Foody, G. M. and Atkinson, P. M. (2007), 'Shoreline Mapping from Coarse-Spatial Resolution Remote Sensing Imagery of Seberang Takir, Malaysia', *Journal of Coastal Research* **23**(6), 1399–1408.

National Oceanic and Atmospheric Administration's: National Data Buoy Center (2011), National Oceanic and Atmospheric Administration's, http://www.ndbc.noaa.gov/.
**URL:** *http://www.ndbc.noaa.gov/*

NHC (1988), Hurricane Gil, Technical report, National Weather Advice, NOAA.

NHC (2010), Weather National Advicer, NOAA, http://www.nhc.noaa.gov/.
**URL:** *http://www.nhc.noaa.gov/*

Niedermeier, A., Romaneeben, E. and Lehner, S. (2000), 'Detection of Coastlines in SAR Images using Wavelet Methods', *IEEE Transactions on Geoscience and Remote Sensing* **38**, 2270–2281.

NOAA (1998), 'Our Restless Tides: A brief explanation of the basic astronomical factors which produce tides and tidal currents'.
**URL:** *http://www.co-ops.nos.noaa.gov/*

Overton, M. F., Grenier, R. R., Judge, E. K. and Fisher, J. S. (1999), 'Identification and analysis of coastal erosion hazard areas: Dare and Brunswick Counties, North Carolina', *Journal of Coastal Research* **Special Issue No.28**, 69–84.

Pajak, M. J. and Leatherman, S. (2002), 'The High Water Line as Shoreline Indicator', *Journal of Coastal Research* **18**(2), 329–337.

Parker, B. B. (2003), 'The Difficulties in Measuring a Consistently Defined Shoreline -The Problem of Vertical Referencing-', *Journal of Coastal Research* **38**, 44–56.

Parker, D. C. and Wolff, M. F. (1965), 'Remote sensing', *International Science and Technology* **43**, 20–31.

Pearre, N. S. and Puleo, J. (2009), 'Quantifying Seasonal Shoreline Variability at Rehoboth Beach, Delaware, Using Automated Imaging Techniques', *Journal of Coastal Research* **25**(4), 900–914.

Pilkey, O., Cooper, A. and Lewis, D. (2009), 'Global Distribution and Geomorphology of Fetch-Limited Barrier Islands', *Journal of Coastal Research* **25**(4), 819–837.

Plant, N., Aarnikhof, S., Turner, I. and Kingston, K. (2007), 'The performance of shoreline detection models applied to video imagery', *Journal of Coastal Research* **23**(3), 658–670.

Plant, N. G. and Holman, R. (1997), 'Intertidal beach profile estimation using video images', *Marine Geology* **140**, 1–24.

Pugh, D. (2004), *Changing sea levels: Effects of tides, weather and climate*, Cambridge University Press, Cambridge.

Richards, J. A. and Jia, X. (1999), *Remote Sensing Digital Image Analysis. An Introduction*, Springer, Praxis, New York.

Robertson, W., Whitman, D., Zhang, K. and Leatherman, S. P. (2004), 'Mapping Shoreline Position Using Airborne Laser', *Journal of Coastal Research* **20**(3), 884–892.

Robinson, I. S. (2004), *Measuring the Oceans from Space. The principles and methods of satellite oceanography*, Springer, Praxis, Germany.

Ruggiero, P., Kaminsky, G. M. and Gelfenbaum, G. (2003), 'Linking Proxy-Based and Datum-Based Shorelines on a High-Energy Coastline: Implications for Shoreline Analyses', *Journal of Coastal Research* **38**, 57–82.

SEMARNAT and SEDESOL (2009), Programa de Ordenamiento Ecologico del Territorio Costero del estado de Yucatan (POETCY)., Technical report, SEMARNAT, SEDESOL, Yucatan, Mexico.

Shaghude, Y. W., Wannas, K. O. and Lundeen, B. (2003), 'Assessment of shoreline changes in the western side of Zanzibar channel using satellite remote sensing', *Int. J. Remote Sensing* **24**(3), 4953–4967.

Shalowitz, A. L. (1964), Shoreline and Sea Boundaries, Technical report, U.S. Department of Commerce, Coast Author Geodetic Survey.

Stafford, D. B. (1971), An aerial photographic technique for beach erosion surveys in North Carolina, Technical report.

Swain, P. H. (1973), *Remote sensing: The quantitative approach*, Purdue University, West Lafayette.

Teodoro, A. C., Marcal, A. R. S. and Veloso-Gomes, F. (2007), 'Correlation Analysis of Water Wave Reflectance and Local TSM Concentrationsin the Breaking Zone with Remote Sensing Techniques', *Journal of Coastal Research* **23**(6), 1491–1497.

Teodoro, A. C., Veloso-Gomes, F. and Gancalves, H. (2008), 'Statistical Techniques for Correlation Total Suspended Matter Concentration with Seawater Reflectance Using Multispectral Satellite Data', *Journal of Coastal Research* **24**(4C), 40–49.

Trebossen, H., Deffontaines, B., Classeau, N., Kouame, J. and Rudant, J. (2005), 'Monitoring coastal evolution and associated littoral hazards of French Guiana shoreline with radar images', *C.R. Geoscience* **337**, 1140–1153.

Turner, I., Leyden, V., Simmons, G., McGrath, J., Jackson, A., Jancar, A., Aarninkhof, S. and Elshoff, I. (2001), 'Comparison of observed and predicted coastline changes at the gold coast artificial (surfing) reef, Sydney, Australia.'.

Vitousek, P. M., Mooney, H. A., Lubchenco, J. and Melillo, J. M. (1997), 'Human Domination of Earth's Ecosystems', *Science* **277**(5325), 494–499.

Wang, C. and Enfield, D. B. (2006), 'Influences of the Atlantic Warm Pool on Western Hemisphere Summer Rainfall and Atlantic Hurricanes', *Journal of Climate* **19**, 3011–3028.

Wang, C., Zhang, J. and Ma, Y. (2010), 'Coastline interpretation from multispectral remote sensing images using an association rule algorithm', *Int. J. Remote Sensing* **31**(24), 6409–6423.

White, K. and El-Asmar, H. M. (1999), 'Monitoring changing position of coastlines using Thematic Mapper imagery, an example from the Nile Delta', *Geomorphology* **29**, 93–105.

Zakariya, R., Rosnan, Y., Saidin, S., Yahaya, M., Kasawani, I. and Lokman, H. (2006), 'Shoreline detection and changes for Terengganu River mouth from satellite imagery (LANDSAT 5 and LANDSAT 7)', *Journal of Sustainability Science and Management* **1**(1), 47–57.